Relationship between the Micromorphology and Mechanical Properties of Semicrystalline Polypropylene

A thesis submitted for the degree of Doctor of Philosophy

By

Zhaoping ZHONG, B.Sc.

Department of Materials Technology
Brunel University
United Kingdom

April 1996

Dedicated to:

my parents,
my husband L. X. TANG
and my daughters Joanna Ying TANG, Maria Lan TANG

ABSTRACT

The objective of this research project was to carry out the investigation of the relationship between processing conditions, micromorphology and mechanical properties of isotactic polypropylene homopolymer using conventional and shear controlled orientation injection moulding (SCORIM) techniques by systematically changing carefully controlled processing conditions, mould geometry and compound additives.

Both SCORIM and conventional techniques were employed for iPP injection moulding using three moulds of different shapes by varying the processing conditions, including nozzle temperature, mould temperature, injection speed, hold pressure and oscillating patterns of pistons. The results obtained were compared so as to indicate the differences in microstructure and physical properties resulting from the two moulding techniques.

A range of analytical methods were employed. Optical transmitted light microscopy was used to reveal the skin-core morphology and preferentially oriented fibrous textures. Transmitted Electron Microscopy represented the enlargement of the fibrous alignment. Microhardness analysed the hardness and isotropy characteristics by measuring the diagonal lengths of the indentations. Mechanical testing determined Young's modulus, the strength and toughness of the mouldings. X-ray diffraction exhibited the distribution of the α, ß and γ crystalline phases of the iPP mouldings. The WAXS Debye patterns confirmed the existence of the preferred orientation through the thickness of the moulding. Differential Scanning Calorimetry analysed the thermal behaviour from the endothermal and exothermal curves.

In the initial stage of the study, the polypropylene was moulded in the form of a standard tensile bar on a conventional Sandretto injection machine in order to obtain the basic characteristics of the polypropylene study material, which could then be used to compare with those properties to be gained using the SCORIM technique. A ring mould was then used in a Negri Bossi twin injection machine to investigate improvements in uniformity of micromorphology and dimensional reproducibility of mouldings made possible by four live-feed injection moulding. Later, a study was carried out on injection moulding of polypropylene by varying processing conditions, including three hold pressures, two mould temperatures and two nozzle temperatures for both conventional and SCORIM injection processes by using a rectangular bar mould in a Demag injection moulding machine. In the finial stage, the study explores the influences of composition, in essence a limited range of nucleating agents, and processing methods, and aspects of the micromorphology, dimensional control and the mechanical properties of polypropylene.

Polypropylene, as a semicrystalline polymer, represents a class of materials in which mechanical properties are strongly influenced by processing conditions and micromorphology.

ACKNOWLEDGEMENTS

I would like to express my gratitude to Professor Mike J. Bevis (Wolfson Centre, Brunel University) for his patient guidance and continual help and encouragement throughout the period of my study.

My thanks are also due to the other members of Wolfson Centre in Brunel University for their invaluable help and advice, Dr. P. Allan and Dr. J. Gibson. I also wish to thank various members of the Department of Materials Technology in Brunel University for their valued assistance.

The financial support from Ministry of Defence of U.K. is gratefully acknowledged.

I would like to thank my husband for his understanding and support through my writing up.

Finally, I would like to thank my parents for their strong encouragements and enormous support for all my education.

Contents

CHAPTER 1 INTRODUCTION

1.1 Background and Aims of Study

Polypropylene plastic products have been largely manufactured using injection moulding technology, and numerous applications have been found for injection moulded polypropylene. In order to produce final plastic parts with required physical characteristics, it is important to control and manipulate the processing procedure, thus optimising the performance properties of the injection moulded polypropylene [1-3].

It is well known that the microstructure is the dominant factor in determining the properties of materials. In the injection moulding of polypropylene plastics, changes in moulding conditions such as mould temperature, melt temperature and injection pressure can greatly influence the microstructure and consequently the ultimate performance properties of the end products. Therefore, a comprehensive experimental study of the detailed micromorphology under different moulding conditions should be of significant value for the understanding and control of the injection moulding process. More importantly, this can be used to predict and optimise the performance properties of injection moulded polypropylene for practical applications.

The aims of this study were:
(1) To investigate the relationship between processing conditions, microstructure and physical properties of polypropylene using injection moulding techniques and a variety of materials characterisation methods.

(2) To compare two different methods of injection moulding of polypropylene: conventional and shear controlled orientation injection moulding (SCORIM).

(3) To study the effect of nucleating additives on the micromorphology which governs the physical properties of injection moulded polypropylene.

This dissertation is divided into five chapters.

Chapter 1 is the literature review concerned with the history of polypropylene production, morphology, nucleation, crystallisation and polymer processing. In the

review of polypropylene morphology, history of the polymer morphology, spherulitic development, molecular and crystal structure, kinetic theories are included.

Chapter 2 describes the selection and preparation of materials, instrumentation and the injection moulding programmes used for preparing polypropylene mouldings, instrumental testing methods and the details of etching technique for polypropylene samples. This chapter is an extension to the literature survey of applied testing techniques to polypropylene mouldings. Microtomy, optical microscopy, Transmitted Electron Microscopy (TEM), microhardness testing, mechanical measurements, x-ray diffraction, WAXS Debye flat plate technique, Differential Scanning Calorimetry (DSC) and density measurement were elucidated.

Chapter 3 presents the experimental results of studies on effects of processing conditions on micromorphology and mechanical properties of polypropylene. In this study, both conventional and SCORIM techniques were employed for injection moulding of a propylene homopolymer using three moulds of different shapes by varying the processing conditions, including nozzle temperature, mould temperature, injection speed, hold pressure, oscillating pattern of pistons and operating pressure of pistons.

A wide range of techniques have been used to investigate the micromorphology and physical properties of a single grade of polypropylene. These included: polarized transmitted light microscopy, TEM, distortion measurements, mechanical testing, x-ray diffraction, WAXS Debye flat plate technique and DSC.

Chapter 4 concentrates particularly on the study of the relationship between processing conditions and mechanical properties of polypropylene with the addition of nucleating agents by conventional and SCORIM injection moulding techniques. The experimental results of x-ray diffraction presents that the concentration and distribution of α, ß and γ-phases exhibit notable dependence on selected processing conditions which are associated with differences in mechanical properties.

Chapter 5 discusses the results presented in chapter 3 and 4. The micromorphology of injection moulded iPP can be controlled by the processing parameters, and the mechanical properties of iPP are dependent on the morphology of the mouldings.

The discussion explores the influences of composition, in essence a limited range of nucleating agents, and processing methods, namely SCORIM and conventional mouldings, on aspects of the micromorphology, dimensional control and the mechanical properties of polypropylene.

1.2 Polypropylene and its History of Production

Polypropylene is a crystalline thermoplastic polyolefin resin. The molecular structure of polypropylene can possess three types of steric configurations: isotactic, syndiotactic and atactic. The stereoregularity of polypropylene is of great importance for the properties and its applications. The commercial form of polypropylene is of isotactic configuration as shown in the following:

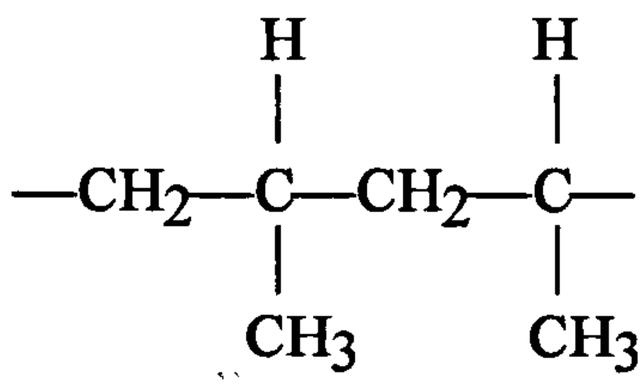

Commercial isotactic polypropylene is a semicrystalline polymer and is mainly isotactic in nature. Syndiotactic polypropylene has been mainly of scientific interest to date, while atactic polypropylene has no useful properties as a solid engineering material [4-6].

The history of crystalline polypropylene is unique from the following standpoints:
1. Polypropylene was the first high melting crystalline aliphatic hydrocarbon.
2. Polypropylene has been the subject of perhaps the most scientific research and printed matter of any crystalline polymer.
3. Crystalline polypropylene was the subject of the longest, most costly contest, between companies, for invention of any chemical composition.
4. Crystalline polypropylene is the only hydrocarbon polymer impacting on a Nobel prize.

The discovery of the first polyolefin is semicrystalline (low density) polyethylene in 1933-1935 [7]. Direct polymerisation of ethylene to polyethylene was achieved by the high pressure polyethylene process of the ICI (1935-1939). As a result of a

happy accident (the right amount of air impurity), ethylene was polymerised to a high polymer at extremely high pressure. Due to the effect of a methyl group, propylene did not polymerise to a high polymer at similar conditions. Rather high molecular weight propylene polymers were made in the 1940's (with catalysts such as $HBr/AlBr_3$), but they were nevertheless grease-like [8].

In 1953 a process suitable for polymerisation of ethylene at atmospheric pressure and moderate temperature (50-75°C) was discovered by Ziegler at the Max-Planck-Institute für Kohleforschung Mühlhein/Ruhr [9]. The essence of this process is the utilisation of a co-ordination catalyst system containing the components $TiCl_4$ and Al-alkyls, or more generally metal alkyl (group I-III) and a reducible compound of the transition elements (group IV-VIII). The so-called low pressure or high density polyethylene obtained in this process is stiffer, stronger and more heat resistant than the conventional low density polyethylene. It is an essentially linear polymer with a comparatively high degree of crystallinity: melting point 135°C, density about $0.95 g/cm^3$.

Shortly after the discovery of high density polyethylene, it was found by Natta that propylene and higher α-olefins can also be polymerised by the use of co-ordination catalysts [10]. In 1954 Dr. Giulio Natta further testified that it was his idea to polymerise propylene into two different forms of polypropylene: an essentially amorphous, rubbery and soluble fraction and a highly crystalline, hard and insoluble fraction. Natta, P. Pino and G. Mazzanti filed U.S. Patent Applications 514,097 and 514,099 claiming a process and crystalline polymers, respectively, of various α-olefins including propylene on June 7, 1955. Polypropylene density and melting point were given as $0.92 g/cm^3$ and 160°C respectively. The Nobel prize in Chemistry in 1963, recognised their outstanding contributions to polymer science.

Natta soon discovered that $TiCl_3$ was a more efficient producer of crystalline polypropylene than $TiCl_4$, and that the violet ("delta") crystalline form of $TiCl_3$ was preferred over the others. Natta was the first to use the term "Ziegler catalyst", and "Ziegler-Natta" catalysts soon became the principal basis of a rapidly growing polypropylene industry.

In May of 1953, E. F. Peters of Standard (Indiana) used the cobalt-molybdenum catalyst of Carmody to attempt the polymerisation of propylene at room temperature.

After one month reaction time, boiling xylene extraction of the catalyst yielded a small amount of polypropylene (Precipitated by cooling the xylene) which infra-red examination showed to have a much lower $-CH_2-/-CH_3$ ratio than Carmody's polymers and to have some crystallinity. Standard Oil (Indiana) Patent Application No. 462,480, filed by Alex Zletz on October 15,1954, recited a density between 0.85 to 0.95g/cm³, a softening point above 120°C, and a viscosity above 0.1poise for polypropylene. The experimental work on olefin polymerisation with molybdenum catalyst eventually led to a commercial process for ethylene polymerisation [11].

In early 1955, Vandenberg at Hercules Powder Co. discovered the use of hydrogen to control molecular weight of polyolefins made with Ziegler-Natta type catalysts [12], and this remains the principal method of control today.

Technology for the early polypropylene plants stemmed from polyethylene process technology. In fact, some of the polypropylene plants still in operation today were originally constructed for high density polyethylene manufacture with Ziegler catalysts [13]. The early plants used a slurry technique which is still the most widely practised commercial process for producing polypropylene, and although major improvements in both catalyst activity and stereospecificity have occurred during the past forty years, for some plants expensive catalyst and amorphous polymer removal steps are still necessary.

One of the oldest of the commercial polypropylene processes is solution polymerisation. It is generally considered obsolete. But the higher temperature (140 to 150°C) necessary to keep the polymer in solution results in the production of greater amounts of normally undesirable amorphous polymer than by other commercial processes.

A bulk or liquid monomer propylene polymerisation process is designed to take advantage of high polymerisation rates associated with bulk polymerisation and high heat transfer rates characteristic of loop reactors. This technique was commercialised by Phillips Petroleum Company in 1963. A bulk polymerisation system in which the heat of reaction is controlled by vaporisation of propylene was developed and used commercially by Dart Industries.

A gas-phase process for producing polypropylene was commercialised by BASF in

a small plant in Germany in the mid-1960's. The polymer initially produced had higher than normal amorphous content and low stiffness and hardness properties. By 1983, it was claimed that this process had the ability to produce higher crystalline products needing no removal of amorphous polymer and minimal stabilisation [14].

The essential factor in commercial production of highly crystalline polypropylene is obviously the catalyst system. The most major development in the 1980's is supported titanium catalyst. The goal of the development of supported catalysts was activity and stereospecificity sufficiently high to avoid both catalyst and amorphous polymer removal.

Since the 1950's, polypropylene has been gaining increasing importance and applications as a member of the thermoplastic materials family. This is mainly due to the fact that polypropylene has many excellent properties [15]. These include great impact strength, chemical and thermal resistance, resistance to stress and flex cracking, good ability of process and the ability to form high strength composites with glass fibre reinforcing. All these properties are a direct result of its isotactic steric molecular structure.

Polypropylene like other crystalline polyolefins, is soluble only at elevated temperatures. Isotactic polypropylene displays good solubility above 80°C in so-called 'good' solvents such as xylene, tetralin, chlorinated aromatic and aliphatic hydrocarbons, etc. In 'poor' solvents such as esters, ethers, higher alcohols, etc. Polypropylene becomes soluble only at considerably higher temperature.

Crystalline polypropylene is now being produced world-wide annually. Major applications of crystalline polypropylene are injection moulded components, especially for the automotive industry and for electrical applications, fibres and monofilaments, film and sheet, pipe and conduit, and blow moulding and other extruded products. Although homopolymer is the principal product, random and block copolymers containing small amounts of ethylene are also commercially important [16]. It is anticipated that the demand for polypropylene will continue to grow for the rest of this decade and new applications requiring specialised types of polymers will continue to emerge [17, 18].

1.3 Morphology of Polypropylene

1.3.1 History of the Polymer Morphology

Crystalline polymers show ordering at a variety of dimensional levels, from interatomic spacings to macroscopic measures. The study of polymer morphology is primarily concerned to elucidate this organisation, and understand of certain properties, deformation and other mechanical behaviour. In addition, the textures revealed are the products of processes whose mechanisms may also be illuminated by examination of their microstructural consequences. Furthermore, the morphology is a record of the past history of a sample which, with sufficient understanding may be read to disclose not only crystallisation, annealing or deformation treatments to which it has been subjected but can also provide an indication of certain intrinsic properties, such as the molecular mass range within a specimen or the nature and extent of molecular branching [19].

Historically, the first detailed knowledge of polymer morphology obtained was that of the crystal structures, i.e. chain packing using the techniques of x-ray crystallography. In addition to the sharp, crystalline reflection used for the structural analysis, polymer samples generally show diffuse, liquid-like diffraction indicative of more disordered molecular arrangements. Such localities are commonly referred to as amorphous regions. Nevertheless, the apparent juxtaposition of crystalline and disordered molecular arrangements has given rise to much speculation as to how this might be achieved by the linear thread-like molecules recognised to be characteristic of crystallizable polymers.

For many years the fringed-micelle model held sway. A sketch of a possible arrangement is shown in Figure 1.1. The sufficiently long molecules will probably be entangled in part and the regions of crystalline order restricted in size. An individual molecule would be like to pass through different regions of order and disorder. The concept of two kinds of order has, and continues to, provided the basis of an explanation for the variable densities, melting points, etc., shown by crystallised polymers —— and is the reason for their often being described as semi-crystalline. The fraction of the material supposed to be fully-crystalline is known as the (degree of) crystallinity of a sample and is a widely used parameter in polymer

science.

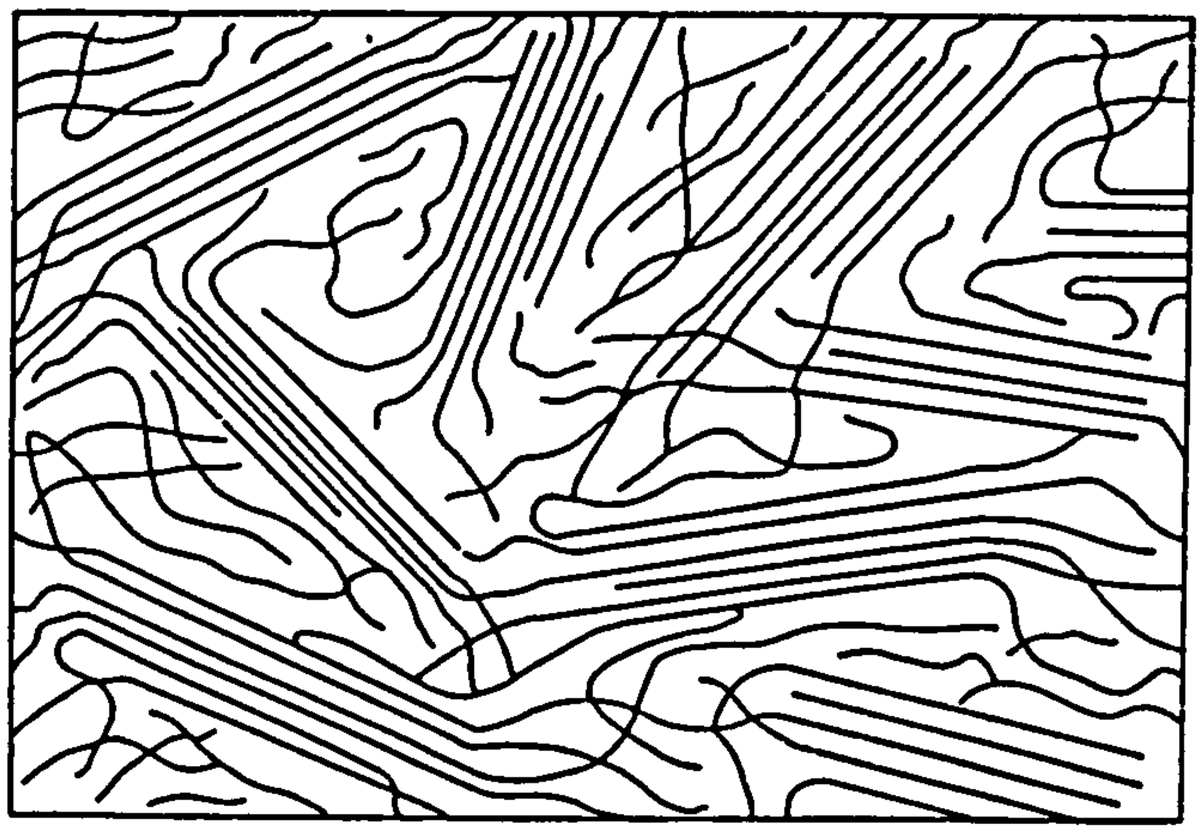

Figure 1.1 The fringed-micelle model of polymeric texture [20]

The textural scale of the fringed-micelle model was believed, primarily on the basis of crystallite size estimated from the widths of x-ray diffraction rings, to be on the scale of a few tens of nm. Such dimensions were not then observable at a time when the first electron microscopes were just being developed. Not until 1945 was it appreciated, first for polyethylene and subsequently for other polymers, that there was additional ordering, on the scale of several μm. This is due to the prevalent crystallisation of high polymers as spherulites and literally little spheres.

The study of spherulites with the polarizing optical microscopy then became the major area of polymer morphology to be investigated. At this stage the link of morphology with properties becomes particularly evident. The study became important to understand what the morphological texture is, how it formed, how it can be controlled and modified to give improved properties if possible.

It was by no means obvious how the supposed fringed-micellar arrangement of molecules at the 20 nm level fitted within spherulites two orders of magnitude larger in scale, particularly in view of the fact that the molecular chain is generally tangential to spherulites instead of radial as had been expected. Matters introduced the first generation of modern electron microscopes, coinciding with the synthesis of highly linear and stereoregular polymers following Ziegler and Natta, led to the discovery of individual polymer crystals grown from very dilute solutions. And

Keller deduced correctly the more remarkable fact that molecules — typically 5-10 μm long —— lay in the crystals with their lengths across the thin dimension (12nm) of the lamellae [21]. The inescapable conclusion was that the chains must fold back on themselves repetitively at each crystal surface alternately, a phenomenon now known to be widespread and called chain folding (Figure 1.2). These above two discoveries of polymer lamellar crystals and chain folding lie at the heart of understanding of polymer morphology.

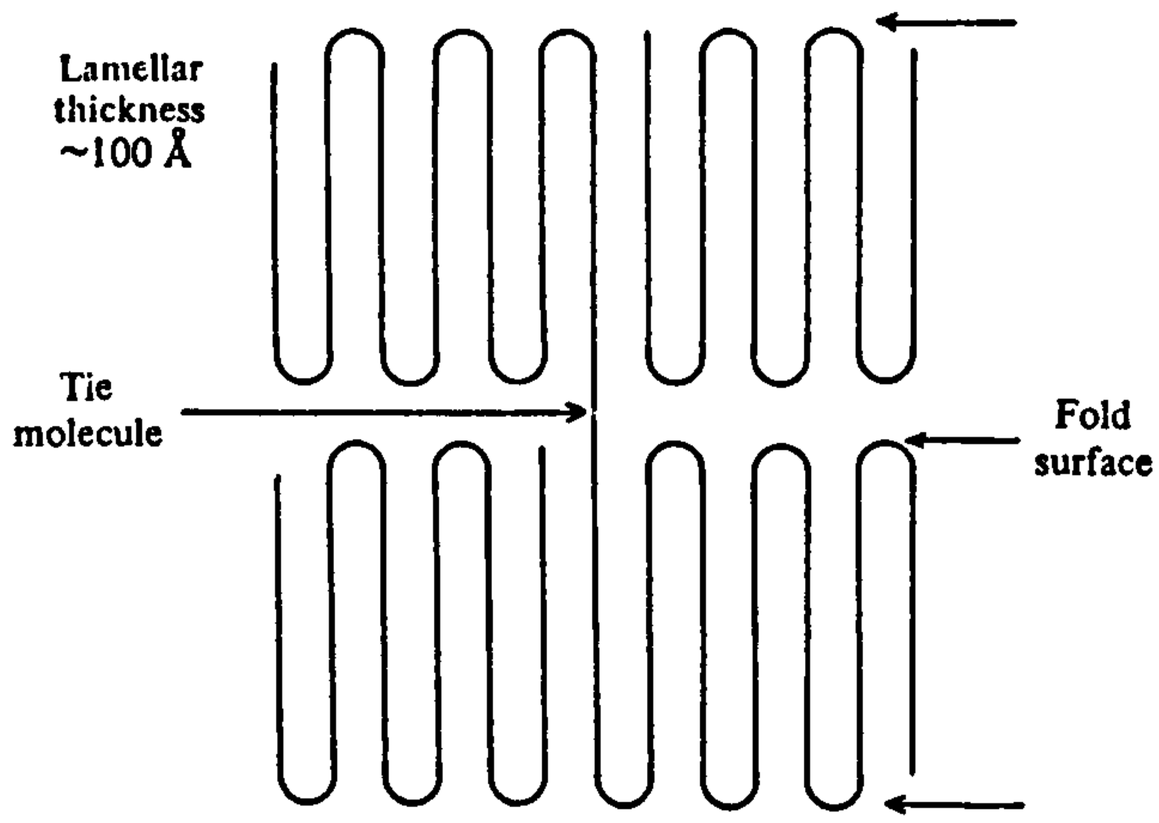

Figure 1.2 Schematic of a chain folded conformation [22]

1.3.2 Spherulitic Development

The polypropylene spherulitic structure is shown in Figure 1.3. The bright contrast derives from birefringence and indicates a crystalline entity. The Maltese cross occurs when the principal optical directions of the radial units fall parallel to those of the polarizing microscope. The significance of the cross remaining stationary while a specimen rotates is then that each radial unit has the same extinction directions. This, in turn, signifies that the major refractive index is then parallel to one of the polarizers.

This fine structure will also serve as a means of identifying a spherulitic entity. In the first instance, how a spherulite develops depends on how it is nucleated. A common progression is shown in Figure 1.4, beginning with a fibre and evolving through sheaf-like embryos before attaining a spherical envelope. Then they become polyhedral until neighbouring spherulites impinge. When nucleated simultaneously

they will share a planar interface, otherwise the common boundary will be a hyperboloid of revolution (see Figure 1.1). This succession of shapes for the same object growing isothermally makes it preferable to define the nature of a spherulite not in terms of whatever outer profile it happens to have formed, but rather on the basis of the constant nature of its fine structure. This simply refers to different stages in development as mature.

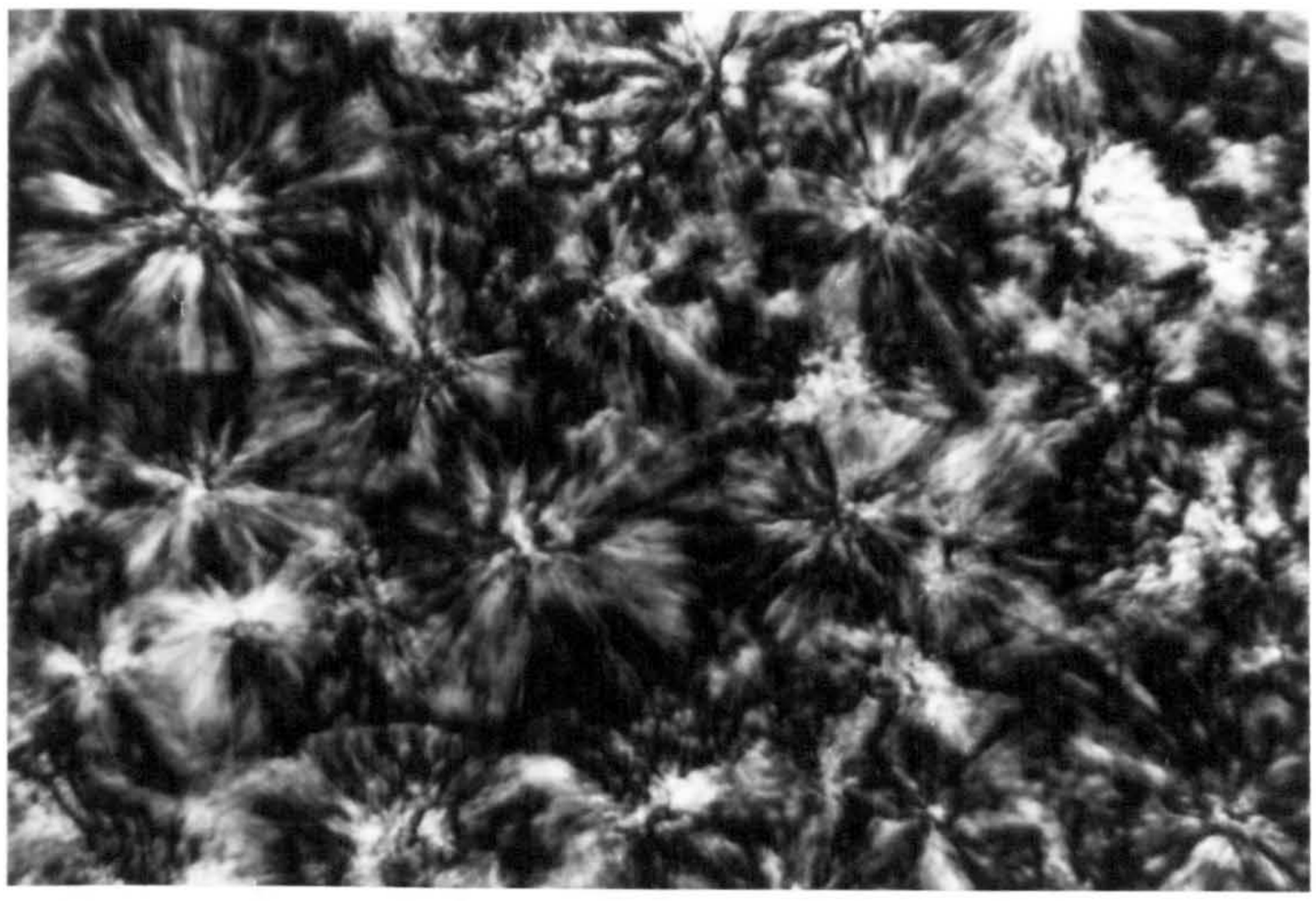

Figure 1.3 Optical polarized micrograph of polypropylene spherulites

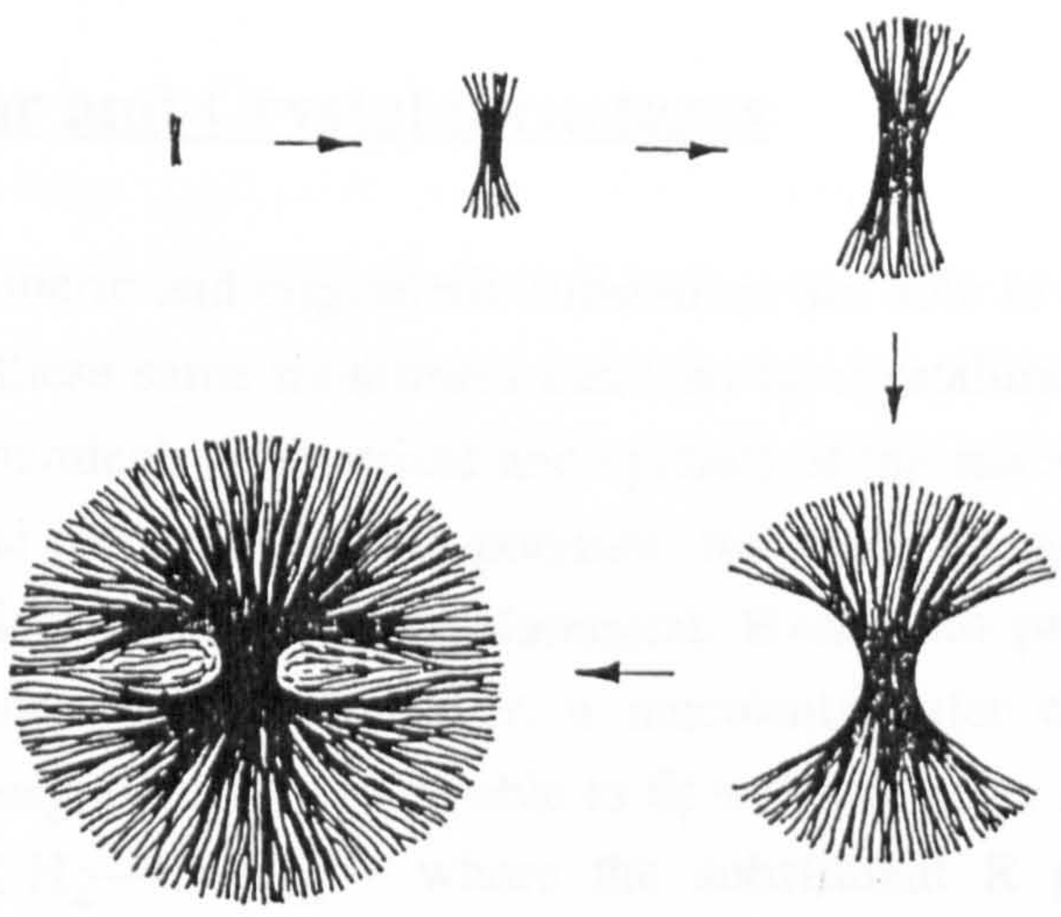

Figure 1.4 A common progression of habits leading to the spherical form of a mature spherulite [19]

Mature spherulites have the same crystallographic axis along every radius. In this they differ from dendrites, which are also highly branched solids but possess a common single crystal orientation. Even this distinction should not be pressed too far because the two have no clear divide but merge continuously as growth conditions vary.

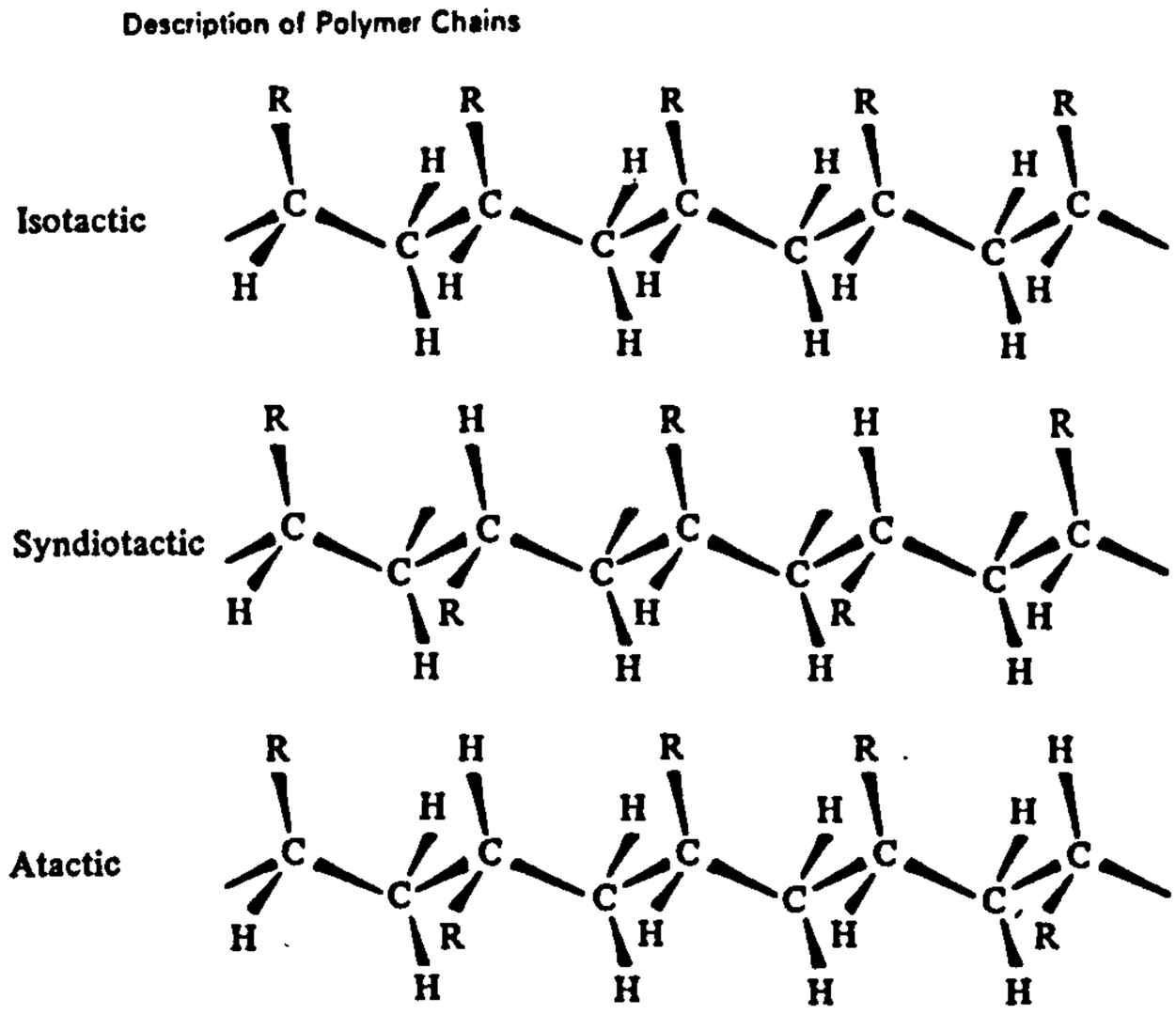

Figure 1.5 Chain configurations in poly(α)olefins [23]

1.3.3 Molecular and Crystal Structures

Practically all monomeric and oligomeric substances are able to crystallise, whether or not polymers of these same monomers can also be crystalline depends primarily on the regularity (chemical, geometrical and spatial) of the macromolecular chains. In general terms, the more regular the polymer, the more likely it is to crystallise. The need for chemical regularity is fundamental. Even with perfect chemical and geometrical repetition along it, however, a macromolecular chain must also be spatially regular if neighbours are to be able to fit well together. A example is given by polyolefins —[CH_2—CHR]$_n$— where the substituent R groups have to be systematically arranged along the chain to permit crystallisation. There are two spatially ordered arrangements: isotactic and syndiotactic. As Figure 1.5 shows that the pendant groups have the same placement or an alternating one in relation to

atoms in the main chain respectively. Disordered sequences are known as atactic. It is a commonplace that whereas atactic polystyrene and polypropylene can not crystallise, their isotactic counter parts will do so.

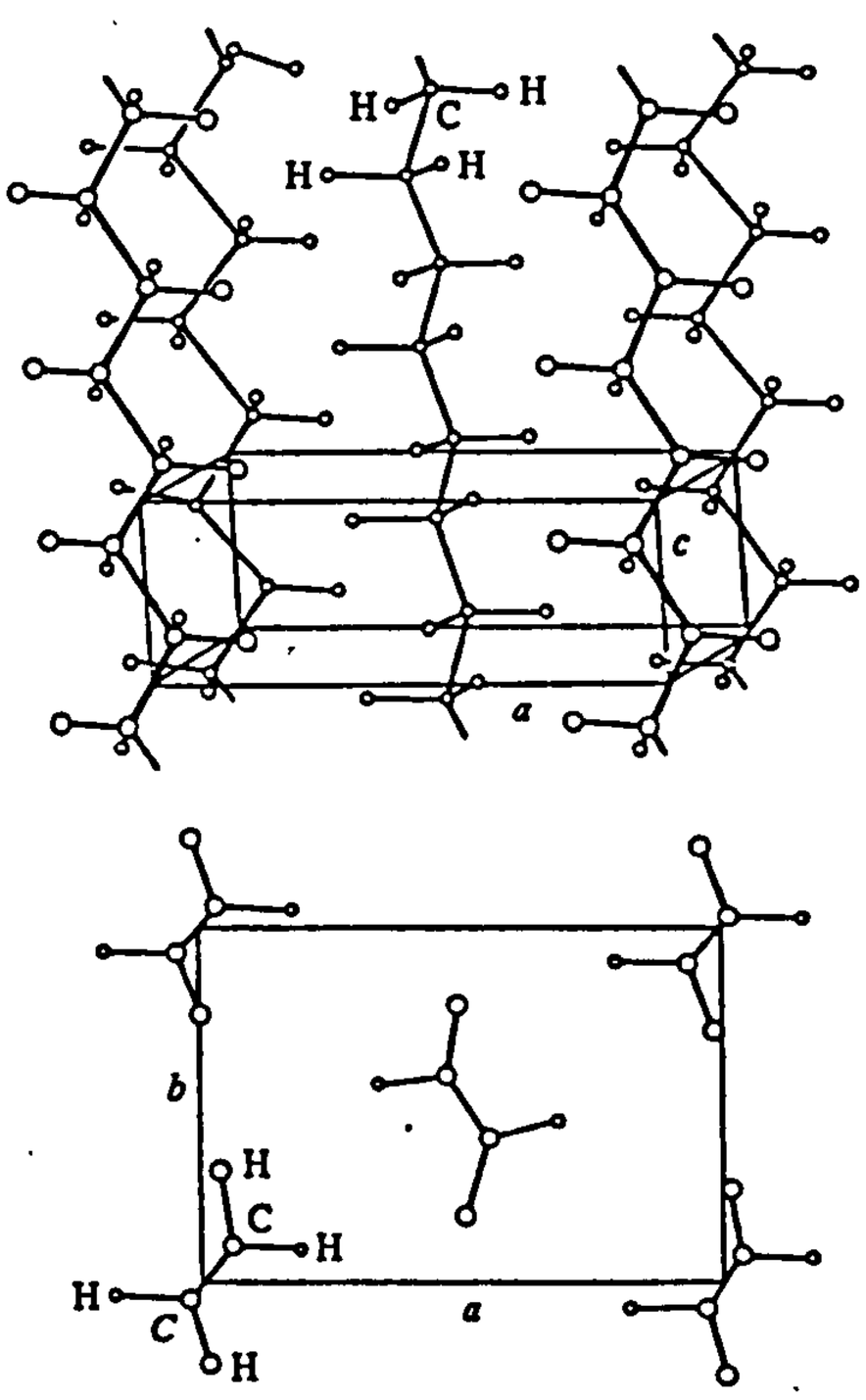

Figure 1.6 The orthorhombic polyethylene structure [20]

To the extent that molecular chains can be regarded as rigid rods with the van der Walls' bonding between molecules weaker than intramolecular covalent linkages, they will tend to pack together in a simple hexagonal array, i.e. with sixfold co-ordination. Certain structures are indeed, truly hexagonal; for example, hexagonal polypropylene and disordered high-pressure phase of polyethylene. More often, however, lower symmetries prevail, such as in orthorhombic polyethylene (Figure 1.6) or monoclinic polypropylene (Figure 1.7) which are distorted hexagonal structures [24]. Nylon-6 is also polymorphic exhibiting both monoclinic and pseudohexagonal forms. Nylon-66 is under most conditions in a triclinic form. Polyethylene terephthalate crystallises to a triclinic crystalline form. Other factors can also intervene. The phenyl groups of polystyrene place the isotactic molecule in a 3_1 helix whose circumscribed triangular prism brings threefold co-ordination. In a similar way it is the provision of optimum packing of the side groups to which the

tetragonal structure of isotactic poly(4-methylpentene-1) is attributed. Sometimes constituent groups cause a chain to adopt a more planar than rod-like shape with consequences for the crystal structure. Thus the all trans-planar zigzags of the n-paraffins and polyethylene can pack together either in the distorted hexagonal structure of the orthorhombic form (Figure 1.6) or they may adopt the slightly higher energy monoclinic subcell in which they are all parallel.

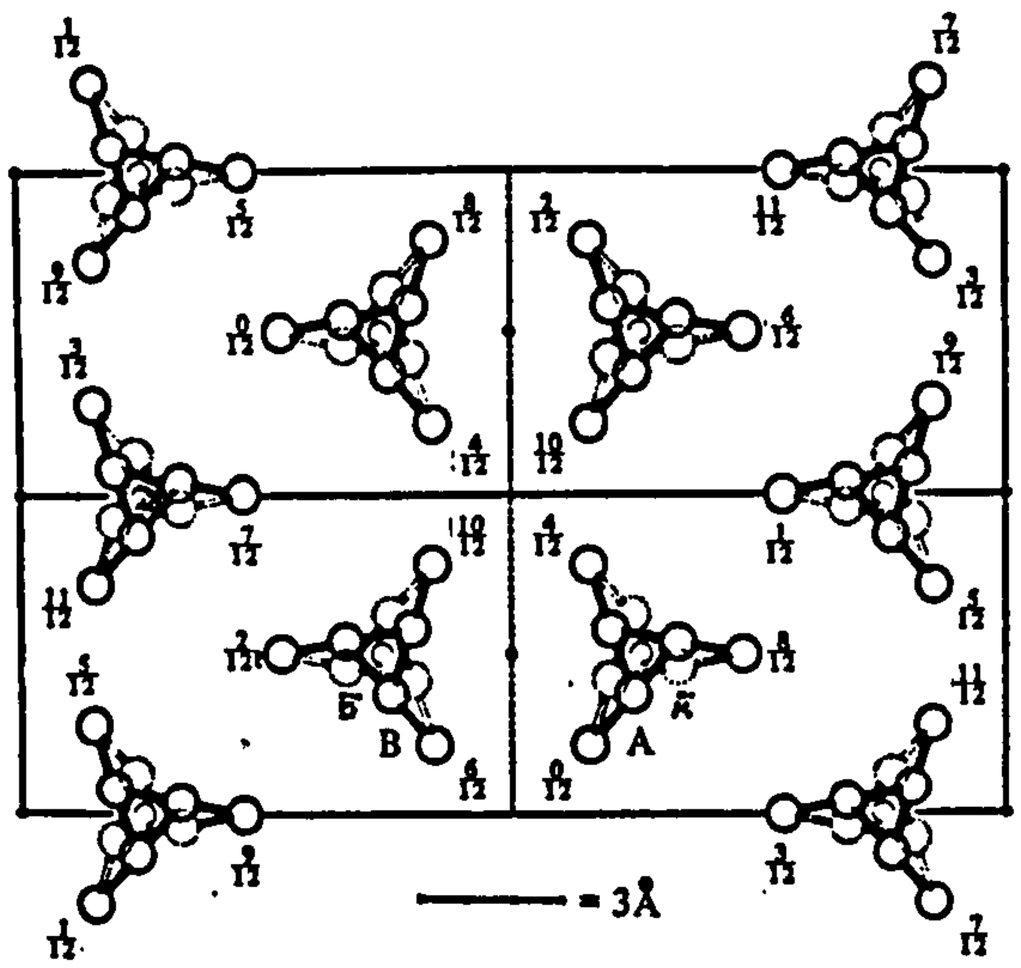

Figure 1.7 The monoclinic polypropylene structure, projected on {001} [24]

1.3.4 "Shish Kebab" Morphology

The "Shish Kebab" is a composite structure of narrow central thread (~30 nm in diameter) strung with small platelets. It was in connection with interlamellar links whose narrow fibrils can become to overgrown with platelets in the characteristic fashion when they are allowed to nucleate growth from additional polymer solution. In short the Shish Kebab is regarded as nucleation of fibrils followed by epitaxial overgrowth of lamellae sharing a common chain-axis orientation along the fibre. The fibre itself results from strain-induced crystallisation, i.e. from distorted molecular conformations in which chains have been brought and maintained parallel for long enough to nucleate crystallites. There are many circumstances where this occurs. Polymers frequently show Shish Kebab form due to crystallisation occurring almost simultaneously with polymerisation. Most systematically, however, Shish Kebabs have been produced by flow-induced crystallisation. This is a large subject

of great technical importance, being related to processes of moulding and extrusion.

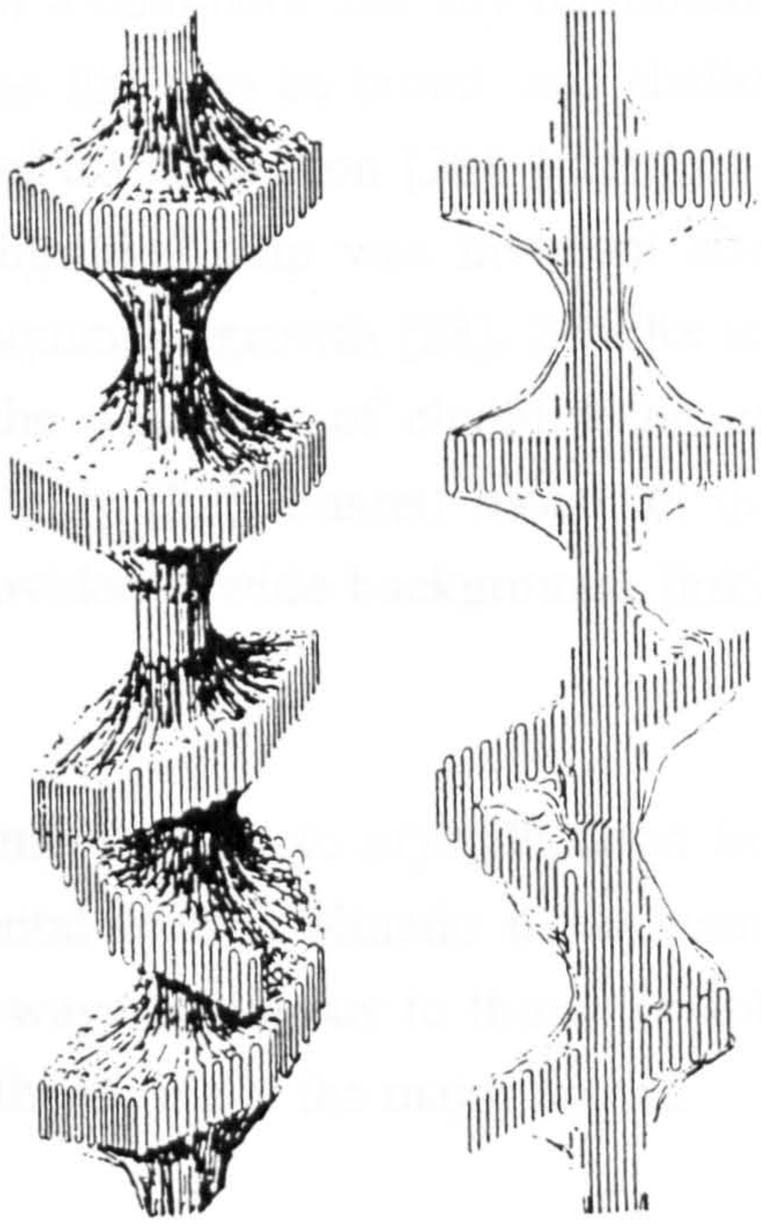

Figure 1.8 Schematic molecular model of the Shish Kebab morphology. [25]

Figure 1.8 is shown a schematic structural proposal. This behaviour is that molecular conformations are being drawn out, the more so for longer molecules. The extension in the flow field will tend to form a series of nuclei in a row but positively discourage molecular background. The row nuclei containing reasonably chain-extended molecules may deposit, under suitable conditions of low temperatures and modified flow, lamellar overgrowth. Pennings pioneered the route to high modulus and high strength fibres by forming fibres in a Couette apparatus [25].

1.3.5 Kinetic Theories

Modern theories of the lamellar thickness are kinetic theories, that is they assume that the observed lamellar thickness is that which grows fastest and is not necessarily the most stable crystal which could have been grown. There have also

been various equilibrium theories which have provided the explanations.

F. C. Frank paraphrased a comment that any minimum in free energy predicted on equilibrium grounds was likely to be broad and shallow especially in comparison with the free energies of crystallisation [26]. Lauritzen and Hoffman assumed that the thickness of a chainfolded strip was invariant after nucleation [27]. Sanchez made the theories of sequential growth [28]. Schultz summarised the theory which substantially predates the discovery of chainfolding and was concerned with the development of crystallinity [23]. Bassett based on the comprehensive review of kinetic theories and provided a wide background, linking the various theories and their development [19].

The application of kinetic theories to crystallisation from the melt is an empirical rather than a fundamental matter. Kinetic theory continues to be used for melt crystallised samples in ways analogous to those for solution crystallisation. In this dissertation the kinetic theory is not the major aspect.

1.3.6 α-, ß- and γ-Crystalline Forms in Polypropylene

Isotactic polymers crystallise in the three basic crystalline forms: monoclinic (α-form), hexagonal (ß-form) and triclinic (γ-form). The α structure was first determined by Natta and Corradini, to consist of molecular chains ordered in a 3_1-helical conformation packed monoclinically [24]. The dimensions of the unit cell are:

a = 6.65±0.05 Å,	b = 20.96±0.15 Å,	c = 6.65±0.04 Å
α = 90°	ß = 99±1°	γ = 90°

The monoclinic α-form is stable at room temperature.

The ß structure was recognised by Keith and Padden [29] and later by Turner-Jones et al., who calculated the unit cell dimensions to be [30]:

a = 19.08 Å,	b = 19.08 Å,	c = 6.49 Å
α = 90°	ß = 90°	γ = 120°

The hexagonal ß-form appearing under certain cooling conditions is unstable and changes into the monoclinic structure already on mild heating. The conditions in

cooling influence to fair extent also the size of crystallites.

The γ structure based on a triclinic lattice was identified by Turner-Jones et al. [30]. The unit cell dimensions were first reported by Turner-Jones et al., but modified more accurately by Morrow and Newman [31], in samples of very low molecular weight fractions:

a = 6.54 Å,	b = 21.40 Å,	c = 6.50 Å
α = 89°	ß = 99.60°	γ = 99°

The γ structure was found to be favoured by hydrostatic pressure [31-33].

In 1964, Turner-Jones reported that stereoblock fractions obtained by solvent extraction of normal commercial polypropylene cooled from above their melting points gave γ-form crystallinity as well as normal α-form. The low temperature fractions, obtained over the approximate range 35——70°C using petroleum ether or xylene as solvents, were of high molecular weight and crystallised entirely in the γ-form.

Since then highly isotactic polypropylene, as opposed to stereoblock polymer has been obtained in the γ-form free of α-form by crystallisation under very high pressure by Kardos [32] and Pae [34] and also independently in these laboratories. Very low molecular weight isotactic polymer has also been shown to crystallise in the γ-form by melt crystallisation and from certain solvents [35]. Brücker and meille determined the crystal structure of the γ-form of isotactic polypropylene by using the Rietveld method of analysis of x-ray powder diffraction data, and confirmed the proposed structure following a packing energy analysis that compared the internal energy of α- and γ-phases [36-38].

The α-, ß- and γ-form determinations, together with measurement of degrees of crystallinity were measured by x-rays. The introduction of experimental techniques led to advances in the understanding of polymer morphology. The use of different techniques to complement each other is essential in morphological enquiry and is likely to involve more and more methods as the sophistication of textural characterisation increases.

1.4 Nucleation and Crystallisation

Nucleation and crystallisation can be described as the thermal and kinetic processes which allows the formation from a structurally disordered phase, of a stable solid phase with a regular ordered geometry. These ordering processes take place as a consequence of the decreasing free energy of the system when the melt is cooled below its liquid temperature.

1.4.1 Nucleation

There are two basic nucleation processes: first, primary nucleation is the birth of the new solid phase or nucleus within the melt. Then secondary nucleation is the process of crystal growth which requires nucleation at the growing interface.

The primary nucleation can be initiated by several different ways. The nucleation of crystalline phases can take place in the following types of mechanisms:

1) Homogeneous nucleation involves the spontaneous aggregation of polymer chains below the melting point in the manner which is reversible up to the point where a critical size is reached. Beyond that point, the subsequent addition of chains is irreversible and growth may be considered to have commenced. The distribution of these regions is random throughout the bulk of polymer and their rate of appearance is usually considered to involve a first-order depending on time.

2) Heterogeneous nucleation arises from adventitious impurities either randomly distributed throughout the bulk or possibly localised on a surface. With this type of nucleation a limited number of growth centres becomes effective instantaneously once the temperature of crystallisation is reached.

3) Self-nucleation cases by polymer crystals which are chemically identical to the crystallising polymer, but have survived the prior dissolution or melting step [39].

1.4.2 Nucleation and Growth

The polarizing microscope has also been much used to study the growth rates of spherulites. The extent over which growth rate can be measured depends on spherulite size and this in turn depends on the relation between nucleation rate and growth rate [40]. In simple terms, if nucleation is slow and growth fast by comparison, a few large spherulites will result. Conversely, rapid and considerable nucleation will lead to profusion of spherulites which may well be immature. Polyethylene often behaves in this way resulting in a texture of very many small embryos which may be barely recognisable as such.

Figure 1.9 shows that the quantity is remarkably linear with time at a given temperature, except when spherulites near impingement or when the viscosity of the melt is deliberately reduced. This is a crucial aspect in the spherulitic growth.

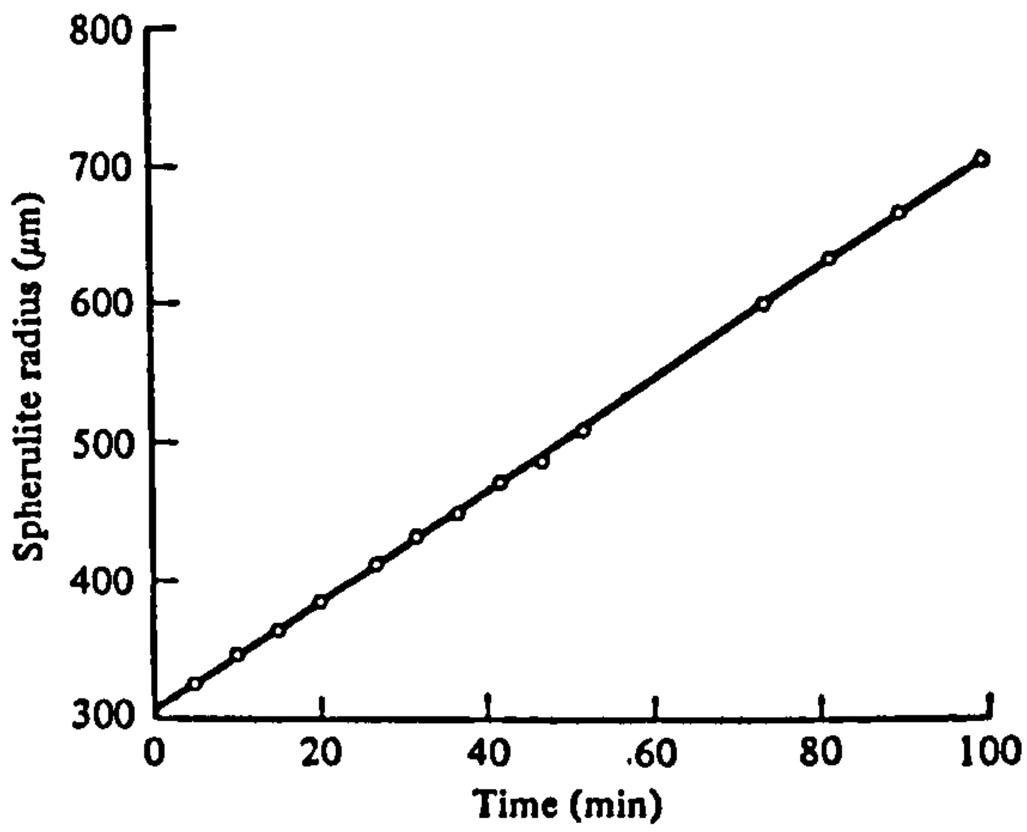

Figure 1.9 Linear isothermal radial growth rate of a spherulite growing from a blend of 20% isotactic and 80% atactic polypropylene [41]

The variation with crystallisation is shown in Figure 1.10. It has been recognized, however, that the characteristic shape is a consequence of growth being slowed by increasing viscosity at lower temperatures and by diminishing thermodynamic drive as the melting point is approached. For polyethylene, growth is so fast that only the higher end of this curve can be realised while for other polymers such as isotactic

polypropylene and isotactic polystyrene the whole range can be measured.

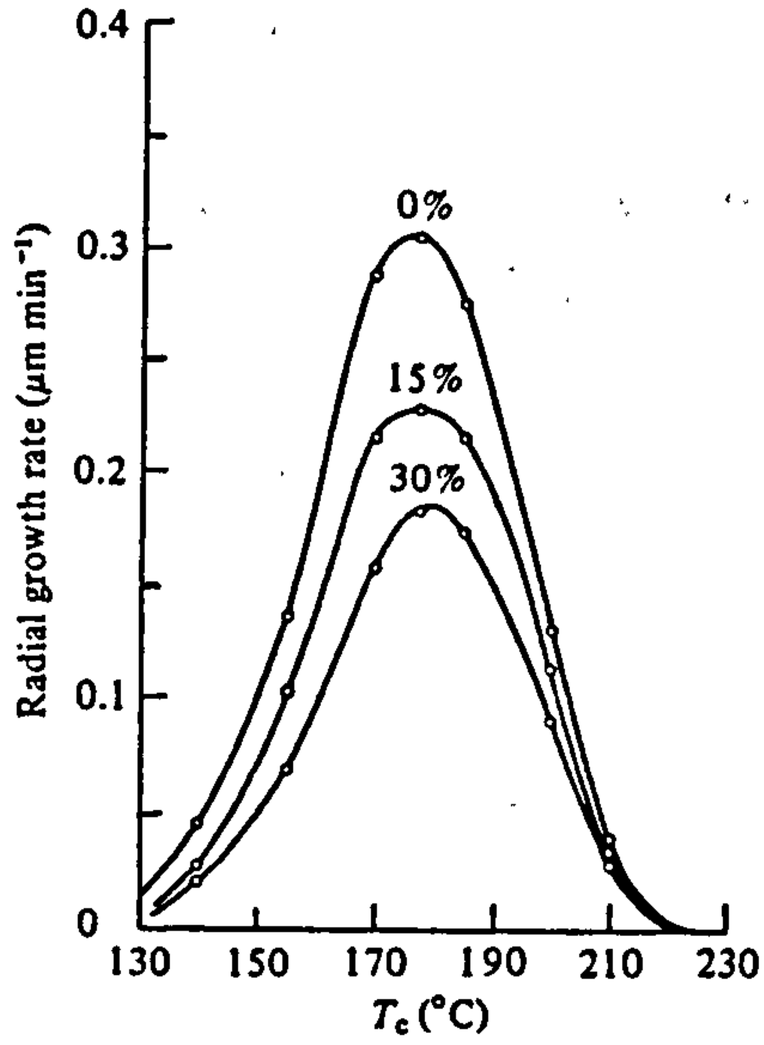

Figure 1.10 Variation of radial growth rates with crystallisation temperature in isotactic polystyrene and blends containing 15% and 30% of atactic polymer [41]

It is possible to control the spherulite size. Because the nucleation in polymers is almost always heterogeneous in origin, i.e. it is initiated on non-polymeric particles. Were it homogeneous, forming on the polymer itself, many fewer possibilities would present themselves. That nucleation is generally heterogeneous is demonstrable in two ways. Firstly, if a polymer is melted and recrystallised then spherulites will often reappear at their original sites. It is usually supposed that this is due to nucleation in cracks of, i.e., foreign particles. It is necessary to hold the polymer for considerable times at temperatures well above its melting point if the melt is taken to successively higher temperatures before recrystallisation. A second experiment of considerable importance is the droplet experiment whereby a sample is dispersed into separate microspheres say 20 μm in diameter prior to crystallisation. The explanation is that the few heterogeneous nuclei have been isolated in their own droplets and rendered impotent so far as the remainder of the sample is concerned, which subsequently crystallises homogeneously. In a bulk sample, however, once heterogeneous nucleation has started growth will proceed through the entire sample. This is the basis for adding heterogeneity deliberately to samples to control spherulite size and development.

No matter whether nucleation is heterogeneous or homogeneous it is still strongly affected by molecular weight, with longer molecules usually initiating crystallisation of the polymer. Presumably this is because the longer a molecule is, the greater the chance of being able to adopt a suitable conformation. The loss of the longer molecules and also the creation of additional very short ones, both help to grow fewer and more open spherulitic structures. There is a wide range of techniques to study the nucleation and growth rates for polypropylene, such as: optical microscopy, mechanical testing, x-ray diffraction and electron microscopy.

1.4.3 Crystallisation

It is well known that polymer molecules can be crystallised, and this depends on the type of polymer and its molecular microstructure. The difference between crystalline polymers and most other crystalline solids is that they are normally only semicrystalline. This is indicated from the density of the crystalline polymers which is normally between the expected fully crystalline polymer and the amorphous polymer. Crystallinity generally means three-dimensional molecular level structural order. Crystals are described in terms of three-dimensional lattice systems. Beginning with the highest level of crystalline symmetry and decreasing to lower levels of symmetry, one has cubic, hexagonal, orhombic, tetragonal, orthorhombic, monoclinic and triclinic. Metals largely crystallise into lattices with high levels of symmetry such as cubic. Polymers usually crystallse into lattice systems with lower symmetrys such as orthorhombic, monoclinic and triclinic. The degree of crystallinity and the size and the arrangement of the crystallites of the semicrystalline polymer determine the physical and mechanical properties of the polymer materials.

General requirements for the crystallizability of polymer molecules are geometrical regularity of the molecular structure (high degree of activity), a sufficient packing efficiency of the polymer chains and sufficiently favourable conditions for the kinetics of crystallisation [42]. Even under the most favourable conditions polymers will never achieve full crystallinity because of chain entanglements, structural imperfections and insufficient rate of crystallisation.

The physical properties of a polymer are determined by its structure, particularly in the case of crystalline polymers. Polymer molecules with a particular molecular

structure aggregate to form crystals, and in turn aggregate to form spherulites. The manner of aggregation of molecules determines the crystal structure. The aggregation of crystals produces the morphological structure (spherulitic or single crystal). X-ray methods are the most important tools in elucidating property structure relations.

The relationship of fabrication or processing conditions to structural order in polymer systems is of great importance. Polymer products including fibers, films and moulded articles play an increasingly important role in commerce. The performance of these products is determined by the character of their structural order. In homogeneous polymers such structural order includes: (1) orientation of polymer chains, (2) existence of crystalline order and its nature, (3) superstructure voids and cracks. In heterogeneous systems such as block copolymers, rubber modified plastics and blends one must also specify phase size, shape and distribution [43].

A major characteristic of the crystallisation of polymers is the strong dependence of the rate of cooling on the crystallisation temperature. The nucleation density of a pure polymer is affected by cooling rate, slow cooling producing a lower nucleation density than quenching. The numerical values for crystallinity in isotactic polypropylene will always have to be below that for tacticity inasmuch as tacticity is a necessary but not a sufficient prerequisite for crystallisation. Numerical values for the degree of crystallinity will, of course also depend on the conditions of crystallisation and after thermal treatment [44], on the molecular weight and molecular weight distribution of any particular sample.

Crystalline polypropylene may occur in two different morphological forms: crystallisation from very dilute solutions leads to the formation of lamellar crystals whereas crystallisation from the melt leads to the formation of spherulites. The orientation of polypropylene molecules in these structures has produced the concept of chain folding which is particularly in the field of polyolefins. Two crystalline forms: α(monoclinic) and ß (hexagonal)are present in commercially available materials with α as the predominant form [45, 46]. The spherulites of different types depend on the rate of cooling and the level of stress and pressure during crystallisation [29, 47-49].

1.4.4 Polymer Modification

The need for polymer modification is due to the inherent limitations of the properties of the original materials. The modifications are an attempt to overcome these limitations by providing for the improvement of properties, e.g. the flexural modulus of plastics materials is an order of magnitude less than that of traditional high stiffness engineering and construction materials.

After incorporating the fillers of the other materials in the original materials, the properties required may be achieved. The fillers include fibrous fillers such carbon fibre [50], inorganic fillers such as talc [51], flame retardants [52], polymeric and rubber fillers such as ABS [53], EPR [54], or etc. The use of adding glass fibres to plastic materials is the most common applications to significant improvement of performance of engineering thermoplastics. Glass reinforcement increases the properties of rigidity, tensile strength, creep and heat resistance, fatigue strength, environmental stress, cracking resistance and chemical resistance [55, 56].

On the other hand, employment of a nucleating agent at a given set of processing conditions enables a degree of control over percentage crystallinity, spherulite size and the rate of crystallisation. Nucleating agents in the presence of composition increase the crystallisation rate that decrease the cycle time and influence the mechanical properties of semicrystalline polymers [57]. Polypropylene crystallisation begins at crystallisation sites. Nucleating agents increase the number of crystallisation sites in a polymer, resulting in an increase in the overall crystallisation rate and a decrease in the spherulite size [58]. Recently, Smith et al. have synthesised and tested 15 compounds as nucleating agents for polypropylene. They found trinaphylidene sorbitol, tri-(4-methy-1-naphylidene) sorbitol, tri-(4-methoxy-1-naphylidene) sorbitol, and dibenzylidene xylitol are efficient nucleating agents of polypropylene [59]. Nucleating agents increase the impact strength, tensile strength, tensile elasticity modulus and clarity of semicrystalline polypropylene.

1.5 Polymer Processing

The general aim of polymer processing is to transform a resin , originally in the form of random particles, into a commercial product of predetermined shape and dimensions. Processing includes all those steps through which a polymer resin goes between polymerisation and fabrication into plastic articles. These products are produced by a wide variety of polymer processing techniques depending on the shaping operations. The principle processing methods used for polymer fabrications include injection moulding, extrusion and blow moulding.

1.5.1 Processing Methods

Extrusion is by far the most important processing method for polyolefins [60]. Extrusion serves to melt and homogenize the polymer and to deliver a constant rate of flow at constant pressure to the die. Extrusion processes led to articles including pipes, rods, profiles, wire coating, sheets films, filaments and fibres, etc.

The blow moulding process is mainly used for the manufacture of bottles, containers and other hollow articles [61]. The equipment includes a conventional extruding machine and the blow moulding set-up. The process is as follows: a molten tub of polymer is formed from a heavy walled tube from a downward directed extruding machine die; the air can be blown through the die, or through the mould base, or through an inserted needle.

Other processing methods which are to be mentioned only include thermoforming [62] and Plasmas [63], lamination [64], plastic coating [65], foaming [66], heat sealing of films [67], etc.

1.5.2 Injection Moulding

Injection moulding is one of the most widely employed methods for fabricating polymer articles, being characterised by high production rates and accurately dimensiones of products. Accordingly, during the injection moulding process the polymer undergoes simultaneous mechanical and thermal influences while in the fluid, rubbery and glassy states [68, 69]. There are many factors that effect the

process——melting temperature, temperature profile, injection velocity in the cylinder, mould temperature and melt flowing patterns. Plastic materials have different heat histories, molecular weights, molecular weight distributions, degrees of polymerisation and impurities. In processing, the material is heated by convection, conduction and shearing. The heat content of the plastic changes as it moves through the cylinder and mould.

The general fabrication operation in injection moulding concerns first melting the raw polymer material, then injecting the melt into a cold mould under pressure (injection pressure) and finally cooling and solidifying to obtain the polymer articles of the desired shape and of other required physical characteristics [70]. The plastic is compressible, stretchable, elastic and subject to changing properties after removal from the mould. It changes its dimensions and properties after processing, and these properties may differ depending on the direction of the material flow in the mould.

The engineering aspects of injection moulding operation and process flow mechanics have so far been given a lot of attention [71-73]. This is of great importance to maximising production rate and to controlling part strength and appearance characteristics. Conventional injection moulding, however, has many disadvantages. One of the main setbacks is the dependence on the compressibility of polymer melt in the mould cavity. Thus, there is still a need to improve mouldability characteristics and mould design.

Advances have often resulted from the introduction of new techniques and, to that extent, the history of the subject parallels that of corresponding technical advance. During the last decade, new techniques for injection moulding were developed which have brought about considerable benefits to plastics industry. The shear controlled orientation technology (SCORTEC) was among the newly developed techniques. SCORTEC is two related technologies, shear controlled orientation injection moulding (SCORIM) and shear controlled orientation extrusion (SCOREX), developed at Wolfson Centre in Brunel University. SCORIM has firstly been widely promoted under the name "Multiple Live-Feed Moulding" (MLFM) [74]. The main principle of shear controlled orientation technology is to influence the microstructure of a solidifying polymer melt by a controlled macroscopic shearing action of the said melt. When the processes are applied to materials which possess alignable constituents, the orientation of these elements can be effectively

managed by the macroscopic shearing of the solidifying melt. The process is completed when the desired orientation is 'locked in' by the controlled solidification of the polymer matrix [75].

The MLFM device can be fitted between the mould cavity and the nozzle of the injection machine. This device divides the feed and carries a piston in each of the channels to the mould. The pistons, activated by auxiliary hydraulics, provide the additional packing pressures, the frequency and amplitude of their movement during the fill and hold stages of the cycle being controlled by a micro-processor.

The conventional injection moulding technique supplies the molten moulding material to a cavity through an entrance which may subsequently be divided into a number of runners to various gating points within the cavity. The pressure to all these gating points is, however, supplied by the single feed point. The MLFM technique differs from the conventional injection moulding is for the single feed (as in the case of conventional injection moulding) from the injection moulder to be split into a plurality of feeds to supply the oscillating pressure method [76-79]. Each one of these multiple feeds is capable of supplying pressure to the mould cavity independently both of each other and of the injection pressure, keeping the material in the gates molten or 'live' when the mould is filled and packed. The solidifying melt can also be subjected to shear, to oscillating packing pressures or to static packing pressures. As a consequence, the limitations of the conventional mould packing techniques described in the publications such as dependence on the compressibility of the polymer melt in the cavity can be overcome [80].

SCORIM provides for elimination of mechanical discontinuities which result from the initial mould filling process, including voids, cracks, sink-marks and weld-line defects. This technique can also achieve shearing control and reproducibility of the dimensions of mouldings and reduce quality assurance problems, particularly in thick sectioned products and full advantage can be taken of the physical properties of the raw material polymers [81], whether thermoplastic, liquid crystal or thermoset. More importantly, the process also allows short fibres in reinforced mouldings to be oriented as required either uni-directionally or in laminated structures [82]. This technique also results in enhancement of strength and stiffness, moulding to closer tolerances and controlling of thermal expansion.

1.5.3 Development of Microstructural Studies in Polymer Processing

In polymer processing operations, molten polymers emerge from dies into a stress field which deforms the melt into a final article of fabricated shape. The properties of the fabricated parts are determined in crystalline polymers by the micromorphology and orientation which are in turn related to the processing history and the crystallisation process.

Ziabicki and Kedzierska studied the melt spinning process, and used birefringence as a measure of molecular orientation under various spinning conditions [83, 84]. After then, a number of works were reported quantitative details regarding the effects of melt spinning and drawing variables on the nature of the crystallinity and molecular orientation and, in turn, their influence on the mechanical properties [85-87]. Also, Dees and Spruiell proposed a detailed model of the morphology developed in melt spun linear filaments based on the 'row structure' concepts of Keller et al. [88, 89].

Spruiell and White have pointed out that an integral part of the problem during melt spinning is the interaction of rheology factors (stretching of the melt), heat transfer from the running threadline, and the crystallisation kinetics of the polymer [90].

Katayama et al. obtained x-ray patterns, and measured temperature, birefringence and diameter profiles on running spin lines of polyethylene, polypropylene and polybutene-1 [91]. They appear to be the first to have demonstrated that crystallisation kinetics may be greatly enhanced during melt spinning, as compared to quiescent conditions, due to the molecular orientation caused by the stretching and cooling of the melt. Furthermore, Nadkarni and Schultz have studied the crystallisation induced by elongational flow during the melt spinning of polyethylene and employed a variety of techniques such as wide-angle x-ray scattering, density, scanning electron microscopy and differential scanning calorimetry to characterise the microstructure of the as-spun fibres. They also attempted to correlate physical properties and structural features of the spun fibre samples with processing variables [92].

Many studies have been made to evaluate the influence of extrusion conditions on the physical, mechanical and morphological properties of the ultra-drawn fibres [93, 94]. In particular, Porter et al. have assessed the properties of the resulting fibres by a variety of techniques such as density, birefringence, thermal expansion, differential scanning calorimetry, small- and wide-angle x-ray scattering, tensile modulus, strength and recovery [95]. Orientation distributions in blow moulded polystyrene bottles have been investigated by White and Agarwal using birefringence [96]. Biaxial orientation factors were determined as a function of position along the length of the bottle. The orientation was found to be low end primarily in the transverse direction.

On the other hand, there have been relatively few similar studies on polymer processing operations other than melt spinning. Most of the studies have concentrated on the crystalline character of the films, including in many cases careful quantitative evaluations of the crystalline orientation [97, 98]. Maddams and Preedy and later by White et al. appear to be the most important studies of the development of crystalline orientation and morphology of polyethylene film to date [99, 100].

In the area of thermoplastic injection moulding, much of the effort has been directed to the modelling of the process, in order to throw some light on the thermo-mechanical history of the material during processing [101, 71]. Other work has concentrated on the study of the morphology and orientation in injection moulded parts [102, 103]. Earlier work has concentrated on the measurement of internal stresses in thermoplastic mouldings mainly by means of polarizing optics such as birefringence [104], analysis of x-ray scattering [105] and directly by measuring thermal shrinkage and by determination of mechanical anisotropy [106].

Menges and Wubken have studied orientation in polystyrene mouldings by means of heat shrinkage measurements [107]. They have concluded that the flow direction is the main direction of orientation in plane-shaped mouldings and that maximum orientation is observed at the surface, while minimum orientation is observed at the centre of the mouldings. Furthermore, increasing the melt and cavity wall temperatures tends to reduce the frozen-in orientation, while increasing the injection rate tends to marginally increase the orientation at the surface but significantly reduces the internal orientation. Similar results have been reported by Bakerdjian

and Kamal on the basis of birefringence measurements in polystyrene mouldings [108]. The latter workers have observed a more complex behaviour of the orientation distributions in conjunction with polyethylene mouldings. They have attributed the complexity of polyethylene to the interaction between orientation and crystallisation phenomena.

Fleissner and Paschke have studied the influence of melt temperature on the development of orientation as measured by birefringence and heat shrinkage measurements, and its effect on the mechanical properties of thin-walled (1mm) injection mouldings of high density polyethylene [109]. They attributed the differences in mechanical properties to the lower orientation at higher melt temperatures, and to the molecular weight differences between the high-flow and low-flow materials. They have found that for high-flow materials, increasing the melt temperature in the range 140°C to 340°C tends to decrease the notched impact strength, while for low-flow materials, the notched impact strength tends to increase as the melt temperature is increased. Furthermore, the tensile yield stress is observed to decrease as the melt temperature is increased, due to the lower orientation. The elongation at yield tends to increase for high-flow materials but decreases for low-flow materials.

A number of works have been reported on the development of morphology in the injection moulding process and its influence on the ultimate properties of the moulded parts. Clark and Boehme have studied the structure development in injection moulded acetal homopolymer and its influence on the mechanical properties of the moulded part under different moulding conditions [110]. They observed by optical microscopy that the microstructure of injection mouldings consists of a composite of different morphologies forming a laminate structure. Three types of morphology occur: a skin of high molecular orientation, a less highly oriented intermediate 'transcrystalline layer', and a spherulitic core. Clark points out that the skin represents that portion of the melt crystallising during the filling period with a structure interpreted as an overgrowth of fold-chain lamellae on fibre nuclei similar to the well-known "Shish Kebab" from stirred solutions, expect for the less extended chain nature of the fibril domains. The transcrystalline and spherulitic regions result from crystallisation under low melt stress. Furthermore, the variation in skin thickness in a moulding is due to the expected decreases of melt velocity with distance from the gate and its corresponding influence on the creation of fibre

nuclei. Boehme has observed that the thicknesses of the three developing zones are influenced both by the moulding procedure and the mould temperature, which in turn, modifies the mechanical properties and the dimensional stability of the moulded part [111].

Kamal et al. have studied the morphological zones and orientation in injection moulded polyethylene [112]. A variety of experimental techniques have been employed, including polarized light microscopy, infrared measurements, density and differential scanning calorimetry, with the aim of elucidating the orientation and morphological effects in polyethylene injection moulding. They concluded that the properties of injection moulded plastics parts are affected by resin properties, moulding geometry and moulding conditions. Kamal and Moy have employed sonic modulus and wide-angle x-ray diffraction measurements together with the above mentioned techniques to estimate the distribution of tensile moduli in injection moulded polyethylene [113].

Woebcken and Heise used the x-ray diffraction technique to relate crystallite orientation in polyethylene injection mouldings to mechanical properties and processing conditions [114]. They observed significant interactions between microscopic structure, on the one hand, and both processing conditions and the properties of the moulded articles, on the other hand.

In view of the above, the morphology and orientation and their distributions in plastics parts reflect the thermo-mechanical history of the resin resulting from the interactions between the resin and the process which incorporates the effects of equipment and processing conditions. In turn, the microstructure, as reflected by morphology and orientation and their distributions, plays a major role in influencing the ultimate properties of plastics articles.

1.6 Summary

Polypropylene, as a semicrystalline polymer, represents a class of materials in which morphology and mechanical properties are strongly influenced by processing conditions and resin characteristics. The study of relationships between micromorphology and mechanical properties of semicrystalline polypropylene is

very important for understanding what the morphological texture is, how it formed, how it can be controlled and modified to give improved properties if possible. The spherulite size depends on the relation between nucleation rate and growth rate. The degree of crystallinity and the size and the arrangement of the crystallites of the semicrystalline polymer determine the physical and mechanical properties of the polymer materials.

Injection moulding is the most commonly used processing method to produce a broad range of intricately shaped plastics end-products. In order to produce final plastic parts with required physical characteristics, it is important to control and manipulate the processing procedure. The SCORIM technique can provide for better management of the microstructure and control of microporosity in injection mouldings and, consequently, improvement in the optimisation of the physical properties of the moulded parts.

CHAPTER 2
MATERIALS AND EXPERIMENTAL TECHNIQUES

2.1 Materials

2.1.1 Polypropylene

A commercial isotactic polypropylene homopolymer manufactured by I.C.I. as Propathene GYM43, was used throughout the investigation. It is a general purpose, injection moulding grade with a melt flow index 10.5 g/10mins at 230°C according to ASTM D1238. Physical property data relating to the GYM43 homopolymer is given below:

Property	Test Method	Unit	GYM43 PP
Melt flow index (MFI)	230°C/2.16 kg	g/10 mins	10.5
Density (mean)		kg/m³	905
Tensile yield stress	ISO 527	MPa	34.5
	ASTM D638M (50mm/min)	kg/cm²	350
Flexural modulus	ISO 178 (2mm/min)	GPa	1.50
	ASTM D790M	kg/cm²	15300
Izod impact strength	ISO 180 (0.25mm notch radius)	kJ/m²	23°C 4.0
			0°C 2.5
			-20°C 2.0
			-40°C -
Embrittlement temperature	ICI method	°C	>23
Rockwell hardness	ISO 2039/2, ASTM D785	R scale	95
Vicat softening temperature (10 N force)	ISO 306A BS 2782:120A	°C	154
Heat distortion temperature	ISO 75/A and /B		
A-1.8 MPa (18.6 kg/cm²)	ASTM D648-A and B	°C	65
B-0.45 MPa (4.6 kg/cm²)		°C	100

2.1.2 Nucleating Agents for Polypropylene

Two different nucleating agents were chosen in the study of the effects of low percentage of nucleating agents on the modification of morphology and mechanical properties of polypropylene.

(1) Geniset DP 60/1 Nucleating Agent

The Geniset product was supplied by Schering Polymer Additives Group (Polymer Additives Group, Schering Industrial Chemicals, Gorsey Lane, Widnes, Cheshire), containing a controlled mixture of isomers of dimethylbenzylidene sorbitol (MDBS). The recommended processing temperature range was from 220° to 240°. The nucleating agent used is in granular form (Geniset DP 60/1) which was pelletized from a mixture containing 7.5% Geniset MD in a polypropylene homopolymer carrier.

(2) ADK STAB (NA-11) Nucleating Agent

ADK STAB (NA-11) was supplied by Asahi Denka Kogyo K.K. (Furukawa BLDG, 3-14 Nihonbashi-Muromachi 2-chome, Chuo-ku, Tokyo, 103 Japan). Its chemical name is sodium 2,2'-methylene bis-(4,6-di-tert-butyl phenyl) phosphate and its formula is $C_{29}H_{42}O_4PNa$. It is supplied in a white fine powder form. It can upgrade the heat deflection temperature, flexural modulus and impact strength of polymer and is reported to give remarkable transparency at low concentration and to raise the crystallisation temperature.

Data of physical properties of ADK nucleating agent are shown in the following table:

Property	Unit		ADK STAB (NA-11)
Molecular weight			508
Melt point	°C		>400
Volatility	°C	10% weight loss temp.	432
TGA	°C	20% weight loss temp.	434

10°C/min.	°C		30% weight loss temp.	436
under air	°C		40% weight loss temp.	441
	°C		50% weight loss temp.	445
Solubility	g/100g		Water	0.00
	of solv. at 25°C		Methanol	82.7
			Ethanol	9.7
			Acetone	0.02
			Benzene	0.01
			n-Hezane	0.00
			Ethyl acetate	0.02
			Chloroform	0.01
Toxicity	mg/kg	Acute oral LD50, rat >7,800		
			Ames test	Negative
			Skin irritation	Negative
			Eye irritation	Negative

2.1.3 Other Materials and Reagents

2.1.3.1 Chemical Liquids for Etching

1) Orthophosphoric acid, H_3PO_4 (supplied by BDH Ltd., Poole, England). The minimum assay is 85.0% and it is corrosive.

2) Sulphuric acid, H_2SO_4 (supplied by BDH Ltd., Poole, England). The assay is between 97 and 99%. It is a general purpose regent and corrosive. The density is about 1.835g/ml at 20°C.

3) Potassium permanganate, $KMnO_4$ (supplied by BDH Ltd., Poole, England). It is a general purpose regent. It contains 99% minimum $KMnO_4$, 0.02% maximum Chloride and 0.03% maximum of Sulphate (SO_4).

2.1.3.2 Chemical Liquids for Density Measurements

(1) Propan-2-ol (BDH Ltd., Poole, England)
The formula is $(CH_3)_2CHOH$ and the density is 0.789g/ml. The minimum assay is 99.7%. It is highly flammable and can be miscible with water.

(2) Digol (supplied by BDH Ltd., Poole, England)

The formula is $O(CH_2CH_2OH)_2$ and the density is 1.115g/ml. The minimum assay is 99.5%.

2.2 Conventional and SCORIM Injection Moulding Processing

A Sandretto Torino 6GV-50 injection moulding machine was used for the preparation of conventional standard tensile bars (see Figure 2.1) using a two cavity mould. For those injection mouldings, two different melting temperatures and two different injection velocity profiles were used with the constant mould temperature for the production of injection mouldings. The injection velocity control was achieved through a preset velocity profile. The velocity programme was provided by 10 velocity command points for a given shot. The processing conditions are shown in the following table:

Table 2.1 Injection processing conditions of conventional standard tensile bar

Melt temperature (°C)	Mould temperature (°C)	Injection speed (%)
200	30	15
		60
220	30	15
		60

Shear controlled orientation injection moulding technology (SCORIM) provides routes for the management of fibre orientation and microstructure in moulded polymer materials. SCORIM has been formerly promoted under name "multiple live-feed moulding" (MLFM) [74, 80, 82]. The main principle of shear controlled orientation technology is to influence the microstructure of a solidifying polymer melt by a controlled macroscopic shear action of the melt. When the process is applied to materials which possess alignable constituents, the orientation of these elements can be effectively managed by the macroscopic shearing of the solidifying melt. The process is completed when the desired orientation is 'locked in' by the controlled solidification of the polymer matrix [75].

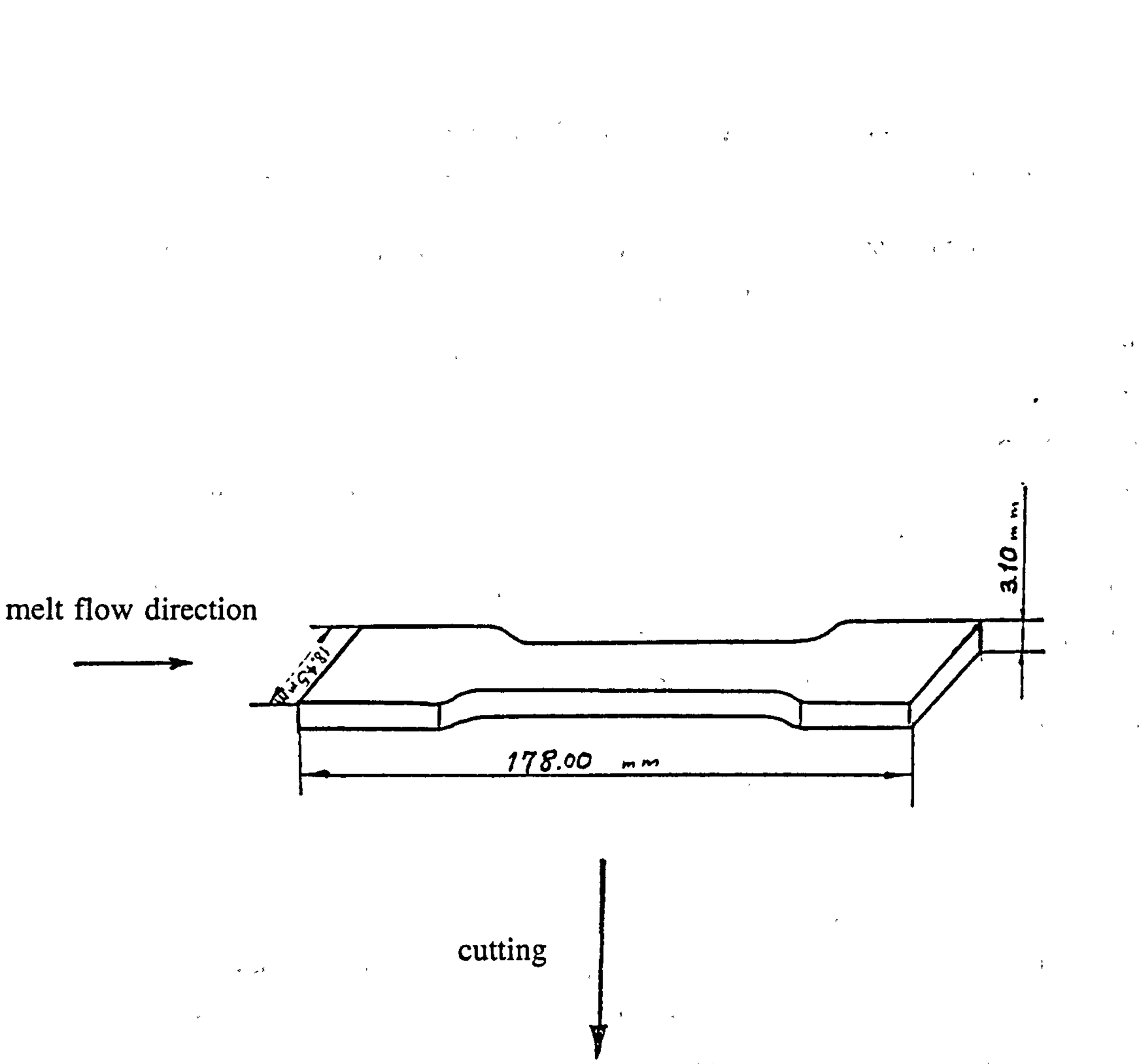

Figure 2.1 Schematic diagram showing the moulding and positions of the sections cut from standard tensile bar by microtomy

The four live-feed arrangement is based on a Negri Bossi NB 130-90/90 twin injection machine to produce conventional and MLFM ring mouldings. The dimension of the screws of Negri Bossi machine is ϕ38mm. The microprocessor control for the four live-feed system was built to specification by Technology Concepts, Cwmbran, South Wales. The Dimigraphic 100 microcomputer is a microprocessor based control system used for the digital control of all operational parameters of the Negri Bossi injection moulding machine, including the visual display of graphs and the process control. The control parameters are grouped according to function and visually represented on 20 pages which can be immediately and easily retrieved at any time. Up to 50 operating stages are possible during the moulding cycle, and these may be selected from the ten stages available for setting conditions in terms of stage duration, frequency of piston movement, compression pressure, decompression pressure and mode of piston operation.

The system controls the temperature of each zone according to the value set. Sixteen zones of temperature control are available. Five speeds can be set as well as the positions at which they start. The possibility to select five different speeds allows an injection profile to maintain a constant material speed during mould filling.

The hold pressure is monitored by a force transducer located behind a pin incorporated in the mould ejection system. The measurement is indirect since the transducer fitted to an ejector pin measures the force that the pressure built up in the cavity transmits through the ejector pin itself. Both the ejector pin and the transducer are fitted to, must have the same cross sectional area for all moulds used so as to keep constant the ratio between cavity pressure and force transmitted.

The cavity pressure chosen is related with the following aspects: mould design; the type of plastic material being used; the moulding physical, mechanical and dimensional features. The cavity pressure is also a function of both the viscosity of the material being moulded and the injection speed, the lower the injection speed or holding pressure, the lower will be to determine the cavity pressure. As a consequence, the pressure value to be set will be different from the pressure value relevant to the plastic material which is desired in the mould.

The arrangement of the MLFM device of four pistons is shown in the Figure 2.2. Four equiangular gates were designed on a ring mould. The dimensions of the ring

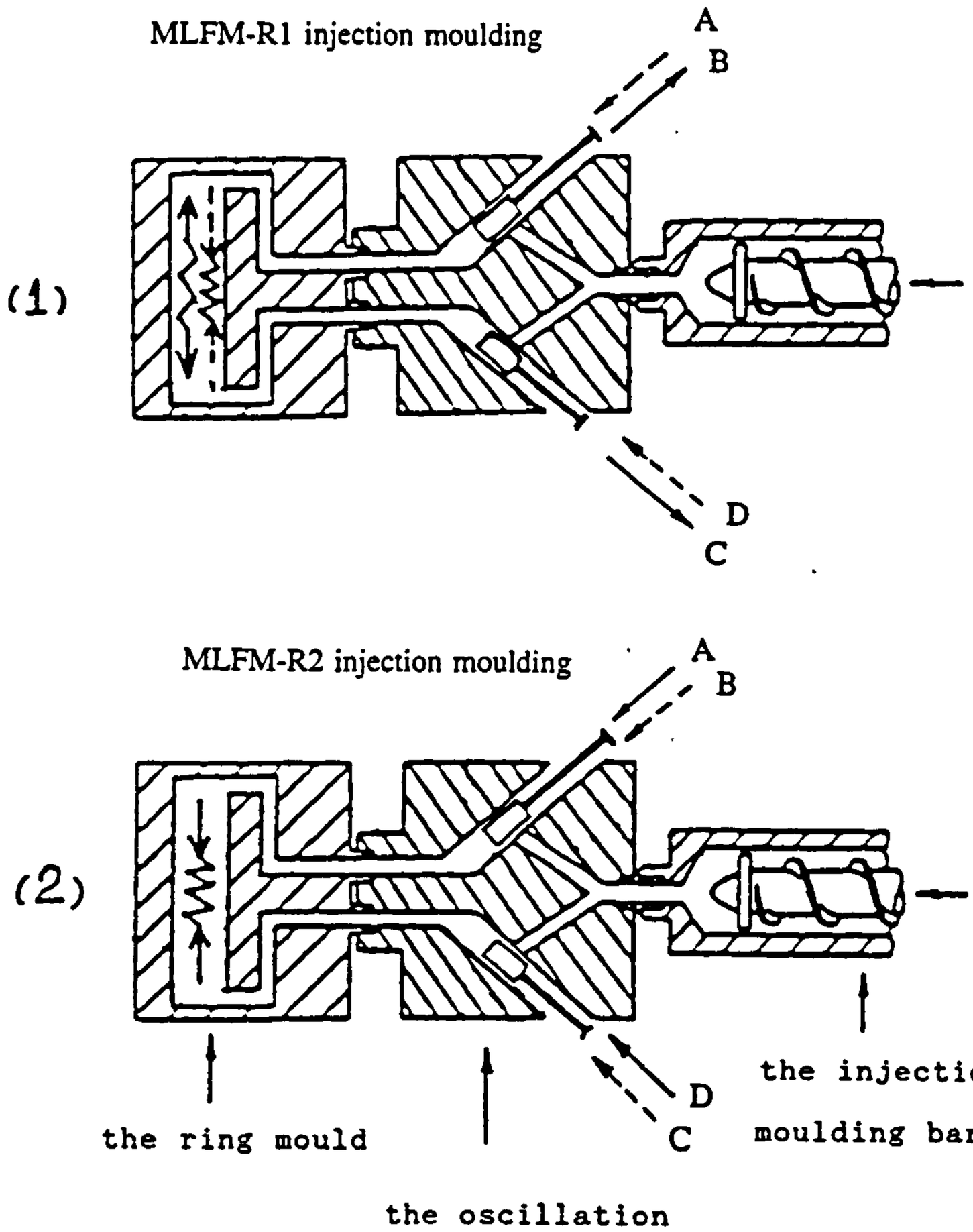

Figure 2.2 Schematic diagram of the modes of operation of the MLFM device (piston B behind piston A, piston D behind piston C)

mould is illustrated by the moulding diagram in Figure 2.3. Each ring sample has four gates and four weld lines. The four-gated moulding packed using the four live-feed arrangement by alternate operation of live feeds A-D and B-C, or simultaneous operation of live feeds A-B-C-D. This erased the internal weld line and provided for the optimum circumferential alignment.

In injection moulded polypropylene plastics, changes in moulding conditions such as melt temperature and injection velocity can greatly influence the microstructure and consequently the physical properties of the end products. Changes in injection moulding technique would also result in moulded polypropylene of different microstructures and thus different physical properties. Three processing programmes were carried out in order to compare the physical properties of the moulded polypropylene for both conventional and MLFM ring mouldings. The processing conditions used are shown in the following table.

Table 2.2 Injection processing conditions of conventional and MLFM ring mouldings

Processing	Conventional	MLFM-R1	MLFM-R2
Nozzle temperature (°C)	190		
Barrel temperature (°C)	190, 180, 170		
Zone (1-5) temperature (°C)	195		
Mould temperature (°C)	37	37	33
Injection speed (%) left barrel right barrel	47 57		
Hold pressure (bar)	34	10	8
Hold pressure time (sec)	80	300	150

A Demag D150 NC III-K injection machine was used to produce conventional and SCORIM rectangular bar mouldings. The injection moulding processes were controlled by a linked computer. The machine is electrohydraulically controlled. The dimension of the screw of Demag machine is ϕ45mm and it is general B type of screw which is applicable for all materials with average viscosity and for mouldings with average wall thicknesses.

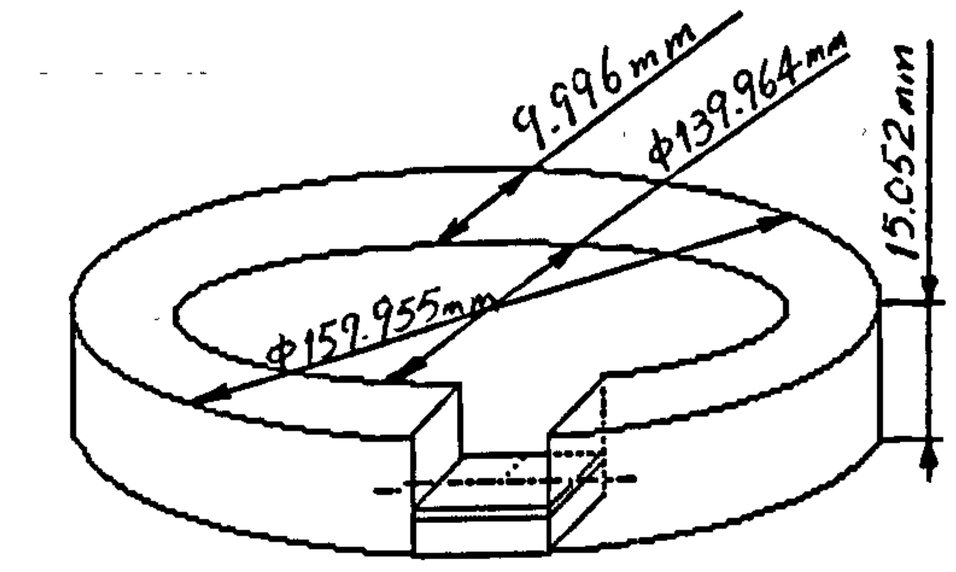

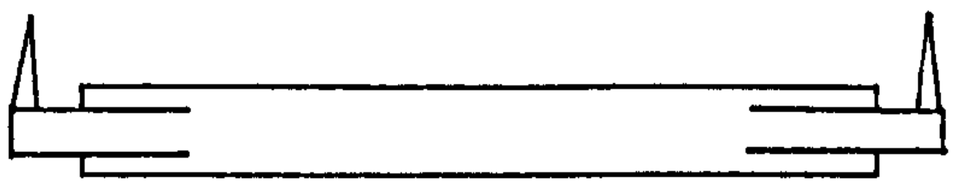

gate A

gate B

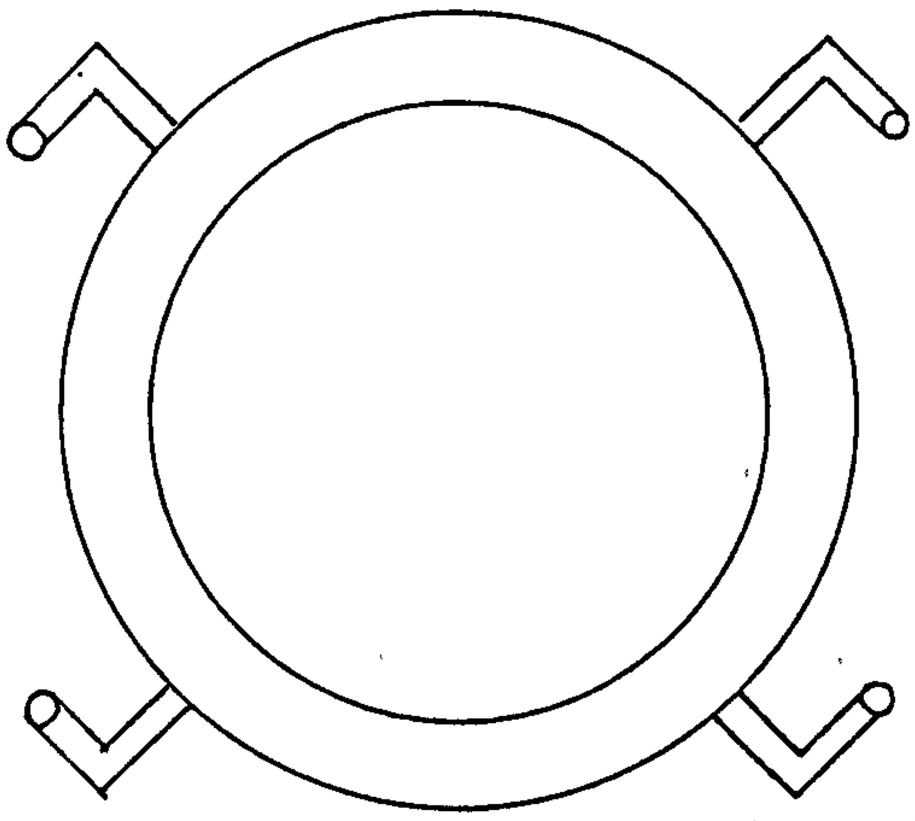

gate C

gate D

Figure 2.3 Schematic diagram showing the section cut from ring moulding for transmitted light microscopy

In general, the choice of the screw cylinder diameter depends on the following factors:

1) volume and material of the moulding;

2) flow property of the melt, very viscous melts require high injection pressure if thin-walled mouldings are to be produced;

3) ratio of flow path/wall thickness within the mould. Thin wall or very long flow paths require high injection pressure;

4) shape of the gate, e.g. pin gates in most cases require a high injection pressure.

The temperature of the screw cylinder feeding zone is controlled by computer. It is set in display temperatures, with plus/minus tolerances. The screw speed selected depends particularly on the material to be processed. The injection sequence, the strokes, pressures and speeds to be chosen depend on the article being moulded and on the mould design, and must therefore be determined by moulding trials. The injection program stages are controlled by a microprocessor which allows to set up to 20 separate stages of mould packing. In addition the stage duration, frequency, compression and decompression pressures can be set for the different packing stages. The compression pressure is applied on the stage which the piston is pumped forth in order to compress the melt in the cavity. The decompression pressure is applied on the stage which the piston is pumped back to relax the melt in the cavity.

The dimensions of the rectangular bar mould cavity can be expressed by a moulding diagram. Figure 2.4 shows the sections of a rectangular bar moulding parallel and perpendicular to the melt flow direction. The twin nozzles of the SCORIM feed the cavity through the two sprues situated at points A and B. Figure 2.5 shows the activation of the two pistons 180° out of phase that causes a macroscopic shear to be applied to the melt solid interface within the mould cavity. The processing conditions employed in the experiments are shown in Table 2.3. Two nozzle temperatures, two mould temperatures and three hold pressures were used to produce the conventional and SCORIM rectangular bar mouldings.

The processing conditions for different injection programmes are shown in Table 2.4. The injection programmes SCORIM-2C was modified to 2CM1 and 2CM2. In the SCORIM-2C program, the oscillating mode *A* was used. In the SCORIM-2CM1 program, the oscillation pattern of pistons was changed to mode *B*. In the SCORIM-2CM2 program, the oscillating mode *C* was applied.

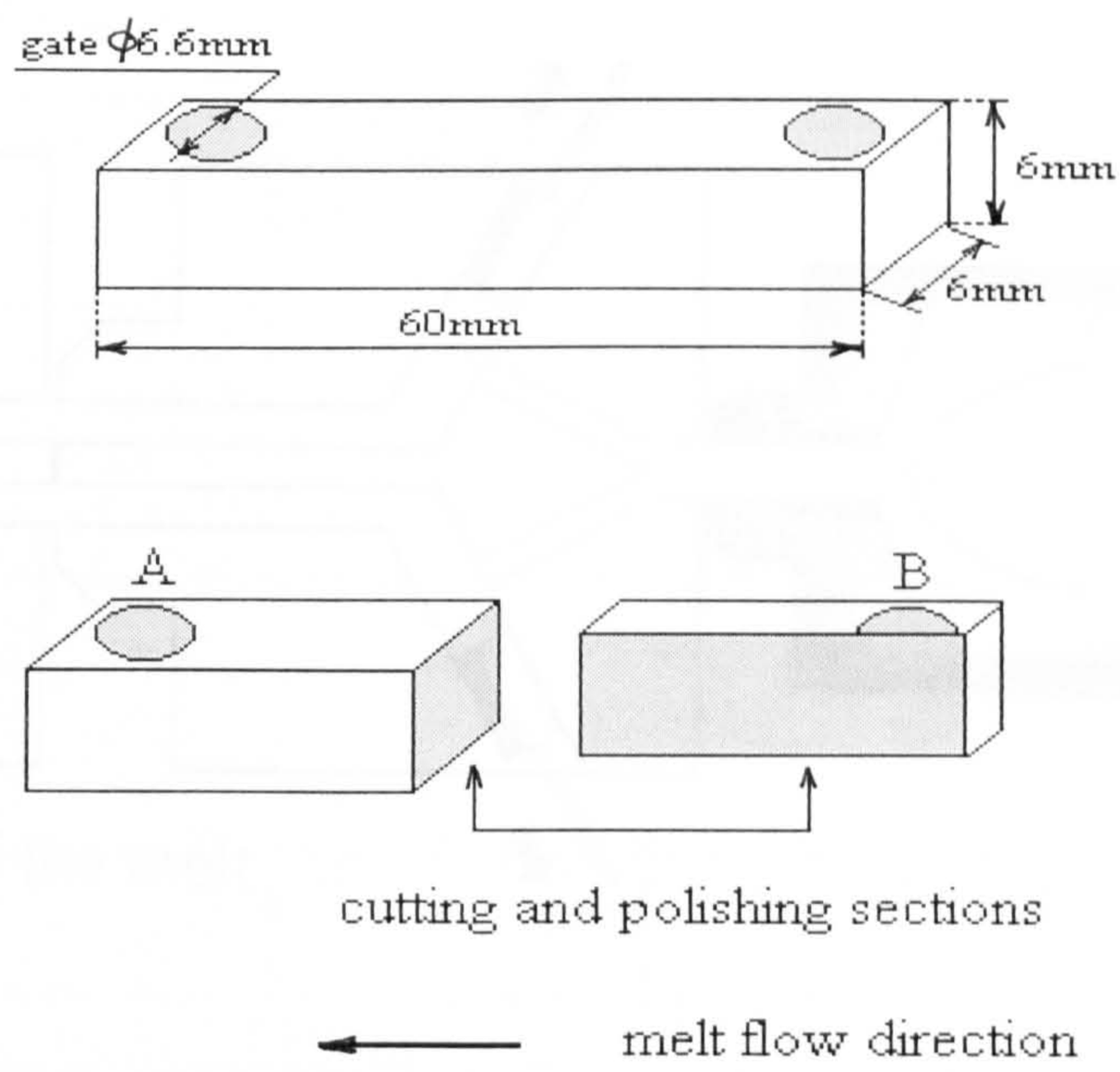

Figure 2.4 Schematic diagram showing the sections cut from rectangular bar moulding for transmitted light microscopy

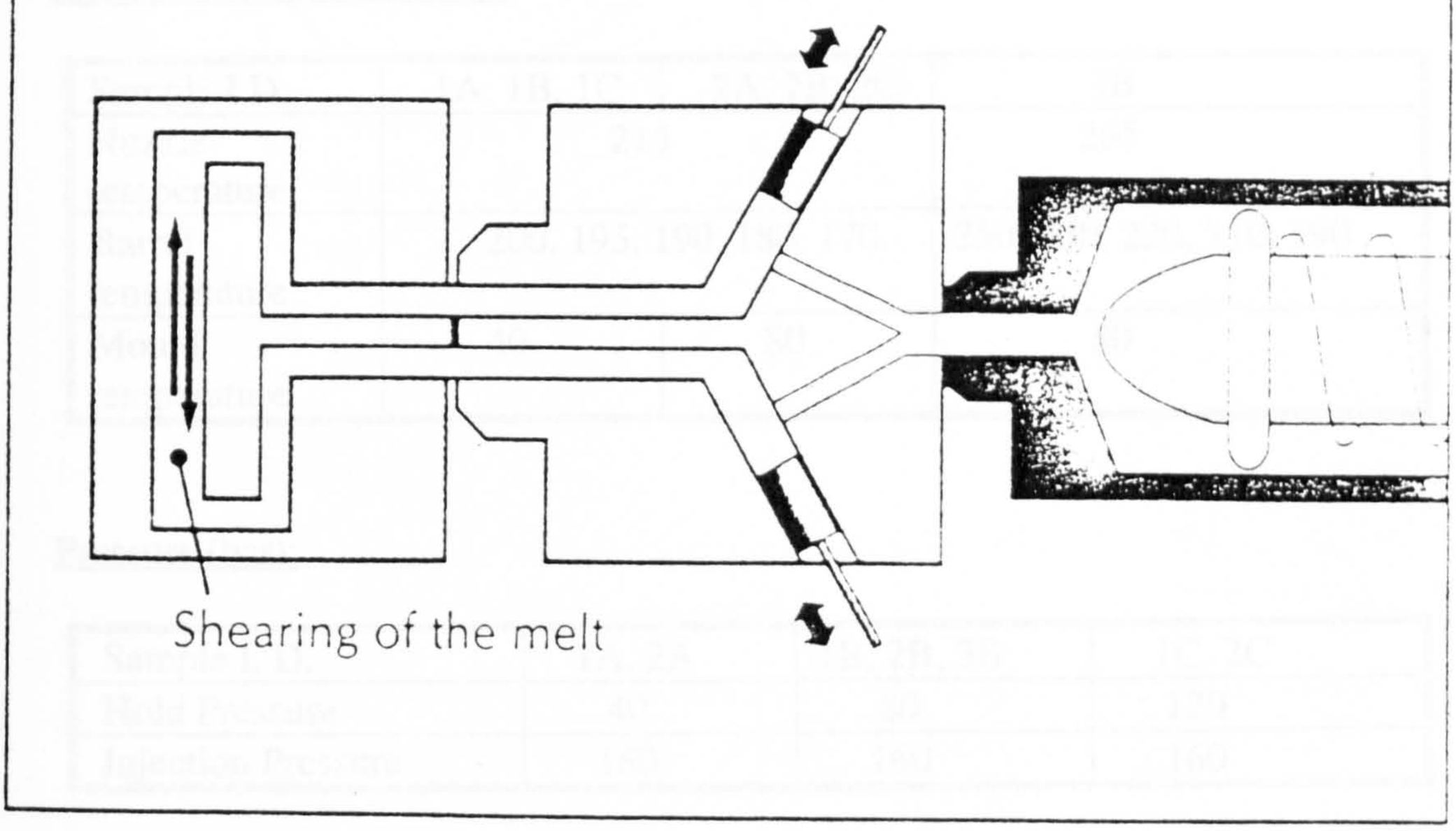

Figure 2.5 Schematic diagram of the mode of operation of the SCORIM device

Table 2.3 Conventional and SCORIM processing conditions for the rectangular bar moulding

Injection Temperature (°C):

Sample I.D.	1A, 1B, 1C	2A, 2B, 2C	3B
Nozzle temperature	215		265
Barrel temperature	200, 195, 190, 180, 170		250, 230, 220, 210, 190
Mould temperature	40	80	80

Pressure (bar):

Sample I. D.	1A, 2A	1B, 2B, 3B	1C, 2C
Hold Pressure	40	80	120
Injection Pressure	160	160	160

Time (sec):

Sample I. D.	1A, 1B, 1C	2A, 2B, 2C	3B
Hold Pressure Time	96.5	96.5	99.5
Cooling Time	20	25	30

Speed (%):

Injection Speed: 100
Plastics Screw Speed: 32
Screw Return After Plastics: 10

Table 2.4 SCORIM processing conditions for the rectangular bar moulding

Injection Temperature (°C):

Nozzle: 215
Barrel: 200, 195, 190, 180, 170
Mould: 80

Pressure (bar):

Hold Pressure: 120
Injection Pressure: 160

Time(sec):

Sample ID No.	SCORIM-2C	SCORIM-2CM1	SCORIM-2CM2
Hold Pressure Time	96.5	106.5	106.5
cooling Time	15	20	15

Speed (%):

Injection Speed: 100
Plastics Screw Speed: 32
Screw Return After Plastics: 10

Stroke: (mm)

Dosing Stop: 14
Start Holding Pressure: 13

Three oscillating modes *A, B, C* are illustrated as follows:

mode *A*: after the cavity had been filled, through both channels, the pistons were moved under different compression and decompression pressure at the same frequency but with a 180 degree phase difference causing the melt to move forth and back. The effect of this oscillating mode is to shear the melt within the mould cavity.

mode *B*: the two pistons were pumped back and forth under different compression and decompression pressure at the same frequency and in phase. The pistons worked as two separate oscillating packing pressure heads. The effect of this oscillating mode is to alternately compress and decompress the melt in the mould cavity.

mode *C*: the two pistons were operated in phase under the same compressing and decompressing pressure at the same frequency to ensure efficient packing of the melt in the mould cavity.

2.3 Microtomy and Light Microscopy

In the investigation of spherulitic morphologies, polarizing light microscopy has been the predominant and most informative tool. The microscopy possesses the overriding advantage of revealing textures and their distribution in direct space. It also allows the view to assess the situation directly, with the considerable gain in information that implies. Microscopy can be used to investigate the nature of the textural elements, i.e. the type of model which can then be used in the interpretation of results produced by other techniques.

There are some shortcomings for microscopy. Microscopy examines only a small part of a specimen at a time, increasingly so the higher the magnification, with the result that the problems of deciding what is a representative morphology and the enlargement of the image, what is usually required is a parameter average over the whole sample. Microscopy can only provide this by statistical sampling procedures whereas other methods may give the result straight away.

The purpose of using optical microscopy is to gain an interpretation of the characteristics. Semicrystalline polymers are complex mixtures of amorphous and crystalline phases. It is generally assumed that their morphology consists of thin crystalline lamellae separated from each other by amorphous layers and connected by tie molecules through the amorphous layers. Crystalline lamellae and amorphous inter-lamellar layers can form spherulites or other types of morphological textures. Spherulites are the basic morphology for polymers crystallised from the melt. They are usually obtained in the processing such as extrusion or injection moulding. The use of optical microscopy techniques provides valuable qualitative and quantitative information on polymer morphology.

The crystallisation procedure of conventional injection moulding of polypropylene leads to three-dimensional spherulites. When such a spherulite is observed by transmission optical microscopy, between crossed polarizers, a Maltes cross occurs along the polarization axes of the polarizers.

Microscopy can be used to observe the spherulitic structure by cutting suitably thin sections of spherulites and exam them. It is very important to cut sections without causing severe distortion. Most polymers are too soft for adequate sectioning at room temperature and sections of the correct thinness are difficult to obtain. The effective method is cooling polymers and make them brittle.

In this study, the specimen temperature was controlled by a Nitrogen cooling system. The cooling equipment consists of a block with two tubs which are filled with liquid nitrogen and surrounds the cutting area. The temperature was chosen by changing the current values. The range of current was from 0 to 20 Å and this range correlated with a temperature range from room temperature to -20°C. For the polypropylene samples, the cooling temperature of the microtome should be lower than their glass transition temperature (Tg=10°C), in order that the sample becomes brittle and a good cutting effect is realised.

This cooling system produced specimens which are hard enough to cut. The knife was moved towards the specimen by means of the coarse knife movement control until it was almost touching the specimen. The specimen edge could be aligned parallel to the knife edge, and the specimen moved past the knife edge with small

movements of the coarse knife control until all of the specimen face was being cut. Then the specimen was moved past the cutting edge and the forces were transferred to the specimen from the cutting edge resulting in a thin layer of material being detached from the surface. Then the specimens were mounted in immersion oil on glass slides and coverslips.

The quality of sections of the specimens used for microscopy is depended on the working conditions of the microtome, such as knife angle, holding stage angle, the cutting thickness of the sample and cutting system. The following aspects are shown the conditions used in this study:

1) The condition of the selected blade was examined by using reflected light microscopy to see the edge of the blade.

2) The blades used were fixed on the angle about 35° to obtain the optimum for the polypropylene sample.

3) The holding stage was parallel to the horizontal-plane.

4) The cutting direction was parallel to the melt flow direction.

5) The cutting speed was controlled manually. If cutting was too fast, the specimen rolled up. If the cutting was too slow, the thickness of the specimen was not uniform. The cutting speed needs to be variable because different materials have different characteristics and the optimum cutting conditions can be obtained by using different cutting speeds.

An Reichert-Jung MicroStar 110 optical microscope fitted with a Nikon M-35 camera, and a Reichert Austria optical microscope with camera in the transmitted light mode, were used for the examination of the microstructures exhibited by the microtome thin sections of injection moulded polypropylene. The magnification of the eye lens used was 10× times and the magnification of objectives were 4×, 10× and 25× times.

2.4 Microhardness Testing

The term hardness can not be precisely defined, as it comprises many characteristics of a plastic. The most commonly quoted hardness values are obtained by indentation testing. The more important characteristics which are studied are:

1) indentation under load and after the release of the load;

2) resistance to abrasion in terms of loss of weight or change in optical properties. The optical properties usually studied are transmission and reflection;
3) scratch resistance.

A Leitz Wetzlar Vickers microhardness indent was used for microhardness measurements. The diagonal lengths of the indentations measured were defined by the applied load. The range of the measuring load for indentations is from 0.49N to 19.61N. Indenting and dwelling time have been set in the factory at about 30 seconds. In the standard Vickers microhardness testing, the indent is a square-based pyramid with angle between opposite faces of 136°. The objectives used were 10× times for scanning and 50× times for measuring. After focusing the eyepiece scale with the eye lens the 50× objective is focused on the indentation with the fine adjustment. The indentation must not be bordered by dark diffraction bands. There is the aiming axis in the eyepiece on the centre of the indentation. In order to obtain measurable indentations, polishing the surface of the sample is often need. Since mechanical polishing may change the surface, the thickness of the layer removed should always be noted. The minimum degree of the polishing cloth used was 1μm.

For polypropylene samples studied, a load of 0.98N was applied for 30 seconds, followed by 3 mins recovery period before measurements of diagonal lengths. The indentations can be produced and measured as follows:

1. Focus on the division of the eyepiece graticule and zero the fine scale.
2. Focus the microscopic image and chose the testing area of the sample for the indentation into the centre of the field of view.
3. Move the testing diamond into the indenting position. Press cable release fully and let it go. The diamond will slowly descend on the object.
4. Rotate the micrometer eyepiece and align one corner of the indentation with the edge of a line of the coarse scale.
5. Zero the fine scale. The scale unit of the fine is 0.5μm. 0.1μm can be estimated.
6. Align the opposite corner of the indentation with the edge of another line of the coarse scale.
7. Read the fine scale. The line intervals of the coarse scale (20μm each) minus the difference between this and the previous reading represents the length of the diagonal. The diagonal lengths of the polypropylene moulding produced in this study were usually smaller than 20μm when the 0.98N load was applied.

8. Turn the micrometer eyepiece through 90° measure the other diagonal of the indentation.

With Vickers indentations obtain the mean of the two diagonals, the following equation (2–1) was used to calculate the Vickers microhardness (HV) in kg/mm²:

$$HV = 1.8544 \cdot \frac{P}{X \cdot Y} \qquad (2\text{–}1)$$

where P is the applied load in kilogram;

X is the length of the indentation diagonal perpendicular to the melt flow direction (mm).

Y is the length of the indentation diagonal parallel to the melt flow direction (mm).

and the isotropy ratio (ΔMH) was calculated by the follow equation (2–2):

$$\Delta MH = [\, 1 - (\frac{X}{Y})^2 \,] \cdot 100\% \qquad (2\text{–}2)$$

2.5 Mechanical Measurement

An Instron tensile testing machine (model 1195) was used to measure Young's modulus and fracture stress of the standard tensile bar mouldings and the ring mouldings. The test conditions used were: crosshead speed 50 mm/min, full scale load 2kN, chart speed 100mm/min and gauge length 70 mm. The equation (2–3) used to calculate the Young's modulus (E) was shown in Appendix 1.

For the determination of tensile stress, strain, modulus and toughness of the conventional and SCORIM rectangular bar mouldings, an Instron tensile testing machine (model 4206) was used. Through an optional IEEE-288 interface, an IBM XT personal computer is interfaced to the Instron 4206. The limit panel provides the ability to set both minimum and maximum limit levels associated with load, extension and strain. Nine load capacities ranging from 10N to 150kN are available for testing. An optional X-Y plotter is used to obtained load/stress *vs.* extension/strain graphs. An optional printer provides permanent records of load,

stress, extension, strain, modulus, energy and preset points values after each testing.

The crosshead speed applied accorded to the ASTM D638-80 depending the shape of the samples. All measurements were taken on a gauge length of 10mm by using an extensometer except the measuring of the breaking stress. Elastic modulus values were based on tests made at a strain rate of 1mm/min and fracture stress at a strain rate of 50mm/min. The tensile modulus results of the iPP injection mouldings are presented and represent an average of 4 or more samples for each processing condition.

The tensile testing results are usually expressed in terms of a stress-strain diagram which differs from material to material. The typical stress-strain diagram for a plastic under tensile testing is shown as follow:

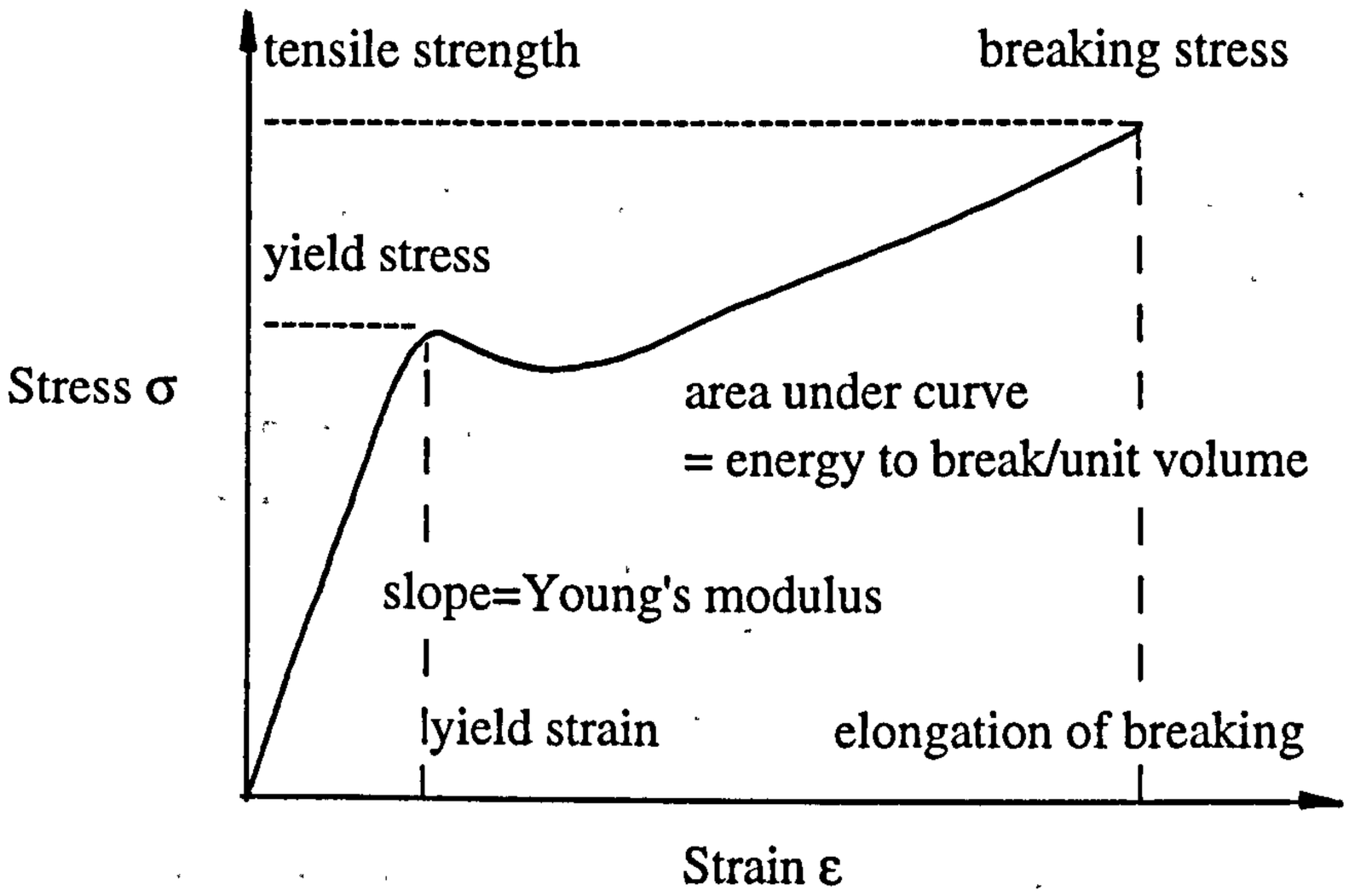

Six parameters can be obtained from such a diagram. These are:

1) Young's modulus of elasticity. This is the ratio of stress to strain in the elastic region in which Hooke's law holds, either closely or approximately. It is the slope of the initial steep portion of the curve;

$$\text{Young's modulus } E = \frac{\sigma}{\varepsilon} \qquad (2\text{–}4)$$

where σ and ε are the stress and strain values at yield point or end of the curve.

2) breaking stress. This is the maximum tensile strength the material can stand

without breaking;

3) elongation at breaking. This is always quoted as a percentage of the original length;

4) yield stress. This is the stress at which the first sign of non-elastic deformation occurs;

5) yield strain. This is the strain corresponding to the yield stress;

6) energy to break per unit volume. This is the area under the graph, and give a rough measure of the toughness of the material.

2.6 X-ray Diffraction and Debye Flat Plate Techniques

The x-ray diffraction method relates the intensity of the main crystalline peaks, to that of the amorphous halo. X-ray diffraction scans were obtained with Cu-Ka radiation with a Phillips PW1050 x-ray diffractometer, which was controlled by Phillips PW1710 microprocessor and Sietronics Sirray112 software (as see in Figure 2.6). The PW1710 is a microprocessor-based control and measuring system and full automation of x-ray powder diffractometer. The PW1710 electronics provided precise programmed control of goniometer stepping motor drives with step sizes down to $2\theta=0.005°$. Equipping the PW1710 with an optional dual serial RS232 C/V24 interface enable to company with wide range of peripherals. An anti-backlash loop ensured that the target angle is always approached from the same direction, regardless of whether the initial movement is up or down. The scan angle used in the study was from 8° to 32°, and the wavelength was 1.5418 Å. The x-ray tube is copper target using a Nickel filter.

A crystalline substance may be defined as a homogeneous solid having three dimensional regularity and plane bounding faces. Once the crystallographic axes are chosen, a parametric plane may be defined and any other plane described in terms of three indices h, k and l [115]. The indices h, k and l are expressed by the ratios of the intercepts of the parametric plane made on the corresponding axis. A zero value for h, k or l indices its intercept is at infinity; a negative value for h, k or l indices an intercept on the negative side of the reference axis. This notation for describing the faces of a crystal was introduced first by Miller in 1839, and h, k and l are called Miller indices. The following table shows the chosen Miller indices according to the main experimental peaks:

h.k.l.	Peak (degree)	2θ
110	α_1	14.1
300	$ß_1$	16.1
040	α_2	16.9
130	α_3	18.5
111	α_4	21.3
131	α_4	21.8
041	α_4	21.9
060	α_5	25.5

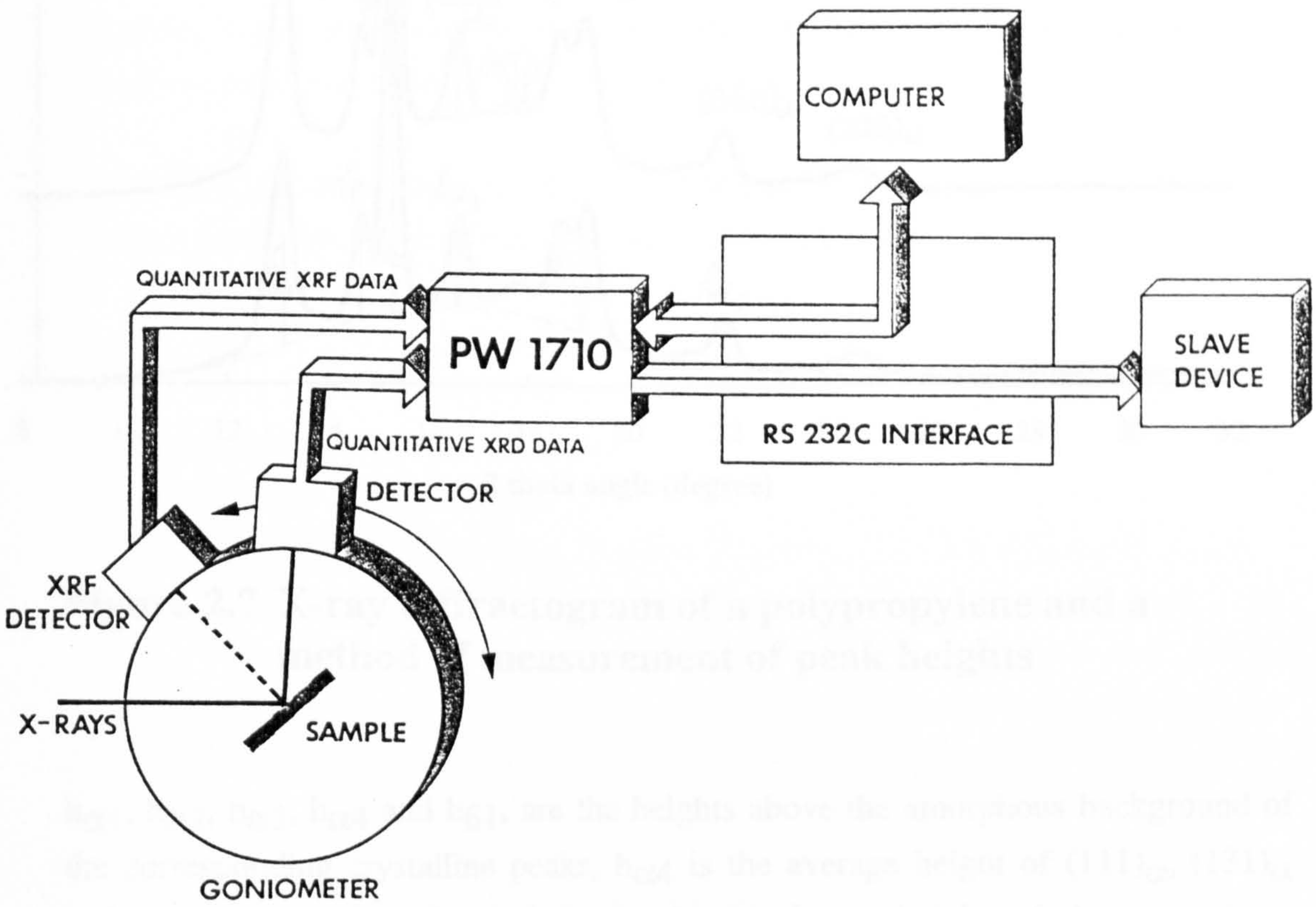

Figure 2.6 The x-ray diffractometer control system

The peak labelling routine searched for peaks over a specified angular range and automatically printed their interplanar d-spacings. The indicated d-values were directly usable for phase identification. A straight background was drawn in between 8° and 32° of 2θ and the diffraction scans were then divided into areas attributable to diffuse scatter from the amorphous region (A) and to sharp diffraction peaks from the crystalline regions (C) as shown by the dotted lines in Figure 2.7.

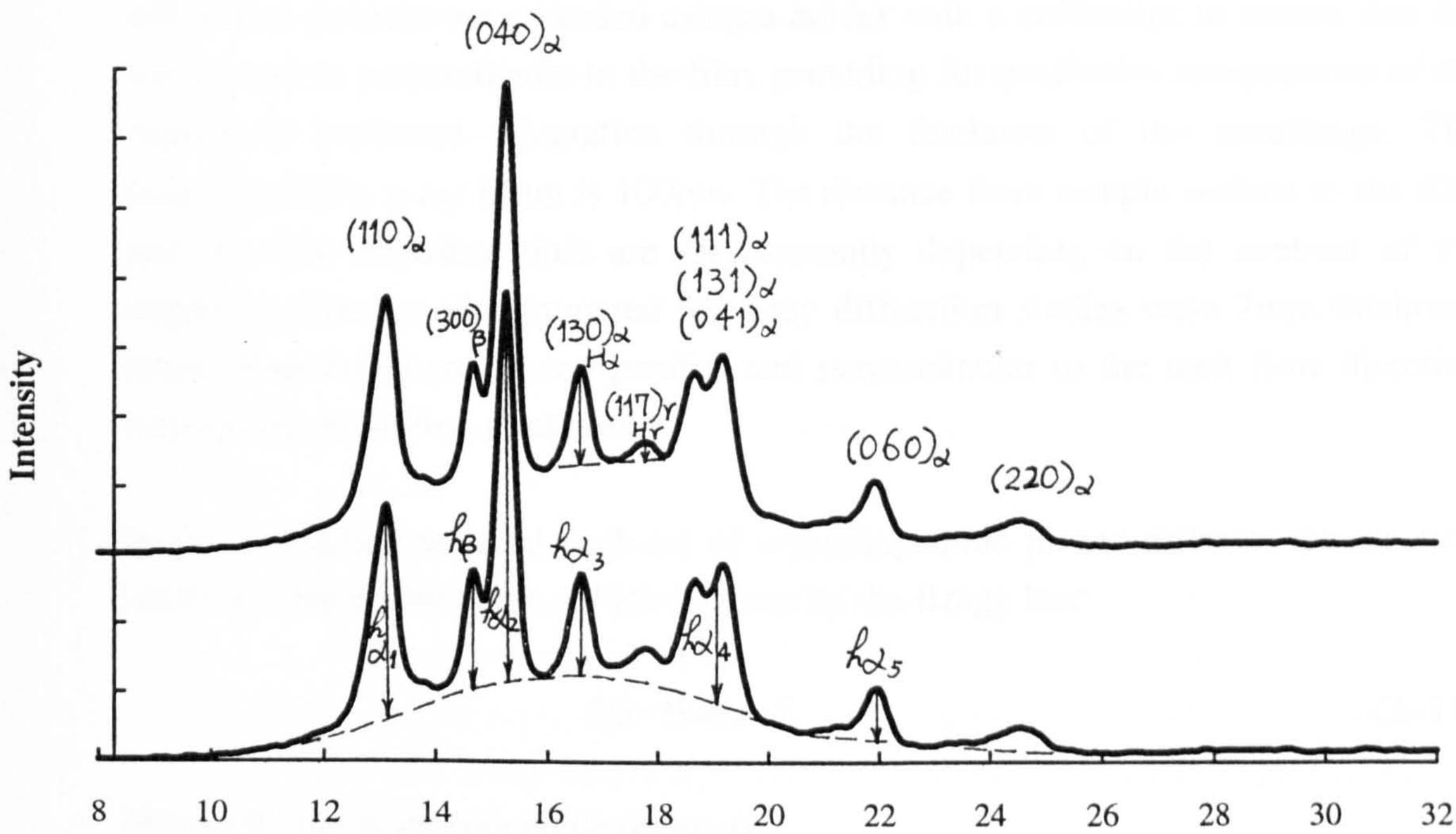

Figure 2.7 X-ray diffractogram of a polypropylene and a method of measurement of peak heights

$h_{\alpha 1}$, $h_{\alpha 2}$, $h_{\alpha 3}$, $h_{\alpha 4}$ and $h_{\beta 1}$, are the heights above the amorphous background of the corresponding crystalline peaks, $h_{\alpha 4}$ is the average height of $(111)_\alpha$, $(131)_\alpha$ and $(041)_\alpha$ crystal peaks and h_a is the maximum height of the amorphous background [116, 30]. The heights of $H_{\alpha 3}$ and H_γ of the α_3 and γ peaks were measured as shown in Figure 2.7 [117]. Appendix 2. is shown the equations to calculate α-phase orientation index A (2–5), ß-phase index B (2–6), crystallinity

index B (2–6), crystallinity index C (2–7), percentage γ crystallinity (2–8), γ-phase index G (2–9) and the degree of crystallinity (2–10).

Semicrystalline polymer gives rise to complex diffraction patterns. The scattering of x-rays by an isotropic polymer sample to give diffraction rings or by an oriented specimen to give the arcs provides information relevant to the spacing of the planes of the molecules in the crystalline phase.

The Debye flat plate technique was also used for x-ray diffraction studies. The x-ray diffraction patterns are recorded using a holder with a collimator to ensure that the x-ray beam is perpendicular to the film, providing for qualitative comparisons of the degree of preferred orientation through the thickness of the mouldings. The diameter of the x-ray beam is 100μm. The distance from sample surface to the film and the film exposure time are set constantly depending on the contrast of the negatives. The samples prepared for x-ray diffraction studies were 2mm thickness taken from the cross section parallel and perpendicular to the melt flow direction through the moulding thickness.

In the crystalline material each set of crystallographic planes diffracts the electron beam to a particular angle, which is given by the Bragg law:

$$2d \cdot \theta = n \cdot \lambda \qquad (2\text{–}11)$$

Where θ : the scattering angle (degree);

λ: the wave length of x-ray;

d: the interplanar distance.

n: the order of reflection;

The calculation method used to analyse the crystallographic data is shown in Appendix 3 (equations 2–12, 2–13).

2.7 Differential Scanning Calorimetry

Differential thermal analysis involves supplying (or removing) heat to a sample at a controlled rate and determining the rate at which this process takes place or is

disturbed by comparing its temperature with that of a reference sample. The melting point distribution and heat of fusion are measured by differential scanning calorimetry. Carefully controlled thermal treatment can be used to characterise the chain distribution presented.

On crystallisation, a polymer gives out an appreciable amount of heat and consequently quite small sample (<10mg) can be used to yield significant effects. Typical weights for standards range from 1 to 10 mg. The accuracy and precision of the sample weight is directly related to the accuracy and precision of the energy measurements made on DSC. Running a large sample at a fast scanning rate can improve the usable sensitivity, while running a small sample at a slow scanning rate can improve the resulting peak resolution.

During melting and crystallisation, the effects show endothermic and exothermic peaks when the sample is heated or cooled. Measurements are usually taken under conditions such that the temperature of the environment is continually increasing or decreasing and of course heat is also emitted or absorbed by the sample during a first-order transition. The steady state rate depends on the conductivity and heat capacity and as the latter changes during a second-order or glass transition such transitions can be determined by this technique. Differential thermal analysis can also be used quantitatively to make comparisons of the degree of crystallinity present after crystallisation by inspection of the area under the curve on melting. This is proportional to the crystallinity and if a suitable calibration is carried out, the actual heat of fusion can be determined.

When a transition such as melting, boiling, dehydration or crystallisation occurs in the sample material, an endothermic or exothermic reaction takes place. The change in power required to maintain the sample holder at the same temperature as the reference holder during the transition recorded as a peak. The testing curve abscissa indicates the transition temperature and the peak area indicates the total energy transfer to or from the sample.

The DSC instruments can analyse solid and liquid samples. Solid samples can be in film, powder, crystal or granular forms. Although quantitative accuracy will remain the same regardless of sample shape, the qualitative appearance of a run will be affected by the sample configuration. Therefore, for maximum peak sharpness and

resolution, a configuration which maximizes the contact surface between the pan and sample is desirable. Materials such as polymer mouldings are prepared by cutting out sections of the sample.

The DSC sample holder is composed of two-mass platinum-iridium sample cells embedded in a large aluminum heatsink. A swing-away lid with a rubber O-ring seal is used to seal the furnaces from the external atmosphere during an analysis. The direct calorimetric measuring principle of the instrument requires that each sample holder has a built-in heater and a temperature sensor. The left-hand furnace is usually used for encapsulated sample materials, while the right-hand furnace is an empty sample container of the type used in the sample cell as reference pen. A high gain, closed-loop electronic system (see Figure 2.8) provides differential electrical power to the heaters to precisely compensate for temperature fluctuation. Therefore the holder temperature is essentially unaffected by the sample behaviour. The differential power required to maintain the balance condition is read out directly in millicalories per second on the recorder and is at all times equivalent to the rate of energy absorption or evolution of the sample.

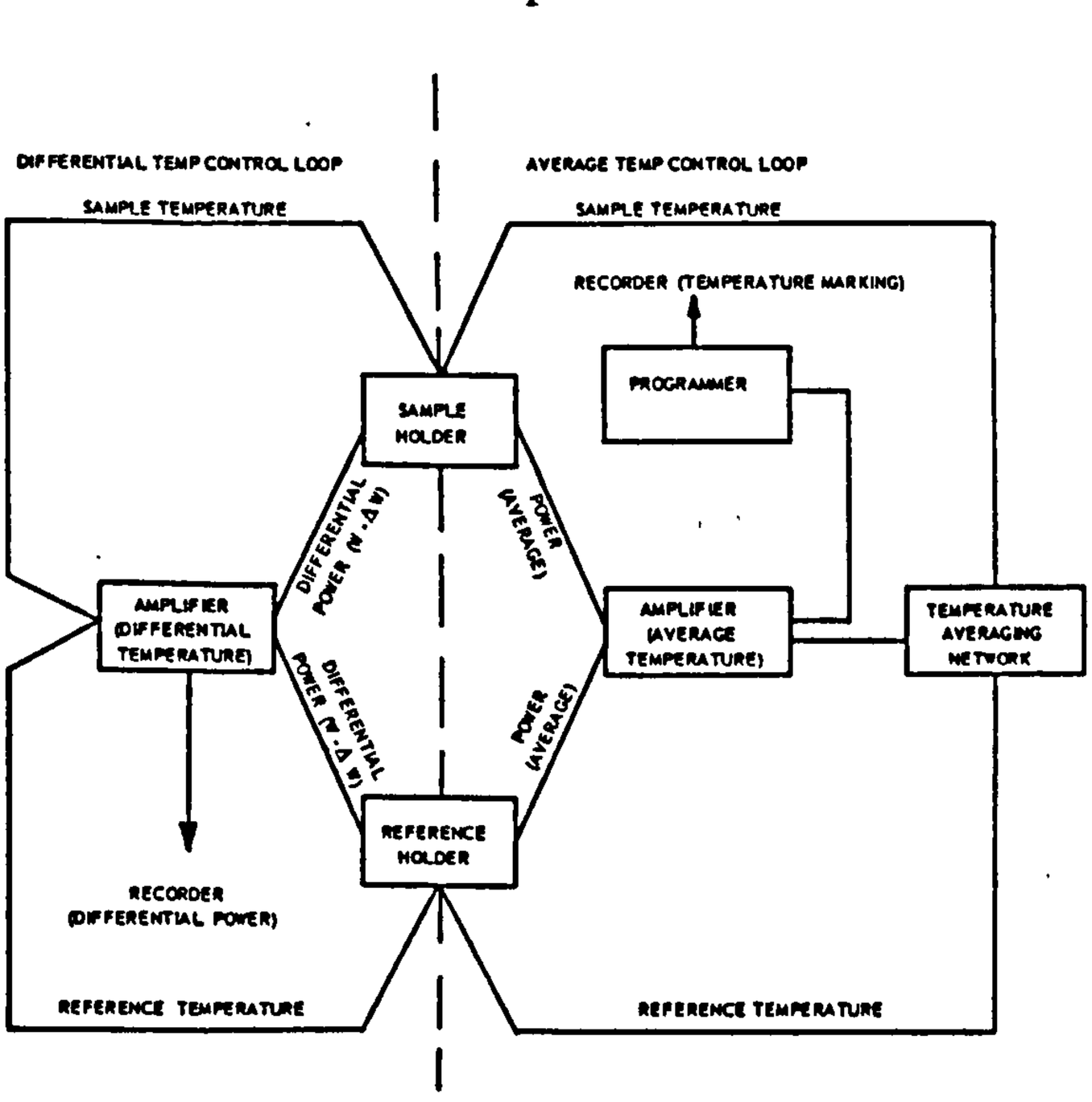

Figure 2.8 The diagram of temperature control system of differential scanning calorimeter

The standard sample pans and covers provided in aluminum, gold and platinum are suitable for most thermal analytical applications. The pan chosen is depended on the temperature range of study. The method of sample encapsulation most widely used is to crimp the sample pan cover in place.

In this study, the heat of fusion ΔH and melt temperature T_m were measured using Perkin-Elmer differential scanning calorimeters DSC-2 and DSC-7. The DSC-2 is a sophisticated instrument connected to a Thermal Analysis Data Station (TADS) for the calorimetric measurement, characterisation and analysis of thermal properties of materials. The DSC-7 is controlled by the DEC Station Personal Workstation. Under the control of the TADS and DEC stations, the DSC-2 and DSC-7 were programmed from an initial to a final temperature through transitions of the sample.

The standard model DSC-2 has an operating range of from 50°C to 725°C. Its range can be extended to -40°C with the Intracooler-1 and the intermediate range subambient accessory, and to -70°C with the Intracooler-2 and the intermediate range subambient accessory. 11 linear precise heating rates and 11 linear independently selective cooling rates are supplied from 0.3125° to 320.0°/min.

The DSC-7 can be used to analyse samples from a temperature of -170°C to 725°C for the study of the endothermic and exothermic reactions. The DSC-7 allows scanning rate of 0.1°C to 500°C/min in steps of 0.1°C/min.

The temperature range used for study was from 320K to 500K. The weights of the samples used ranged from 2-10 mg. The heating rate was 10 or 20°C/min and the cooling rate was 20 or 320°C/min. ΔH was estimated from the area enclosed by the fusion curve and the baseline. The crystallinity $X_{\Delta H}$ obtained from ΔH and is substantially associated with the peak regions. $X_{\Delta H}$ was calculated as follows:

$$X_{\Delta H} = \frac{\Delta H}{\Delta H_0} \cdot 100\% \qquad (2—14)$$

Where ΔH_0 is the heat of fusion of the perfect crystal, assumed to be 33cal/g = 137.08J/g.

2.8 Etching Technique and Transmission Electron Microscopy

2.8.1 Etching Technique

The objective of etching preparation is to render the specimen suitable for observation in the TEM without altering its chemical or physical state. There are many etching techniques depending upon the nature of the materials.

Some prime concerns of selective etching have been the increase in the roughness of polymer surfaces, change the surface chemical constitution, degradation or dissolution of low molecular weights which migrate to the surface, and relieving of residual surface stresses. Every polymer surface, thermoplastic or thermoset, amorphous or crystalline exhibits a different morphology from the bulk. Etching can considerably change the morphology and chemical properties of polymer surfaces. By etching, some polymer surfaces can be converted from hydrophobic to hydrophillic, thus considerably facilitating the application of surface finishes.

Liquid etching is the most widely used method for the modifying of polymer surfaces. Liquid etchs produce increased roughness on polymer surfaces. However, a liquid etching may also change the overall electronic state of the polymer surface by generating unsaturation and polar groups. A liquid etching may also selectively dissolve one of the components of a heterogeneous system, creating a rough surface with numerous pits and holes. A liquid etching often serves both functions of chemical modification and dissolution. Liquid etching is particularly useful for removing low molecular weight fractions which can reside on the surface [118].

In this study, the preparation of specimens for TEM study was carried out on the steps including polishing, etching, cleaning, coating and the replica preparing.

Firstly, the samples were etched according to the following steps:
1) mixture 50:50 sulphuric acid with orthophosphoric acid in a pre-dried flask. The flask was placed in the cooling water bath in order to remove the heat of mixing. The mixing operation must be very carefully carried out.
2) the mixture obtained from step (1) was left in the fridge for 2-3 hours.

3) add 2wt.% potassium permanganate in to the mixture obtained from step (2) with the use of a magnetic stirring machine. It took time to dissolve the potassium permanganate little by little. Then a dark green precipitate of $O_3MnO\text{-}SO_3H_3$ was produced.

4) the samples (polished surfaces) to be etched were placed surface downward in the mixture obtained from step (3) in an ultra-sonic bath at 40°C for 2-3 hours.

Secondly, the etched surfaces of samples were cleaned according to the following five steps:

1) transfer the etched specimen to a mixture of 2% solution sulphuric acid with distilled water, which had been pre-cooled at -20°C for 2 mins in the ultra-sonic bath.

2) washing the etched specimen with 30% solution hydrogen peroxide for 1 minute.

3) washing the specimen with distilled water for 1 minute.

4) rinse in acetone for 1 minute.

5) dry the specimen in a vacuum oven at 40°C for 1 hour.

The etched and cleaned specimens were then coated in an EDWARDS 306 vacuum coater. the specimens were shadowed with a very thin platinum/palladium alloy layer at 45° angle for 2 seconds, followed by coating with a thicker carbon layer at 45° on to the Pt/Pd surface. Polyacrylic acid (PAA) was then spread on the top of the Pt/Pd-C coating layer and left to dry for 24 hours. The Pt/Pd-C-PAA sandwich was removed from the etched surface by peeling off with a razor blade. The thin film was placed with the PAA side down into a bowl of clean water with a dust free surface to allow the PAA to dissolve. The thin film should then float on to the water surface. A piece of 200 mesh copper grid was placed under the water surface and raised under the thin film, and then brought the Pt/Pd-C-grid out off the water surface and placed in desiccating paper to dry. When dry the replica was ready for TEM.

2.8.2 Transmission Electron Microscopy

Electron microscopes were developed in 1936 but only became commercially available in 1946. Now electron microscopes have developed to exploit widely the analytical capability which results from the many different interactions between electrons and materials.

Many of the properties of engineering materials are controlled by microstructural features. For instance many mechanical properties are controlled by line defects. The importance of the high resolving power of electron microscopes is then a key feature in their use. Electron microscopy has had a key role in furthering our understanding of microstructural processes in engineering materials. Scanning electron microscopy (SEM) and transmission electron microscopy (TEM) are the most widely used microscopic methods.

A microscopic examination of an artefact or a process within a material usually involves a combination of microscopic techniques. The attraction of electron microscopy in the examination of engineering materials comes from the high resolving power together with the large range of signals available. These permits a number of magnified images to be formed whose contrast can contain different information about the geometry, crystallography, structure and chemistry from which these signals originate [119].

Electron microscopy has a central position in the development of materials science as a subject. Increasingly, electron microscopy is also seen to have a pivotal role in the more applied end of the subject; in helping to develop accurate data bases, in isolating the cause of failures, and in the inspection and fabrication of devices. For instance, there is now a major interest in using electron beams for machining masks and circuits for use in electron devices.

The basic construction of electron microscopy consists of: electron gun, condenser lens system, specimen stage, objective lens, projector lens system, viewing screen and image recording facility. The condenser lens controls the electron intensity through the specimen,; the objective lens controls the focus of the image on the screen; and the projector lens controls the final magnification of the image.

Figure 2.9 shows the basic imaging arrangement of transmission electron microscopy (TEM), an electron beam from an electron gun illuminates the specimen, usually through an illuminating system of lenses. The radiation interacts with the specimen and is scattered. The scattered radiation is brought to a focus by the objective lens. Then, further magnifying (or projector) lenses produce an image of convenient size. The image is formed from electrons which have passed through

the specimen with only a small loss of energy in the transmission electron microscopy.

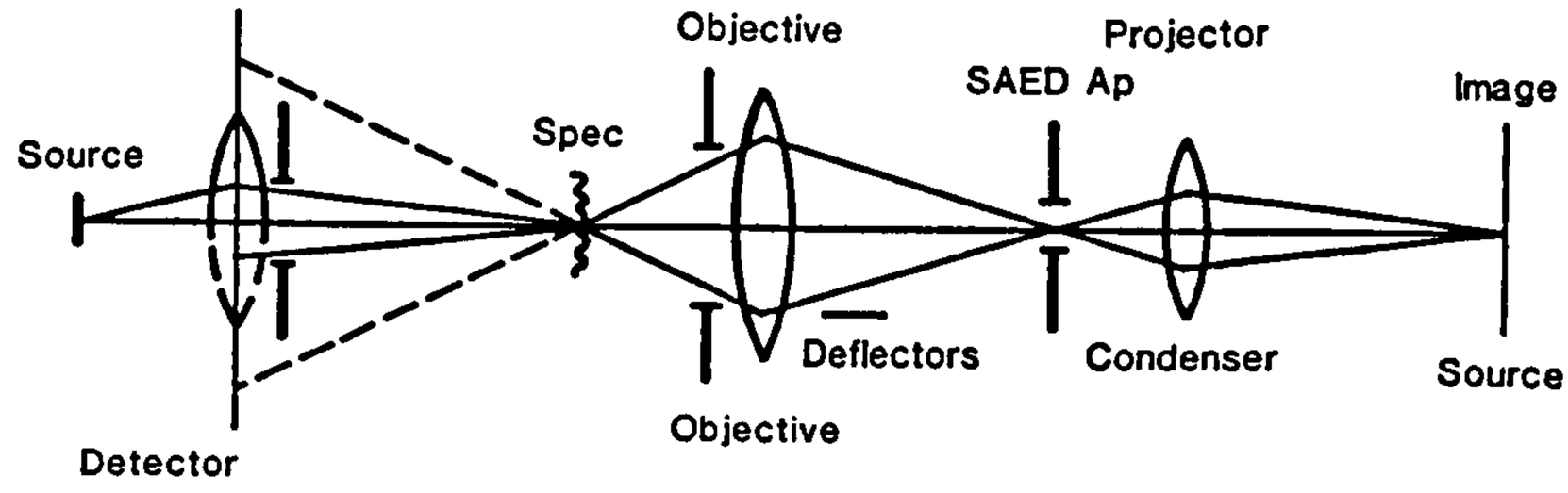

Figure 2.9 The main elements of transmission electron microscopy [119]
(SAED AP is the selected area electron diffraction aperture. Spec is the specimen)

Two important factors determine the essential geometry of the imaging system. The wavelength of the electrons determines the angular range of the scattering from the specimen. The aberrations of the electron lenses limit the angular range of scattered radiation that can usefully contribute to the image.

In the study, A JEOL 100CX transmission electron microscopy (TEM) was used for examination of the replicas. A fine beam of electrons can be focused on a pre-determined area which electron diffraction patterns obtained and hence related to the appearance of the crystal. The orientation of the molecules chain can be observed in the crystal lamella.

JEOL 100CX TEM fitted with a scanning attachment is combined with a link energy dispersive x-ray detector to form a powerful analytical system with a variety of imaging modes. The high resolution transmitted electron image with a point to point resolution of better than 6, together with the associated technique of electron diffraction is used for conventional electron microscopy of polymer, biological and metallurgical materials. The ability to use the microscope in the scanning mode for both secondary and transmitted images coupled with x-ray analysis of elements from Na to U is used to advantage in the study of a wide variety of subject materials. Applications include the characterisation of microfeature in polymer and metallic engineering materials, analysis of supported catalysts and the study of biological tissues and cell contents.

2.9 Density Measurement

2.9.1 Density Testing Method by Weight Measurement

Crystalline polymers are considered to have both crystalline and amorphous phases. Density has long been used as a primary method of estimating the crystalline fraction in polymers. This density testing method is accorded to ASTM D792-66 standard and covers the determination of the specific gravity and density of solid plastics by displacement of liquid and determination of the change of weight in air and in water. The purpose of using this method is to obtain the range of the density for setting up the Tecam density column.

The specific gravity or density of a solid is a property that can be measured conveniently to identify a material, to follow physical changes in a sample, to indicate degree of uniformity among different sampling units or specimens, or to indicate the average density of a large item. Portions of a sample may differ in density because of differences in crystallinity, thermal history, porosity and composition. This method involves weighing one piece of a specimen of 1 to 50 g in water, using a steel sinker with iPP specimens which have less dense than water. Care should be taken in cutting specimens to avoid changes in density resulting from compressive stresses or frictional heating. A corrosion-resistant wire was used for suspending iPP specimen. The water used was distilled.

Calculation of the specific gravity and the density of the samples were as follows:

$$\text{the specific gravity} \quad (23°C) \qquad Sp\cdot gr = \frac{a}{a+w-b} \qquad (g)$$

$$\text{the density} \quad (23°C) \qquad D = 0.9975 \cdot Sp\cdot gr = \frac{0.9975\cdot a}{a+w-b} \qquad (g/cm^3) \qquad (2\text{–}15)$$

a = apparent weight of specimen, without wire and sinker, in air.
b = apparent weight of specimen and sinker completely immersed and of the wire partially immersed in liquid.
w = apparent weight of total immersed sinker and partially immersed wire.

From the weight measuring method, the crystallinity could be calculated as equation (2–15):

$$\text{Crystallinity } X_d = d/d_0 \times 100\% \qquad (2\text{–}16)$$

where the density of the prefect crystal $d_0 = 0.9360$ g/cm³.

2.9.2 Tecam Density Column Method

Tecam density column method accorded to ASTM D1505-60T standard is used to actually measure accurately the density of specimens. The schematic diagram of the Tecam density column is shown in Figure 2.10. In this study, the column contained a mixture of propan-2-ol and digol whose density varies along a linear scale from top to bottom of the column. The choice of liquids varies according to the density range determined from the former density testing method of weight measurement. The temperature was controlled to less than ±0.2°C. Seven standard glass markers floated in the liquid to provide points of reference at intervals throughout the height of the column. The position of the specimen relative to the scale accurately indicates its density (see Figure 2.11).

The density range of the column required was obtained from the density determination by weight measurement. The density range of the column should be wide enough that it accommodates easily all specimens likely to be used but in no event wider than 0.3 gms/ml. It should also be noted that the narrower the range of the column the more accurately can density determinations be made. Calculation of density range is shown in Appendix 4.

2.10 Summary

In view of the above, this chapter is an extension to the literature survey of applied testing techniques to polypropylene mouldings. Both conventional and SCORIM techniques were employed for iPP injection mouldings using three moulds of different shapes by changing the processing conditions. Shear controlled orientation injection moulding technology (SCORIM) provides routes for the management of fibre orientation and microstructure in moulded iPP. Three oscillating modes of pistons were employed to cause a macroscopic shear to be applied to the melt solid

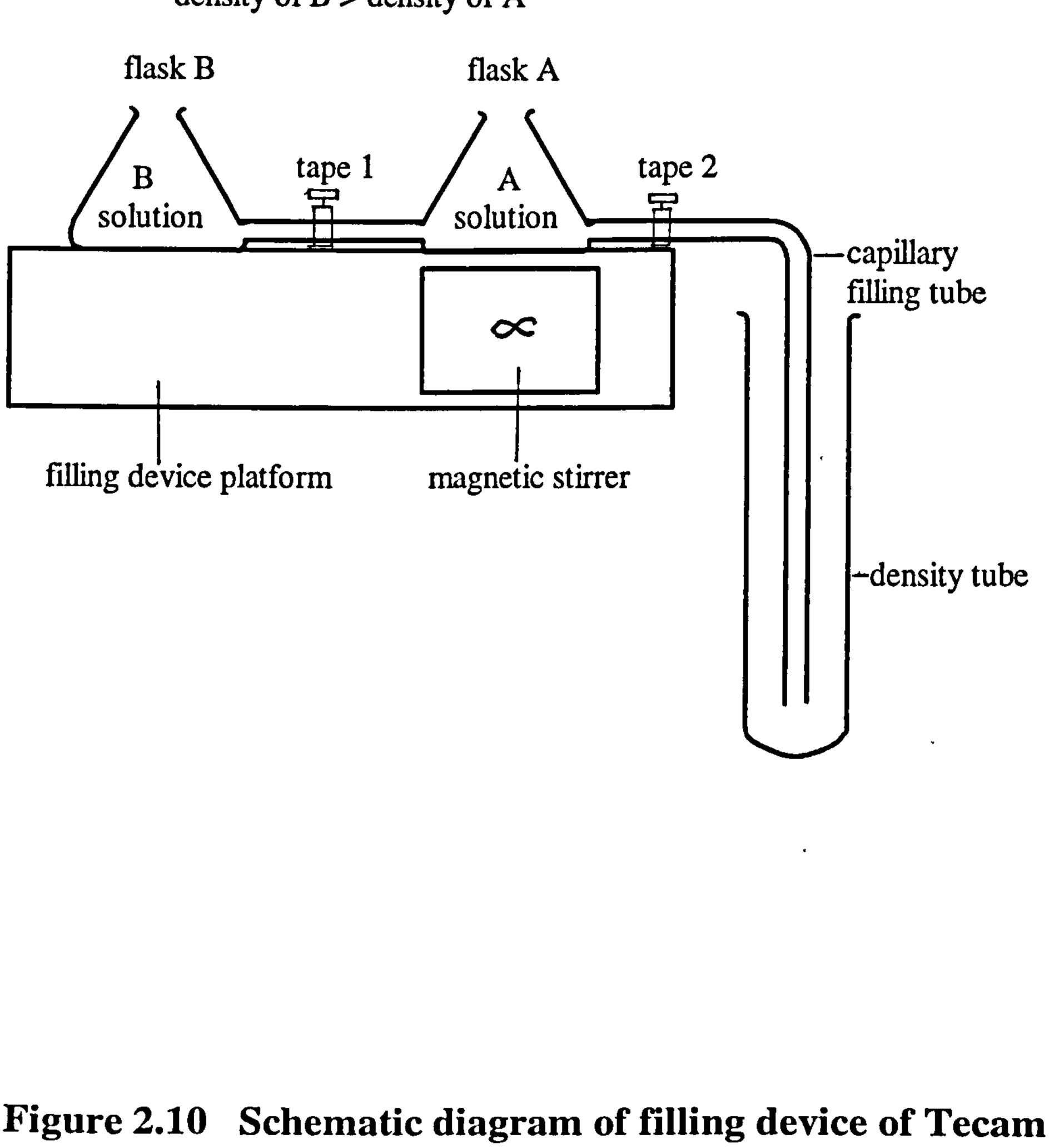

Figure 2.10 Schematic diagram of filling device of Tecam density column

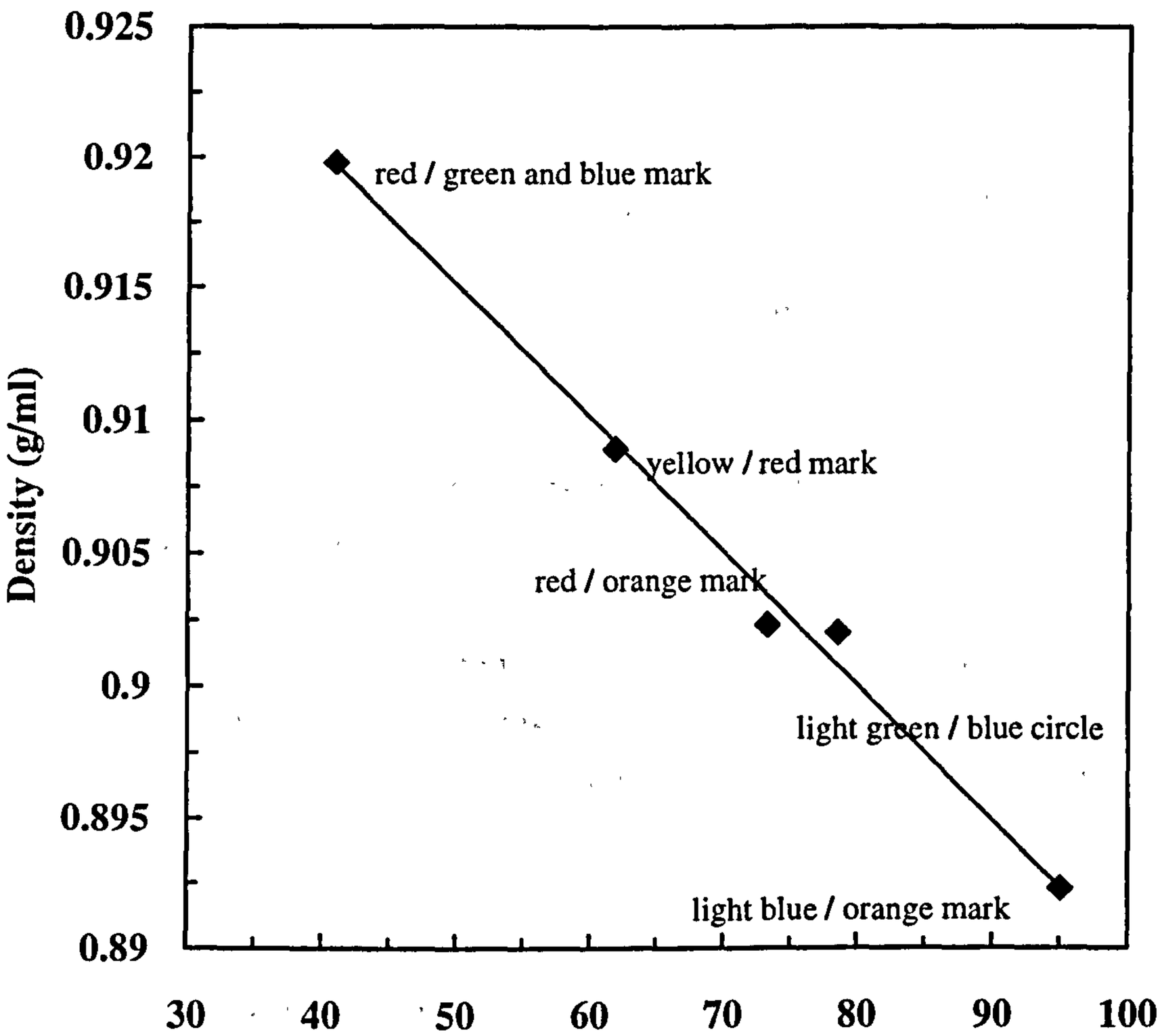

Figure 2.11 Parameter curve of Tecam density column
(Water temperature 24.38°C)

interface within the mould cavity.

The introduction of experimental techniques led to advances in the understanding of polymer morphology. The use of different techniques to complement each other is essential in morphological enquiry and is likely to involve more and more methods as the sophistication of textural characterisation and mechanical behaviour increase.

Light microscopy can be used to reveal the nature of the textural element and gain an interpretation of the characteristics. The etching technique gives the analytical capability to examine a representative morphology and the enlargement of the image by TEM.

Vickers microhardness can be measured by indentation testing to obtain the most commonly quoted hardness of the injection moulded polypropylene samples.

In the mechanical measurement, the determination of Young's modulus, tensile stress, tensile strain and toughness of the conventional and SCORIM mouldings were measured by using Instron tensile testing machines (model 1195 and 4206).

X-ray diffraction studies provided for the concentration and distribution of the α, ß and γ crystalline phases of iPP mouldings by calculating α-phase orientation index A, ß-phase index B, crystallinity index C, percentage γ crystallinity (γ%), γ-phase index G and the degree of crystallinity. The Debye flat plate technique provided for qualitative comparisons of the degree of preferred orientation through the thickness of the mouldings.

Differential Scanning Calorimetry is used to characterise the thermal behaviour and make comparisons of the degree of crystallinity by analysis of endothermic and exothermic processings. Density is used as a primary method of estimating the crystalline fraction in polymers.

CHAPTER 3
EFFECTS OF PROCESSING CONDITIONS ON THE MICROMORPHOLOGY AND MECHANICAL PROPERTIES OF POLYPROPYLENE

3.1 Injection Moulding

In this study, both conventional and shear controlled orientation injection moulding (SCORIM) techniques were employed for injection moulding of a propylene homopolymer, using three moulds of different shapes and by varying the processing conditions, including nozzle temperature, mould temperature, hold pressure, injection speed, piston operating pressure and oscillating mode of pistons. The effects of such different conditions on the micromorphology and physical properties of the moulded polypropylene were investigated. The results obtained were compared so as to indicate the differences in microstructure and physical properties resulting from the two moulding techniques. The principal aim of the study was to identify the most promising lines of investigation to follow in order to realise the maximum benefit of SCORIM applied to unreinforced semi-crystalline polypropylene.

In the initial stage of the study, the polypropylene was moulded in the form of a standard tensile bar on a conventional Sandretto injection machine using a double cavity mould. The purpose of this part of the investigation was to provide the basic characteristics of the polypropylene study material which would then be used to compare with those properties to be gained using the SCORIM technique, which should lead to the enhancement of the physical properties of moulded polypropylene.

A ring mould was then used in the Negri Bossi twin injection machine to investigate improvements in uniformity of micromorphology, shrinkage and tensile strength of mouldings made possible by four live-feed injection moulding.

In the final stage, the study was carried out on the SCORIM injection moulding of iPP homopolymer by varying processing conditions, including three hold pressures, two mould temperatures and two nozzle temperatures for both conventional and SCORIM injection processes. A rectangular bar mould was used in a Demag D150 injection moulding machine to investigate the enhancement of the preferred orientation and physical properties in injection moulded iPP.

3.2 Light Microscopy Study of Microstructure of Injection Moulded iPP

The dimensions of the standard tensile bar mould were 191.60×19.10×3.20 mm^3. Thin sections (~2μm) from the tensile bar mouldings were prepared by microtomy for the examination of transmitted light microscopy. Figure 2.1 shows the sections that were made both at the gate region and at 8/10 of the path length of the tensile bar in the melt flow direction.

The microtome sections were prepared from selected conventional injection moulded iPP standard tensile bar samples for each set of processing conditions. Figures 3.1a and 3.1b show the polarizing transmitted light micrographs gained from the typical gate regions in the conventional iPP samples. The sections were taken at the gate regions of the tensile bar mouldings through the 3mm thickness following the melt flow direction.

The spherulitic structure exhibited the well known skin-core morphology [105]. The skin layer was very thin (0.12 — 0.20mm) and was characterised by a fine spherulitic structure. The morphology between the skin and core shows a oriented and birefringent non-spherulitic structure and it became narrower away from the gate region. It disappeared in the section at 8/10 of the flow path length [120]. In the central core (2.0 — 2.7mm) the isotropic spherulites display a dark Maltese-cross. Figure 3.2 shows the photograph of the spherulitic structure in the skin and core region recorded at high magnification. It is clearly seen that the radial spherulites are in the random arrangement on the core region. The spherulites themselves are crystalline but the spaces between them are not.

Figures 3.3 — 3.5 are the micrographs taken from the four gate regions of MLFM and conventional ring moulding samples respectively. It can be seen that the MLFM processing resulted in shear bands in the regions near the gate A and gate D, and the traces of high shear stress were observed in the area near gate B and gate C (see Figures 3.3 and 3.4). The micrographs of the MLFM ring mouldings also exhibited the wider width shoulders at the four gates. These are in contrast to the conventional injection moulding in which no shear band was observed (see Figure 3.5). Furthermore, macro-voids are evident in the centre of the whole ring moulding

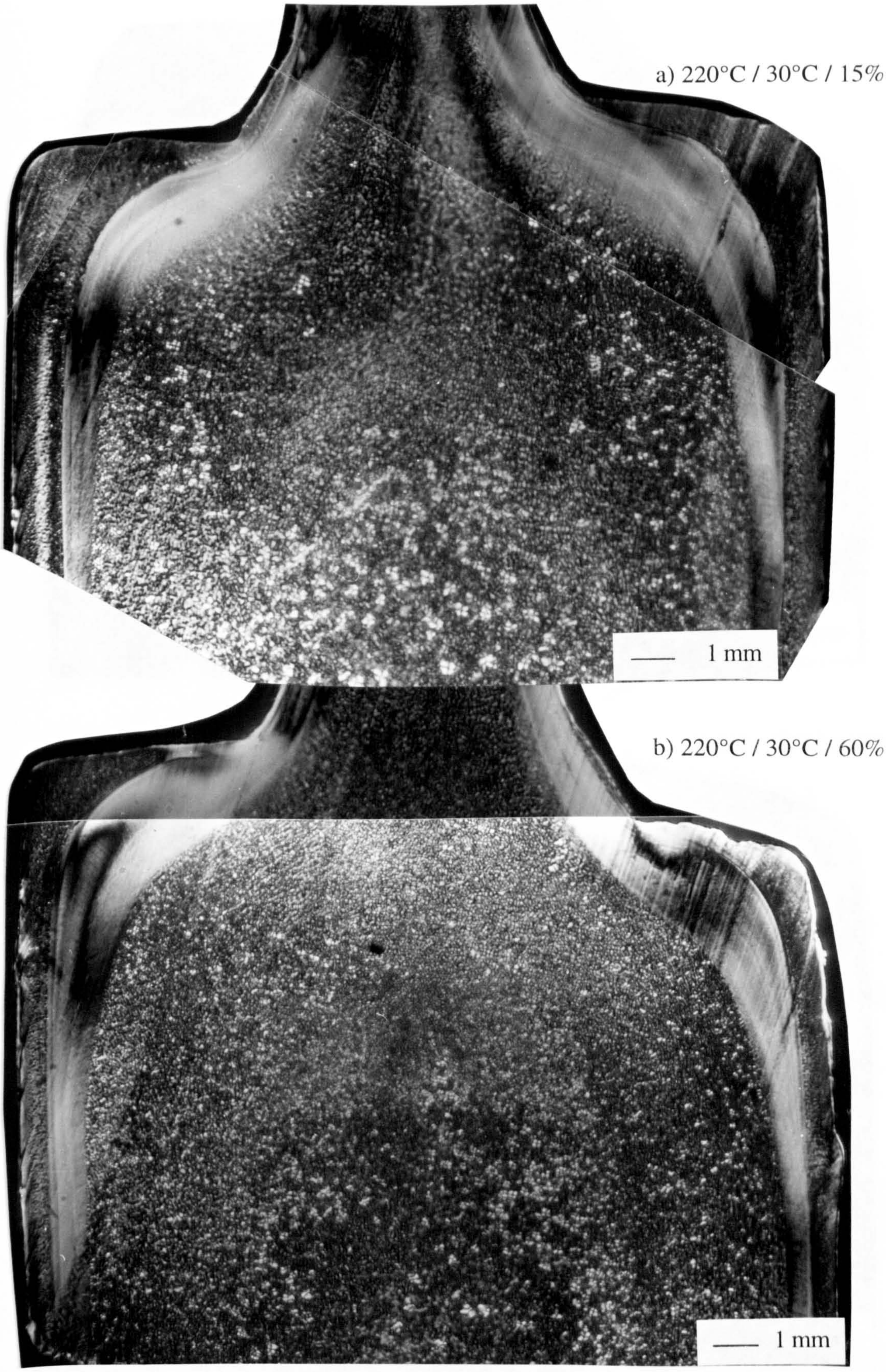

Figure 3.1a Micrographs of the gate regions of standard tensile bar conventional injection mouldings

(Processing condition: nozzle temperature / mould temperature / injection velocity)

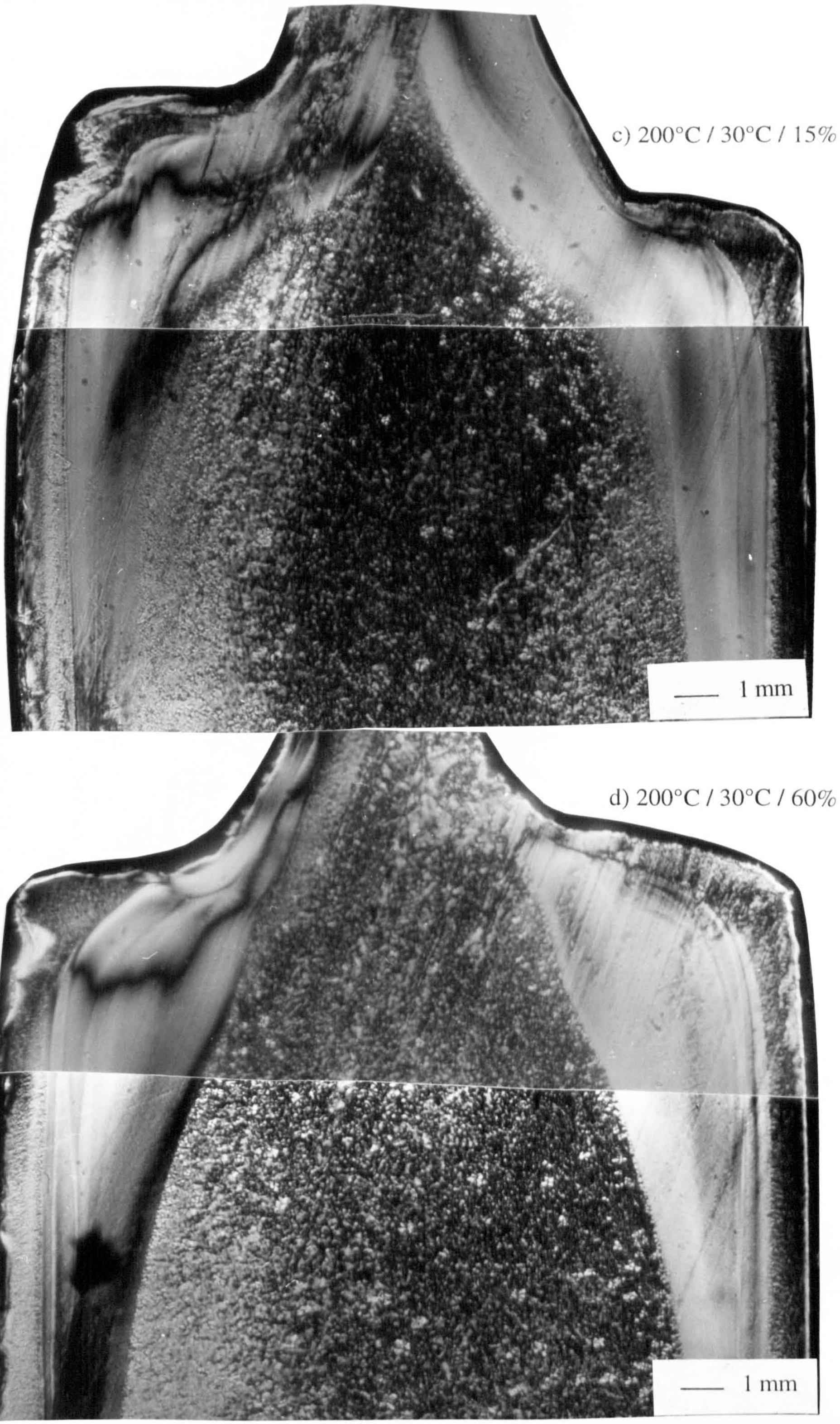

Figure 3.1b Micrographs of the gate regions of standard tensile bar conventional injection mouldings

(Processing condition: nozzle temperature / mould temperature / injection velocity)

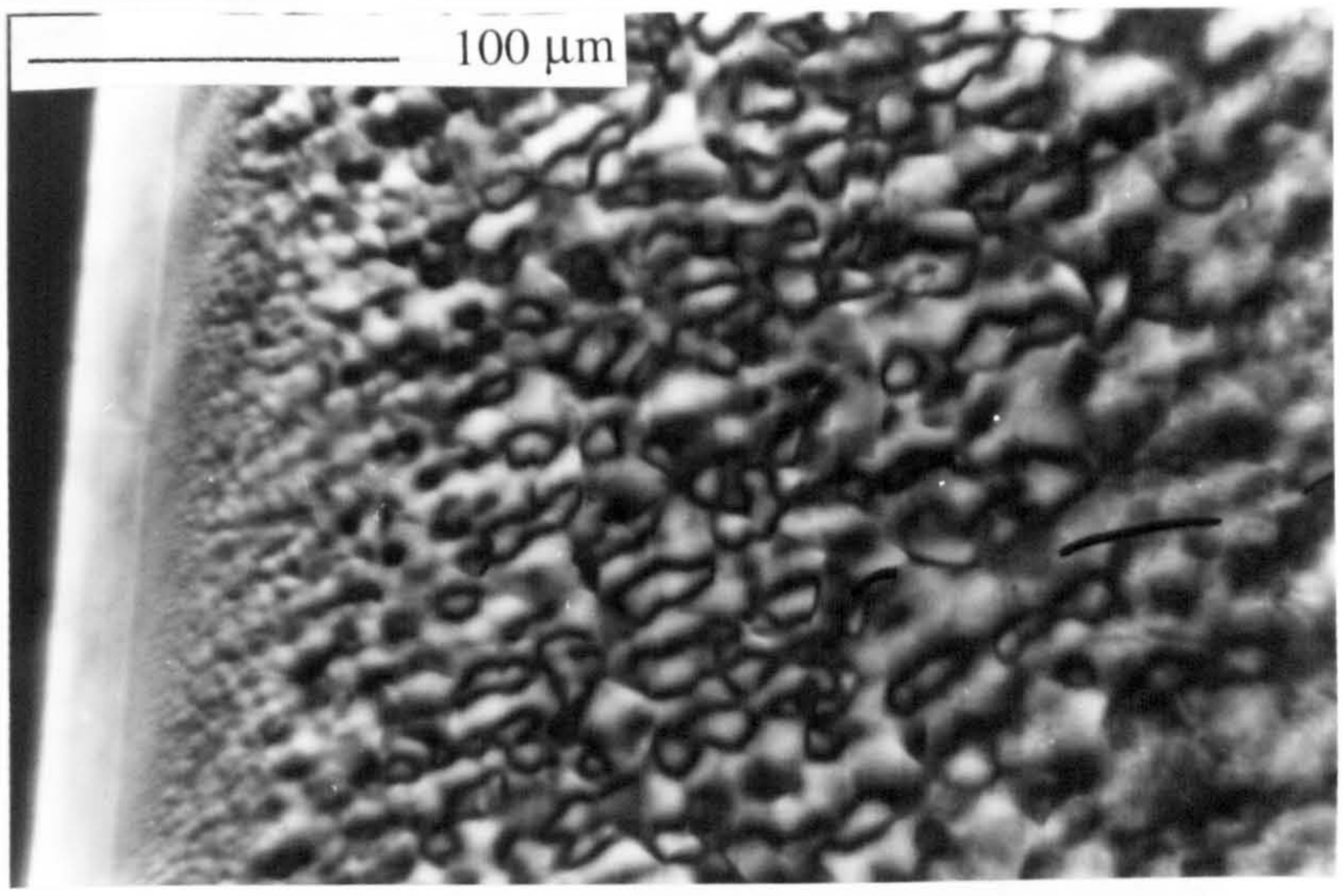

skin layer

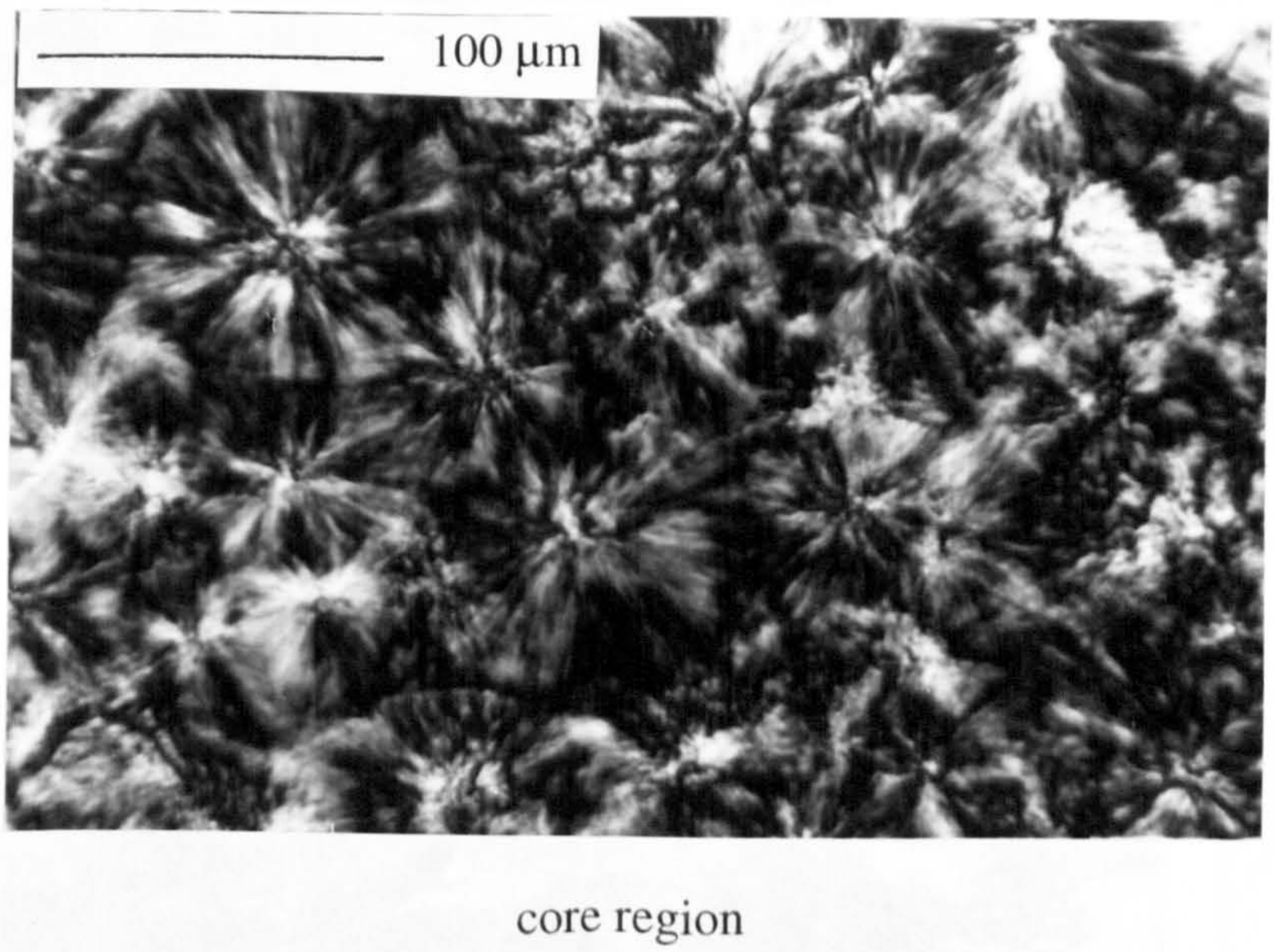

core region

Figure 3.2 High magnification micrographs of the skin layer and the core region in conventional injection moulded polypropylene

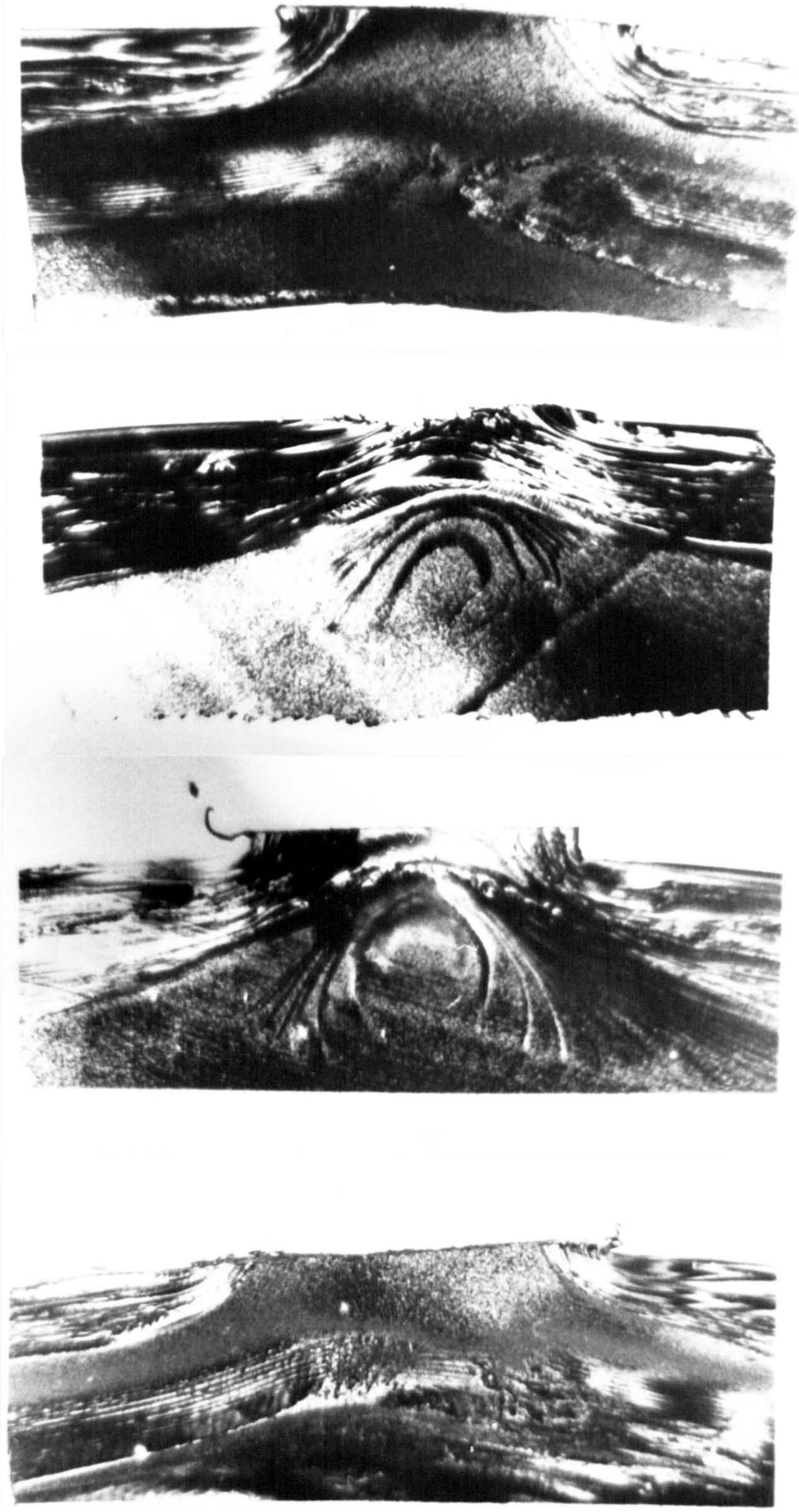

Figure 3.3 Micrographs of the gate regions of MLFM-R1 ring moulding

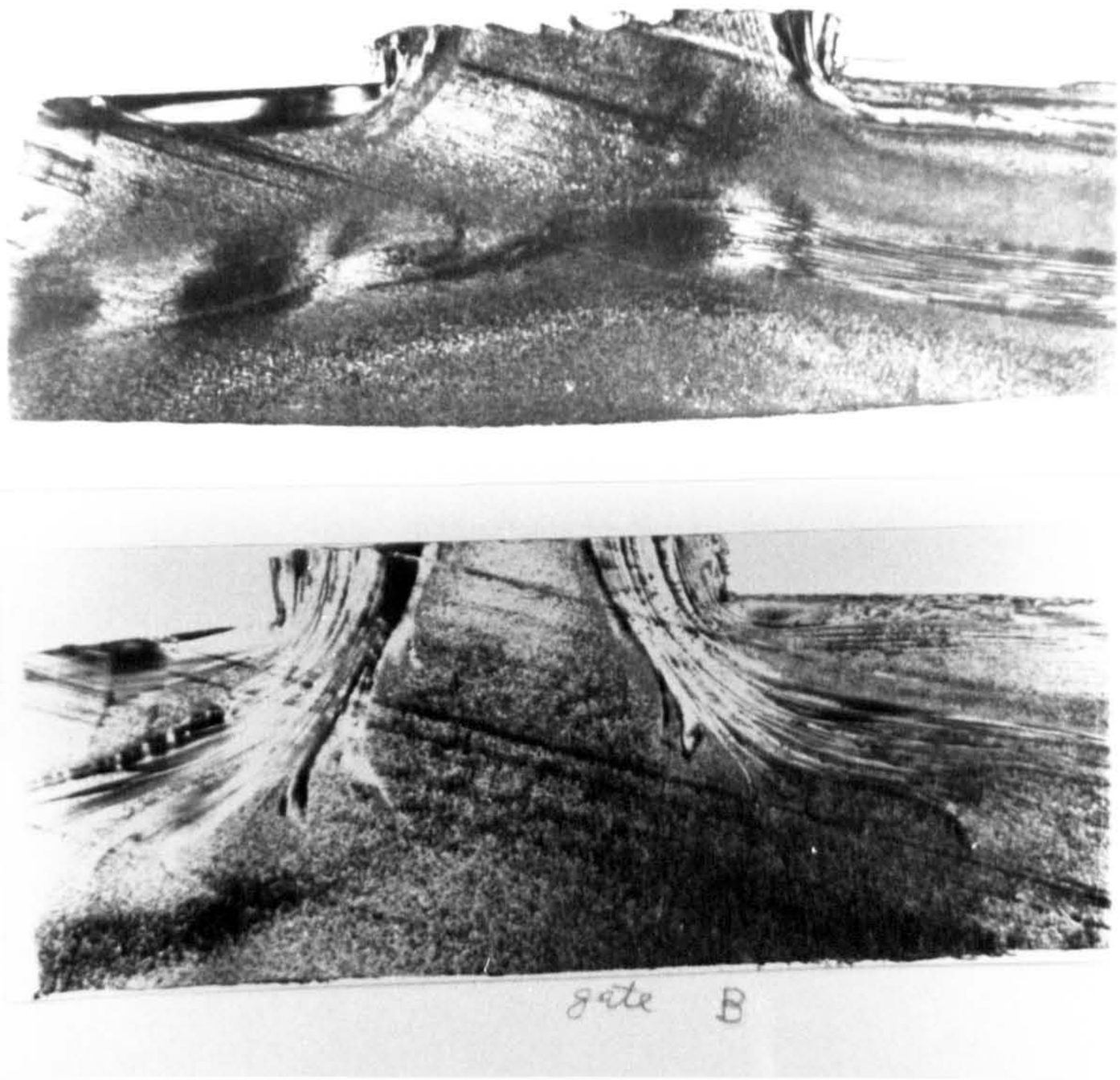

Figure 3.4 Micrographs of the gate regions of MLFM-R2 ring moulding

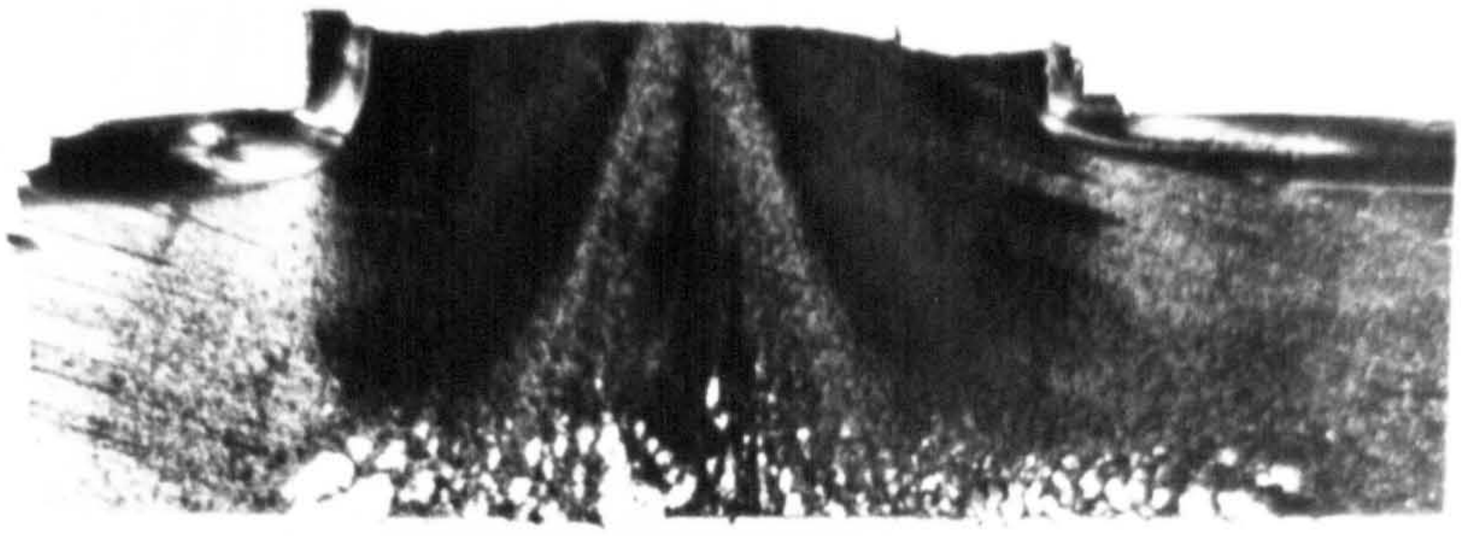

Figure 3.5 Photographs of the gate regions of conventional injection ring moulding

produced using the conventional injection technique.

In order to explain the effects observed on the tensile modulus and fracture stress of the ring and rectangular bar mouldings, an examination of the fibrous lamellar structure in the moulding was made. The whole section of the centre part cut through the moulding thickness of the sections were taken. A polishing technique was used to prepare the whole section of the ring moulding and rectangular bar samples for examination under transmitted light microscopy. The finest polishing cloth was 1μm. Figure 3.6 shows the higher magnification micrographs which were taken from the section parallel to melt flow direction at gate A of the MLFM-R1 ring moulding. It shows a preferred oriented laminate arrangement (X and Y) produced by alternate operation of live feeds A-D and B-C, to give the aligned structures in the area near gate A and D.

Figures 3.7 and 3.8 show the micrographs of the whole sections perpendicular and parallel to the melt flow direction of the rectangular bar mouldings of seven SCORIM processing conditions. The samples were taken 1mm away from the gate (as shown in Figure 3.7) and the main part (Figures 3.8a,b,c) of the bar mouldings. The use of different SCORIM processing conditions for the same mould temperature and nozzle temperature resulted in different microstructures. Figure 3.7 shows 40bar and 80bar hold pressure resulted in a finer spherulitic structure in the sub-skin area and in the core area near the gate region (SCORIM-1A, -1B, -2A, -2B and -3B mouldings), whereas the SCORIM-1C and SCORIM-2C produced under high hold pressure (120 bar) exhibited greater evidence shearing in the sub-skin layer and core region.

All micrographs were taken from the main part of the SCORIM injection mouldings perpendicular to the melt flow direction, and reveal a pronounced shear band in the central layer which is shown as lamellar rings in the left side photos in Figures 3.8(a,b,c). The micrographs on the right side in Figures 3.8(a,b,c) were taken from the corresponding sections parallel to the melt flow direction in the main part of the mouldings. The SCORIM mouldings produced under 120 bar hold pressure (SCORIM-1C and SCORIM-2C) showed the lamellar ring structure with high shear traces through the whole cross section.

Figure 3.9 shows the same sections perpendicular to the melt flow direction in the

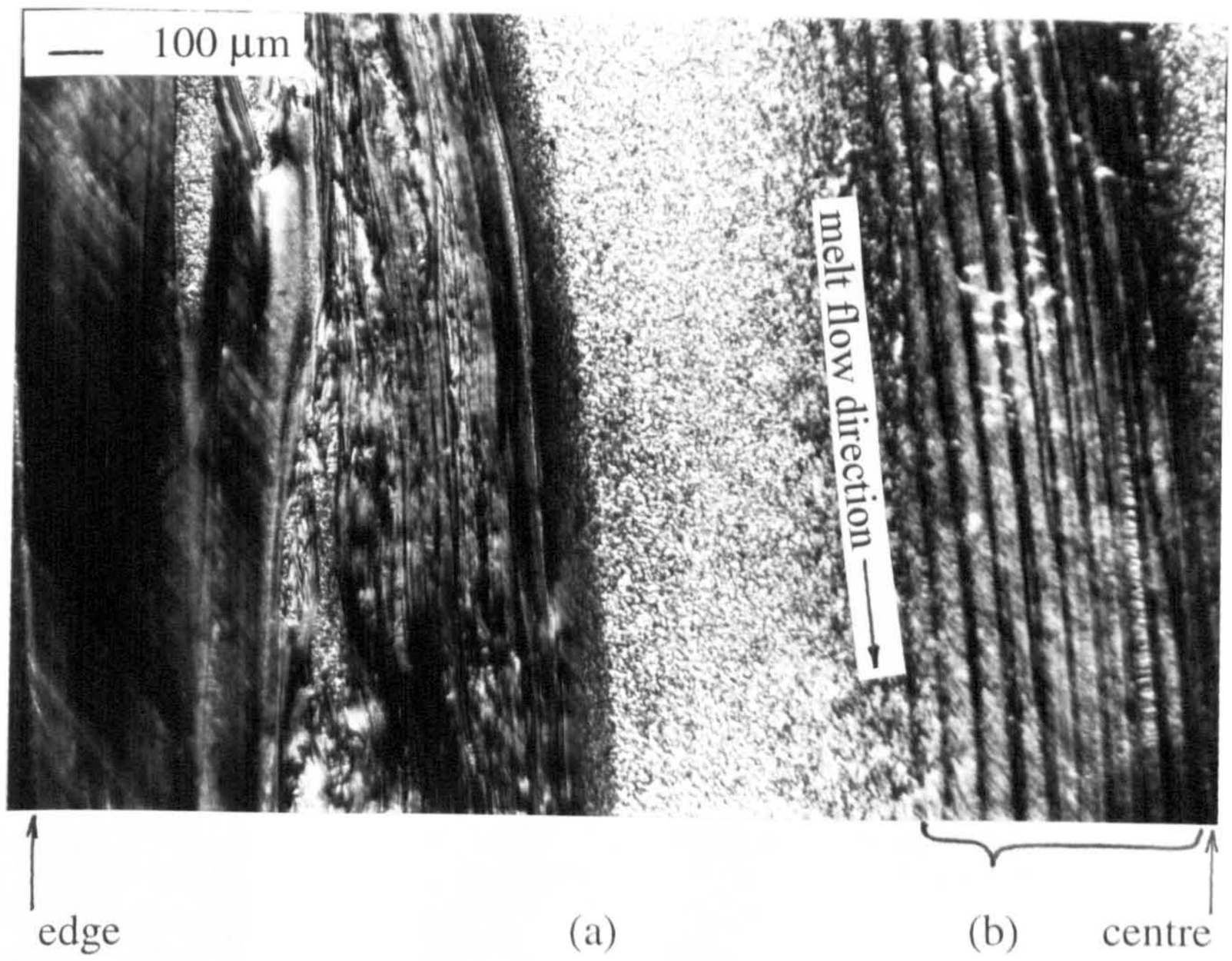

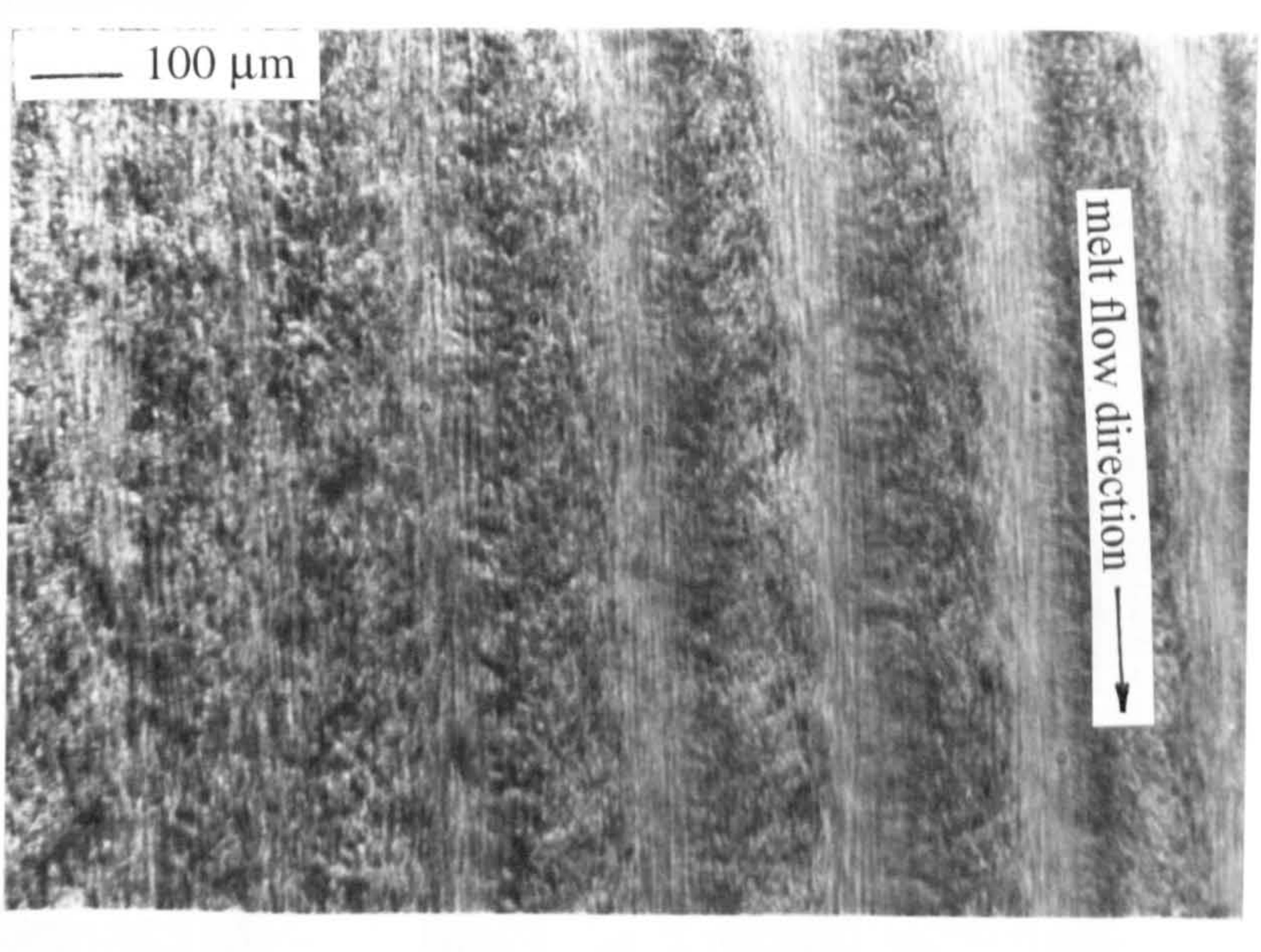

(b)

Figure 3.6 Micrographs of the high magnification at the gate A region of the MLFM-R1 ring moulding

(a) part of cross section parallel to melt flow direction

(b) high magnification of lamellar structure

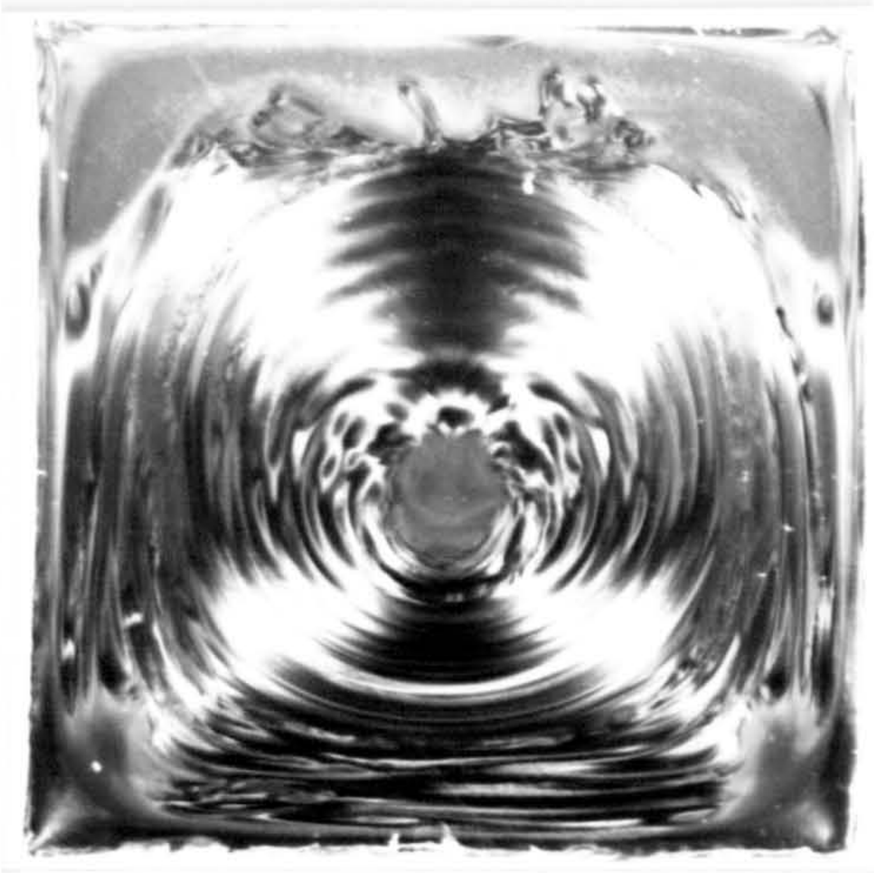

SCORIM-1A
(40°C / 215°C / 40bar)

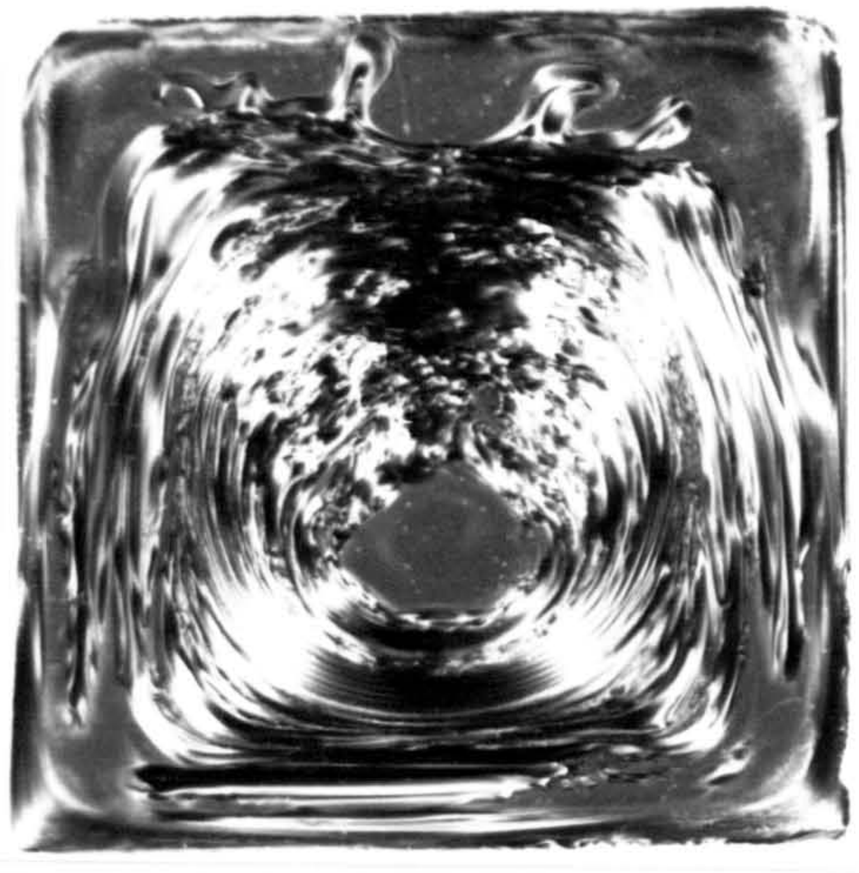

SCORIM-1B
(40°C / 215°C / 80bar)

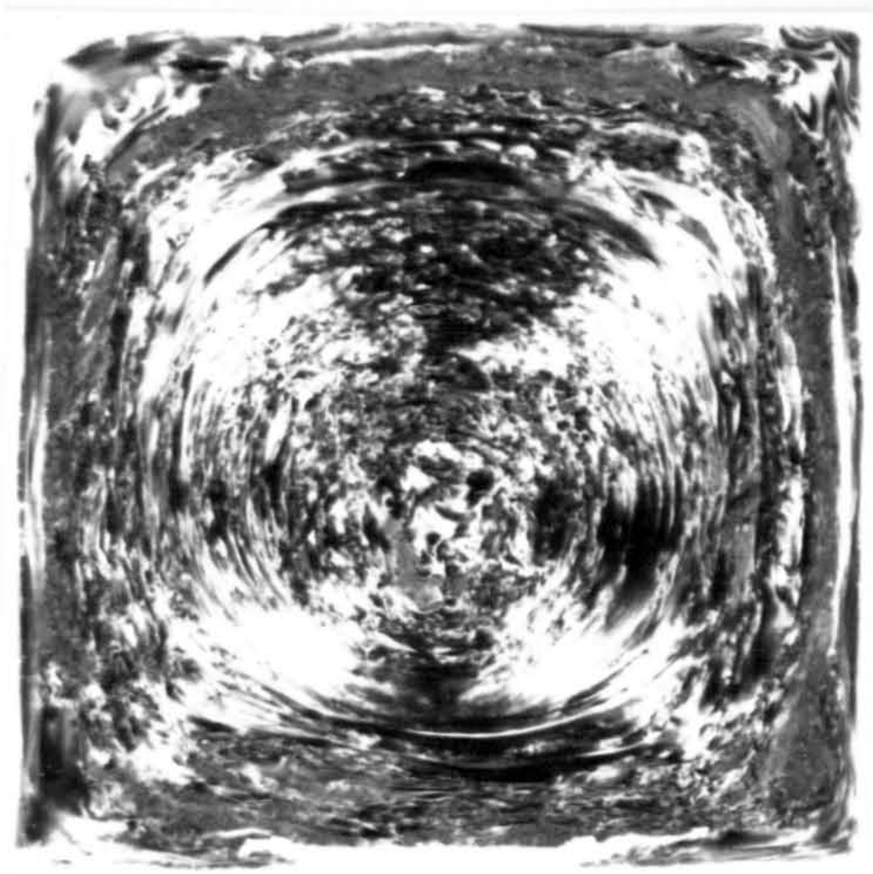

SCORIM-1C
(40°C / 215°C / 120bar)

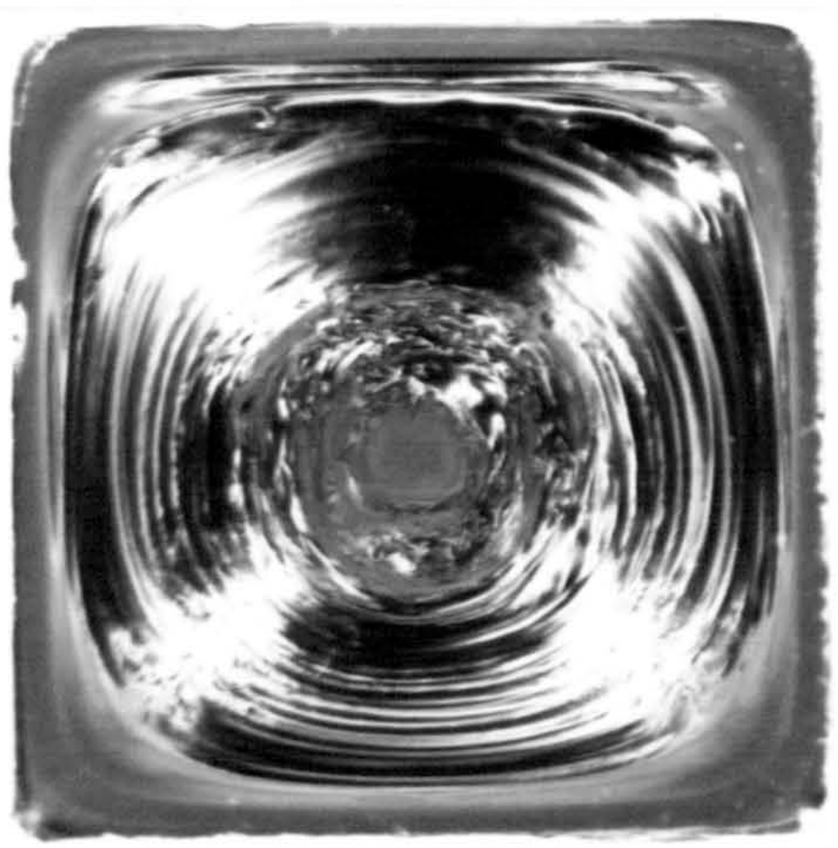

SCORIM-2A
(80°C / 215°C / 40bar)

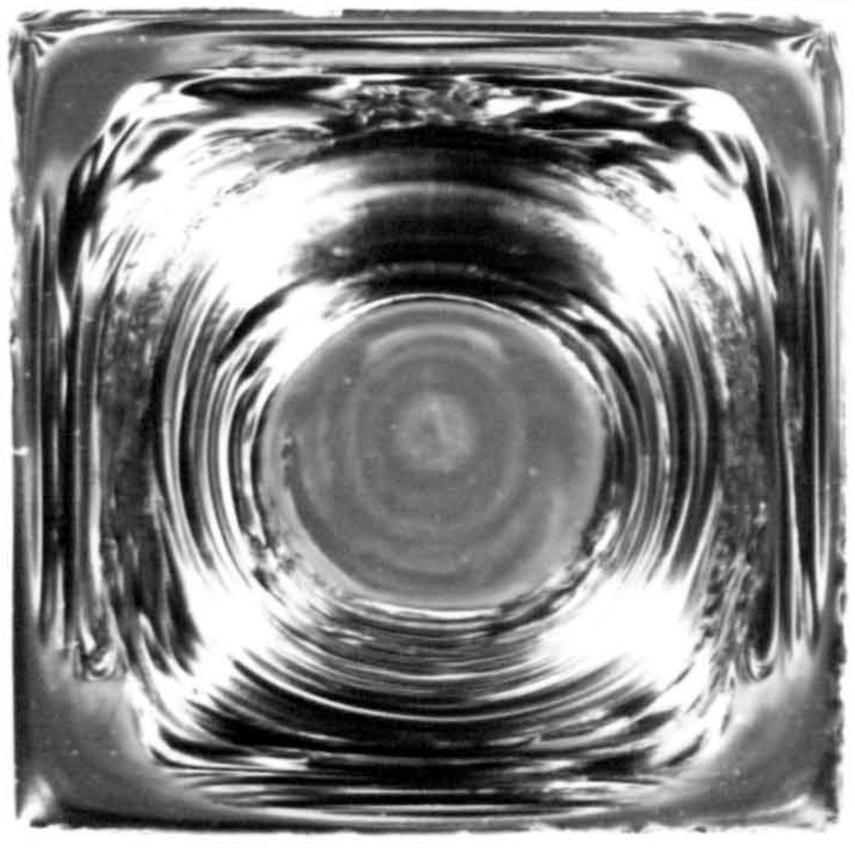

SCORIM-2B
(80°C / 215°C / 80bar)

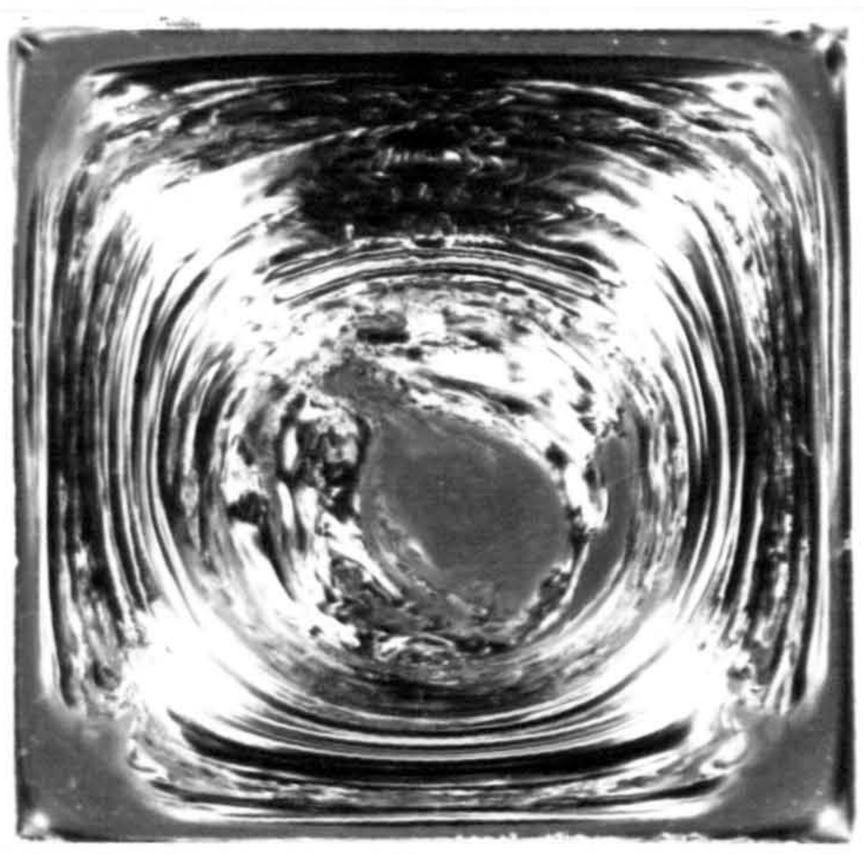

SCORIM-3B
(80°C / 265°C / 80bar)

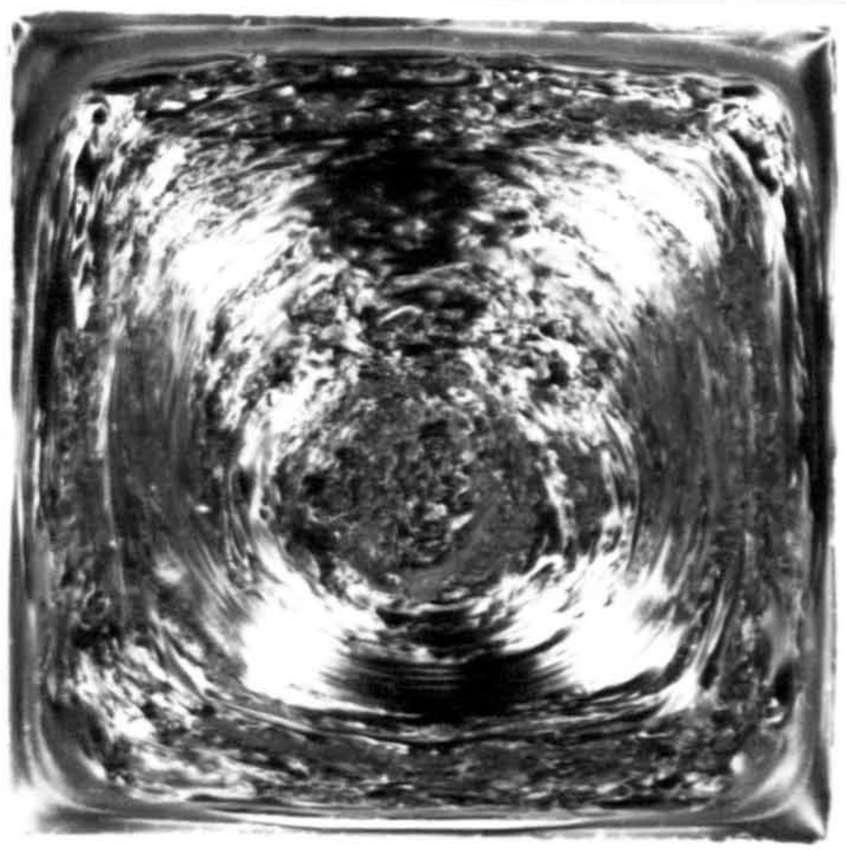

SCORIM-2C
(80°C / 215°C / 120bar)

1 mm

Figure 3.7 Photographs of whole cross sections perpendicular to the melt flow direction at 1mm away from the gate edge in SCORIM rectangular bar samples

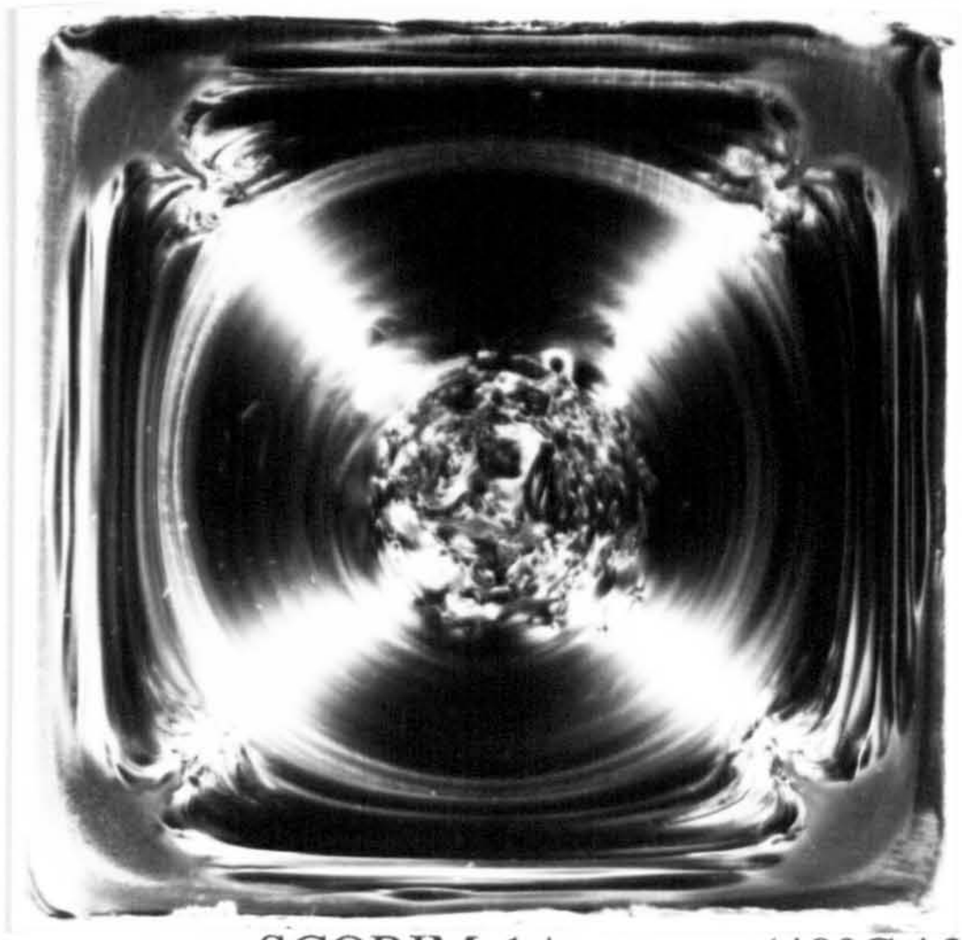

SCORIM-1A (40°C / 215°C / 40 bar) SCORIM-1A

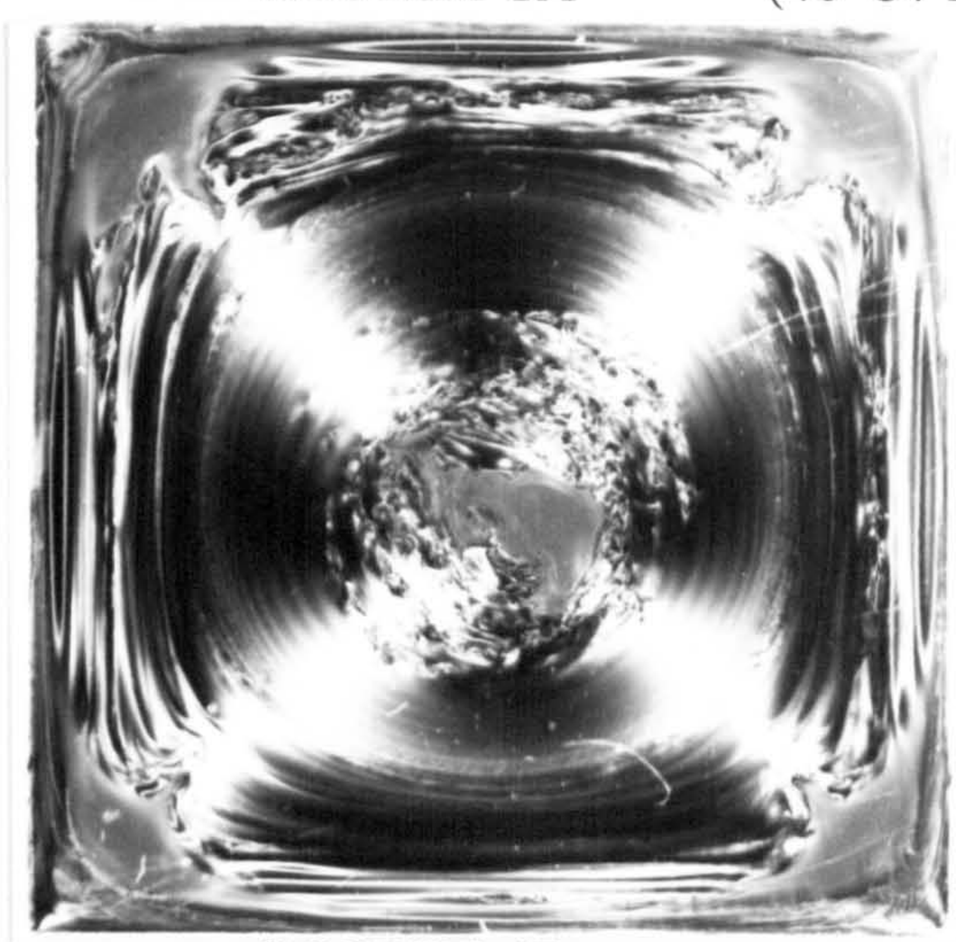

SCORIM-1B (40°C / 215°C / 80 bar) SCORIM-1B

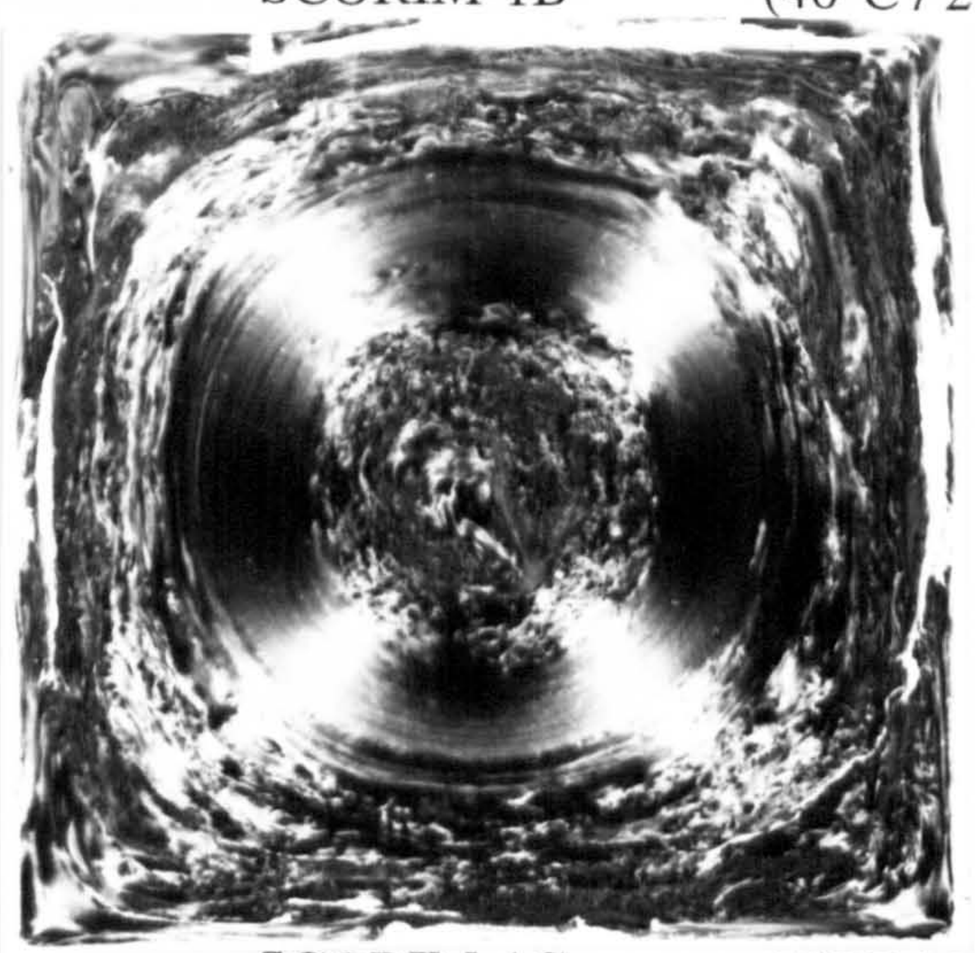

SCORIM-1C (40°C / 215°C / 120 bar) SCORIM-1C

—— 1 mm

Figure 3.8a The photographs of sections in the main part of SCORIM rectangular bar moulding:

(Processing condition: mould temperature / nozzle temperature / hold pressure)
(i). whole cross-section perpendicular to the melt flow direction (left side photo)
(ii). part of cross section parallel to the melt flow direction (right side photo)

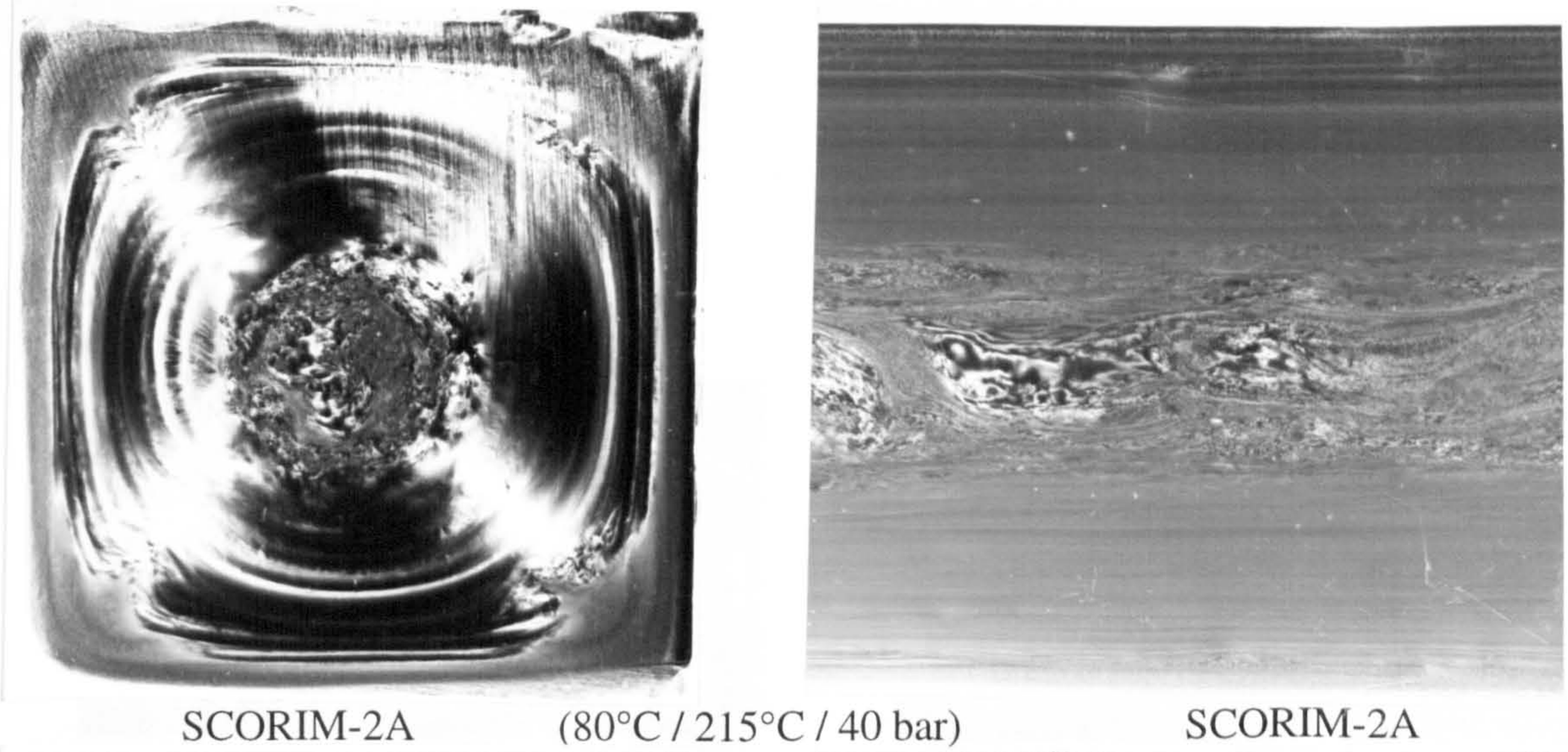

Figure 3.8b The photographs of the sections in the main part of SCORIM rectangular bar moulding:

(Processing condition: mould temperature / nozzle temperature / hold pressure)
(i). whole cross section perpendicular to the melt flow direction (left side photo)
(ii). part of cross section parallel to the melt flow direction (right side photo)

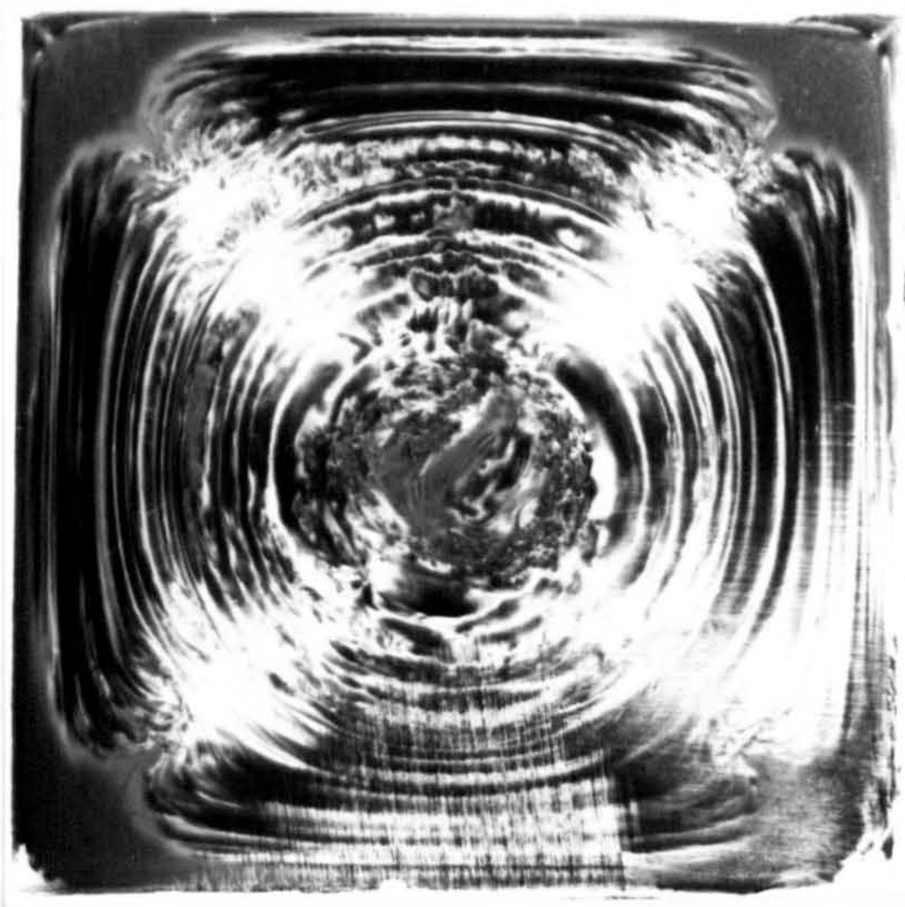

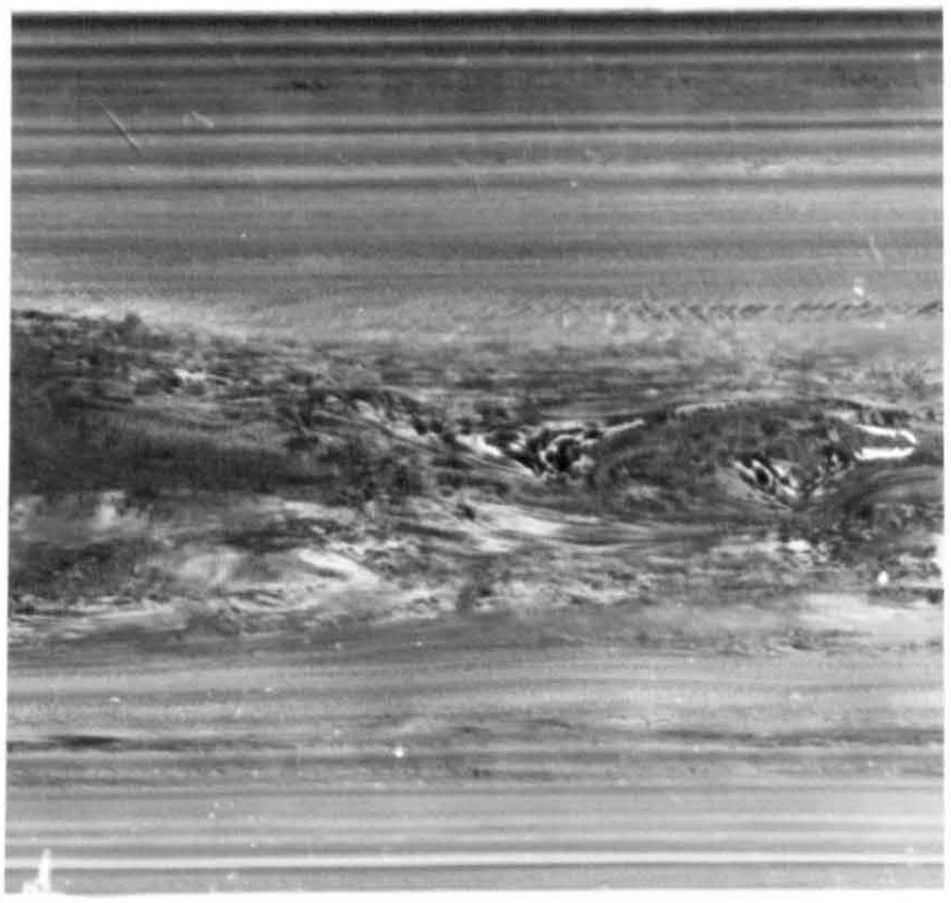

1 mm

SCORIM-3B (80°C / 265°C / 80 bar) SCORIM-3B

Figure 3.8c The photographs of the sections in the main part of SCORIM-3B rectangular bar mouldings:

(Processing condition: mould temperature / nozzle temperature / hold pressure)

(i). whole cross section perpendicular to the melt flow direction (left side photo)

(ii). part of cross section parallel to the melt flow direction (right side photo)

bar mouldings produced using SCORIM and conventional processing conditions. The samples were taken from the main part of the bar mouldings. In the main part of all conventional bar mouldings, the spherulitic microstructure was obtained from the cross sections through the moulding thickness and no shear related structure was observed in these sections. The difference in the micrographs of the SCORIM samples is that the area of the core of the SCORIM-2CM2 moulding is slightly larger than the SCORIM-2C and SCORIM-2CM1 mouldings, and it exhibited a morphology representative of a high shear traces in the core region. Under the limited magnification of polarizing light microscopy, it is difficult to identify differences of further fine details in the mouldings produced using the SCORIM-2C, SCORIM-2CM1 and SCORIM-2CM2 processing conditions. However, the results of x-ray scattering reveal differences details in concentrations of the crystal phases corresponding to processing conditions. The x-ray diffraction results are presented in a following section of this chapter.

There have been some optical microscopic studies of cross-sections of injection moulded crystalline parts [121]. High levels of orientation are found in the area near the mould walls and more isotropic character in the centre of the cross-section. Clark and Heckmann have shown the existence of row structures presumably folded chain lamellae in injection moulded parts using TEM [122, 123]. The core of injection moulded parts is found by optical microscopy to be spherulitic. The outer layers have been found to possess more oriented structures.

3.3 TEM Studies of Injection Moulded iPP

The moulding produced by the SCORIM-2CM2 injection condition was selected for etching and subsequent preparation of replicas for examination with the TEM.

TEM micrographs show (Figure 3.10), in the skin layer, lamellaes are perpendicular and parallel to the melt flow direction. By the SCORIM, iPP melt crystallised under a high shear pressure during injection and solidifying. This is particularly notable near the mould surface. It is considered that the skin layer composed of "shish-kebab" like main skeleton structures, whose c-axis is parallel to the melt flow direction, piled epitaxially with a*-axis oriented lamellar substructure. Crystalline lamellaes, which are "kebabs" fill space, and fibrous crystals which are "shishes"

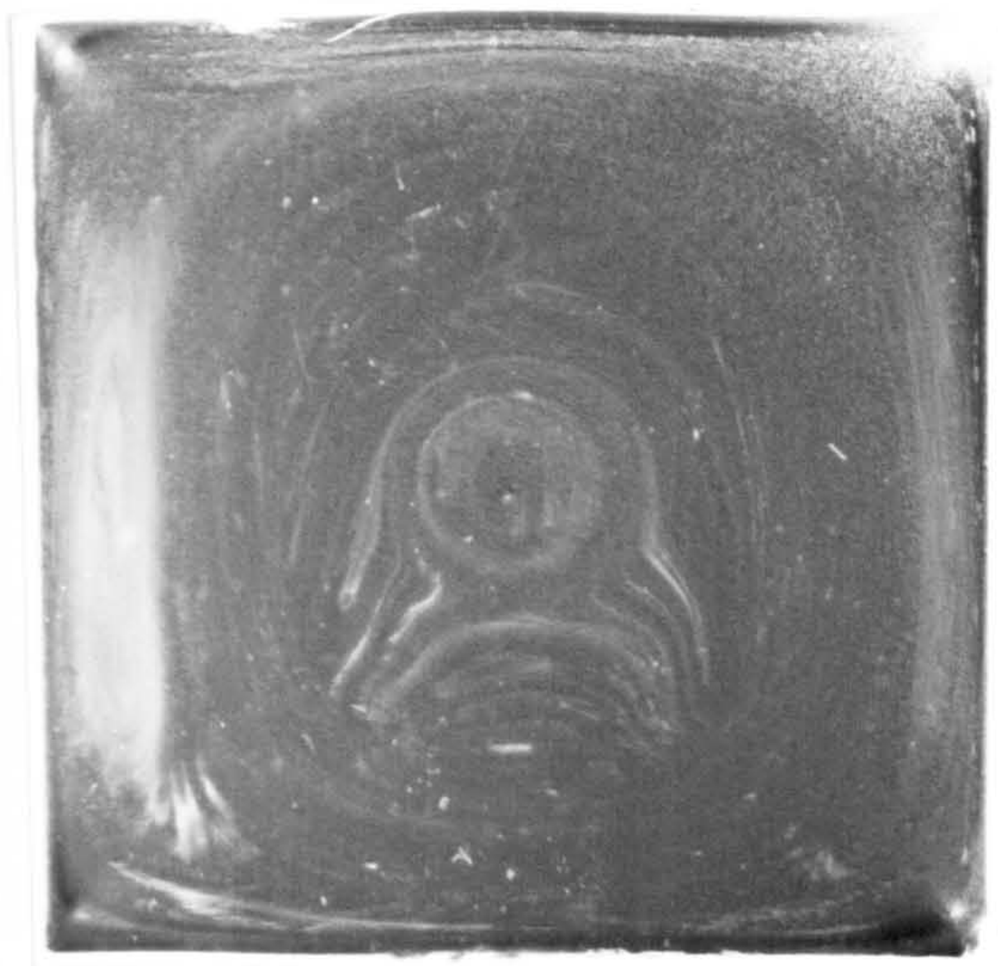

conventional-2B
(80°C / 215°C /80 bar)

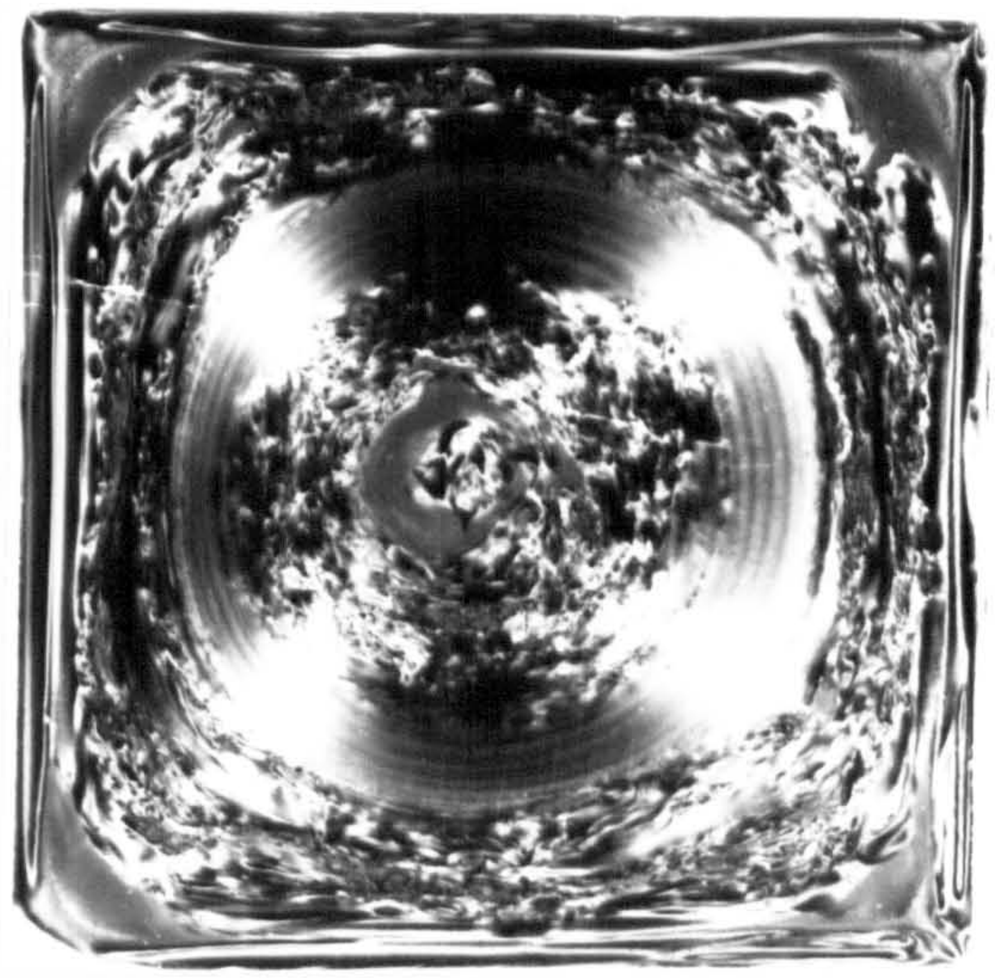

SCORIM-2C

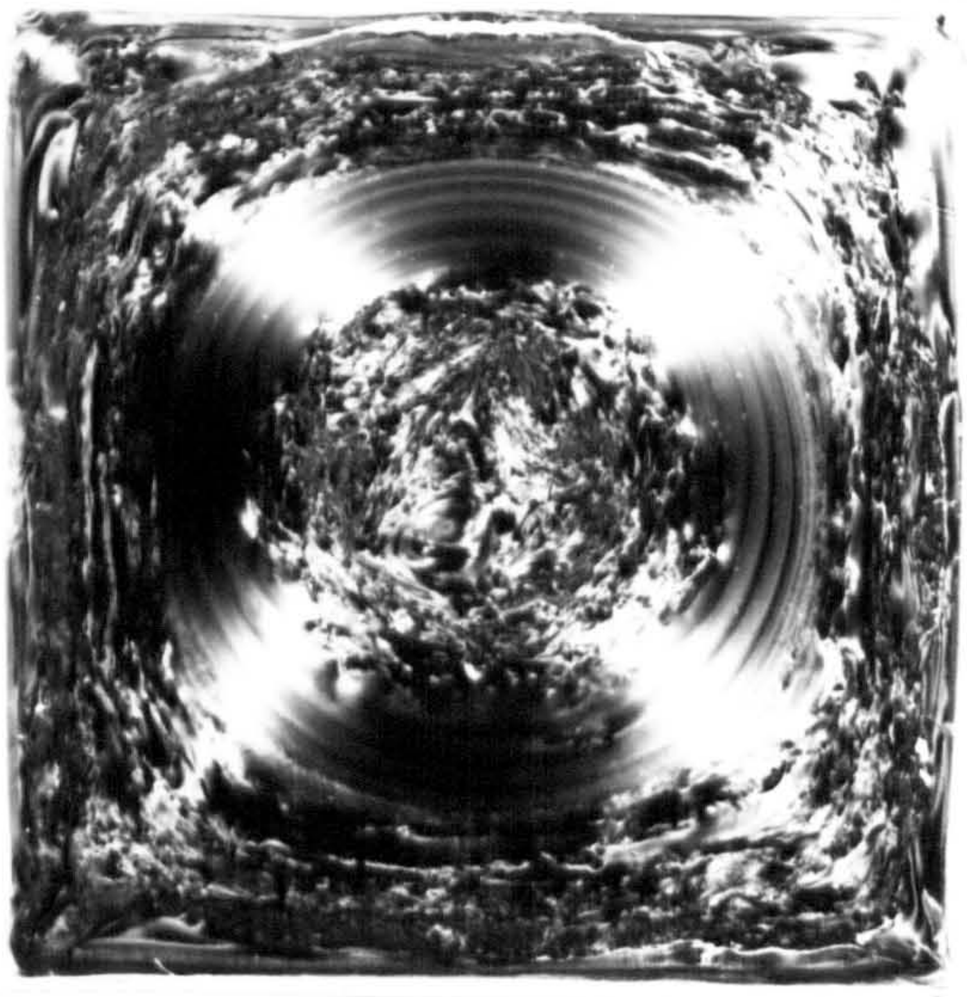

SCORIM-2CM1

1 mm

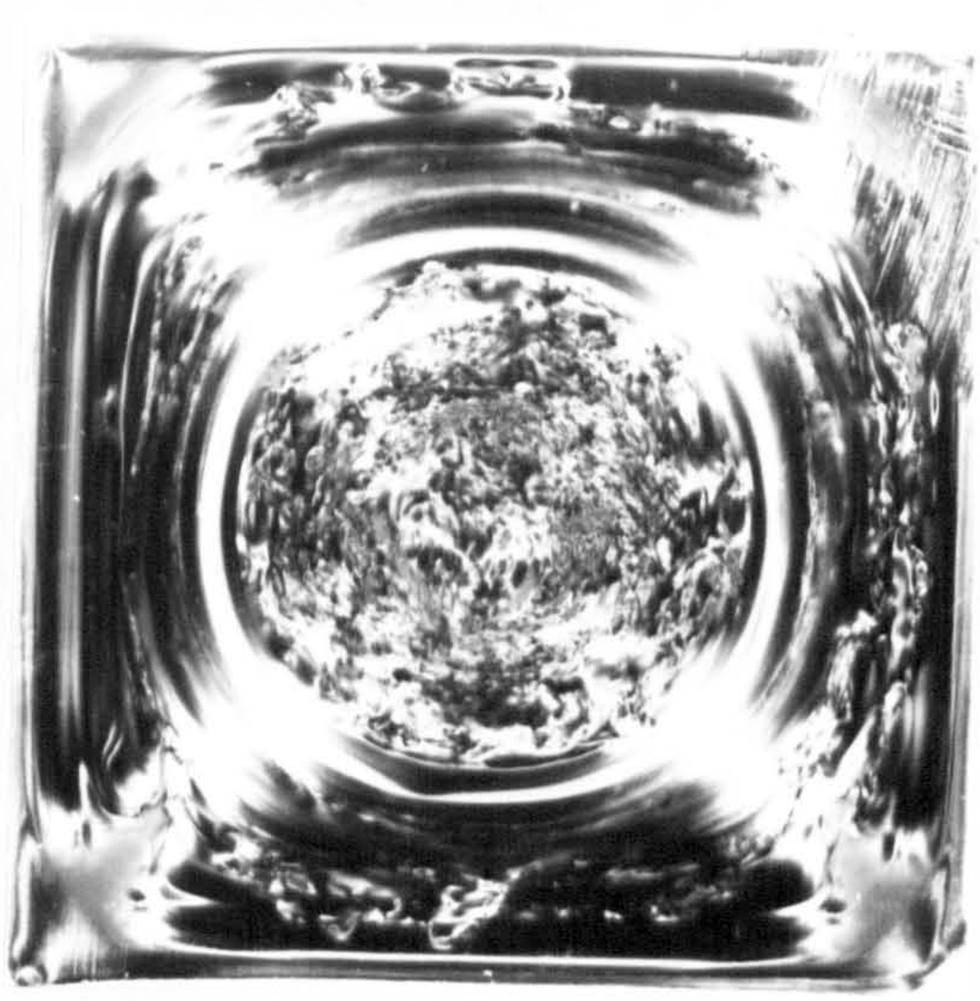

SCORIM-2CM2

Figure 3.9 Photographs of whole cross sections perpendicular to melt flow direction in the main part of SCORIM and conventional rectangular bar mouldings

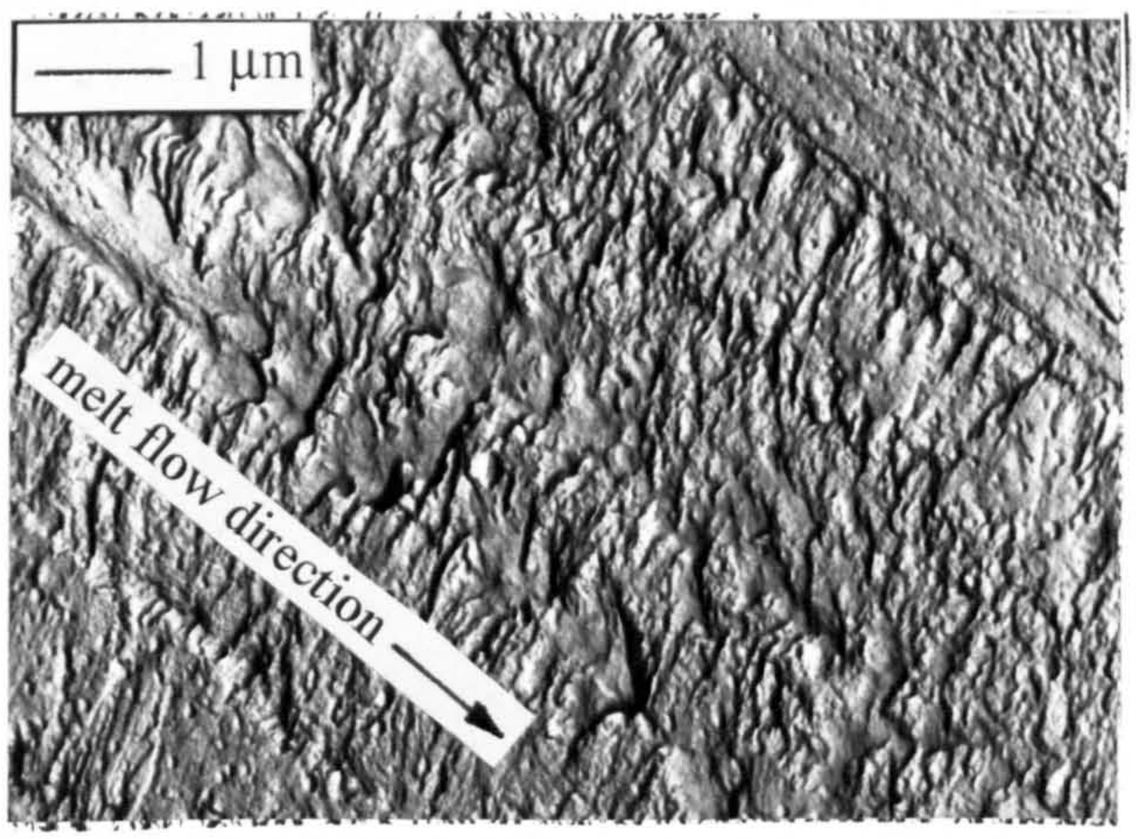

(a)

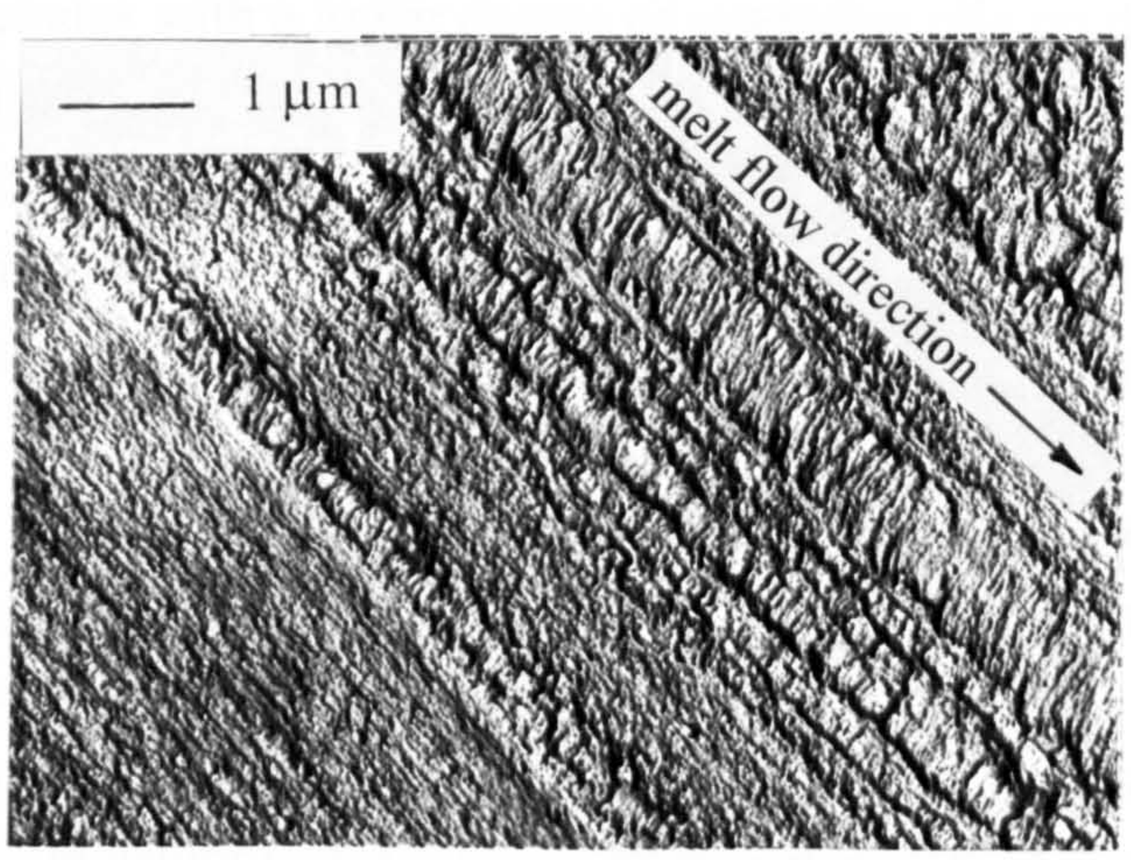

(b)

Figure 3.10 TEM micrographs of the skin region of SCORIM-2CM2 rectangular bar moulding;
magnification ×10,000

penetrate them in the melt flow direction. Some kebabs are linked up with neighbouring kebabs. Although only shishes are as linkage in melt flow direction, in actually, it is considered that there also exists tie molecules which link the kebabs in the melt flow direction. Small and nonuniform lamellae whose a*-axes are parallel to melt flow direction pile epitaxially on the c-axis oriented lamellae which are a component (kebabs) of the shish-kebab main skeleton structure. Amorphous chains fill the space of the above mentioned crystalline structure. The skin layer exhibited a mixed c-axis and a*-axis orientation to melt flow direction which Clark explained its formation by assuming that c-axis oriented component was formed first and a*-axis component was formed by epitaxial overgrowth on the c-axis oriented substrate [124].

Fujiyama explained the formation mechanism of the shish-kebab [125]. Since a melt near the mould cavity surface is applied a high shear stress in injection moulding, the molecular chains in it are extended. On crystallisation by cooling, molecular chains with a high degree of extension gather first and form fibrous crystals and, then, molecular chains with a lower degree of extension pile on the fibrous nuclei by chain folding. Thus, a shish-kebab structure is formed. At this time, a part of molecular chains are rejected from forming lamellae, remain in the space of the main skeleton structure, then do a secondary crystallisation and pile epitaxially on the main skeleton structure. Thus, a*-axis oriented lamellae are formed.

The morphology in the shear layer (Figure 3.11) shows pronounced orientation in all cases (as shown in Figure 3.11a) and the fine features of the shish-kebab lamellar structure are apparent at 26,000 magnification (as see Figure 3.11b). The formation of the orientation is due to the SCORIM processing. When the melting material was sheared in the mould cavity under high oscillating pressure, the melt developed as a lamellar arrangement along the melt flow direction. The heat in the middle layer is retained for a slightly longer time than that in the skin layer, tending to increase crystallisation temperature before the melt solidified. The melt in the middle layer was oriented preferably by the SCORIM to form a highly fibrous lamellar structure in the melt flow direction.

The micrograph of the core region (Figure 3.12) shows relatively little preferential alignment. The crystallisation temperature of the material in the core was maintained for the longest time in the whole moulding. The condition provides for

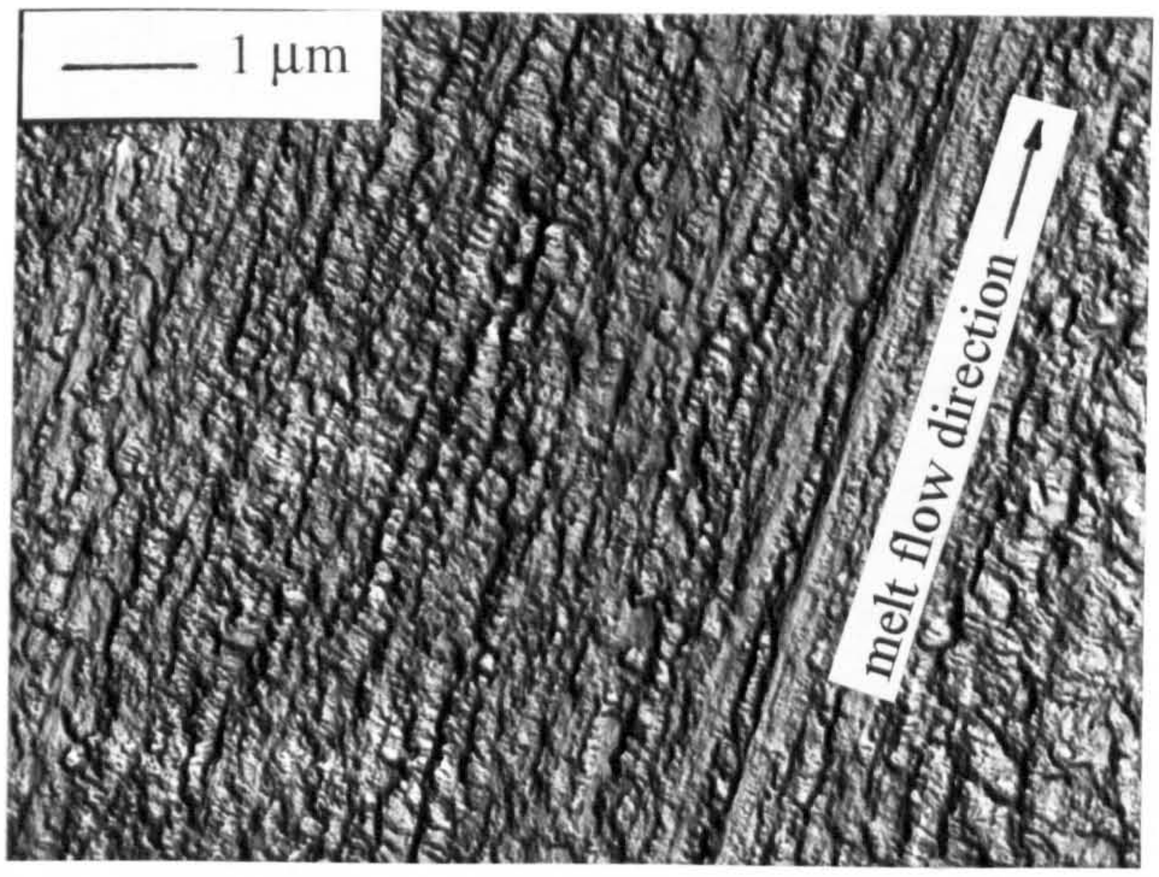

(a)

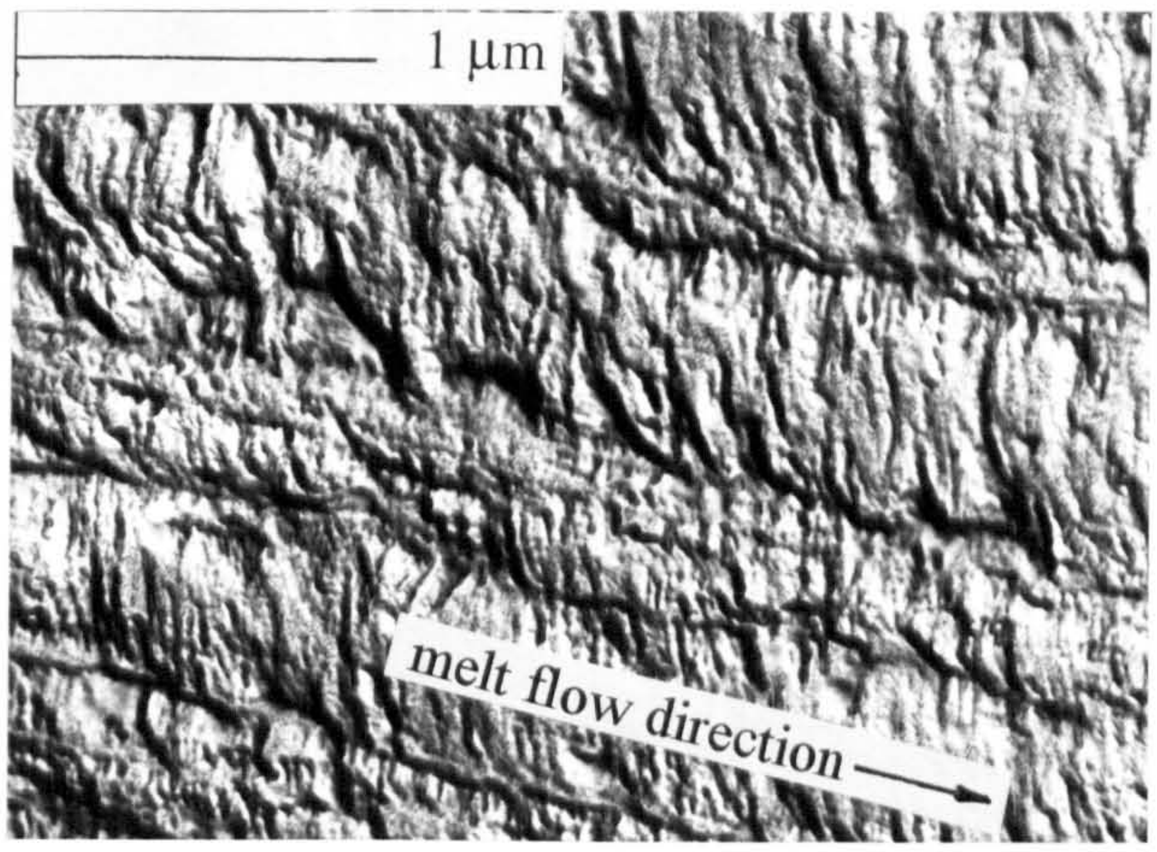

(b)

Figure 3.11 TEM micrographs of the shear region of SCORIM-2CM2 rectangular bar moulding

(a) magnification ×10,000; (b) magnification ×26,000

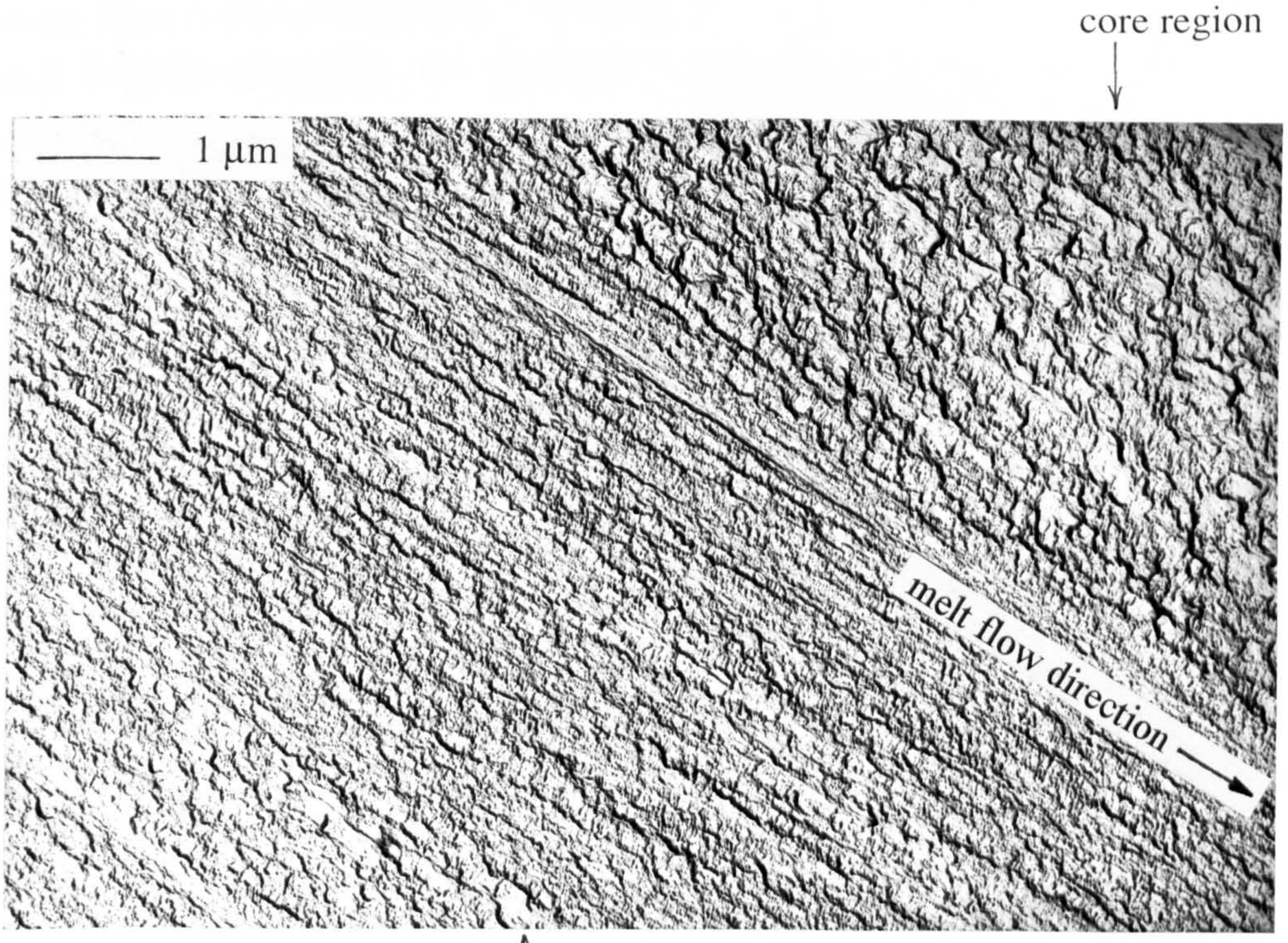

Figure 3.12 TEM micrograph of the shear and core region of SCORIM-2CM2 rectangular bar moulding

magnification ×13,200

larger spherulite size in the core region.

Figure 3.13 shows the schematic model of shish-kebab structure.

For the conventional-2C rectangular bar sample, the emanation of crystalline morphology from a central aggregate was observed in the TEM. Figure 3.14 shows the typical α-phase spherulite and the cross bands of four spherulites. Under the TEM, the spherulitic structures were viewed from skin layer to core region of the conventional injection moulding.

3.4 Microhardness Testing of Injection Moulded iPP

In the microhardness measurements, a Leitz Wetzlar machine (model 7640, Germany) was used to examine the diamond indentation. The lengths of the two diagonals of the diamond indentation are designated as X and Y respectively. Y is parallel to the melt flow direction and X is perpendicular to the melt flow direction. The diagonal lengths of the indentation can reflect the distribution of the hardness and can be related to the anisotropy of microstructure. The samples were prepared for examination by polishing and then coated with carbon.

The dependence of Vickers microhardness (HV) on position through the thickness of MLFM and conventional ring mouldings is shown in Figure 3.15. The testing positions were taken on the section parallel to the melt flow direction and midway between gates A and B, C and D. For the MLFM-R1 ring sample, the HV profiles show similar shapes in the AB region and CD region (Figure 3.15a). A relatively soft skin layer exhibited HV values between 8.9kg/mm² to 10.8kg/mm². A hard region corresponds to the middle layer with the HV peak values in the microhardness profiles which present the preferred orientation within the moulding. Light micrographs have shown the fibrous structure in this region. The core region exhibited smaller HV value than the middle layer.

The HV profile (Figure 3.15b) of the MLFM-R2 ring moulding in the CD region shows the same distribution of hardness through the moulding thickness, which containing the softest skin layer, a hard middle layer and a softer core. The HV values of the MLFM-R2 ring moulding in the CD region are smaller than those of

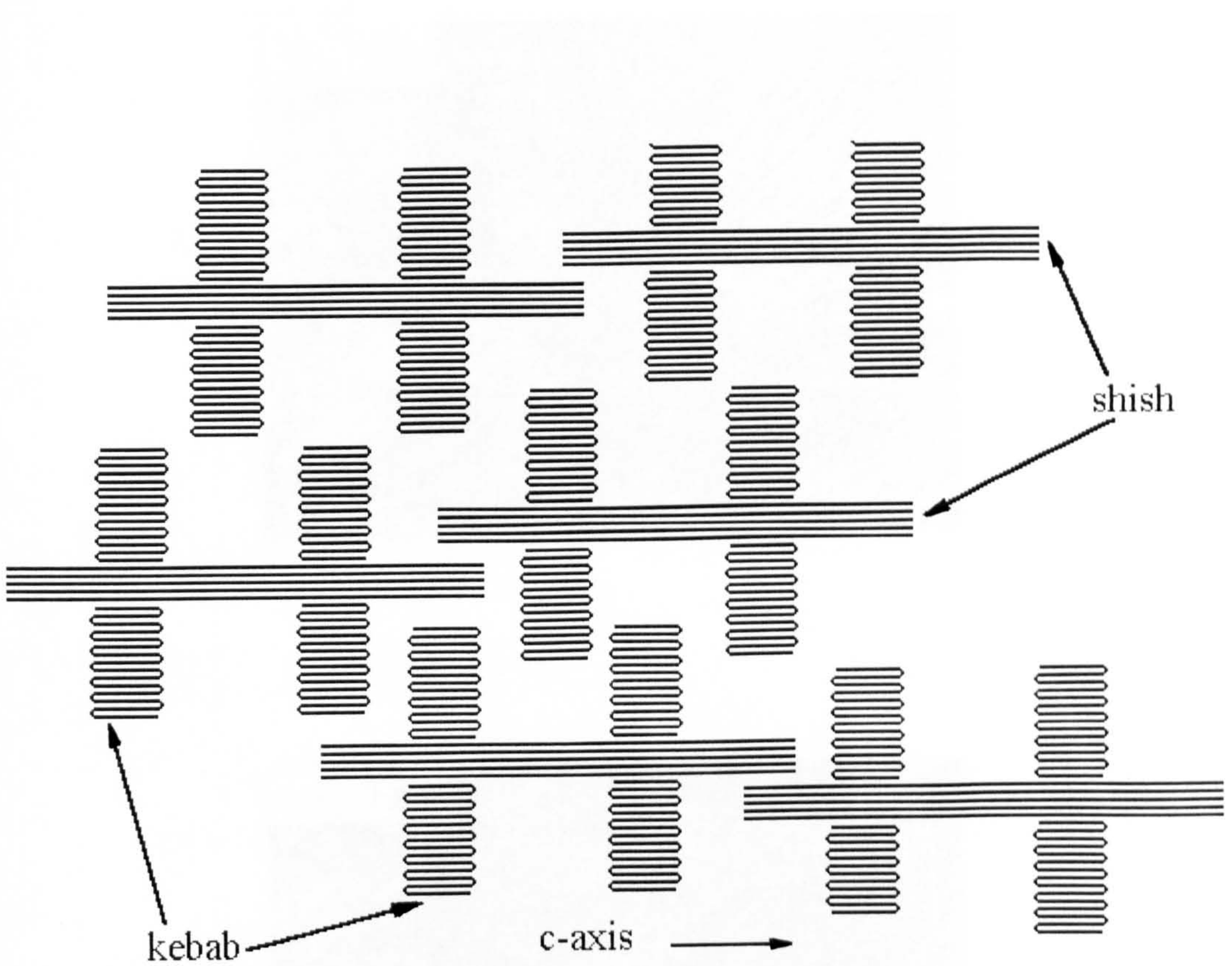

Figure 3.13 Schematic diagram showing the model of shish-kebab structure

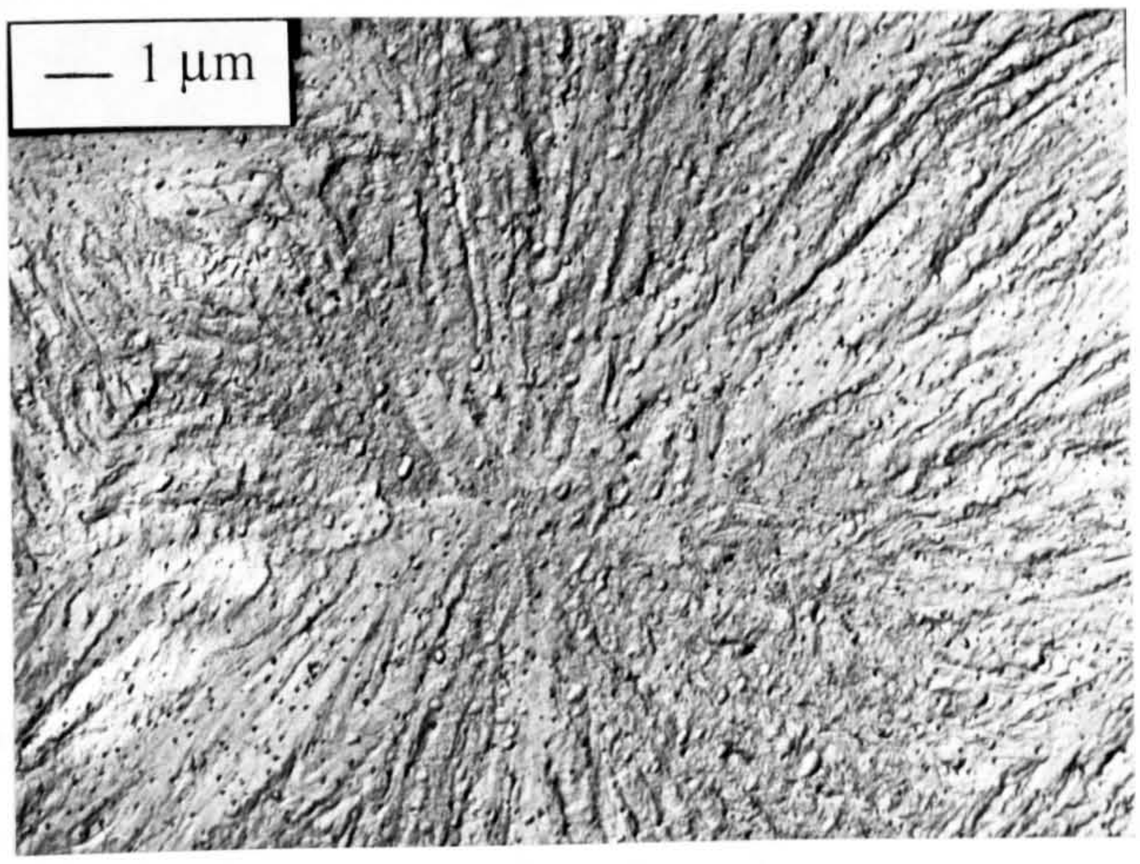

(a)

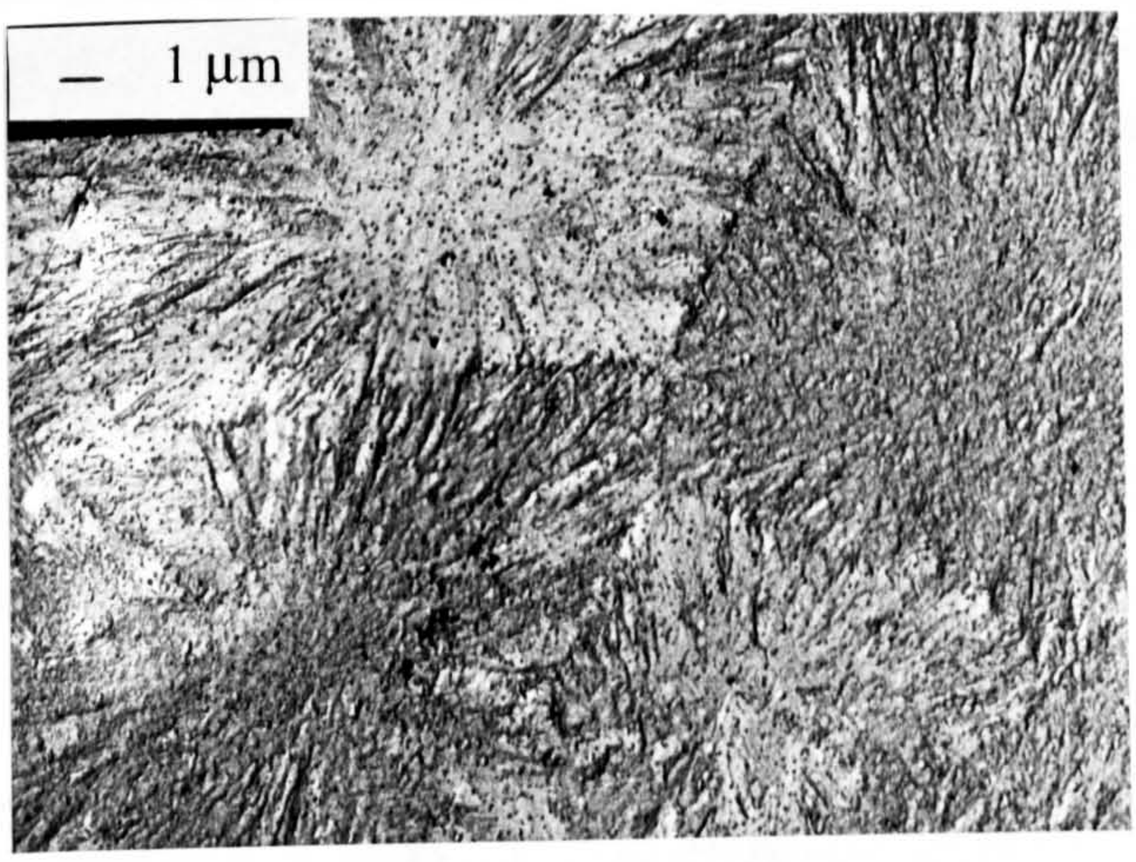

(b)

Figure 3.14 TEM micrographs of the section of conventional-2C rectangular bar moulding
(a) magnification ×5,000; (b) magnification ×3,300

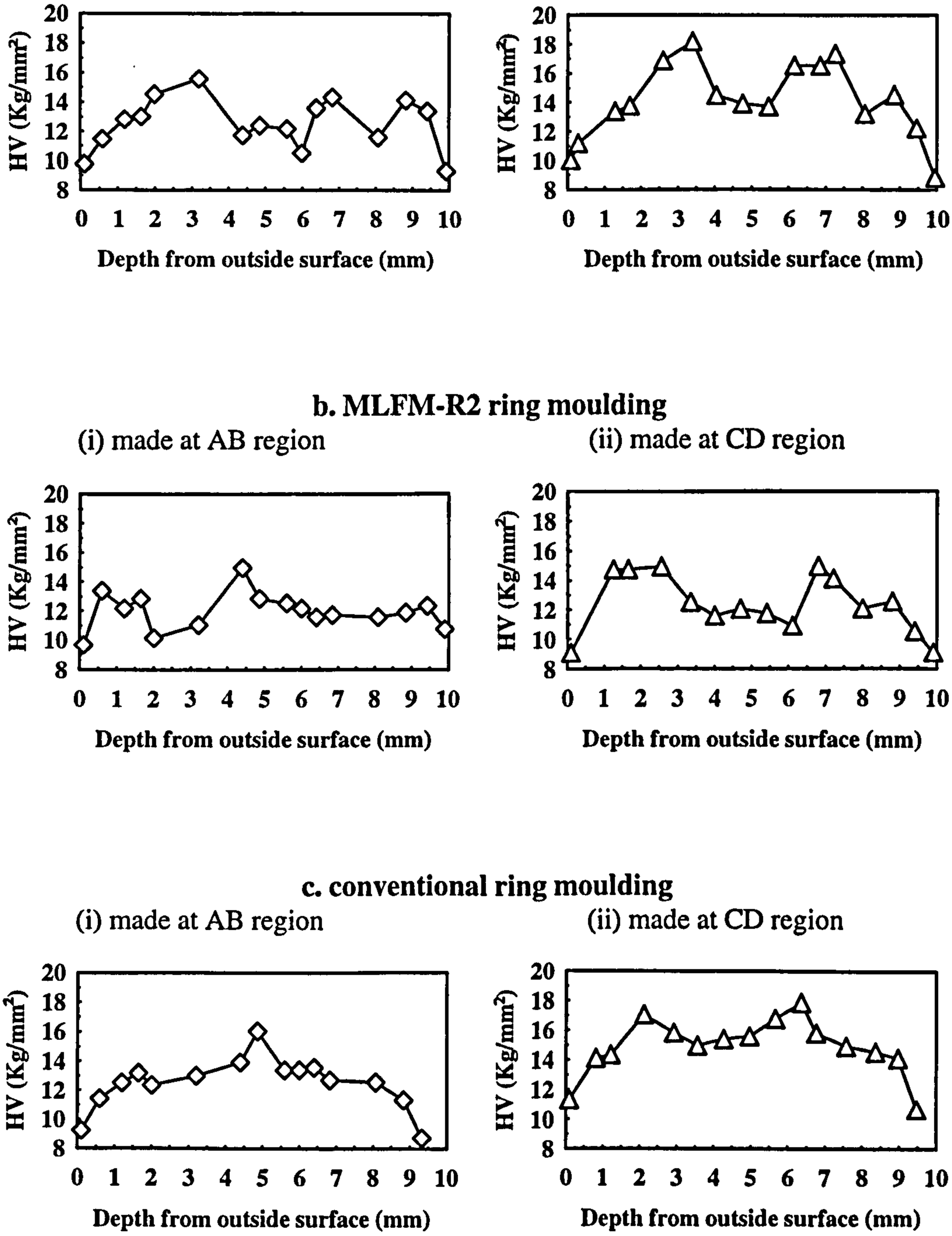

Figure 3.15 Microhardness profiles through the thickness of MLFM and conventional ring mouldings

the MLFM-R1 moulding. The HV profile of the MLFM-R2 ring moulding in the AB region shows a no considerable distribution of hardness through moulding thickness. The difference probably was attributed due to the difference in the MLFM process. In the MLFM-R1 program, the oscillation pattern of pistons was set alternately which would provide high shear stresses in the melt flow direction, relating to the fibrous texture. The melt in the weld line region was sheared to arrange to lamellar structure. In the MLFM-R2 program, the oscillating packing pattern of the pistons was set simultaneously in the processing. The compression pressure was increased when the four pistons were moved down or up together. The melt in the weld region was packed under the high compression pressure.

For the conventional ring moulding, the HV profiles show a different distribution of microhardness in the AB and CD regions (Figure 3.15c). The HV value of the AB region increased from the skin layer to the middle layer and the peak HV value is exhibited by the core region. The HV profile of the CD region gave the highest values in the middle layer, and the HV value of the core is smaller than the values recorded from the middle layer. Both AB and CD regions exhibited the softest skin layer associated with the lowest HV value.

Figure 3.16 shows the Vickers microhardness and anisotropy ratio profiles of the SCORIM-3B rectangular bar sample. The testing points were taken through the thickness on the sections parallel to the melt flow direction and they were 1mm, 2mm away from the gate edge and in the main part of the moulding. The variation in anisotropy identified by microhardness measurement is consistent with the recorded x-ray diffraction patterns and light microscopy.

When the testing sections were 1mm, 2mm away from the gate edge of the moulding, HV profiles (Figure 3.16a,b) exhibited a hard middle layer with the greater HV values, and Y was greater than X, $\Delta MH>0$. This reflects that the microstructure of the middle layer is anisotropic and the c-axis orientation is parallel to the melt flow direction. In the core region, HV profiles exhibited the smaller values, and Y was smaller than X, $\Delta MH<0$ and reflects that the a*-axis orientation exists in the direction perpendicular to the melt flow direction. The skin layer showed a relatively lower HV values. The anisotropic ratio of the skin layer exhibited both c-axis and a*-axis orientation from the region 1mm to 2mm away from the gate. In the skin layer, when the testing points were taken from the section

a. 1mm away from the gate edge

(i) Vickers microhardness

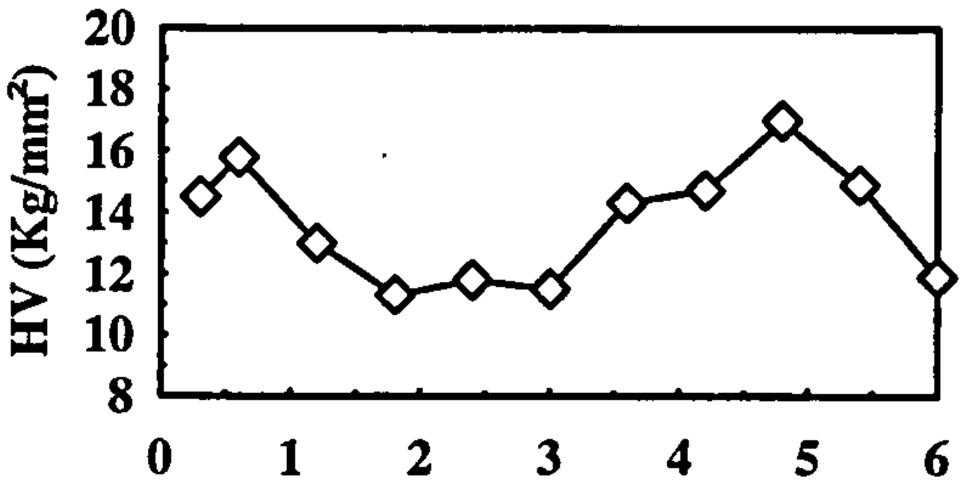

(ii) Anisotropy ratio

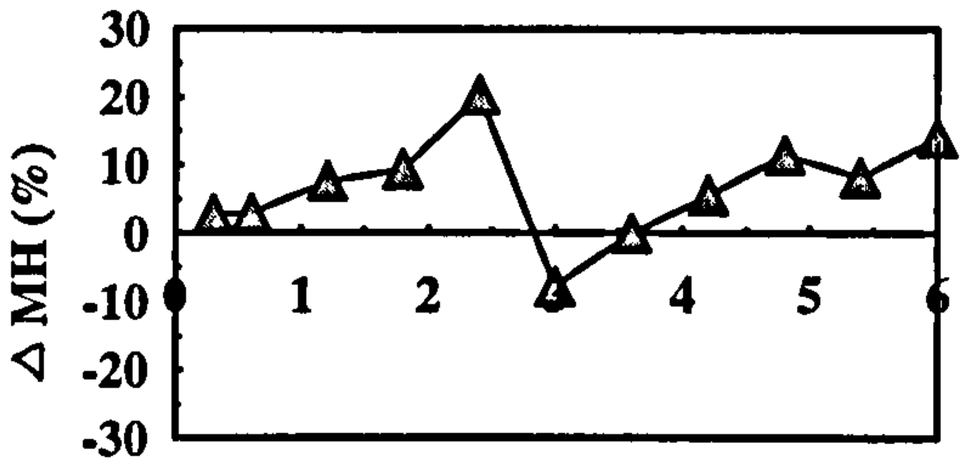

b. 2mm away from the gate edge

(i) Vickers microhardness

(ii) Anisotropy ratio

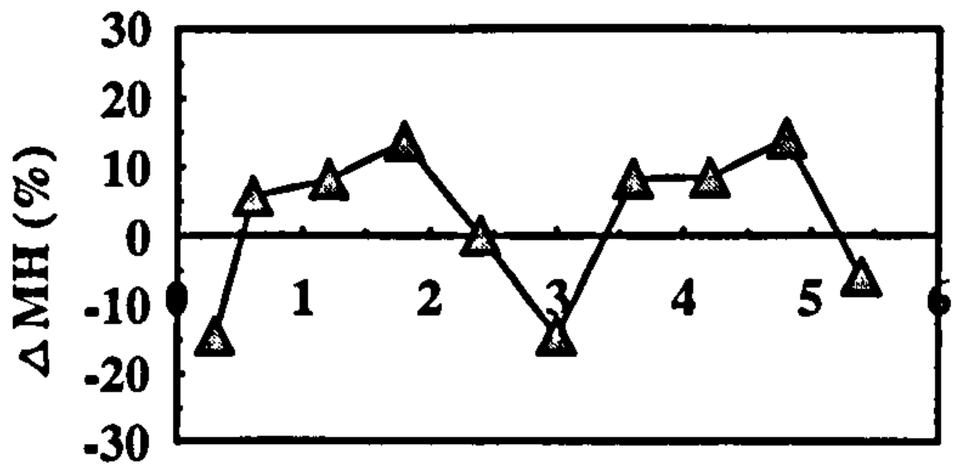

c. the main part of the moulding

(i) Vickers microhardness

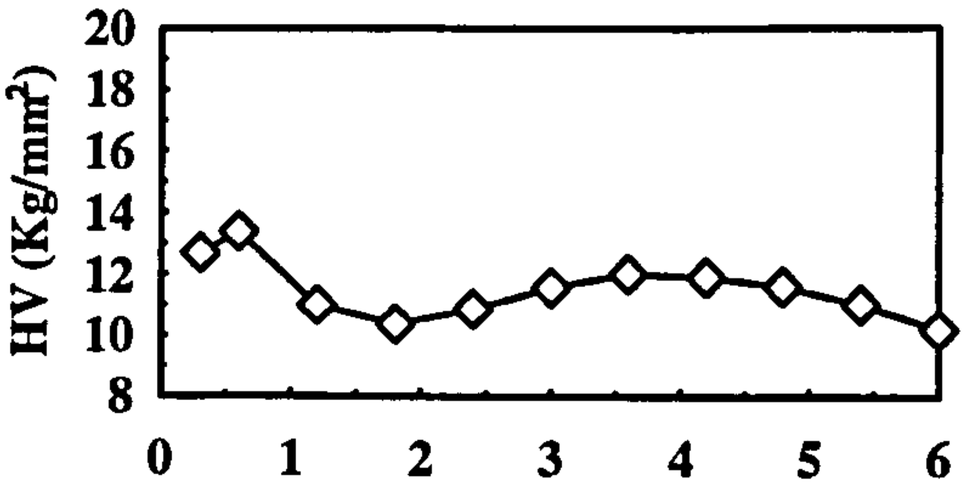

(ii) Anisotropy ratio

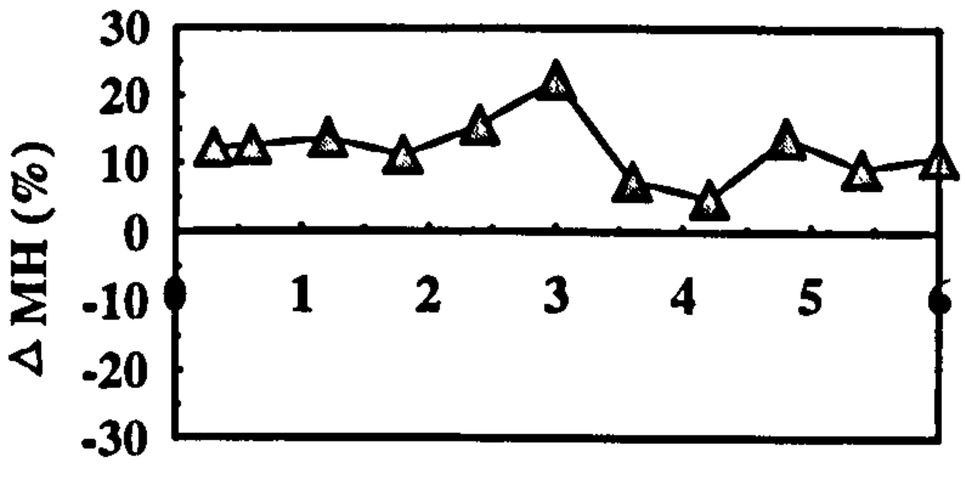

Figure 3.16 Vickers microhardness measurements of SCORIM -3B rectangular bar mouldings

1mm away from the gate, Y>X, ΔMH>0 and reflects c-axis orientation is parallel to the melt flow direction. In the section 2mm away from the gate, Y<X, ΔMH<0 and reflects a*-axis orientation is perpendicular to the melt flow direction.

Figures 3.16c shows the Vickers microhardness and anisotropy ratio profiles in the main part of the SCORIM-3B sample. It was found that Y was predominantly greater than X in the indentations produced, ΔMH>0, exhibiting the anisotropic microstructure and indicating c-axis orientation parallel to the melt flow direction.

Figure 3.17 shows the Vickers microhardness and anisotropy ratio profiles in the main part of three SCORIM mouldings (SCORIM-2C, -2CM1 and -2CM2) and conventional-2C moulding. The testing points were taken through the thickness on the section parallel to the melt flowing direction. It can be seen that the diagonal length Y was greater than X for the indentations produced in all three SCORIM moulding samples, ΔMH>0. This reflects that the microstructure of the SCORIM moulding is anisotropic and biaxial orientation is parallel to the melt flow direction. While in the case of conventional injection moulding less pronounced differences of Y and X values were recorded, ΔMH was quite close to zero and reflects the microstructure of the conventional moulding is isotropic. Microscopy and TEM observations confirmed the existence of the preferably oriented lamellar structure in the SCORIM mouldings and an equiaxed α-phase spherulites in the conventional moulding.

3.5 Distortion Measurements of Injection Moulded iPP Rings

A Mitutoyo Co-ordinate FN503 measuring machine with probe head control unit was used to measure the distortions of the MLFM and conventional ring mouldings. The results of moulding roundness, moulding flatness and surface straightness obtained with the MLFM-R1, MLFM-R2 and conventional injection processings, are summarised as follows:

1) Roundness;

In the measuring of the ring roundness, the centre of a moulding section was chosen as the reference ring. The maximum values for the distortion of roundness were

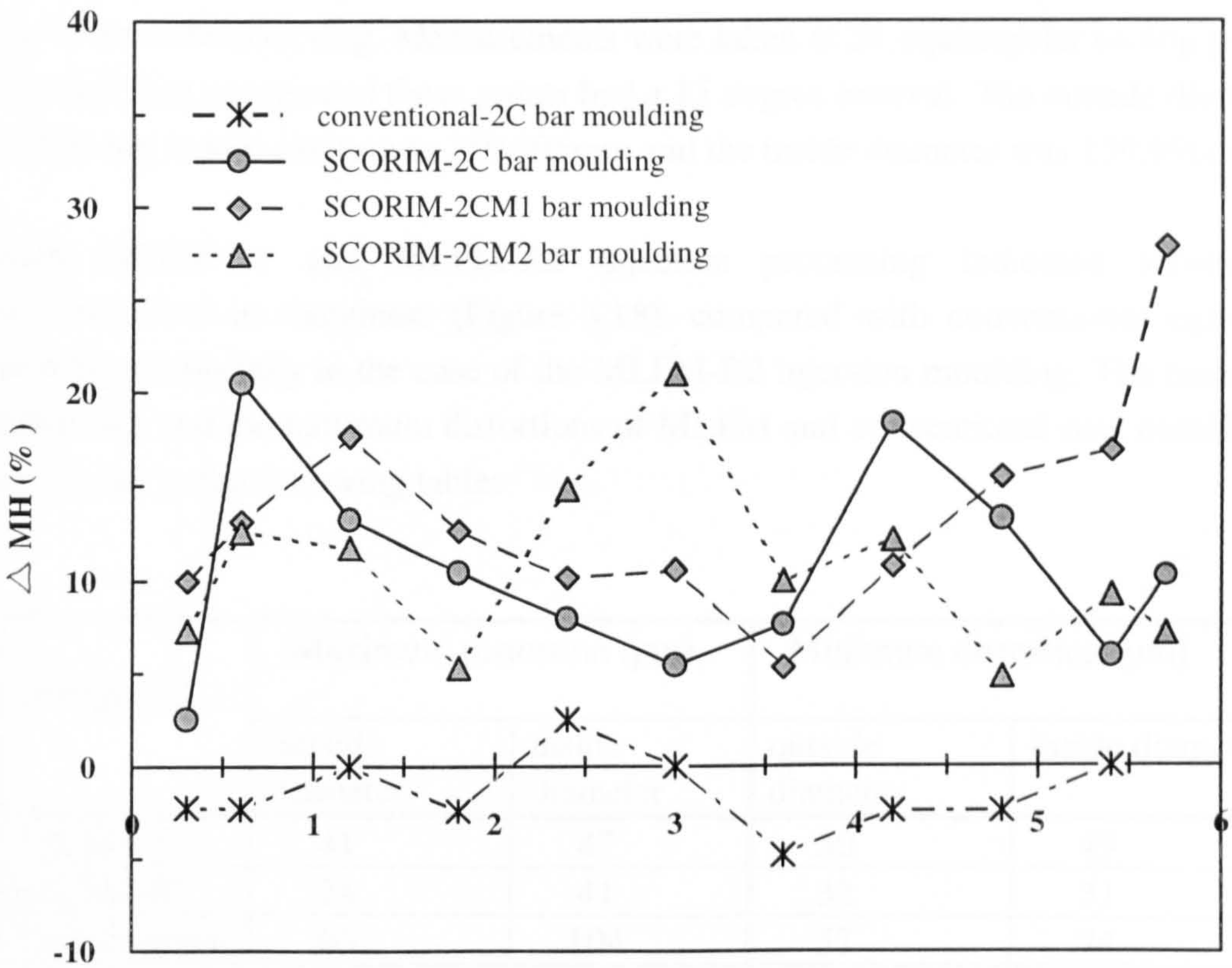

Figure 3.17 Vickers microhardness measurements of the SCORIM-2C, 2CM1, 2CM2 and conventional-2C rectangular bar moulding

taken at the furthest test point outside and inside the reference ring. The minimum values for the distortion of roundness were taken at the closest test point outside and inside the reference ring. Measurements were taken at 24 equiangular testing points for each ring sample and these points had a 15 degree interval. The outside diameter of the ring mould cavity was 159.995mm and the inside diameter was 139.996mm.

Both MLFM-R1 and MLFM-R2 injection processing indicated substantial improvements in roundness (Figure 3.18), compared with conventional injection moulding especially in the case of the MLFM-R2 injection moulding. The recorded maximum and the minimum distortions of MLFM and conventional ring mouldings are shown in the following table:

Sample I.D.	Maximum distortion (μm)		Minimum distortion (μm)	
	outside diameter	inside diameter	outside diameter	inside diameter
MLFM-R1	41	47	50	49
MLFM-R2	24	41	32	31
Conventional	66	104	57	74

The ring mouldings produced using the MLFM injection processing showed less maximum and minimum distortions on the outside and inside dimensions than conventional moulding. The MLFM-R2 ring moulding exhibited least distortion from moulding roundness than either the MLFM-R1 or conventional moulding. The ring mouldings produced by the SCORIM exhibit the better controlled dimension in the moulding roundness.

2) Moulding flatness;

In the measurements of the flatness of the ring moulding, three needles with 120 degree angle were set flat as the reference plane. Measurements were taken at 48 equiangular testing points for each ring moulding sample and every 2 testing points had a 7.5 degree angle.

Ring mouldings produced using the MLFM-R1 exhibited slightly better flatness

a. MLFM-R1 ring moulding

(i) made at outside diameter

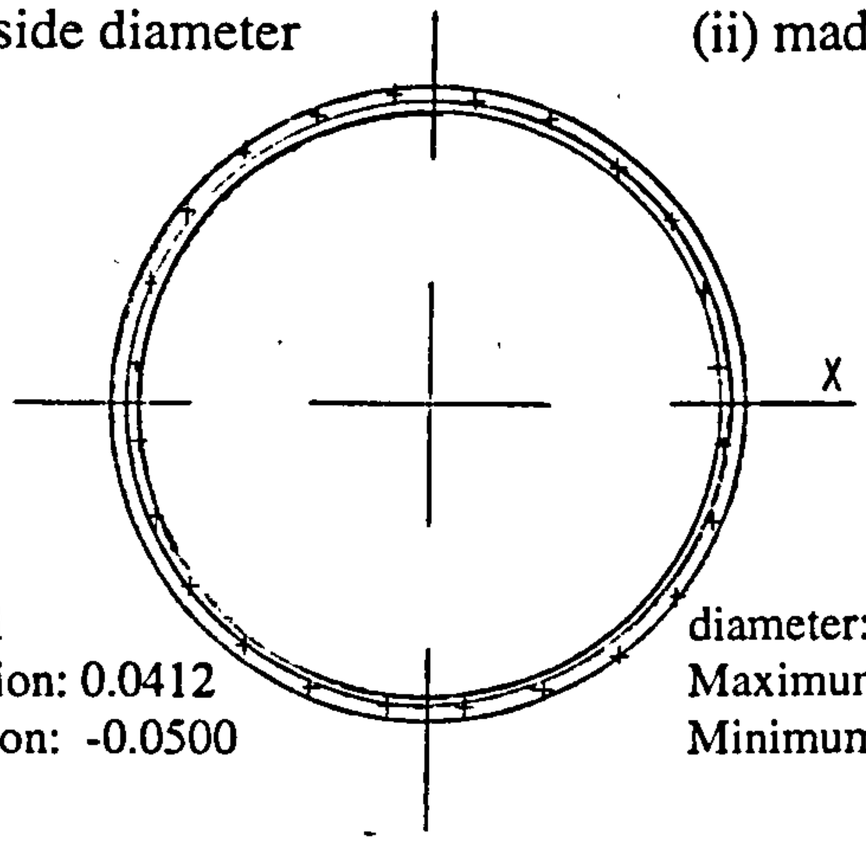

diameter: 158.291
Maximum distortion: 0.0412
Minimum distortion: -0.0500

(ii) made at inside diameter

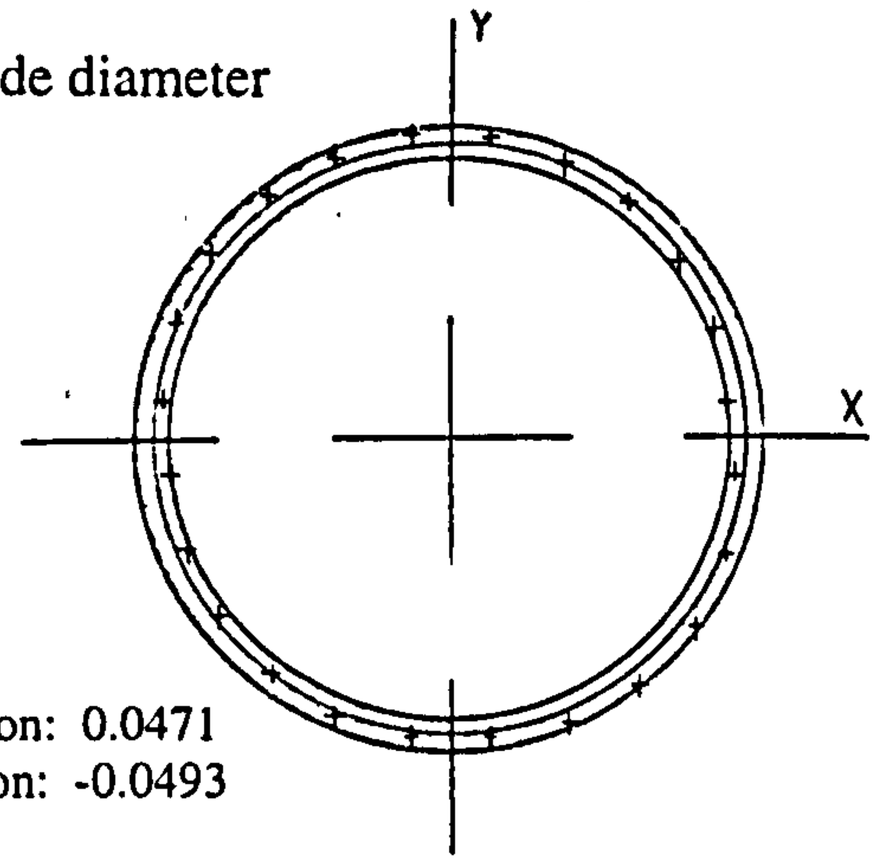

diameter: 138.342
Maximum distortion: 0.0471
Minimum distortion: -0.0493

b. MLFM-R2 ring moulding

(i) made at outside diameter

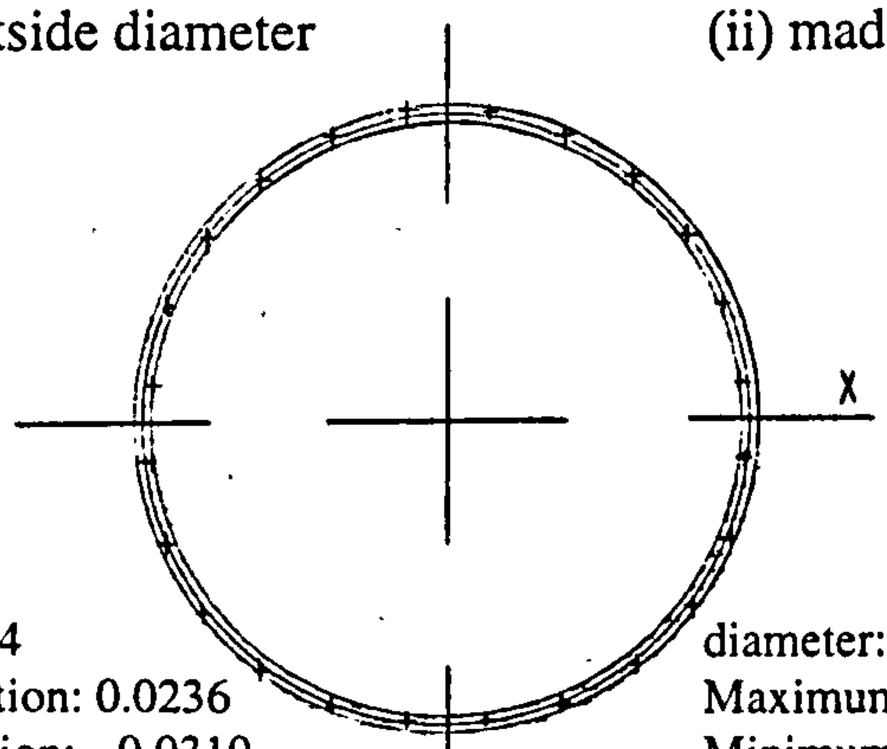

diameter: 158.204
Maximum distortion: 0.0236
Minimum distortion: -0.0319

(ii) made at inside diameter

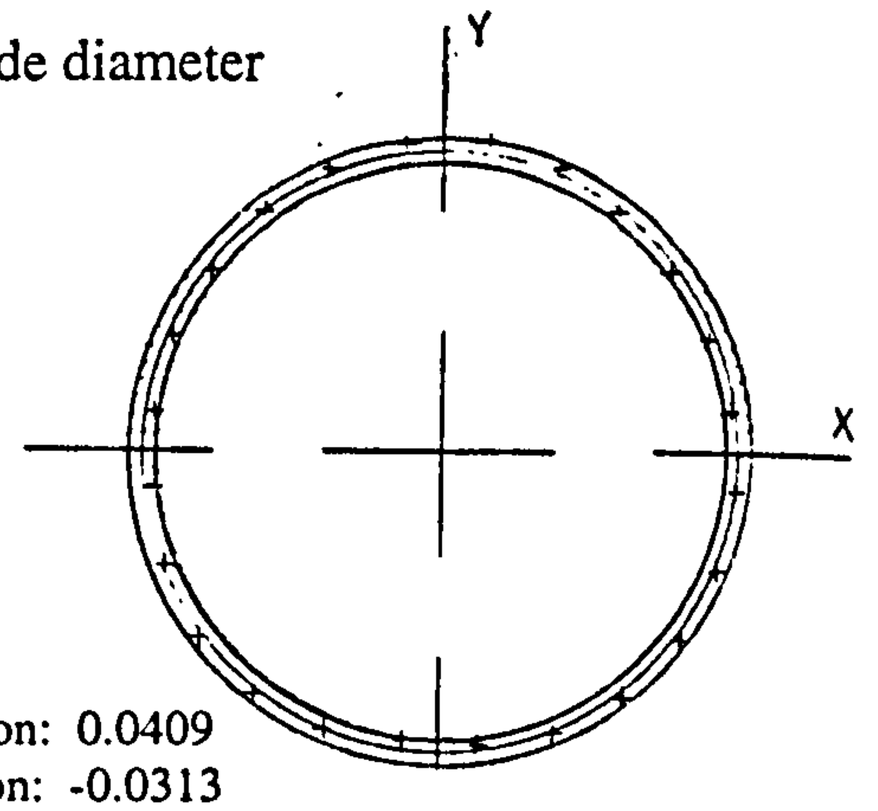

diameter: 138.249
Maximum distortion: 0.0409
Minimum distortion: -0.0313

c. conventional ring moulding

(i) made at outside diameter

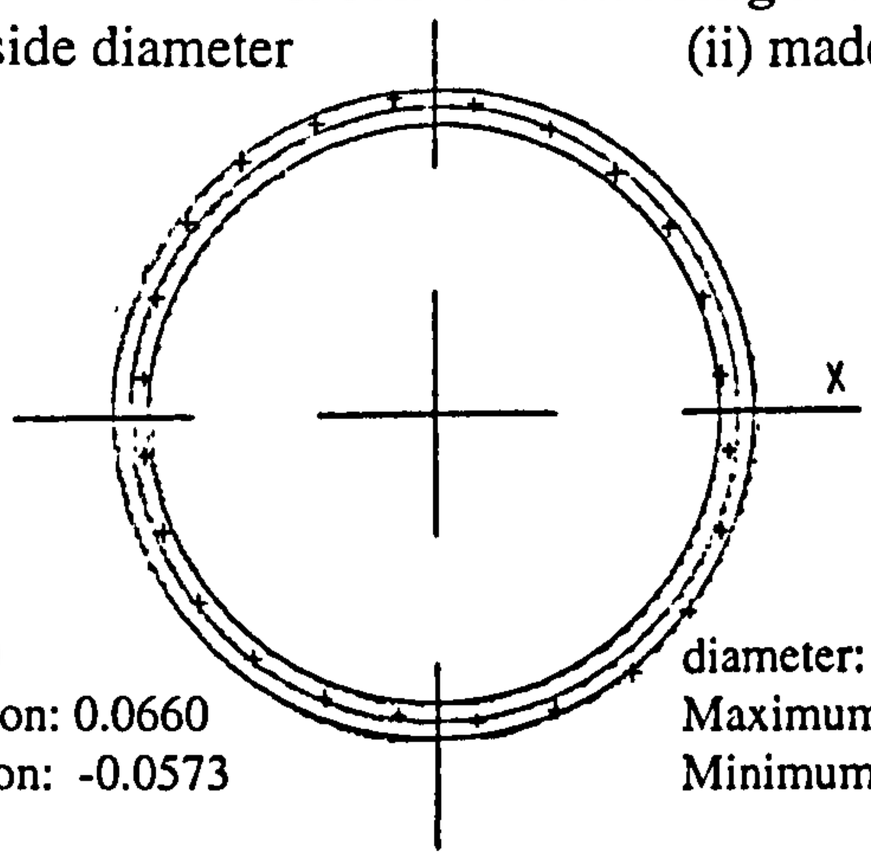

diameter: 157.180
Maximum distortion: 0.0660
Minimum distortion: -0.0573

(ii) made at inside diameter

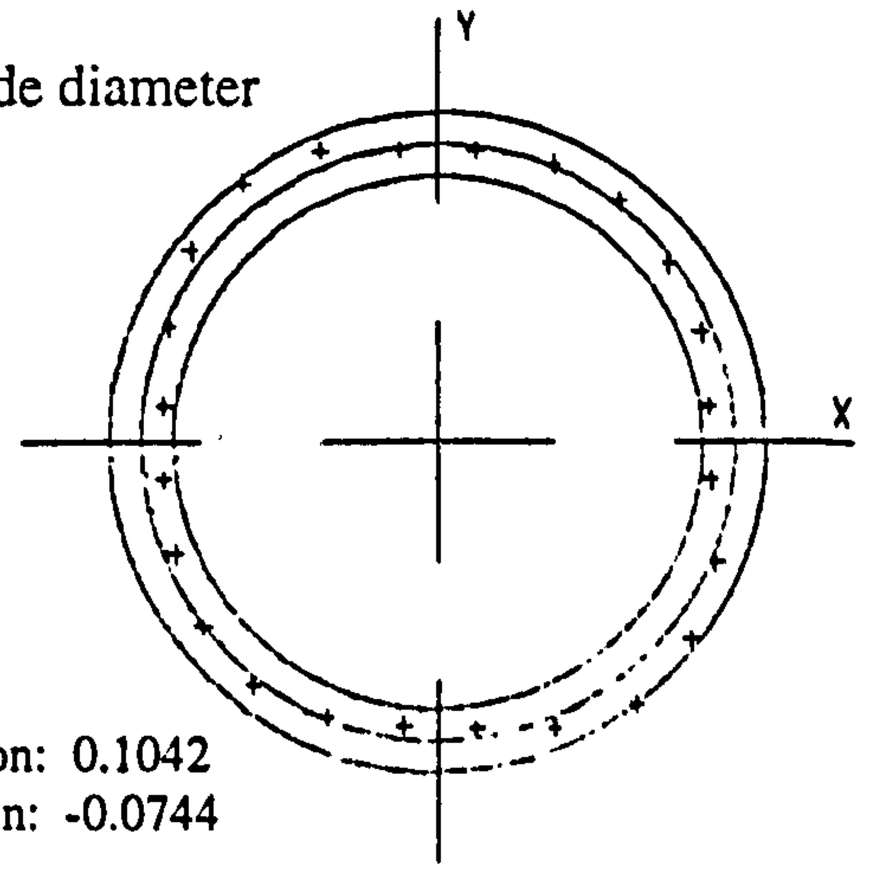

diameter: 137.712
Maximum distortion: 0.1042
Minimum distortion: -0.0744

Figure 3.18 The results of moulding roundness measurements of MLFM and conventional ring samples

(Figure 3.19) than those produced using conventional injection moulding. The maximum difference of flatness was 68.6μm in the MLFM-R1 ring moulding, and was 71.1μm in the conventional ring moulding. Ring mouldings produced using the MLFM-R2 program in this preliminary investigation, exhibited higher deviation (79.8μm) from flatness than either the MLFM-R1 or conventional moulding.

3) Surface straightness;

The surface straightness of the ring moulding samples was measured from the top, bottom, outside and inside surfaces. 9 equiangular testing points were measured on the top surface. 7 equiangular testing points were measured on the bottom surface. 14 equiangular testing points were measured on the outer and on the inner surfaces.

The maximum and the minimum deviations from surface straightness (Figure 3.20) on the top, bottom, outside and inside surfaces in MLFM and conventional ring mouldings were shown in the following table:

Sample I.D.	Maximum deviation (μm)				Minimum deviation (μm)			
	top surface	bottom surface	outside surface	inside surface	top surface	bottom surface	outside surface	inside surface
MLFM-R1	13.4	6.1	12.1	19.1	12.6	4.7	14.5	17.4
MLFM-R2	16.1	9.4	11.0	14.8	8.4	12.0	16.7	10.4
conventional	30.6	17.3	66.4	61.4	39.2	15.2	65.6	59.6

The measurements of surface straightness obtained from all the four surfaces consistently showed the advantages by using MLFM. Much higher deviations from straightness on the four surfaces were recorded from conventional injection moulding especially on the outside and inside surfaces. The ring mouldings produced by the SCORIM exhibit well controlled dimension in moulding surface straightness.

3.6 Mechanical Measurements of Injection Moulded iPP

Table 3.1 shows the results of Young's modulus and breaking stress of the standard tensile bar of conventional injection moulded iPP. The results exhibited that at both

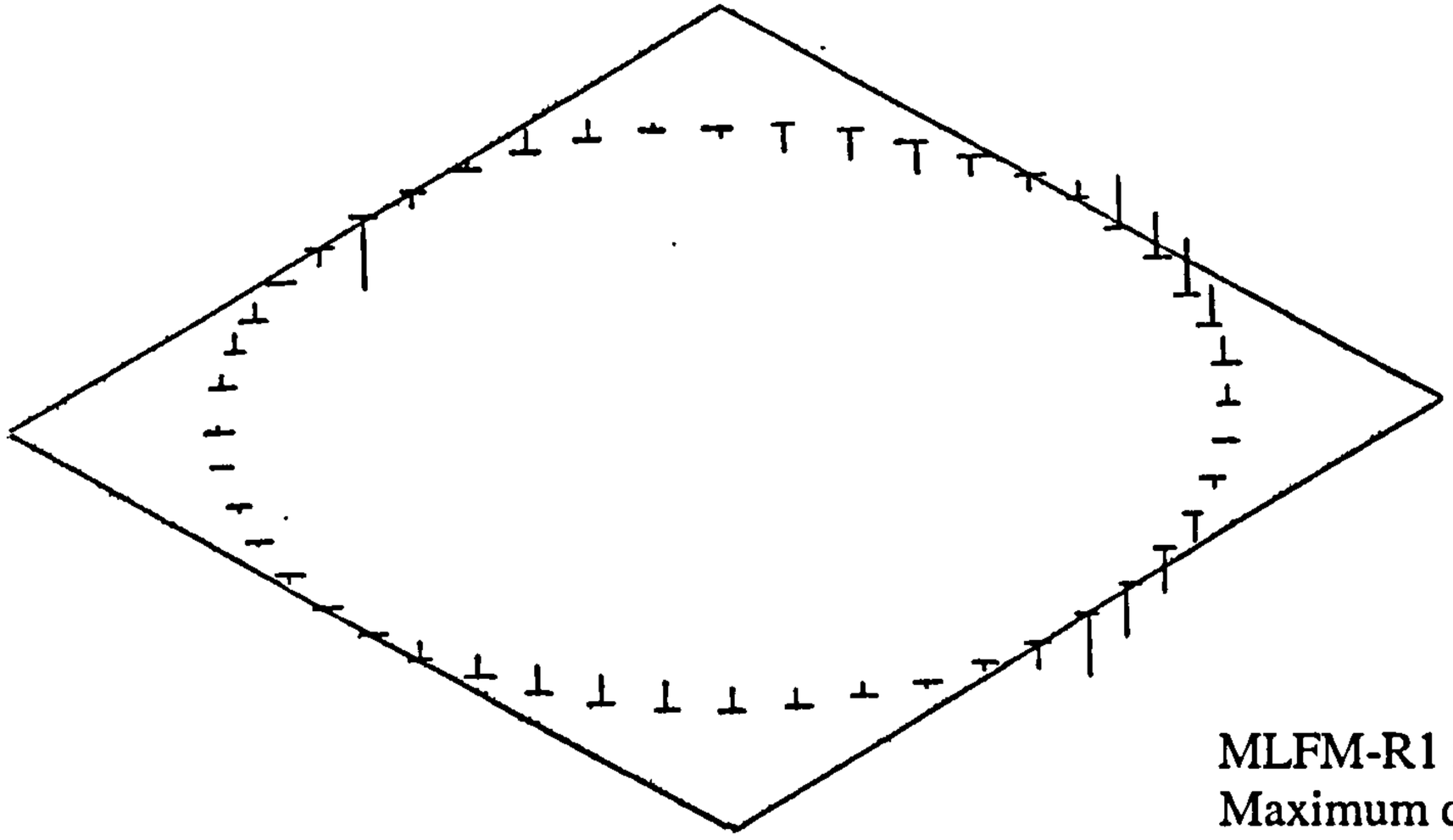

MLFM-R1 ring moulding
Maximum distortion: 0.0301
Mimimum distortion: -0.0386

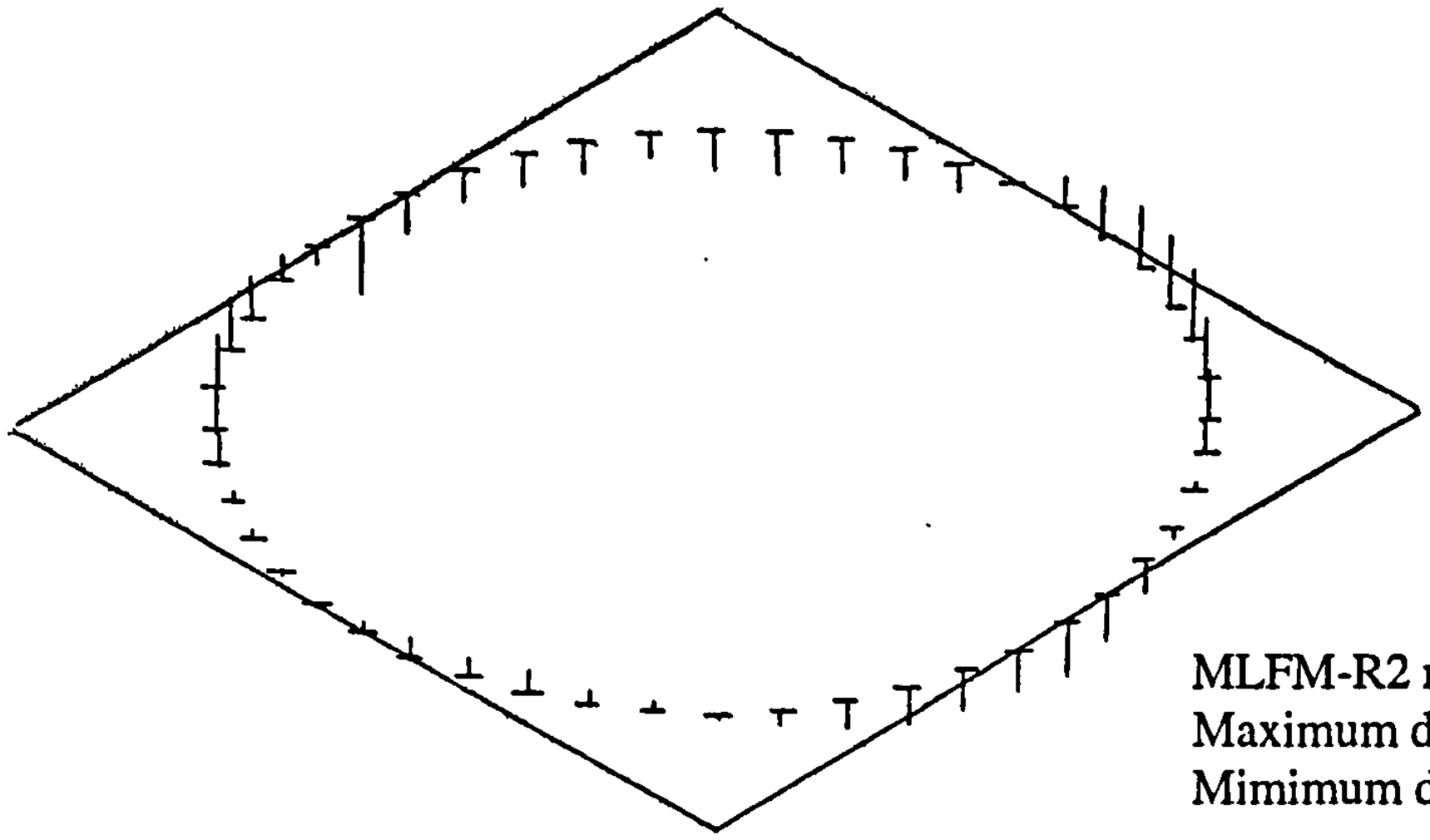

MLFM-R2 ring moulding
Maximum distortion: 0.0381
Mimimum distortion: -0.0417

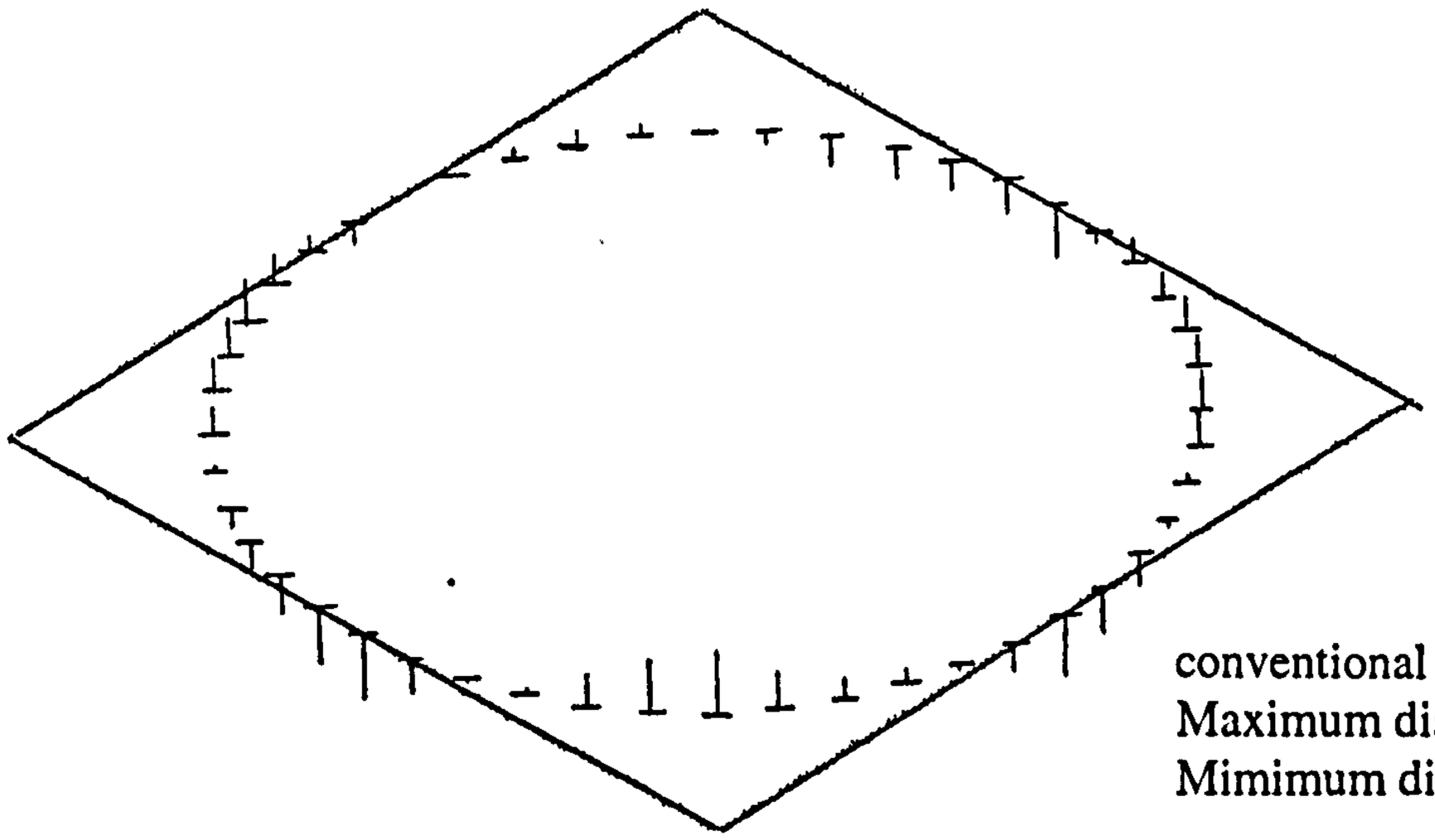

conventional ring moulding
Maximum distortion: 0.0342
Mimimum distortion: -0.0369

Figure 3.19 The results of moulding flatness measurements of MLFM and conventional ring samples

a. MLFM-R1 ring moulding

(i) made at top surface

Maximum distortion: 0.0134
Minimum distortion: -0.0126

(ii) made at bottom surface

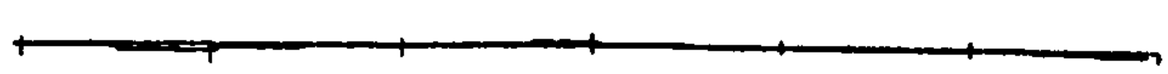

Maximum distortion: 0.0061
Minimum distortion: -0.0047

b. MLFM-R2 ring moulding

(i) made at top surface

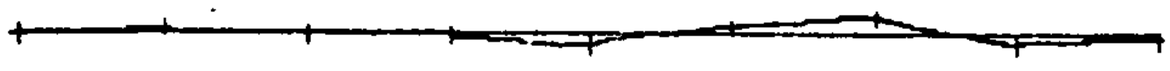

Maximum distortion: 0.0161
Minimum distortion: -0.0084

(ii) made at bottom surface

Maximum distortion: 0.0094
Minimum distortion: -0.0120

c. conventional ring moulding

(i) made at top surface

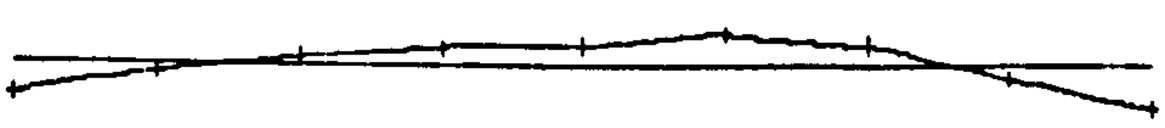

Maximum distortion: 0.0306
Minimum distortion: -0.0392

(ii) made at bottom surface

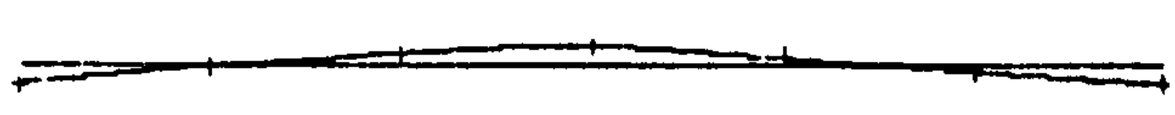

Maximum distortion: 0.0173
Minimum distortion: -0.0152

Figure 3.20a The results of surface straightness measurements on the top and bottom surfaces of MLFM and conventional ring samples

a. MLFM-R1 ring moulding

(i) made at outside surface

Maximum distortion: 0.0121
Minimum distortion: -0.0145

(ii) made at inside surface

Maximum distortion: 0.00191
Minimum distortion: -0.00147

b. MLFM-R2 ring moulding

(i) made at outside surface

Maximum distortion: 0.0110
Minimum distortion: -0.0167

(ii) made at inside surface

Maximum distortion: 0.00148
Minimum distortion: -0.0104

c. conventional ring moulding

(i) made at outside surface

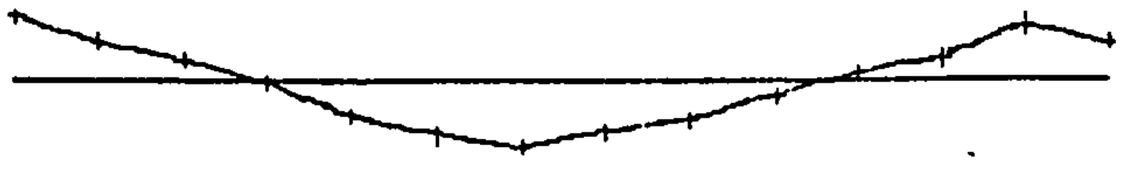

Maximum distortion: 0.0664
Minimum distortion: -0.0656

(ii) made at inside surface

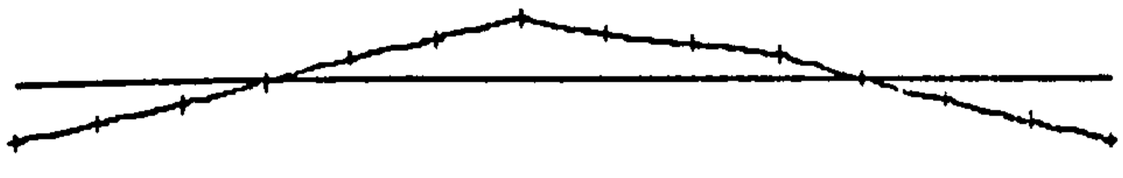

Maximum distortion: 0.0614
Minimum distortion: -0.0596

Figure 3.20b The results of surface straightness measurements on the outside and inside surafces of MLFM and conventional ring samples

Table 3.1 Mechanical results of standard tensile bar conventional injection mouldings

mould temperature/ nozzle temperature/ injection speed	Strain (mm/mm)			Stress (MPa)			Young's Modulus (GPa)
	Peak	Yield	Break	Peak	Yield	Break	
30°C/220°C/ 15%	0.10	0.02	0.65	33.3	14.9	21.3	1.18±0.31
30°C/220°C/ 60%	0.10	0.01	0.58	35.6	15.4	20.7	1.30±0.03
30°C/200°C/ 15%	0.09	0.02	0.17	35.4	14.9	25.9	1.22±0.02
30°C/200°C/ 60%	0.10	0.01	0.60	34.6	15.7	15.8	1.30±0.04

melt temperatures (200°C, 220°C), the higher injection velocity (60%) resulted in a higher Young's modulus (1.30GPa) and a lower breaking stress. The lower melt temperature (200°C) and lower injection velocity (15%) resulted in the highest breaking stress 25.9MPa.

The tensile modulus values of the conventional and MLF injection ring mouldings were calculated from the initial slopes of the load-extension curves under the same testing conditions, and were presented for comparative purposes only. The MLFM-R1 ring mouldings exhibited a significant enhancement in tensile modulus (Figure 3.21a). The average tensile modulus value of the MLFM-R1 ring mouldings was 1.9 times greater than that measured from conventional ring mouldings, and a 9.3% increase in the case of the MLFM-R2 ring mouldings.

The results (Figure 3.21b) of mechanical testing on the weld line regions show that there is a modest increase in the hoop fracture stress of the MLFM ring mouldings, compared with conventional ring mouldings. The average hoop fracture stress was increased by 17% in the MLFM-R1 ring mouldings and by 2.5% in the MLFM-R2 ring mouldings.

The results shown in Table 3.2 indicate that under the corresponding processing conditions the SCORIM rectangular bar mouldings have significantly increased tensile modulus in comparison with conventional bar mouldings. For the SCORIM rectangular bar samples, the mouldings can be distinguished into 4 groups which were shown in Table 3.3 depending on their processing conditions.

In Table 3.3 group-(1), the SCORIM-1A, -1B and -1C mouldings produced under the same lower mould temperature (40°C) and nozzle temperature (215°C), the use of a lower hold pressure (40 bar) resulted in mouldings (SCORIM-1A) with higher Young's modulus value 2.63GPa.

In Table 3.3 group-(2), the SCORIM-2A, -2B and -2C mouldings produced under the same higher mould temperature (80°C) and lower nozzle temperature (215°C), the use of a higher hold pressure (120 bar) resulted in mouldings (SCORIM-2C) with higher Young's modulus value 3.81GPa.

In Table 3.3 group-(3), the SCORIM-1B, -2B and -3B mouldings produced by

(a)

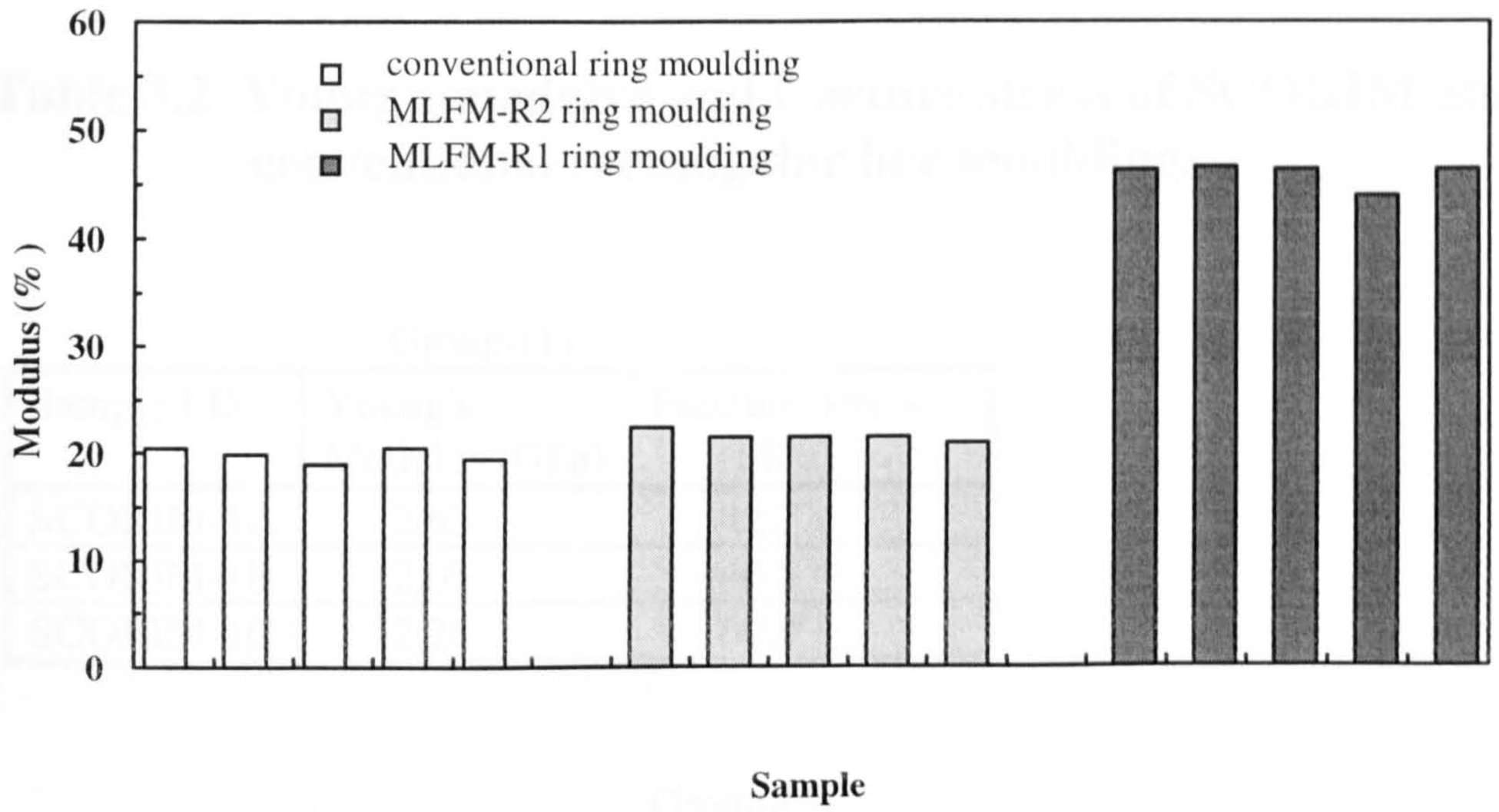

(b)

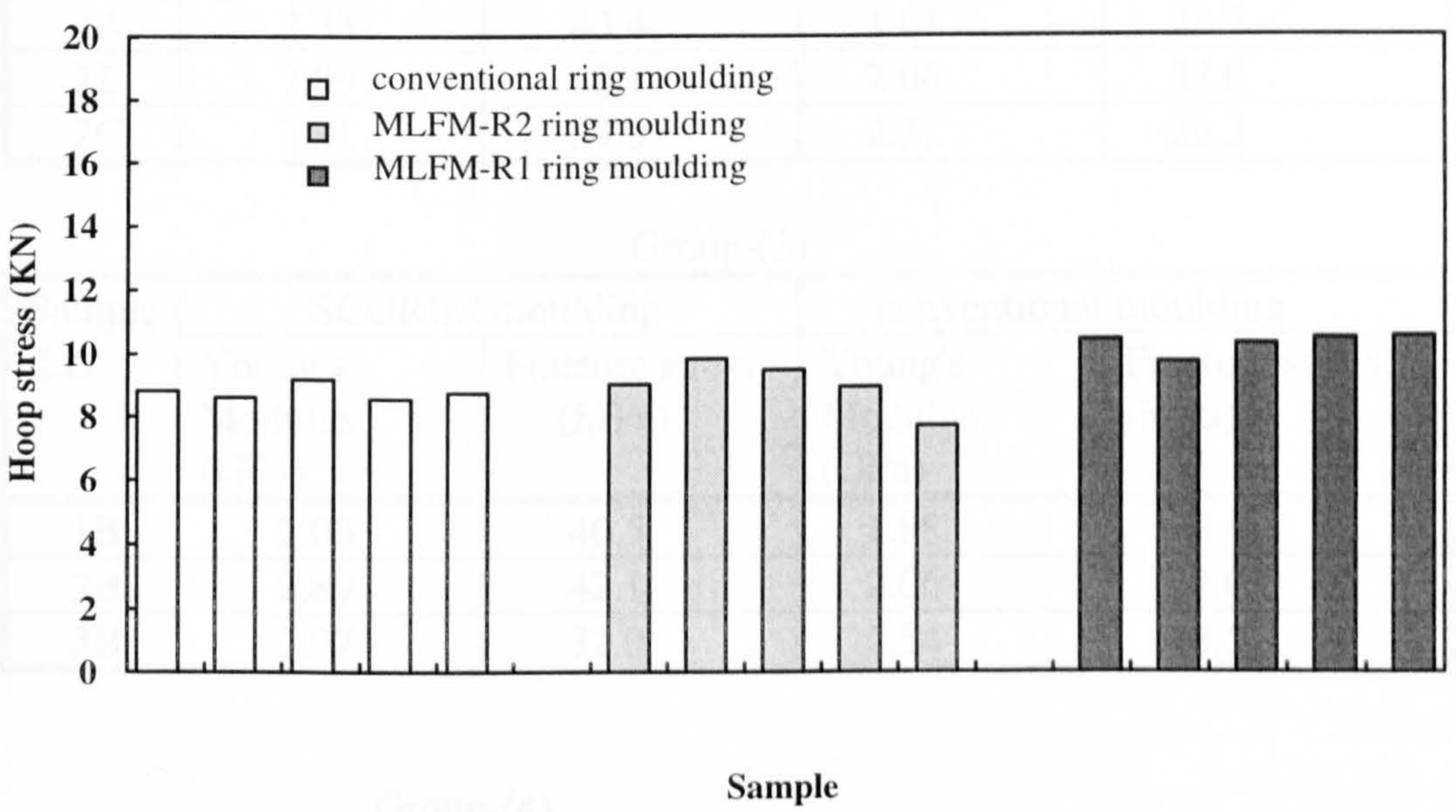

Figure 3.21 Mechanical measurements of the MLFM and conventional ring mouldings

a) tensile modulus b) tensile hoop stress

Table 3.2 Young's modulus and fracture stress of SCORIM and conventional rectangular bar mouldings

Group-(1)

Sample I.D.	Young's Modulus (GPa)	Fracture stress (MPa)
SCORIM-1A	2.63	42.7
SCORIM-1B	2.03	40.5
SCORIM-1C	2.26	60.4

Group-(2)

Sample I.D.	SCORIM moulding		conventional moulding	
	Young's Modulus (GPa)	Fracture stress (MPa)	Young's Modulus (GPa)	Fracture stress (MPa)
2A	2.33	43.4	1.61	28.7
2B	2.89	42.1	2.06	32.0
2C	3.81	59.3	2.31	29.3

Group-(3)

Sample I.D.	SCORIM moulding		conventional moulding	
	Young's Modulus (GPa)	Fracture stress (MPa)	Young's Modulus (GPa)	Fracture stress (MPa)
1B	2.03	40.5	1.88	20.4
2B	2.89	42.1	2.06	32.0
3B	3.97	32.0	2.54	18.5

Group-(4)

Sample I.D.	Young's Modulus (GPa)	Fracture stress (MPa)
conventional-2C	2.31	29.3
SCORIM-2C	3.81	59.3
SCORIM-2CM1	3.68	57.8
SCORIM-2CM2	4.50	56.0

Table 3.3 Mechanical results of SCORIM rectangular bar mouldings

SCORIM-Group(1)

Sample I.D.	Strain (mm/mm)			Stress (MPa)			Young's Modulus (GPa)
	Peak	Yield	Break	Peak	Yield	Break	
SCORIM-1A	0.39	0.02	1.08	51.7	6.5	42.7	2.63±0.21
SCORIM-1B	0.40	0.03	0.86	48.4	13.0	40.5	2.03±0.10
SCORIM-1C	0.61	0.02	0.78	61.5	7.8	60.4	2.26±0.67

SCORIM-Group(2)

SCORIM-2A	0.29	0.02	0.85	46.3	9.8	43.4	2.33±0.29
SCORIM-2B	0.44	0.02	1.15	48.7	10.8	42.1	2.89±0.85
SCORIM-2C	0.58	0.02	0.64	59.9	7.7	59.3	3.81±0.48

SCORIM-Group(3)

SCORIM-1B	0.40	0.03	0.86	48.4	13.0	40.5	2.03±0.10
SCORIM-2B	0.44	0.02	1.15	48.7	10.8	42.1	2.89±0.85
SCORIM-3B	0.25	0.02	0.73	44.6	12.2	32.0	3.97±1.02

SCORIM-Group(4)

SCORIM-2C	0.58	0.02	0.64	59.9	7.7	59.3	3.81±0.48
SCORIM-2CM1	0.61	0.06	0.78	62.4	20.4	57.8	3.68±0.68
SCORIM-2CM2	0.56	0.07	0.64	58.8	24.1	56.0	4.50±0.80

using the same hold pressure (80 bar), the use of a higher mould temperature (80°C) and higher nozzle temperature (265°C) resulted in the mouldings (SCORIM-3B) with the highest Young's modulus value 3.97GPa.

Comparing all of the SCORIM mouldings, the higher modulus values were obtained by using the SCORIM-2C and SCORIM-3B programmes. The processing condition of the SCORIM-2C and SCORIM-3B were 80°C/215°C/120bar and 80°C/265°C/80bar, represented mould temperature, nozzle temperature and hold pressure respectly. The exterior surfaces of the SCORIM-3B mouldings were burnt due to the higher processing temperature, and is not suitable for the large-scale production. So based on the SCORIM-2C, the SCORIM program was improved to the SCORIM-2CM1 and SCORIM-2CM2 to enhance the preferred orientation and tensile modulus of the iPP mouldings (see Table 3.3 Group-4).

For the SCORIM mouldings, the original samples were in the shape of rectangular bar with three layers outside the core (as shown in Figure 3.8). The further modulus measurements incorporated the following considerations:

step (1) The initial sample (square bar) was tested.
step (2) The initial sample was polished so that the skin layer was removed. The resulting bar (still square-shape) was then tested.
step (3) The square bar obtained in step (2) was further cut into a round bar using a lathe to remove the sub-skin layer. Then the resulting round bar was tested.
step (4) The round bar obtained in step (3) was deeper cut to remove the shear layer. Then the resulting round bar was tested.

The testing results obtained according to step (1) to (4) above are summarised in Table 3.4a. The mechanical testing results obtained from the layer removal procedures provided the data necessary for estimation of the moduli in different regions within mouldings and delineated by different microstructures. The modulus value in each region was obtained by the calculation method which is shown in Appendix 5.

After the mechanical removal procedure, the strain of the testing sample was changed slightly with the changing of the area and the shape (square or round) of the sample cross section. In the tensile testing the Young's modulus was measured in the elastic region of the rectangular bar moulding by using a 10 mm

Table 3.4 Mechanical results of rectangular bar SCORIM mouldings by layer removal procedure

a. Modulus testing results of layer removal procedure

layer removel procedure	SCORIM-1A		SCORIM-1C		SCORIM-2A	
	Young's modulus (GPa)	Area (mm^2)	Young's modulus (GPa)	Area (mm^2)	Young's modulus (GPa)	Area (mm^2)
step-(1)	2.63 ±0.21	36.31	2.26 ±0.67	36.80	2.44 ±0.21	36.60
step-(2)	2.26 ±0.13	31.99	2.02 ±0.19	32.80	1.93 ±0.19	21.63
step-(3)	1.89 ±0.13	14.03	2.20 ±0.07	12.15	1.99 ±0.26	13.99
step-(4)	1.37 ±0.32	3.77	1.44 ±0.17	4.99	1.80 ±0.17	8.20

b. Modulus calculated results of each region

Layers	Young's modulus (GPa)		
	SCORIM-1A	SCORIM-1C	SCORIM-2A
skin layer	5.37	4.23	3.18
sub-skin layer	2.55	1.91	1.82
shear layer	2.08	2.73	2.26
core	1.37	1.44	1.80

extensometer. The testing limit of the strain was set to 0.6 mm/mm and the testing rate was 1 mm/min. In order simplify the calculation the strain (ε) in each region was deemed to be constant by using the same testing condition. The calculated results can be used to analyse the distribution of moduli from each region in the SCORIM mouldings.

After removal of skin, sub-skin and shear layers, the moduli of the resulting bar mouldings were changed. Table 3.4b shows the calculated modulus results of each layer within the moulding. The skin layer exhibits a much higher modulus. Both sub-skin layer and the shear layer can also provide some contribution to the modulus of the moulding. The modulus of the core region shows the lowest value within the moulding. So the higher modulus of the mouldings, the wider width of the skin layer and the smaller region of the core.

Kantz et al. made x-ray diffraction measurements on the skin layer in injection moulded polypropylene from various directions and found that crystallites were biaxially oriented to the melt flow direction and the tensile yield strength and mould shrinkage in the melt flow direction were higher as the skin layer was thicker [105]. Matsumoto et al. found using polarizing microscopy that injection moulded polypropylene was composed of multiple layers, and the thickness of oriented layer was governed mainly by resin temperature and mould temperature [126].

In injection moulding, the skin layer is rapidly cooled and the core is cooled more slowly, the crystallisation temperature in the skin layer is lower than that in the core. However, crystallisation occurs under a high pressure and high stress in injection moulding; good conditions for the formation of shish-kebab structure are presented in TEM micrographs (Figure 3.10). The shishes which are fibrous crystals, have a high modulus, and long penetrate the texture in melt flow direction, must hold most of stress. Fujiyama et al. found that the skin layer exhibited a value of dynamic modulus about twice that of core, suggested that the moulding with thick skin layer gives high modulus and high thermal resistance [125].

Following the above views, the program SCORIM-2C was improved to 2CM1 and 2CM2. It significantly resulted in the SCORIM-2CM2 with the greatest modulus value which increased 94.8% in comparison with conventional-2C, and 18.1% in comparison with the SCORIM-2C (see Table 3.3 Group-4).

Table 3.2 shows the fracture stress of the SCORIM and conventional rectangular bar mouldings. Under the corresponding processing conditions the SCORIM bar mouldings have significantly increased 32% — 102% fracture stress in comparison with conventional bar mouldings (see Table 3.2 Group-2, 3).

For the SCORIM samples, produced using both mould temperatures (40°C and 80°C) and the same nozzle temperature (215°C), the use of a higher hold pressure (120 bar) resulted in mouldings with the greatest fracture stress values (see Table 3.2 Group-1, 2). Under the same hold pressure (80 bar), the use of higher mould temperature (80°C) and lower nozzle temperature (215°C) resulted in the greater fracture stress value 42.1MPa (see Table 3.2 Group-3). In comparison with conventional-2C, SCORIM-2C, -2CM1 and -2CM2 exhibited the greater fracture stress values which were 102.4% increased in the SCORIM-2C, 97.3% increased in the SCORIM-2CM1 and 91.1% increased in the SCORIM-2CM2 (see Table 3.2 Group-4).

Thus it can be concluded that the tensile properties of the mouldings are dependent on the processing conditions and techniques. Careful selection of appropriate processing temperatures, injection speed, pressure and operating modes can produce mouldings with enhanced tensile modulus and fracture stress. Microscopy and Vickers microhardness confirmed the existence of the preferably oriented lamellar structure in the SCORIM mouldings and isotropic α-phase spherulitic structure in the conventional mouldings.

3.7 X-ray Diffraction Techniques for Injection Moulded iPP

Isotactic polypropylene crystallised from the melt may occur in three crystalline forms according to the thermal treatments and the mechanical stresses applied to the polymer [116]. The main form is the α form which has a monoclinic lattice. The ß form is hexagonal, and is characteristic of a crystallisation under stress [127], whereas the γ triclinic form arises only under more exceptional conditions [31].

3.7.1 The Wide Angle X-ray Diffraction Measurement of Injection Moulded iPP

Wide angle x-ray scattering profiles were measured with the scattering angle (2θ) from 8° to 32° and the scanning rate was 0.02degree/sec. The wavelength of the x-ray (λ) was 1.5418Å. The peak intensities of the α, ß and γ-phase were obtained from the scattering profiles. The α-phase orientation index A, ß-phase index B, γ-phase index G, crystallinity index C and γ-phase percentage (γ%) were calculated from the corresponding peak heights.

The x-ray diffraction profiles of 2θ angle and peak intensity of the standard tensile bar conventional mouldings are shown in Figures 3.22 and 3.23. At the gate region, the lower melt temperature (200°C) and higher injection velocity (60%) exhibited the higher intensity for crystal phases —— $(110)_\alpha$, $(300)_ß$, $(040)_\alpha$ and amorphous phase (the highest height of ha). The higher melt temperature (220°C) and lower injection velocity (15%) exhibited lower intensity of the amorphous phase.

At the 8/10 of the flow path length, the intensities of all crystal phases and the amorphous phase were increased. The higher melt temperature (220°C) and lower injection velocity (15%) exhibited the higher intensity for crystal phases —— $(110)_\alpha$, $(300)_ß$, $(111)_\alpha$, $(041)_\alpha$ and the amorphous phase.

The results of A, B and C indices are shown in the Table 3.5. In the gate region, the highest α-phase index (A=0.689) was obtained by using lower melt temperature (200°C) and higher injection velocity (60%); the mouldings produced under lower melt temperature (200°C) provided the higher ß-phase index (B=0.20); the highest crystallinity index (C=3.12) was obtained by using higher melt temperature (220°C) and lower injection velocity (15%).

At the 8/10 of the flow path length, the mouldings produced under higher injection velocity (60%) can provide the higher α-phase index, lower ß-phase index and higher crystallinity index. The highest α-phase index (A=0.553) was obtained by using lower melt temperature (200°C) and higher injection velocity (60%); the highest ß-phase index (B=0.229) was obtained by using higher melt temperature (220°C) and lower injection velocity (15%); the highest crystallinity index (C=2.97)

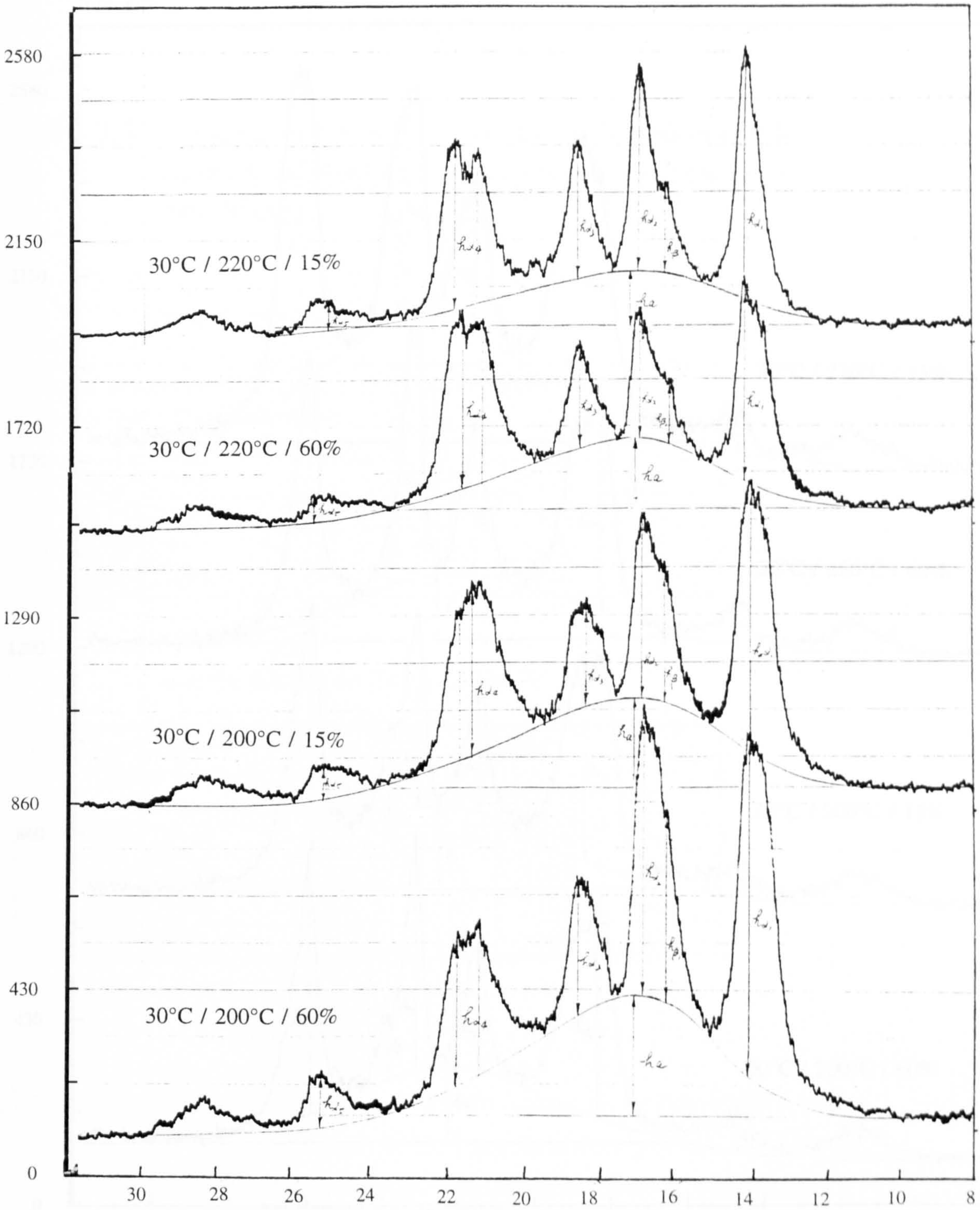

Figure 3.22 X-ray diffractogram of standard tensile bar conventional injection mouldings at each gate region

(Processing condition: mould temperature / nozzle temperature / injection speed)

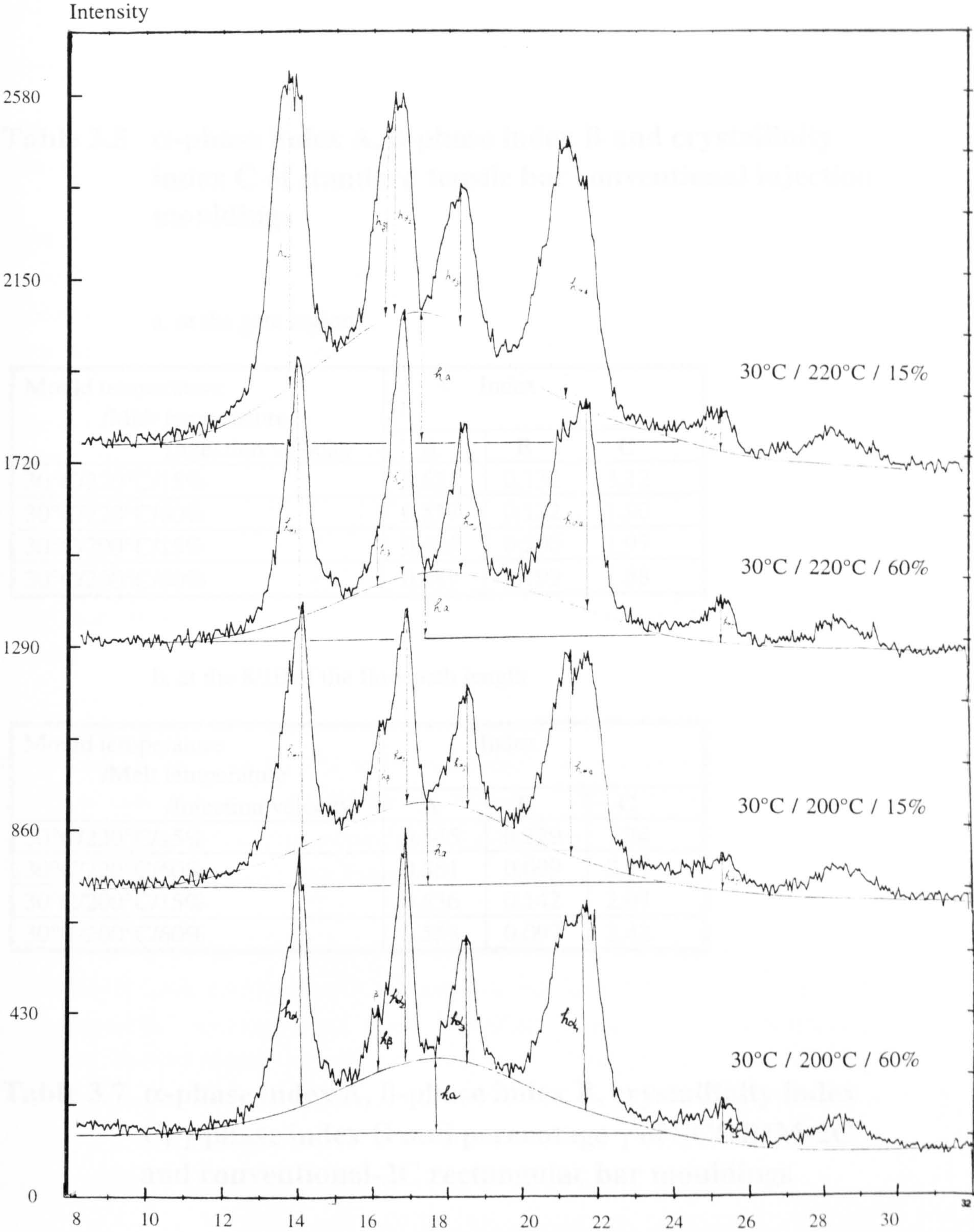

Figure 3.23 X-ray diffractogram of standard tensile bar conventional mouldings at the 8/10 length of the flow path
(Processing condition: mould temperature / nozzle temperature / injection speed)

Table 3.5 α-phase index A, ß-phase index B and crystallinity index C of standard tensile bar conventional injection mouldings

a. at the gate region

Mould temperature /Melt temperature /Injection velocity	Index		
	A	B	C
30°C/220°C/15%	0.621	0.132	3.12
30°C/220°C/60%	0.557	0.132	1.90
30°C/200°C/15%	0.605	0.200	1.97
30°C/200°C/60%	0.689	0.199	1.88

b. at the 8/10 of the flow path length

Mould temperature /Melt temperature /Injection velocity	Index		
	A	B	C
30°C/220°C/15%	0.545	0.229	1.74
30°C/220°C/60%	0.551	0.099	2.97
30°C/200°C/15%	0.536	0.142	2.07
30°C/200°C/60%	0.553	0.097	2.42

Table 3.7 α-phase index A, ß-phase index B, crystallinity index C, γ-phase index G and percentage γ of SCORIM-2C and conventional-2C rectangular bar mouldings

Sample I.D.	A	B	C	G	γ%
SCORIM-2C	0.963	0.220	1.60	0.107	59.1
Conventional-2C	0.538	0.201	1.25	-	-

was obtained by using higher melt temperature (220°C) and higher injection velocity (60%).

Figures 3.24, 3.25 and 3.26 show the x-ray diffraction profiles of MLFM and conventional ring mouldings. Measurements were made on each gate and weld line region for each processing ring sample. Comparing with conventional ring samples, the wide angle x-ray scattering profiles of the MLFM ring samples showed higher intensity of ß-phase $(300)_{\beta}$ at each gate and weld line regions, but a new intense reflection at a Bragg angle (2θ) of 19.68° of MLFM-R1 and 19.83° of MLFM-R2 corresponding to the $(117)_{\gamma}$ reflection in the γ-phase is present. As Turner-Jones states, the presence of reflections with a d-spacing of 4.426Å indicates the presence of the γ-phase, which is in fact the case for the SCORIM mouldings of polypropylene under investigation. The appearance of γ-phase was the main difference between conventional and shear controlled orientation injection moulding process.

Figure 3.27 shows the results of α-phase orientation index A, ß-phase index B, crystallinity index C of MLFM and conventional ring mouldings. Generally, the values of indices A, B and C of the MLFM ring samples at each corresponding region were greater than that of conventional ring sample. The results of A, B, C, G indices and γ% are shown in the Table 3.6.

Figure 3.28 shows the wide angle x-ray diffraction profiles of crystal phases of the SCORIM-2C and conventional-2C rectangular bar mouldings. Comparing with conventional-2C moulding, the x-ray scattering profile of the SCORIM-2C moulding showed higher intensity scattering from crystal planes $(110)_{\alpha}$, $(040)_{\alpha}$, and very weaker intensity from crystal planes $(111)_{\alpha}$, and $(041)_{\alpha}$. The x-ray scattering profile of the SCORIM-2C sample showed the γ-phase $(117)_{\gamma}$ reflection and no γ-phase reflection was observed in the conventional-2C sample.

Table 3.7 shows the results of A, B, C, G indices and γ% of the SCORIM-2C and conventional-2C bar samples. The results of A, B, C, G and γ% of the SCORIM-2C were all greater than those of conventional-2C sample. The α-phase index A of the SCORIM-2C moulding was 1.5 times greater than that of conventional-2C moulding. The conventional-2C moulding did not present any γ-phase.

Figure 3.24 X-ray diffractogram of MLFM-R1 ring moulding on each gate and weld line regions

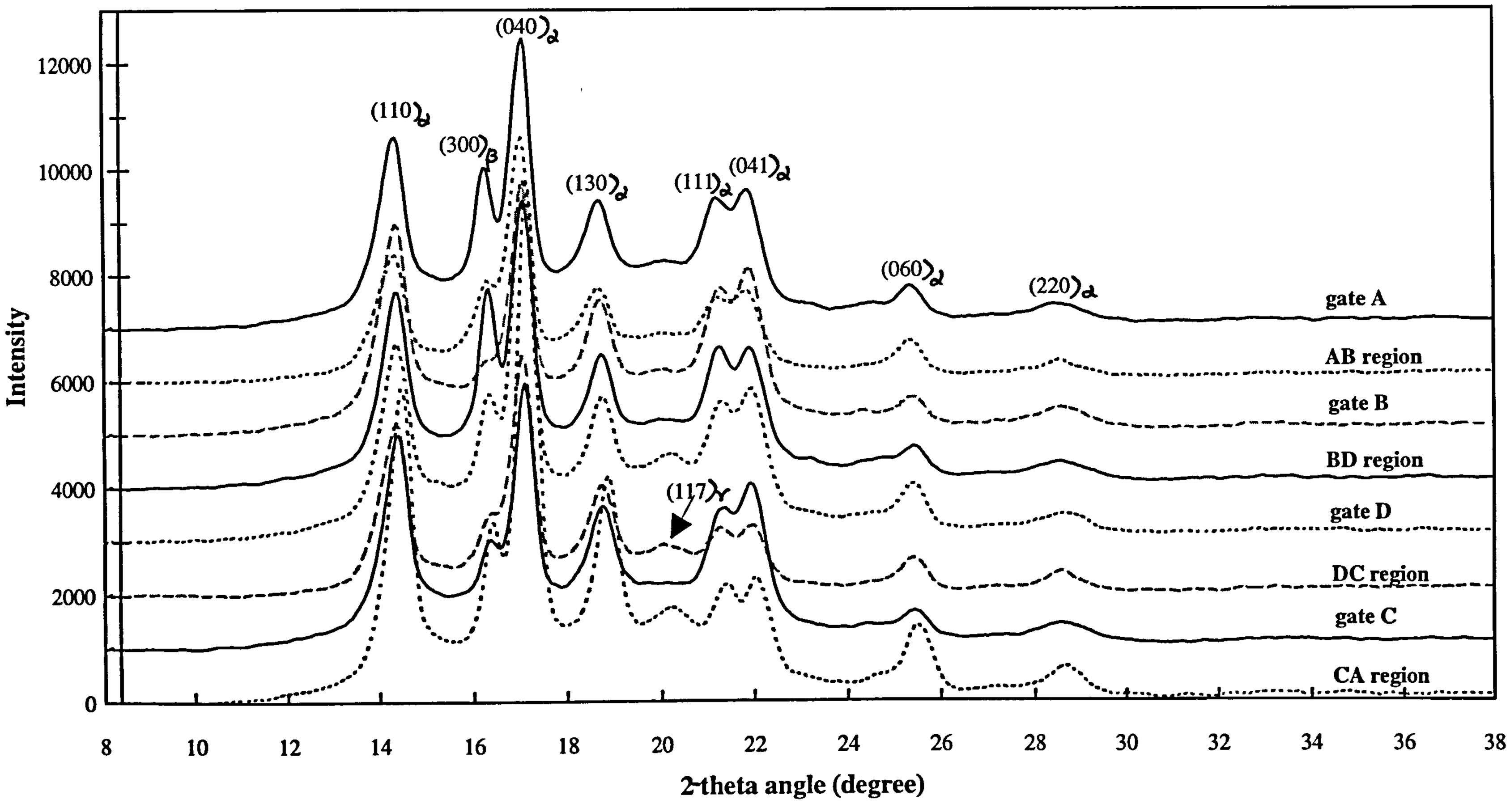

Figure 3.25 X-ray diffractogram of MLFM-R2 ring moulding on each gate and weld line regions

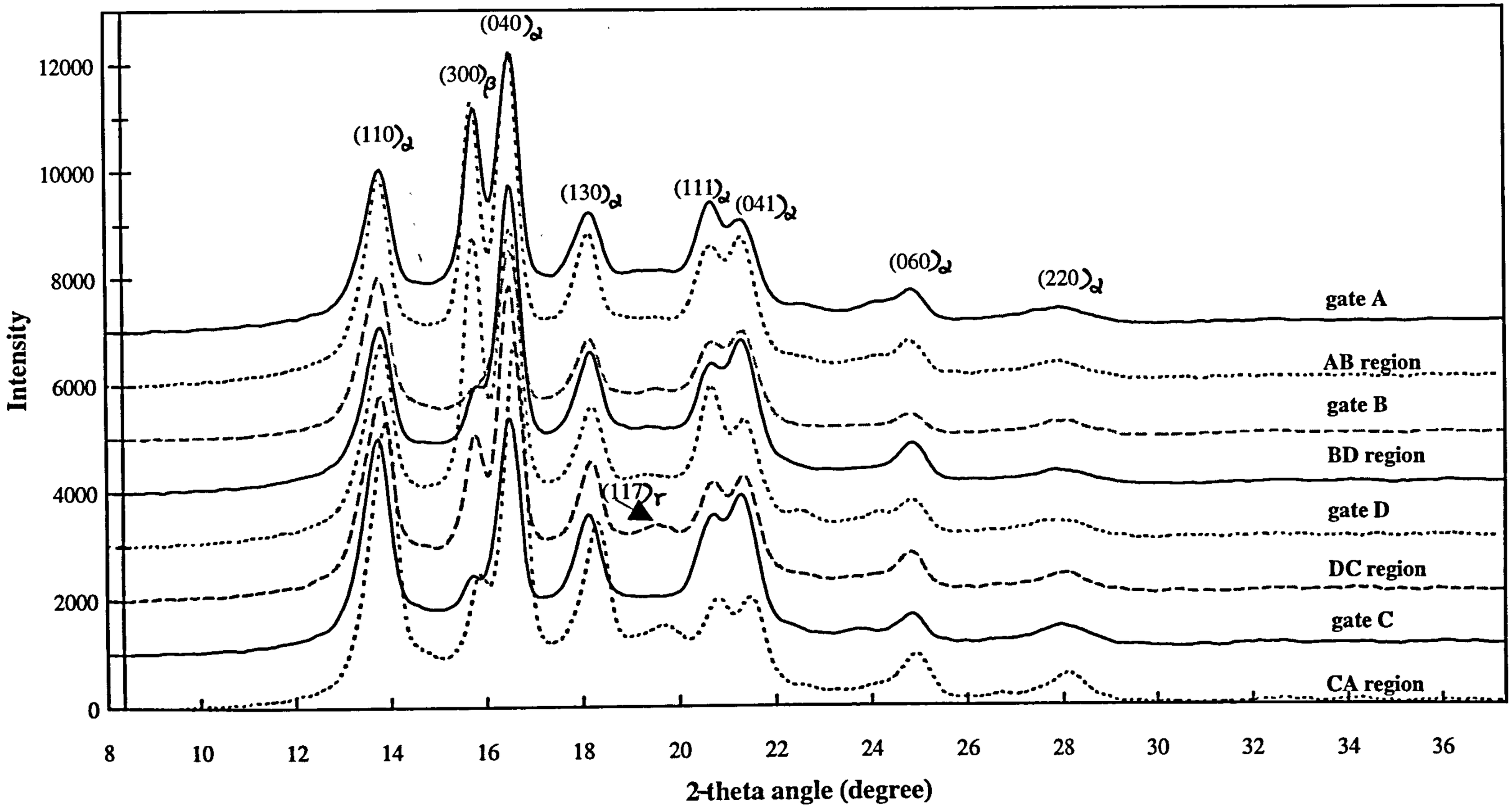

Figure 3.26 X-ray diffractogram of conventional ring moulding on each gate and weld line regions

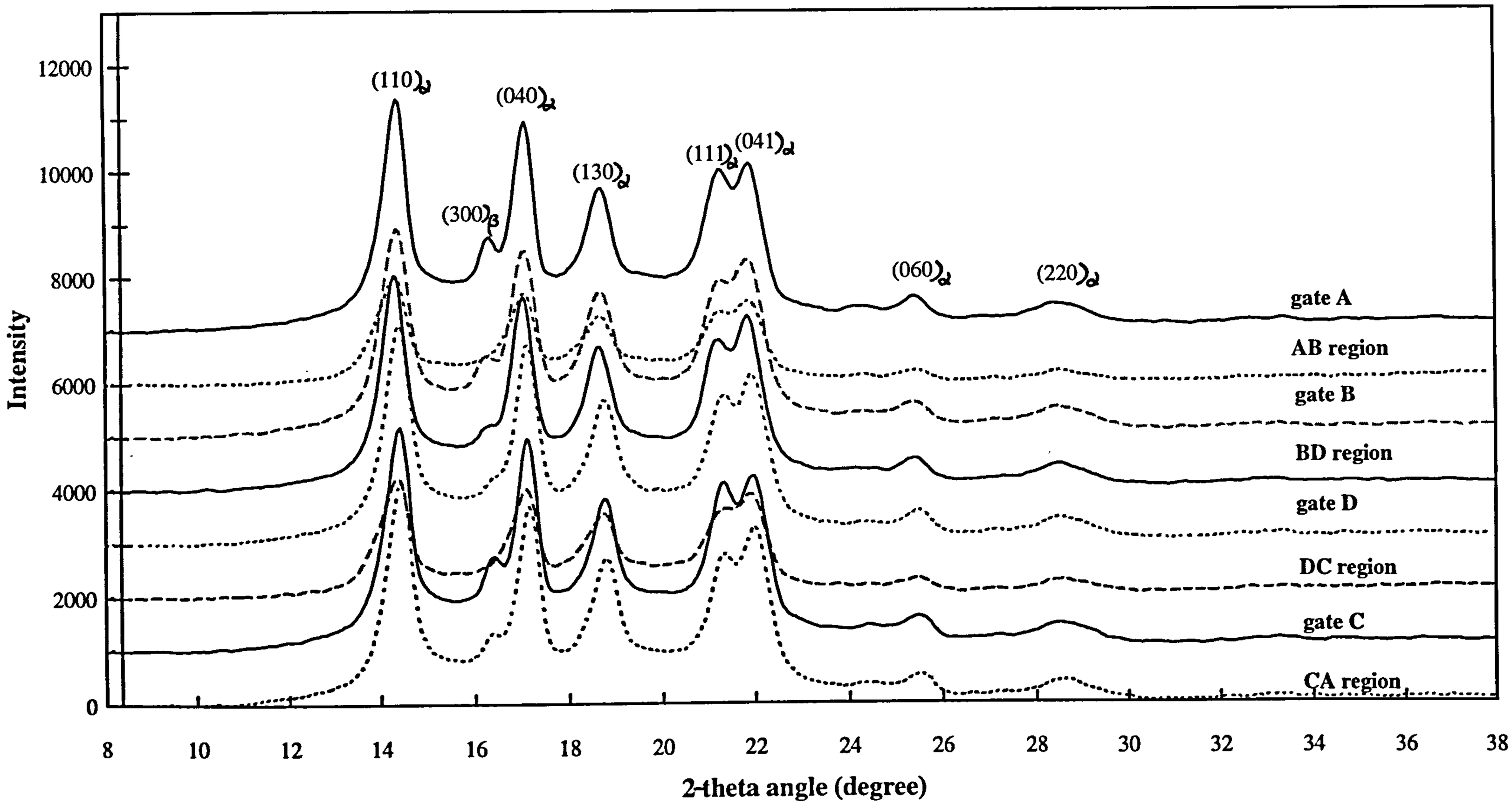

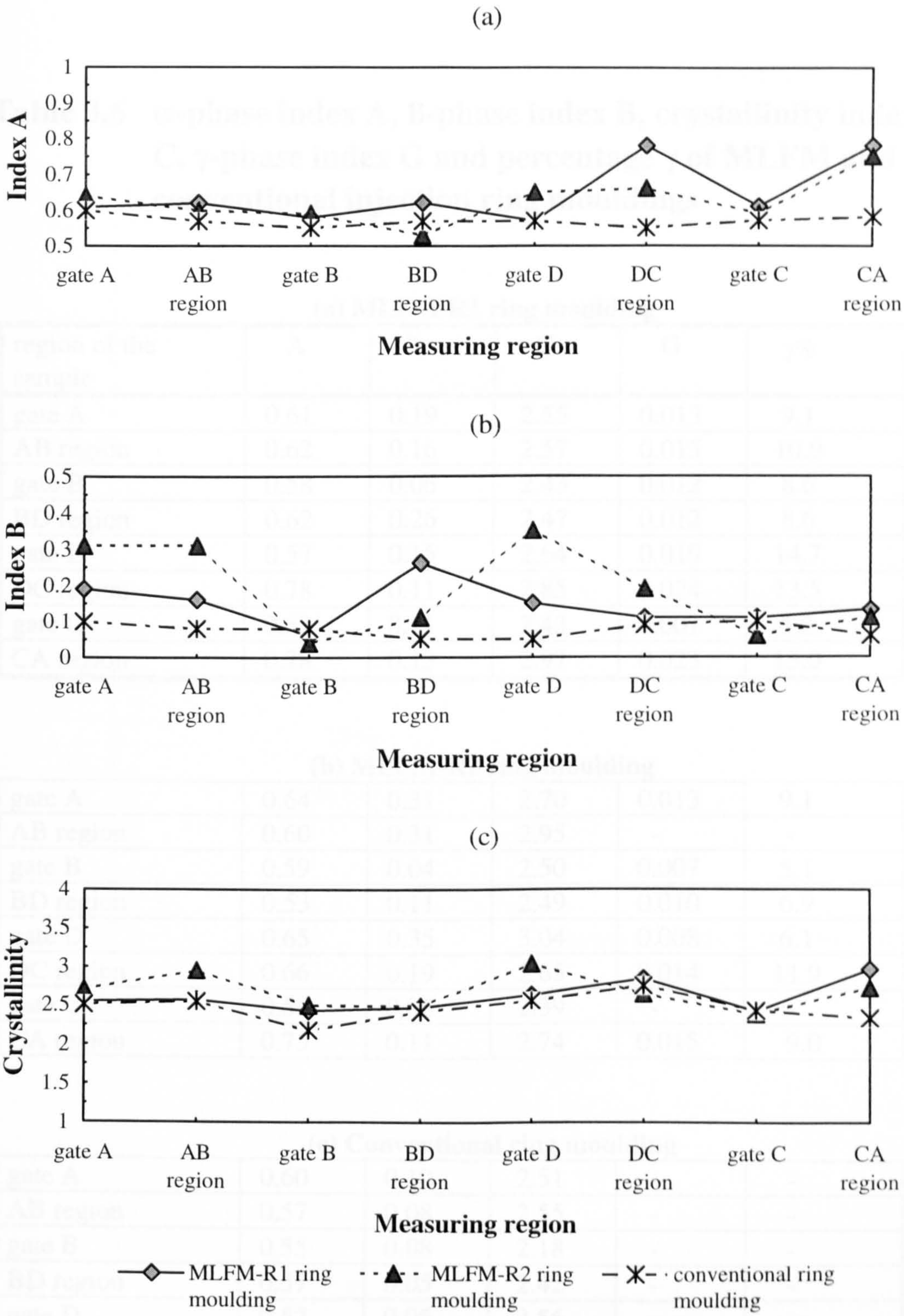

Figure 3.27 The results of x-ray diffraction measurements on each gate and weld line regions of MLFM and conventional injection ring samples

(a) α-phase orientation index A (b) β-phase index B (c) crystallinity index C

Table 3.6 α-phase index A, ß-phase index B, crystallinity index C, γ-phase index G and percentage γ of MLFM and conventional injection ring mouldings

(a) MLFM-R1 ring moulding

region of the sample	A	B	C	G	γ%
gate A	0.61	0.19	2.55	0.013	9.1
AB region	0.62	0.16	2.57	0.015	10.9
gate B	0.58	0.06	2.43	0.012	8.6
BD region	0.62	0.26	2.47	0.012	8.6
gate D	0.57	0.15	2.64	0.019	14.7
DC region	0.78	0.11	2.85	0.024	13.5
gate C	0.61	0.11	2.43	0.007	5.2
CA region	0.78	0.13	2.97	0.023	13.0

(b) MLFM-R2 ring moulding

gate A	0.64	0.31	2.70	0.013	9.1
AB region	0.60	0.31	2.95	-	-
gate B	0.59	0.04	2.50	0.007	5.1
BD region	0.53	0.11	2.49	0.010	6.9
gate D	0.65	0.35	3.04	0.008	6.1
DC region	0.66	0.19	2.65	0.014	11.9
gate C	0.59	0.06	2.39	-	-
CA region	0.75	0.11	2.74	0.015	9.0

(c) Conventional ring moulding

gate A	0.60	0.10	2.51	-	-
AB region	0.57	0.08	2.55	-	-
gate B	0.55	0.08	2.18	-	-
BD region	0.57	0.05	2.42	-	-
gate D	0.57	0.05	2.56	-	-
DC region	0.55	0.09	2.76	-	-
gate C	0.55	0.10	2.51	-	-
CA region	0.58	0.06	2.35	-	-

Figure 3.28 X-ray diffractogram of SCORIM-2C and conventional-2C rectangular bar mouldings

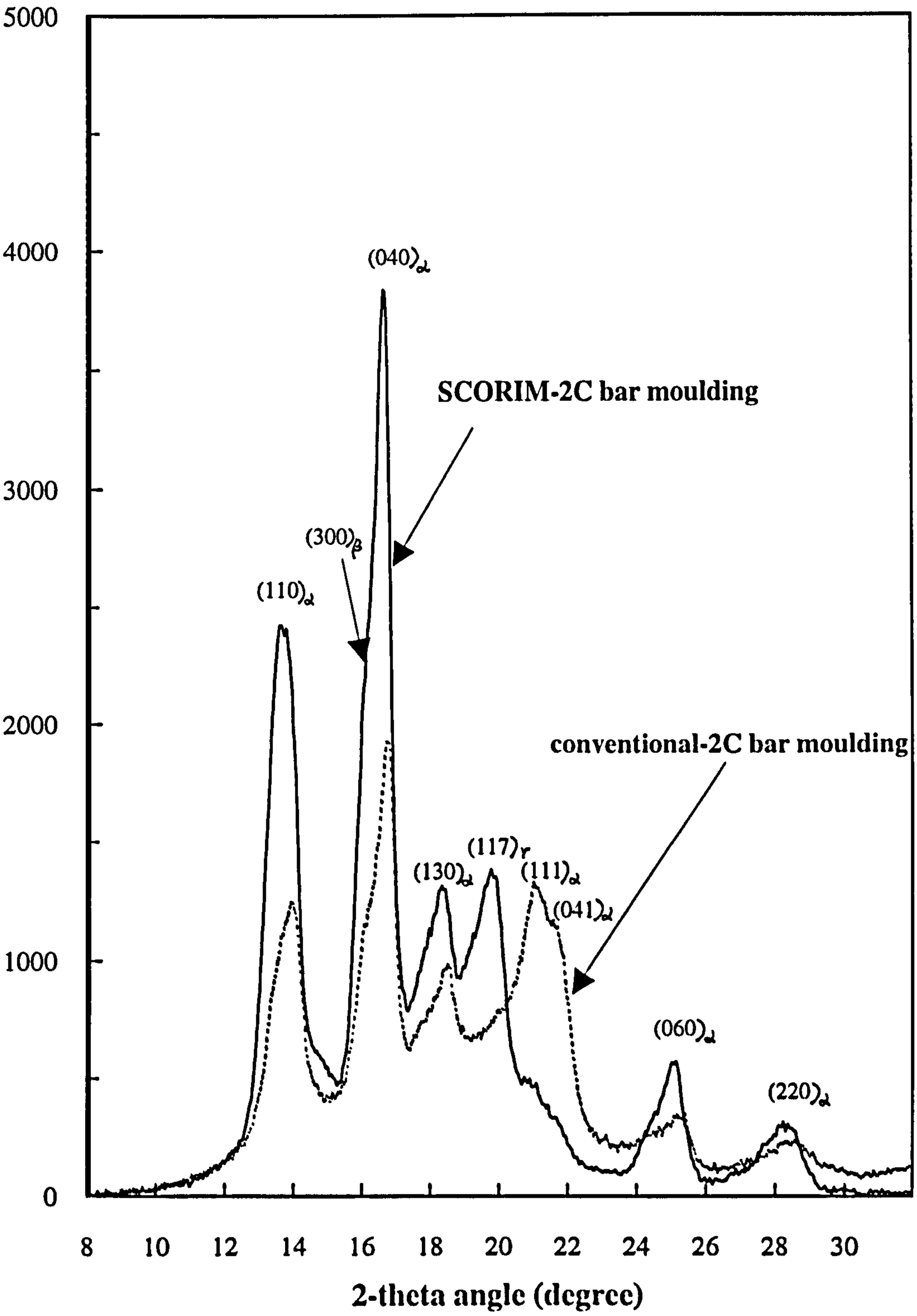

In comparison with conventional iPP mouldings, shear controlled orientation injection moulded iPP samples exhibited high intensity of α-phase, γ-phase $(117)_\gamma$ reflection and contain usually lower percent of amorphous structure.

3.7.2 WAXS Debye Flat Plate Patterns of Injection Moulded iPP

In the x-ray diffraction experiments, the Debye flat plate technique was employed to obtain the ring patterns which can be related to the microstructure of the injection moulding. The WAXS Debye patterns were taken on the same sample as used for wide angle x-ray diffraction or Vickers microhardness measurements. It is well known that the more intense the arcing in the ring pattern, the higher the degree of preferred orientation.

Figures 3.29 and 3.30 show that Debye ring patterns obtained from the midpoints taken from the cross section parallel to the melt flow direction of the MLFM ring mouldings. The testing positions were chosen from the light microscopy photographs which presented the skin, sub-skin, shear and core regions. The samples were the same as used for wide angle x-ray diffraction and Vickers microhardness measurements. The distance from the sample surface to the film was 37.6mm and the film exposure time was 2 hours. The MLFM ring samples exhibited different levels of preferred orientation in each of the layers.

For the MLFM-R1 ring moulding (Figure 3.29), the testing points were taken from 1.10, 1.70, 3.59 and 5.07mm away from the surface in the middle cross section at AB region of the sample. As regards to crystalline structure, the skin layer is mostly composed of the α-form (monoclinic form), but some coexistence with the ß-form (hexagonal form) is also observed; a weak reflection is observed inside the $(040)_\alpha$ reflection of the α-form on the a*-axis direction, which is the $(300)_\beta$ reflection of the ß-form. This was confirmed clearly by a 2θ scan of the MLFM-R1 at AB region. seven Debye rings were observed from the skin layer (1.10mm) and corresponding to reflection from crystal planes $(110)_\alpha$, $(300)_\beta$, $(040)_\alpha$, $(130)_\alpha$, $(111)_{\alpha+}(041)_\alpha$, $(060)_\alpha$ and $(220)_\alpha$. These seven crystal phases were all exhibited the intensity peaks in the x-ray 2θ scattering profile at the same region. But $(117)_\gamma$ reflection was too weaker to appear in the Debye pattern. The Debye patterns of the sub-skin layer (1.70mm) and shear layer (3.59mm) did not exhibited $(300)_\beta$ reflection. The pattern

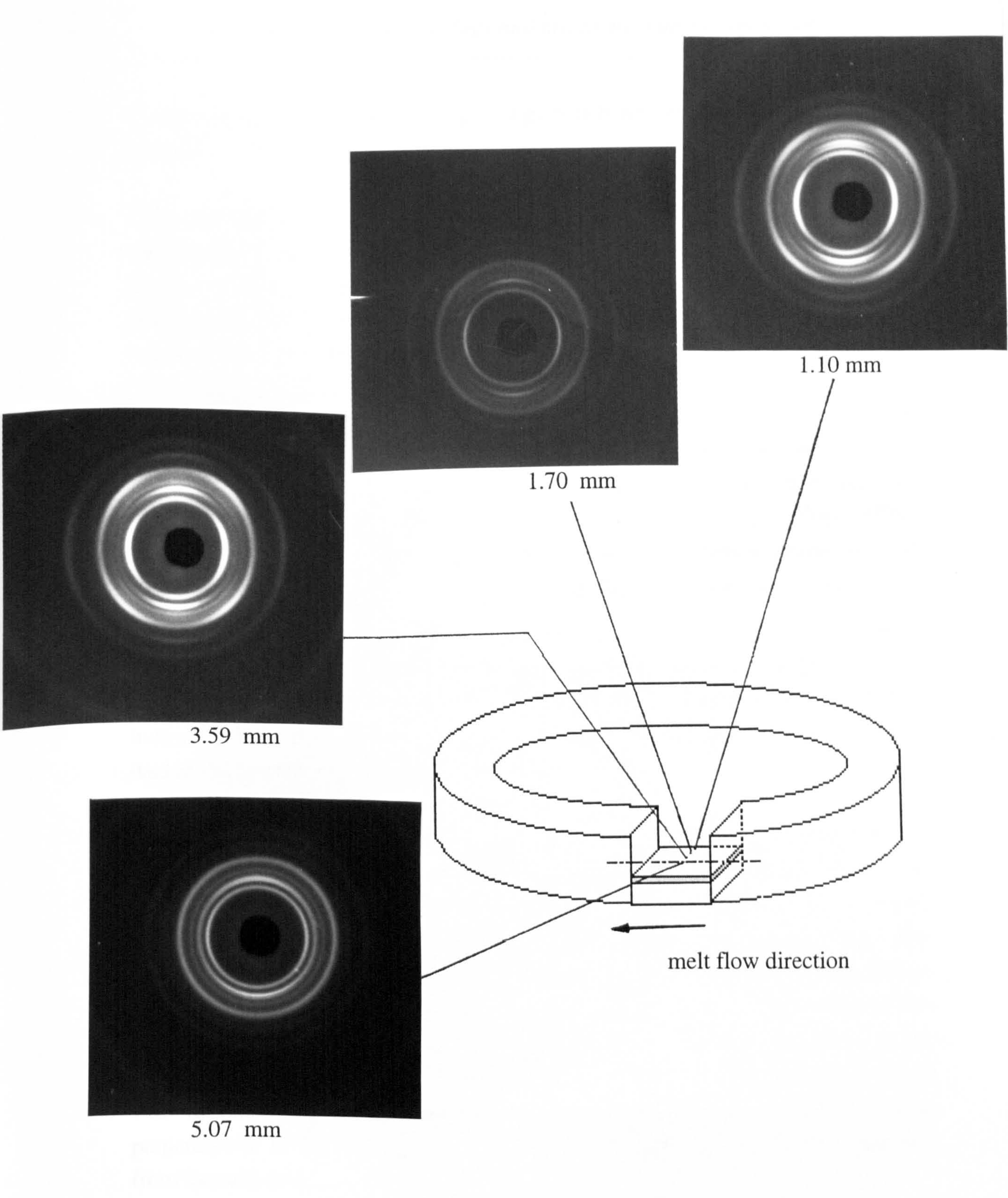

Figure 3.29 Distribution of preferred crystallite orientation in the MLFM-R1 ring moulding

of the core region exhibited isotropic rings which was explained by the isotropic structure in the core region.

Since the amount of the ß-form is small judging from the reflection intensity, it is not essential in analysing the structure of the skin layer. Kantz et al. found that the ß-form existed in the shear zone inside the skin layer of injection moulded polypropylene [105]. Fitchmum and Mencik reported that the ß-form existed at the boundary between oriented layer and core [128].

For the MLFM-R2 ring moulding (Figure 3.30), the testing points were taken from 1.0, 2.0, 3.0 and 5.0mm away from the surface in the middle cross section at CD region of the sample. Seven Debye rings were observed from the skin layer (1.0 mm) and corresponding to reflection from crystal planes — $(110)_\alpha$, $(300)_\beta$, $(040)_\alpha$, $(130)_\alpha$, $(111)_{\alpha+}(041)_\alpha$, $(060)_\alpha$ and $(220)_\alpha$. These seven crystal phases were all exhibited the reflections in the x-ray scattering profile at the same region. But $(117)_\gamma$ reflection was too weaker to appear in the Debye pattern. The ring patterns obtained from sub-skin layer (2.0mm), shear layer (3.0mm) and core region (5.0mm) exhibited similar intense arcing and no $(300)_\beta$ reflection was observed. The results indicate that an oriented structure existed in all the above regions. Crystallographic data of the MLFM ring mouldings is presented in Table 3.8.

Figure 3.31 shows the Debye ring patterns of the SCORIM-3B rectangular bar moulding. The distance from the sample surface to the film was 27.6mm and the film exposure time was 3 hours. The testing points were taken from the cross section parallel to the melt flow direction and 1mm away from the gate edge. The sample was the same as used for Vickers microhardness measurement. The Debye ring pattern obtained from the first point 0.9mm away from the surface exhibited the higher brightness intense arcing, and represented the preferred orientation. In the testing point of sub-skin layer, shear layer and core region, a less intensity of arcing was obtained. When the testing points were taken from the cross section perpendicular to the melt flow direction, the isotropic ring pattern was obtained from the each layer.

Figure 3.32 shows the photograph at higher magnification of the Debye pattern of the SCORIM-3B and SCORIM-1C samples. The testing points were taken from the main part cross section parallel to the melt flow direction. Eleven Debye rings were

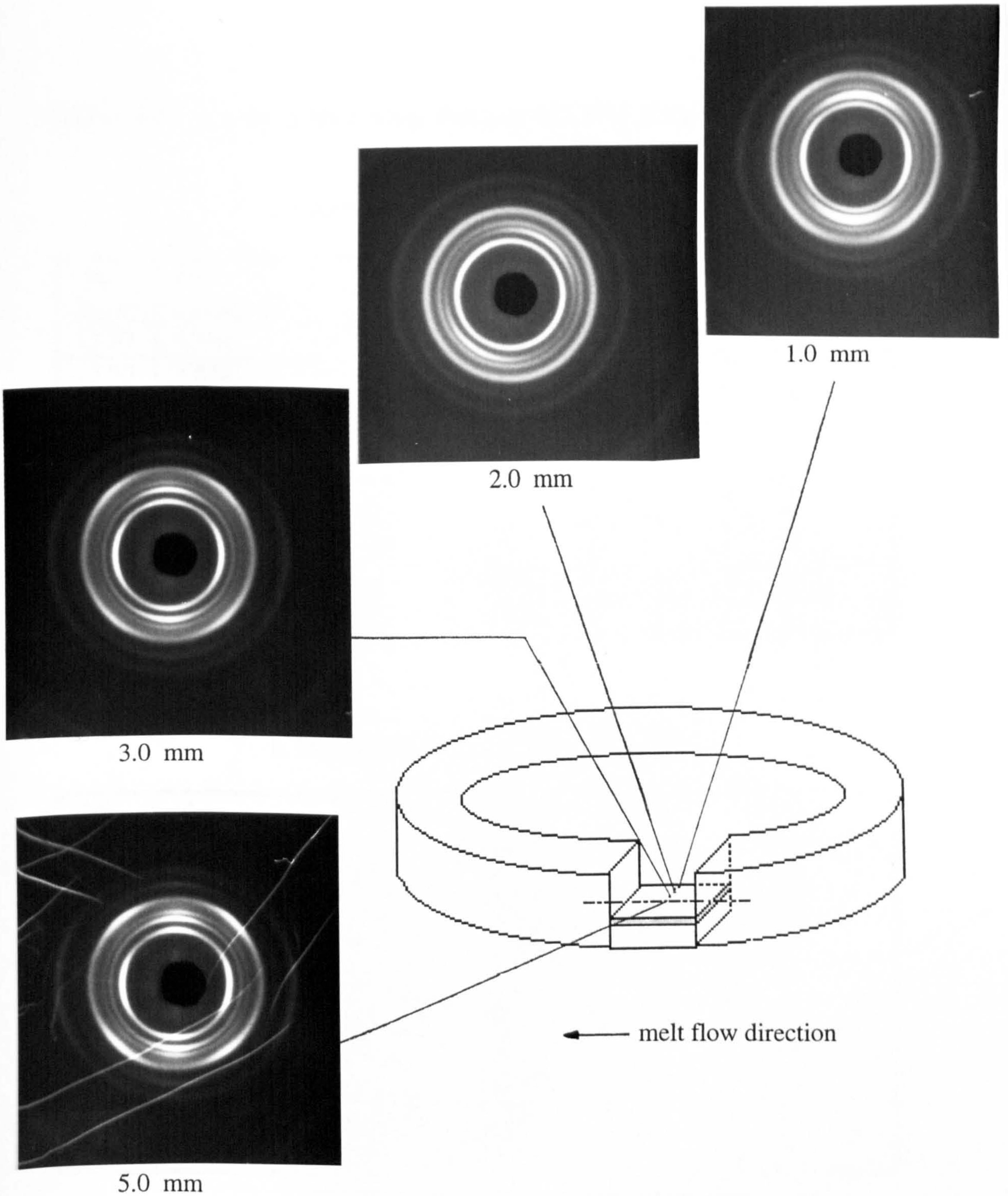

Figure 3.30 Distribution of preferred crystallite orientation in the MLFM-R2 ring moulding

Table 3.8 X-ray diffraction data of MLFM ring mouldings

a. MLFM-R1 ring moulding (AB region)

2θ (degree)	d-spacing (Å)	$d^* = \lambda/d$	Miller index (hkl)	Crystal phase	Relative intensity (%)
13.92	6.364	0.242	110	α	51
15.90	5.572	0.277	300	ß	41
16.67	5.318	0.290	040	α	100
18.35	4.834	0.319	130	α	38
19.68	4.511	0.342	117	γ	20
21.00	4.229	0.365	111	α	34
21.62	4.111	0.375	041	α	37
25.19	3.536	0.436	060	α	16
28.45	3.137	0.491	220	α	8

b. MLFM-R2 ring moulding (CD region)

2θ (degree)	d-spacing (Å)	$d^* = \lambda/d$	Miller index (hkl)	Crystal phase	Relative intensity (%)
13.97	6.340	0.243	110	α	64
15.96	5.554	0.278	300	ß	52
16.72	5.302	0.291	040	α	100
18.45	4.807	0.321	130	α	43
19.83	4.477	0.344	117	γ	23
21.06	4.219	0.365	111	α	36
21.67	4.101	0.376	041	α	38
25.24	3.529	0.437	060	α	14
28.55	3.126	0.493	220	α	7

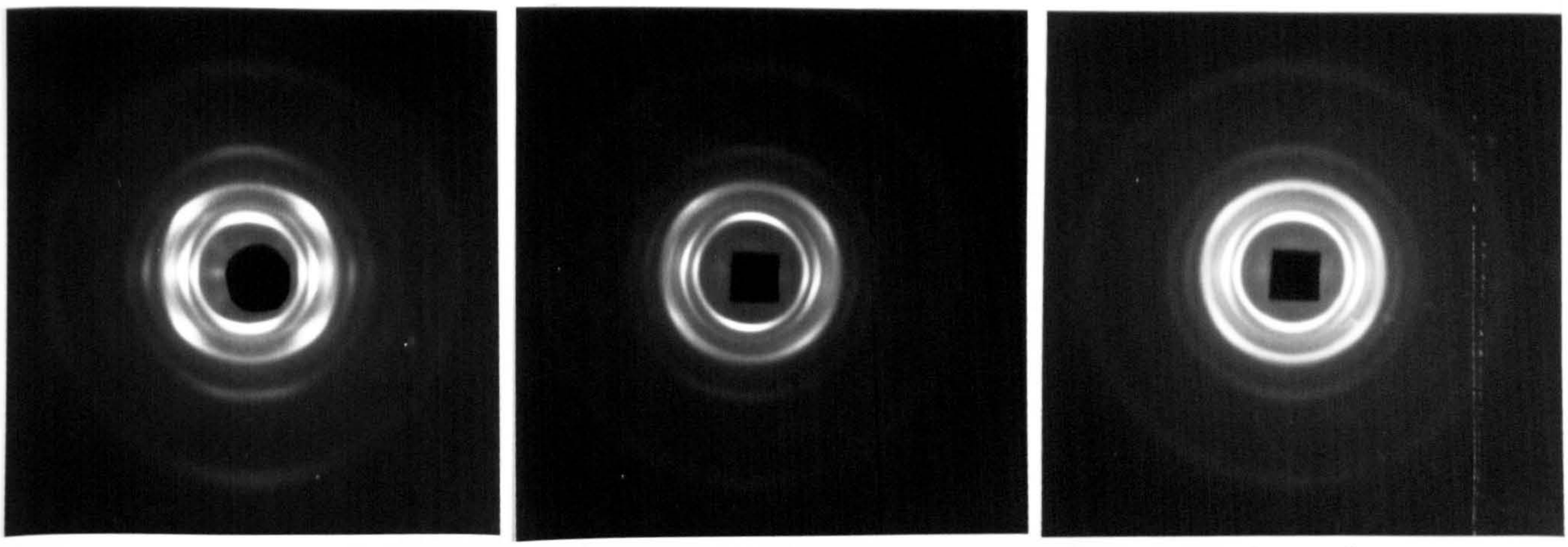

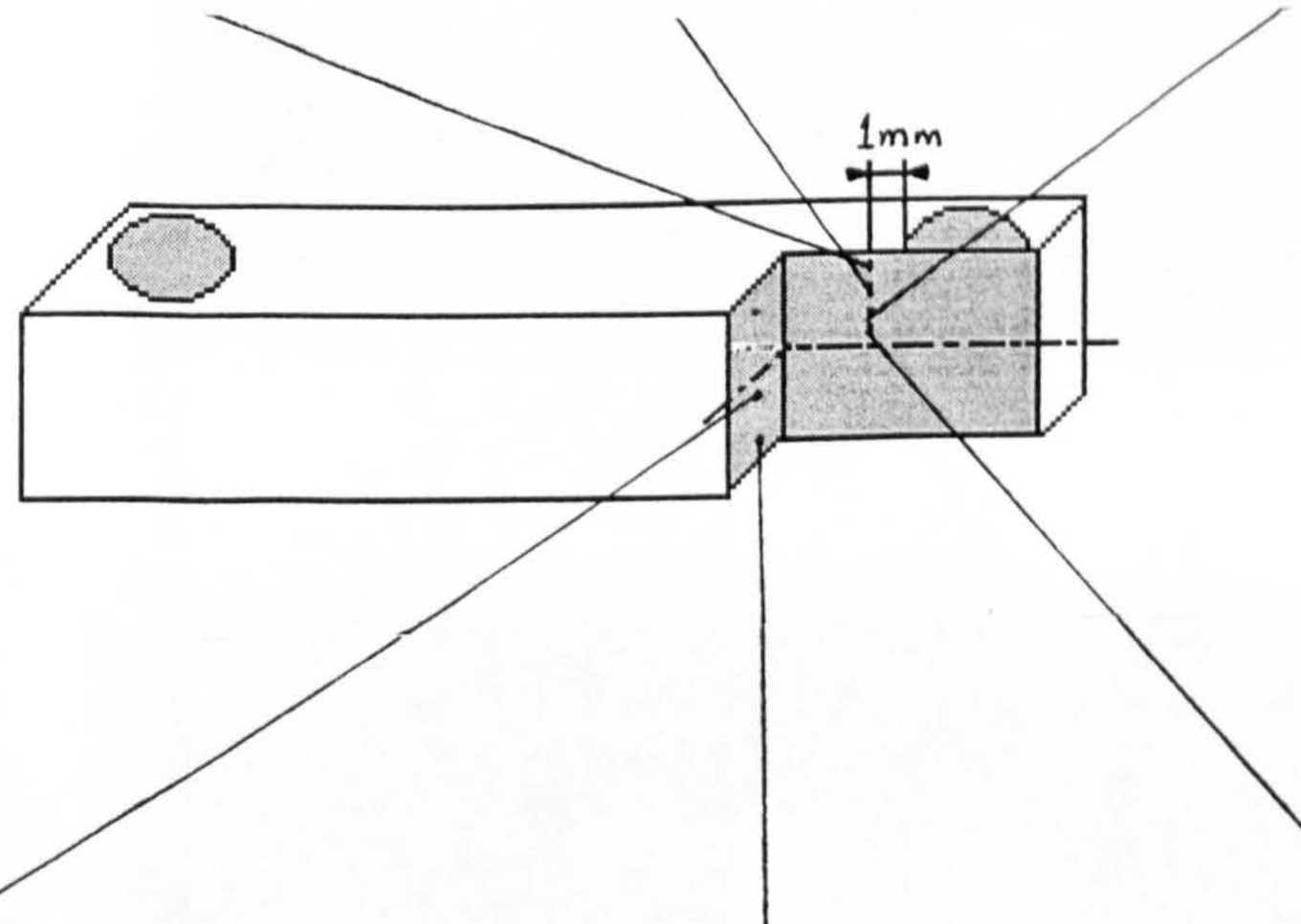

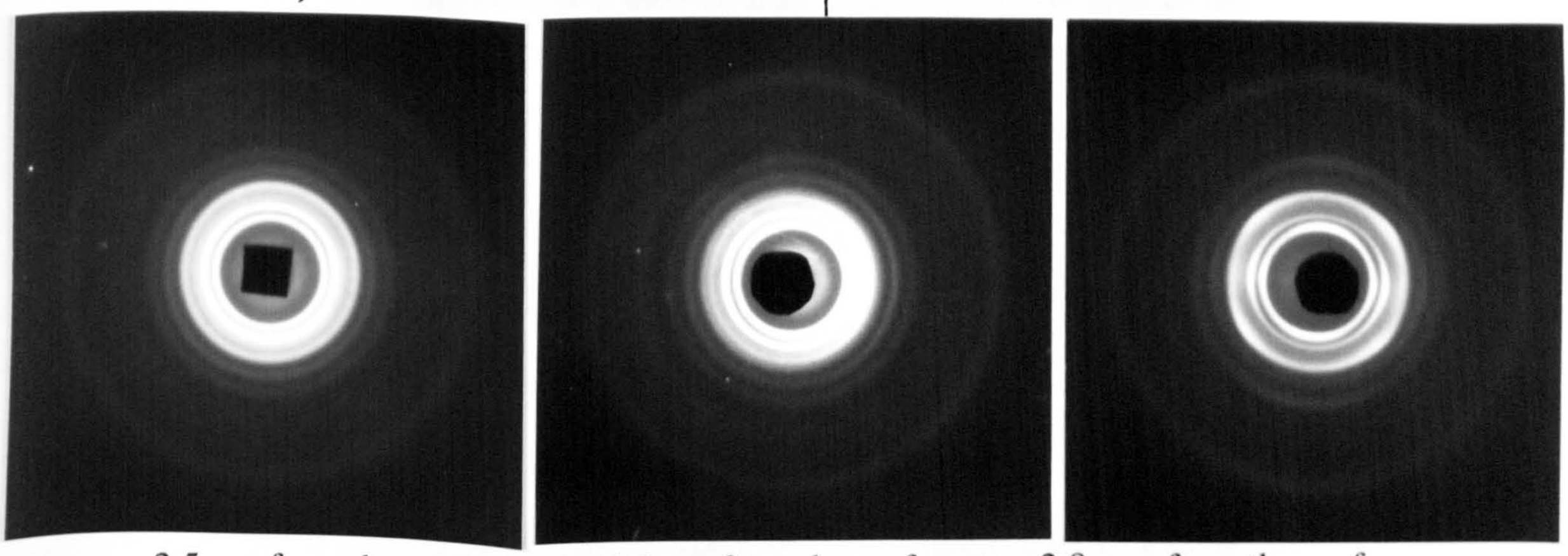

Figure 3.31 Distribution of preferred crystallite orientation in the SCORIM-3B rectangular bar moulding

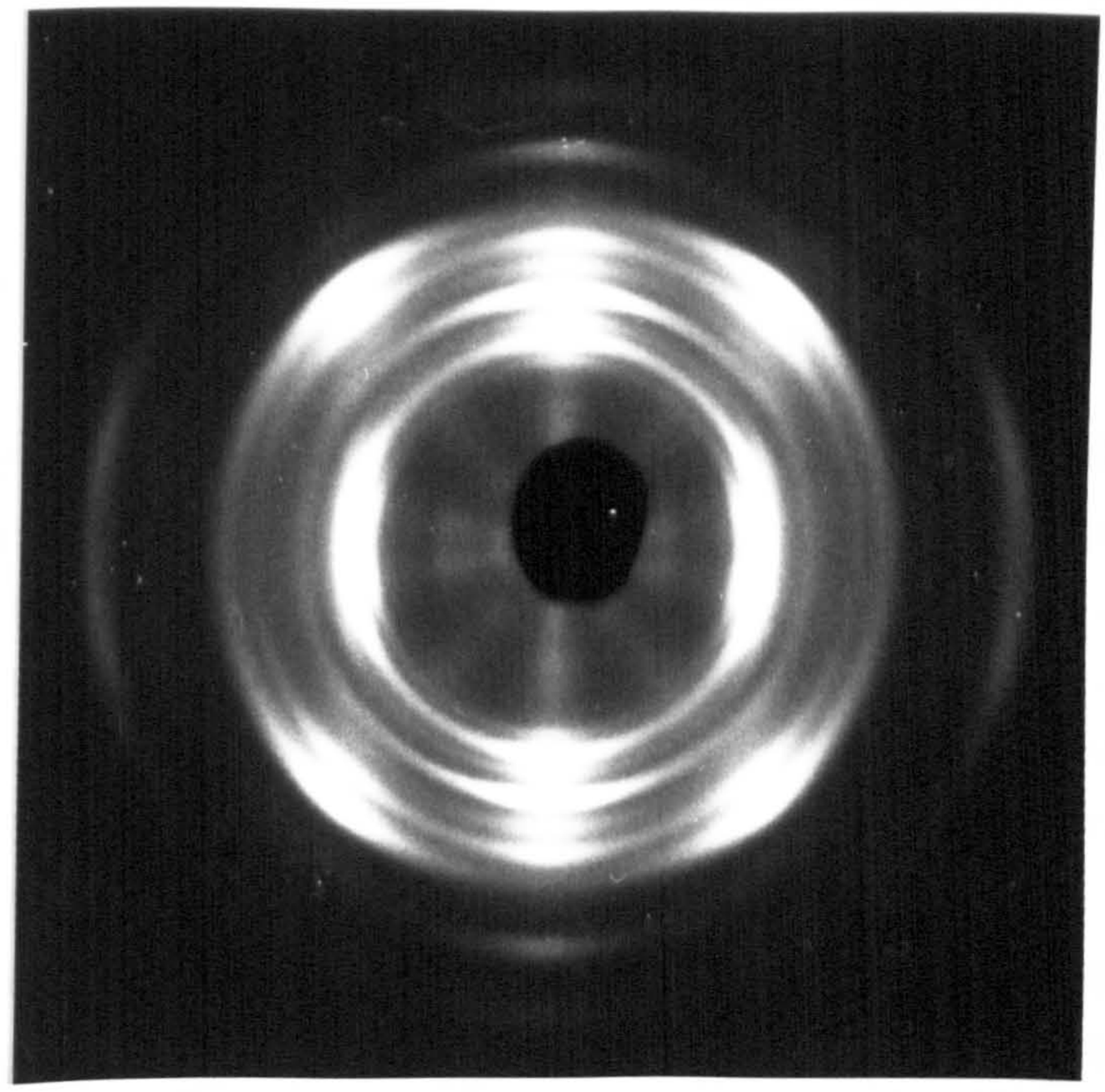

(a) SCORIM-3B

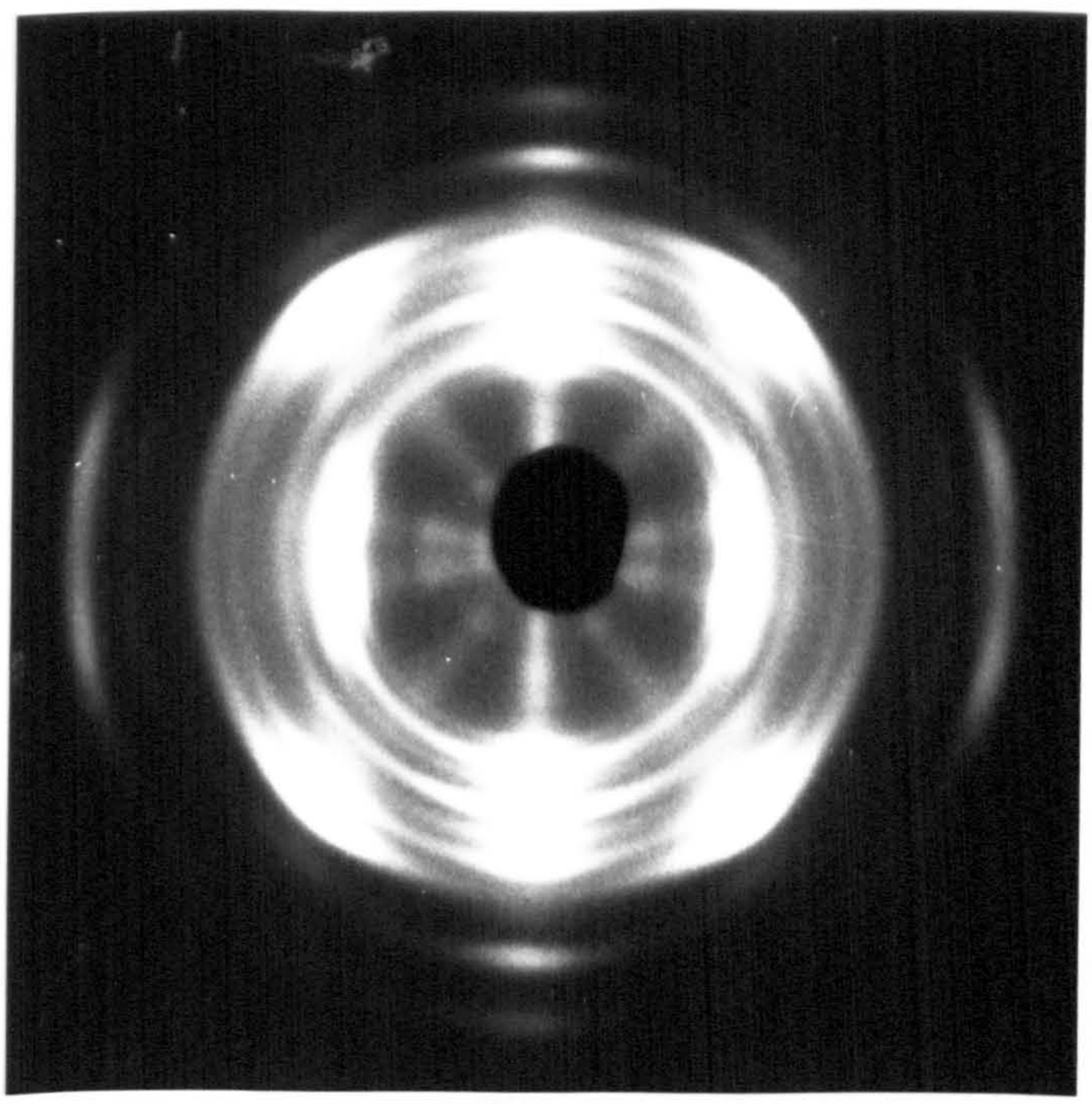

(b) SCORIM-1C

Figure 3.32 Photographs of Debye pattern of the main part of the SCORIM rectangular bar mouldings

(a) SCORIM-3B (b) SCORIM-1C

observed. The first internal unidentified ring corresponded to 2θ of 12.16° and d-spacing of 7.28 Å. The other ten rings were indexed as $(110)_\alpha$, $(113)_\gamma$, $(040)_\alpha$, $(130)_\alpha$, $(117)_\gamma$, $(111)_\alpha$, $(041)_\alpha$, $(131)_\alpha$, $(060)_\alpha$ and $(220)_\alpha$.

Figures 3.33 and 3.35 show the x-ray diffraction patterns of the SCORIM-2C and conventional-2B rectangular bar mouldings. The distance from the sample surface to the film was 37.6mm and the film exposure time was 3 hours. The testing points were taken from the cross section parallel and perpendicular to the melt flow direction (see Figure 3.33). The point positions were measured from the light micrographs (see Figure 3.8). The Debye ring pattern obtained from the cross section parallel to the melt flow direction of the SCORIM-2C sample in the skin, sub-skin, shear and core regions all exhibited the more pronounced arcs and represented the higher level of preferred c-axis and a*-axis orientation. When the samples were taken from the points in the section perpendicular to the melt flow direction, the isotropic ring patterns were obtained from each layer. Crystallographic data is shown in Table 3.9a. Figure 3.34 shows the photograph at higher magnification of the Debye pattern of the SCORIM-2C sample. The testing point was taken from the section parallel to the melt flow direction at the middle layer (as see Figure 3.34a) and perpendicular to the melt flow direction at the core region (as see Figure 3.34b). Nine Debye rings of $(110)_\alpha$, $(300)_\beta$, $(040)_\alpha$, $(130)_\alpha$, $(117)_\gamma$, $(111)_\alpha$, $(041)_\alpha$, $(060)_\alpha$, and $(220)_\alpha$ were observed.

For the conventional-2B moulding, the Debye patterns were taken from the points in the cross section parallel and perpendicular to the melt flow direction (see Figure 3.35). The Debye ring patterns exhibited a less intensity of arcing in the cross section parallel to the melt flow direction, the $(040)_\alpha$ and $(130)_\alpha$ reflections were slightly biased to the melt flow direction. When the testing points were taken from the points in the cross section perpendicular to the melt flow direction, the Debye ring patterns exhibited the isotropic rings in each layer and representing the isotropic structure. Figure 3.36 shows the photographs at higher magnification of the Debye pattern from the conventional-2B sample. The testing points were taken from the section parallel (see Figure 3.36a) and perpendicular (see Figure 3.36b) to the melt flow direction at the sub-skin layer. Six Debye rings of $(110)_\alpha$, $(040)_\alpha$, $(130)_\alpha$, $(111)_\alpha$+$(041)_\alpha$, $(060)_\alpha$ and $(220)_\alpha$ were observed.

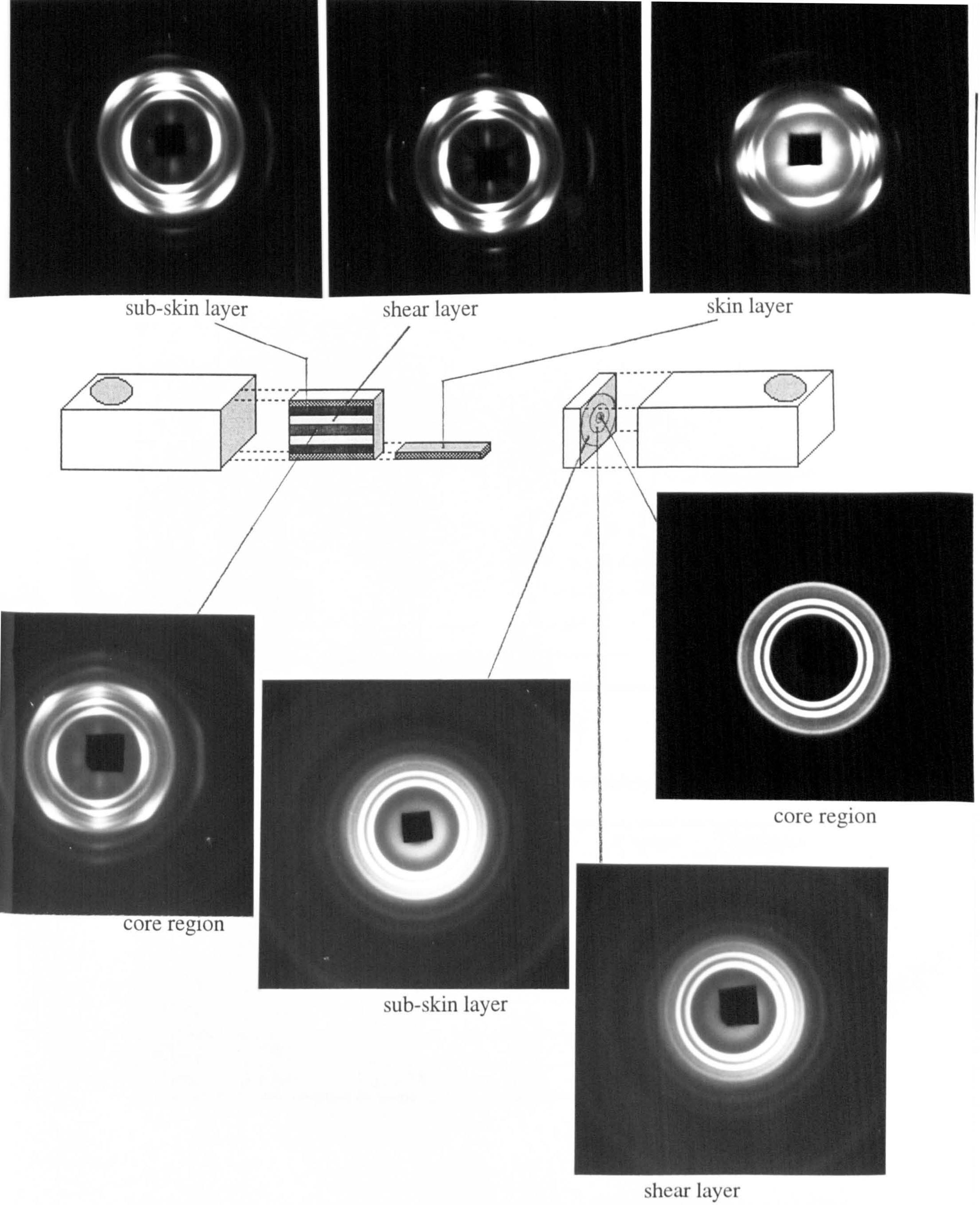

Figure 3.33 Distribution of preferred crystallite orientation in the SCORIM-2C rectangular bar moulding

Table 3.9 X-ray diffraction data of SCORIM-2C and conventional-2C rectangular bar mouldings

a. SCORIM-2C moulding

2θ (degree)	d-spacing (Å)	$d^* = \lambda/d$	Miller index (hkl)	Crystal phase	Relative intensity (%)
13.64	6.492	0.237	110	α	63
16.24	5.457	0.283	300	β	65
16.65	5.324	0.290	040	α	100
18.36	4.831	0.319	130	α	34
19.80	4.483	0.344	117	γ	34
21.11	4.208	0.366	111	α	13
21.66	4.103	0.376	041	α	9
24.39	3.648	0.423	131	α	9
25.07	3.552	0.434	060	α	15
28.29	3.155	0.489	220	α	8

b. Conventional-2C moulding

2θ (degree)	d-spacing (Å)	$d^* = \lambda/d$	Miller index (hkl)	Crystal phase	Relative intensity (%)
14.00	6.328	0.244	110	α	65
16.77	5.287	0.292	040	α	100
18.55	4.782	0.322	130	α	51
21.05	4.220	0.365	111	α	69
21.61	4.113	0.375	041	α	61
25.23	3.530	0.437	060	α	18
28.61	3.120	0.494	220	α	12

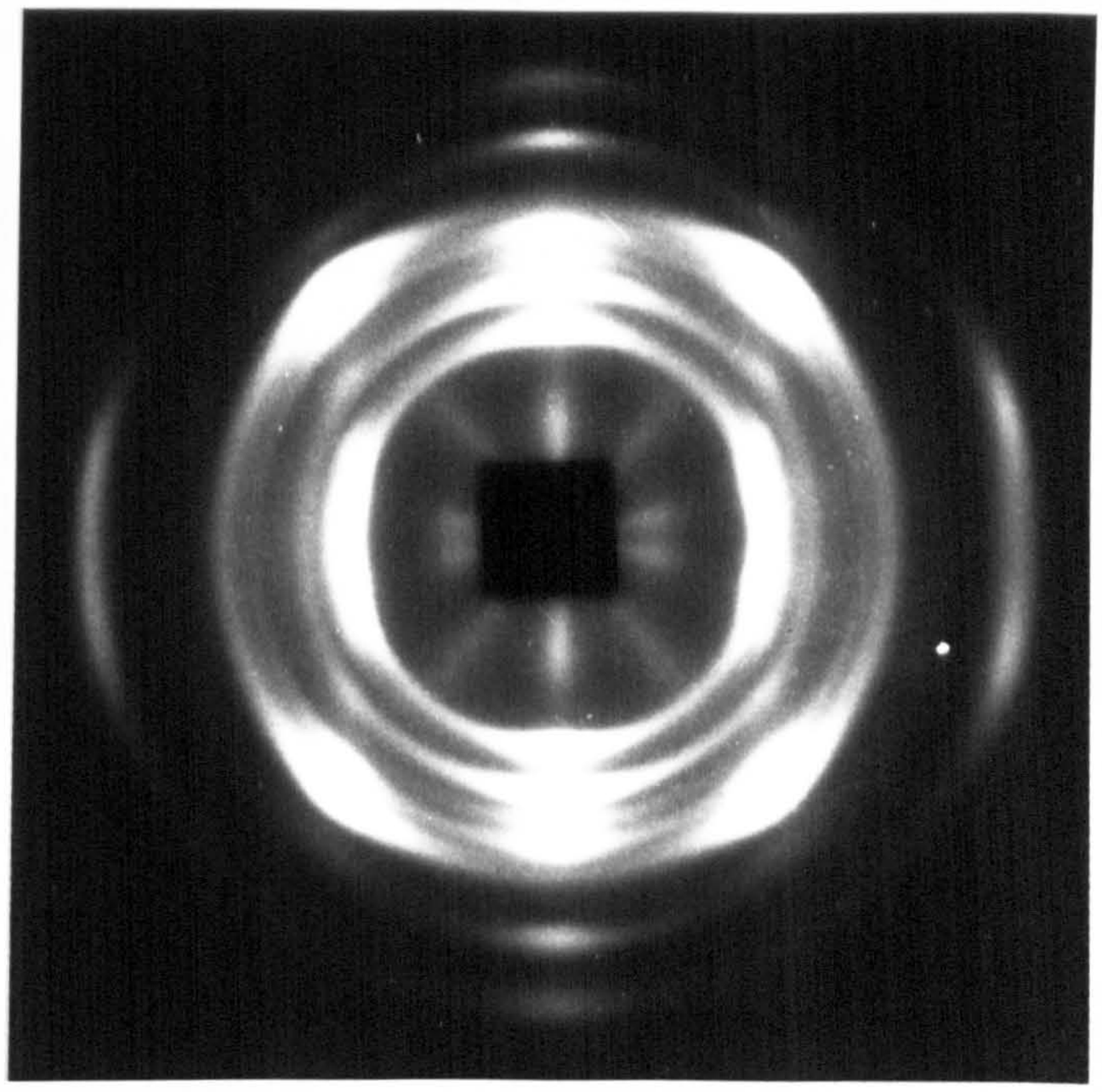

(a)

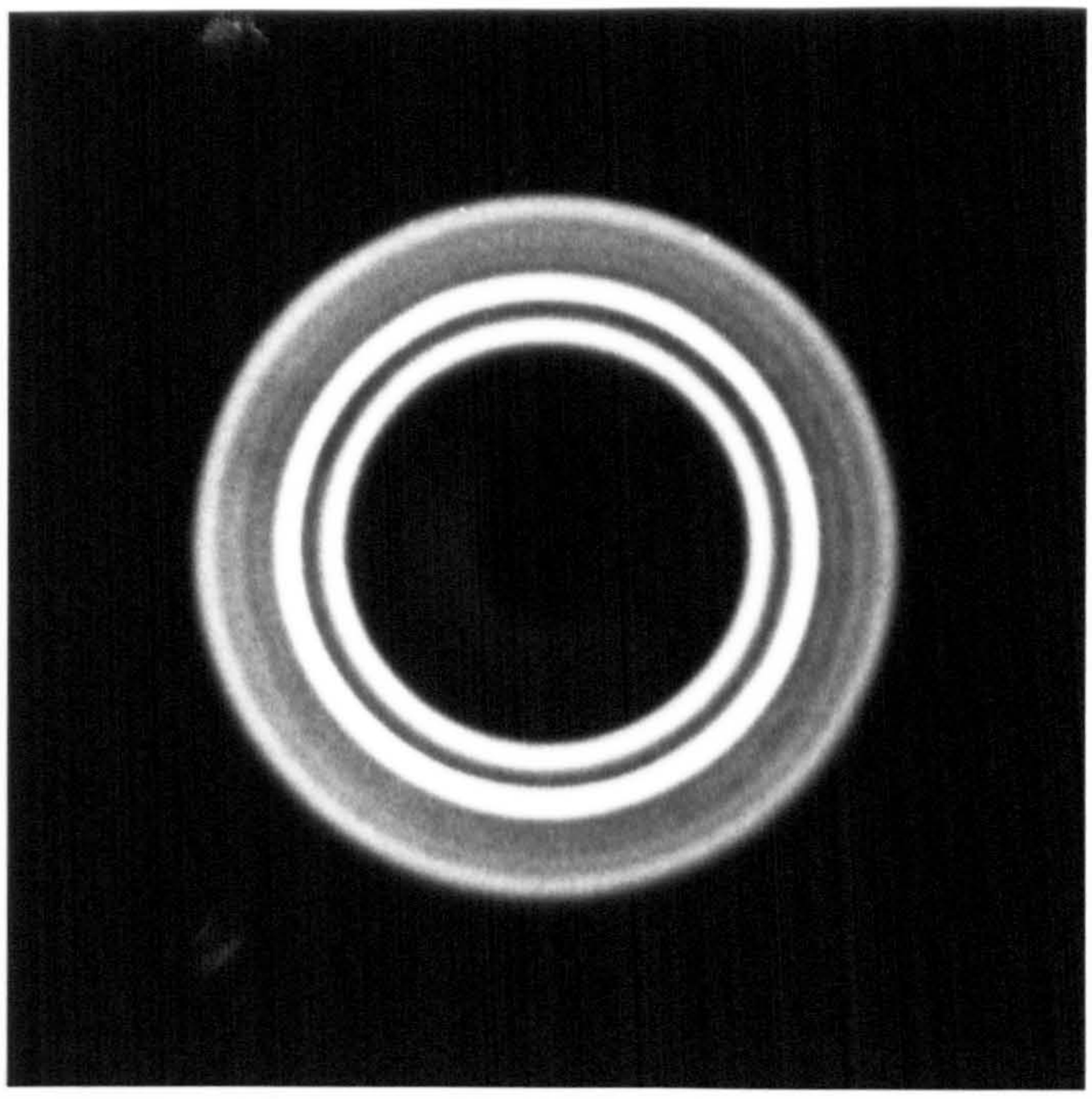

(b)

Figure 3.34 Photographs of Debye pattern of the SCORIM-2C rectangular bar moulding

(a) section parallel to the melt flow direction at the middle layer
(b) section perpendicular to the melt flow direction at the core region

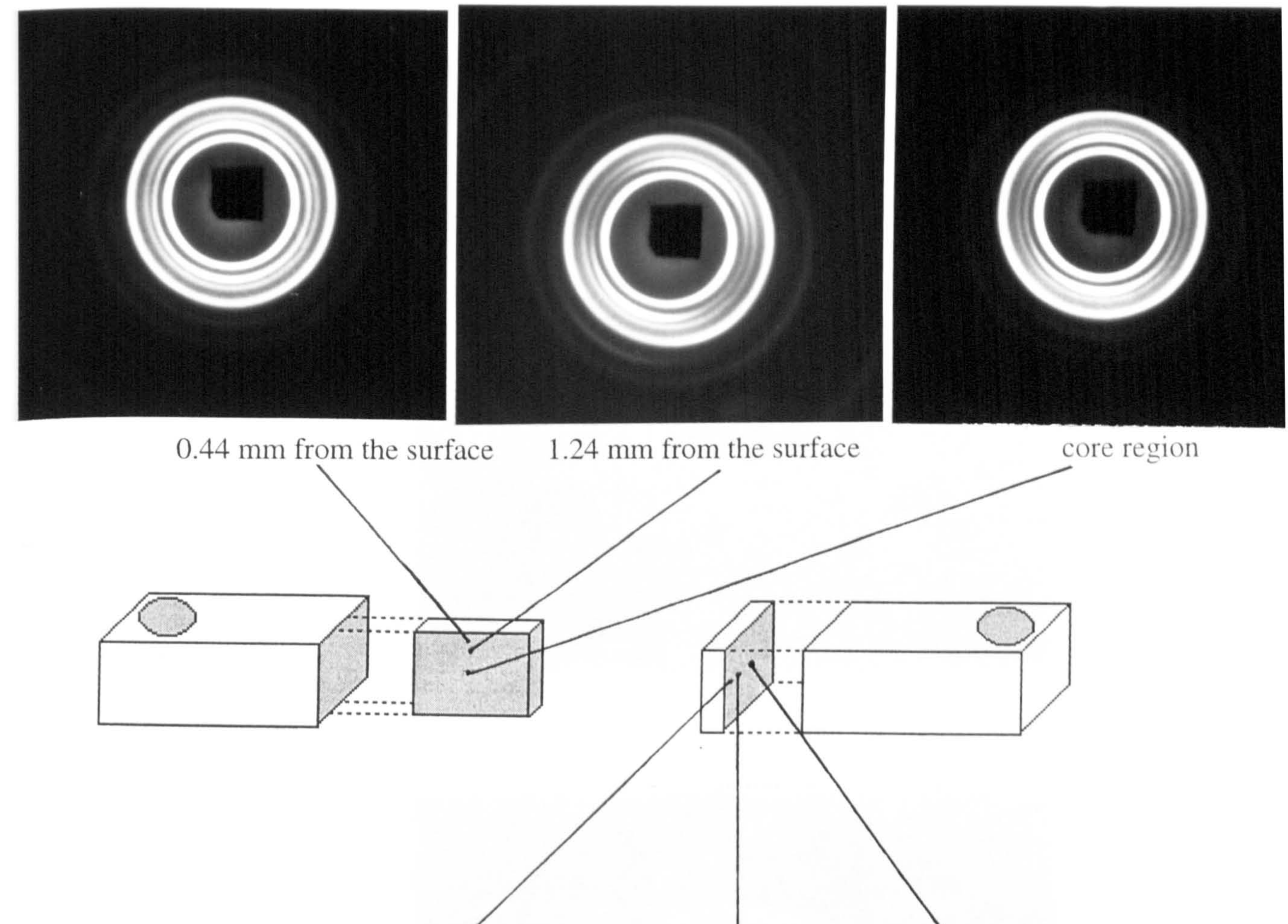

Figure 3.35 WAXS Debye patterns of the conventional-2B rectangular bar moulding

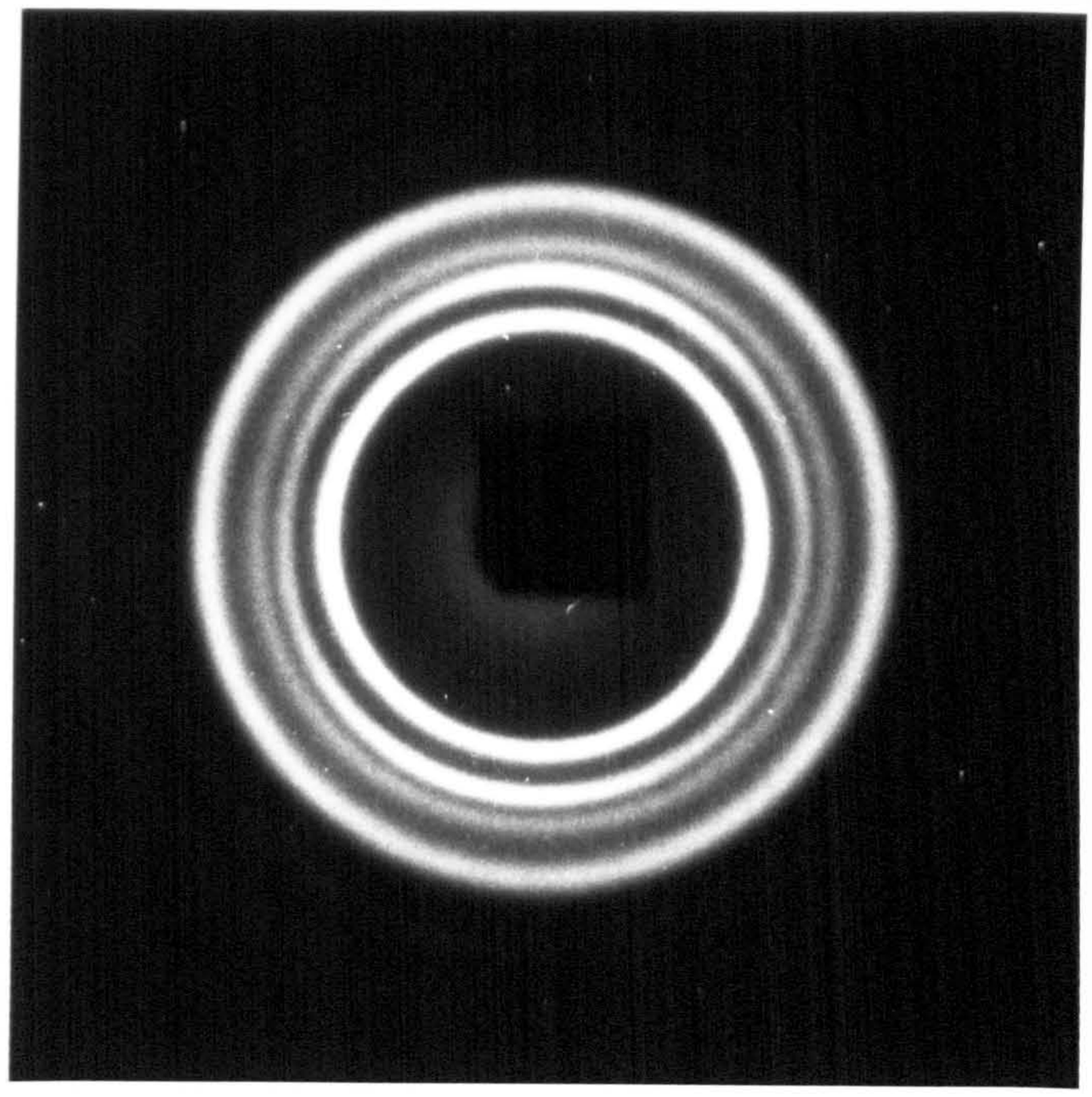

(a)

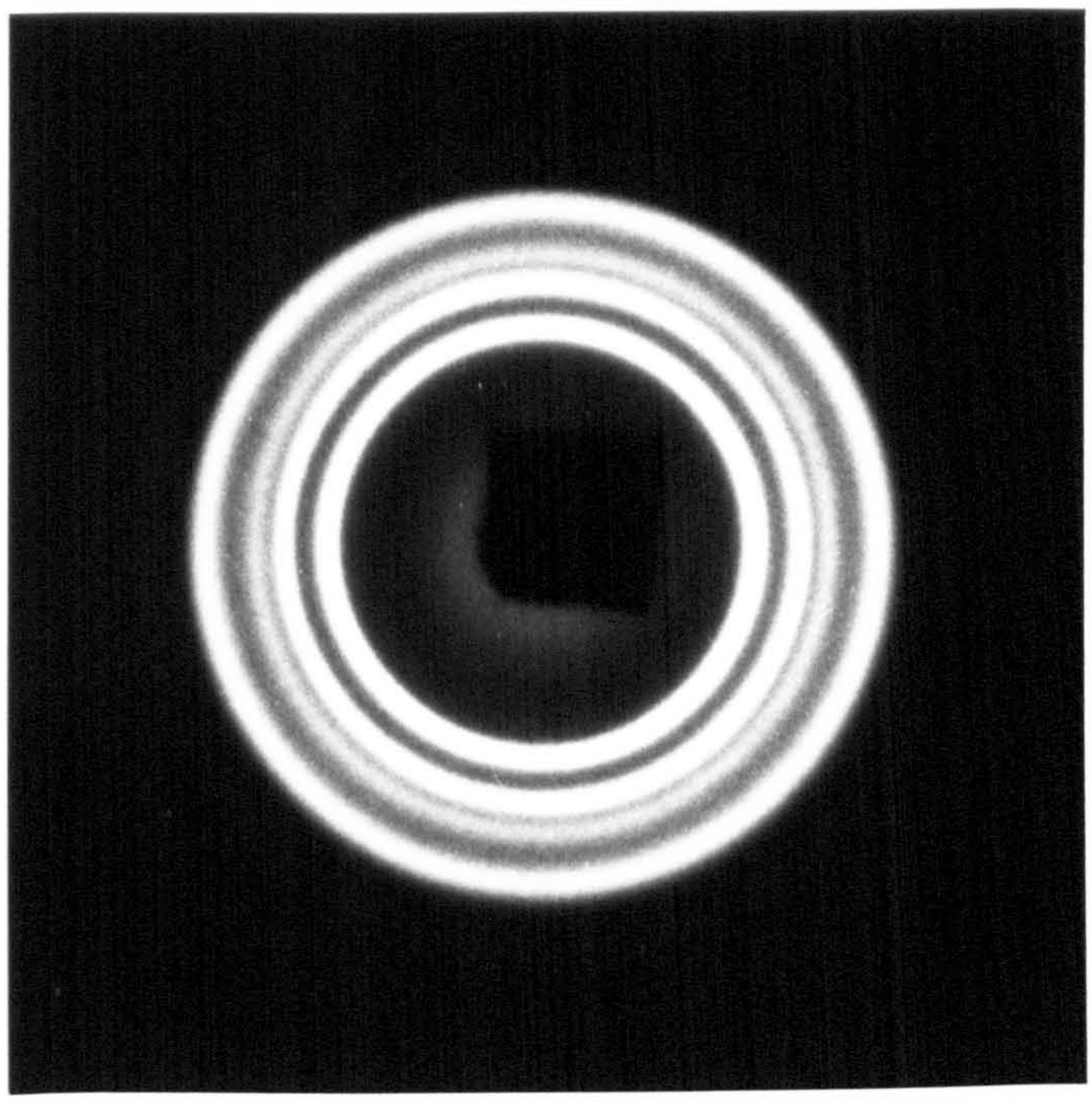

(b)

Figure 3.36 Photographs of Debye pattern at the sub-skin layer of the conventional-2B rectangular bar moulding

(a) section parallel to the melt flow direction

(b) section perpendicular to the melt flow direction

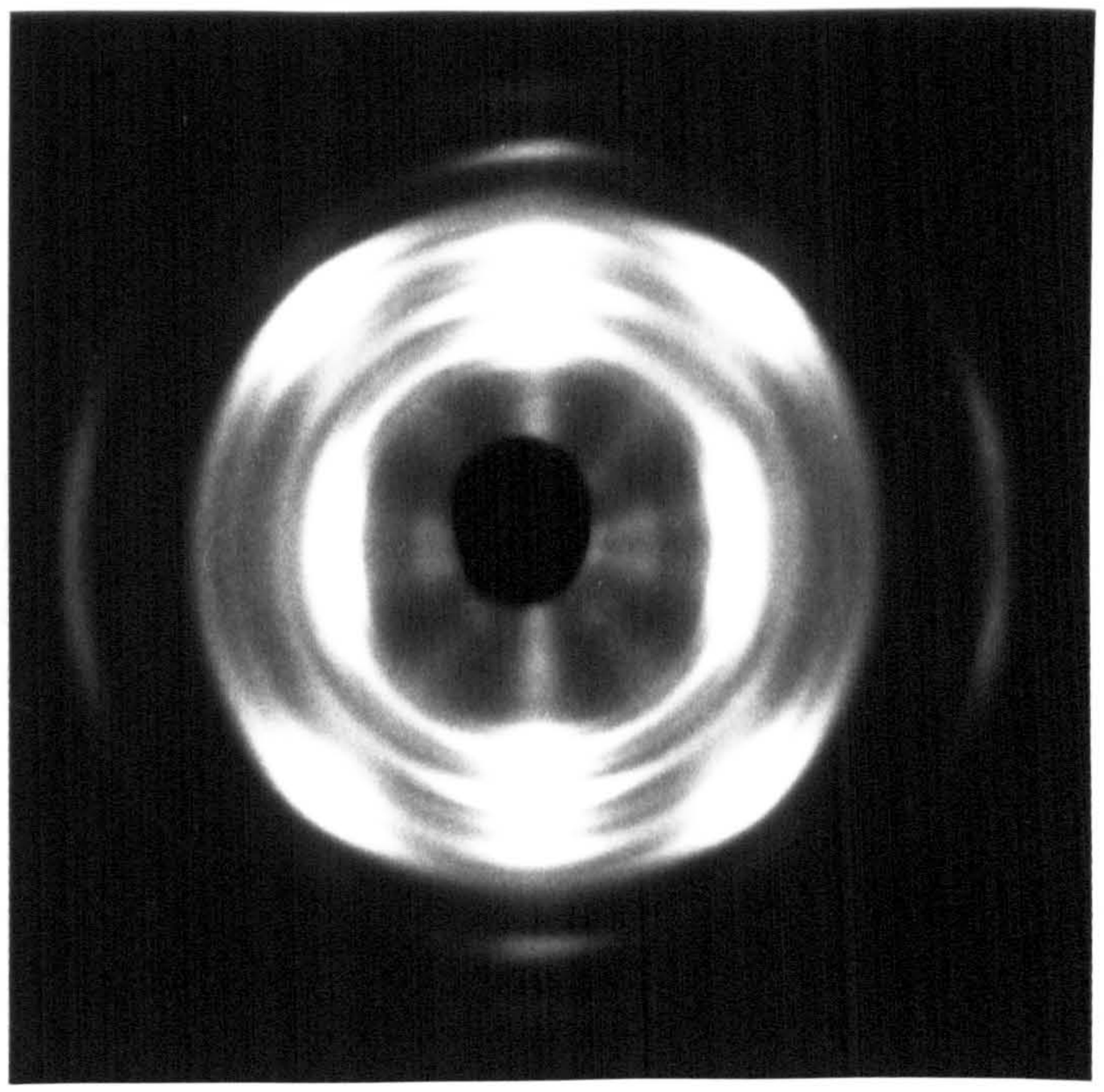

(a)

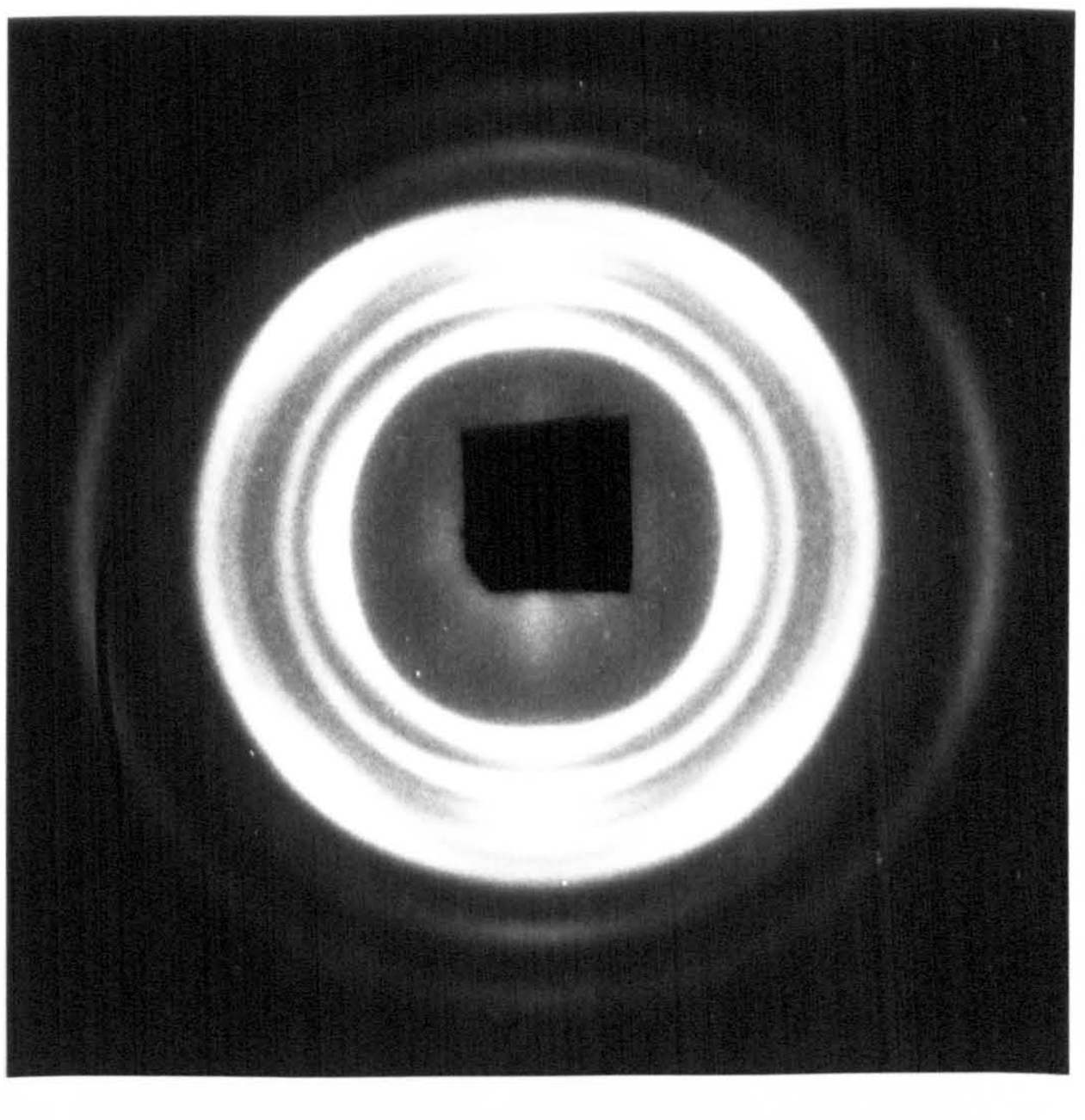

(b)

Figure 3.37 Photographs of Debye pattern at the section parallel to the melt flow direction of the SCORIM-2CM2 rectangular bar moulding

(a) in the middle layer (b) in the core region

Figure 3.37 shows the photographs at higher magnification of the Debye pattern of the SCORIM-2CM2 sample. The testing points were taken from the section parallel to the melt flow direction at the middle layer (as see Figure 3.37a) and perpendicular to the melt flow direction at the core region (as see Figure 3.37b). The sample was the same as used for Vickers microhardness measurement. The Debye ring patterns exhibited the higher level intensity of arcing and represented the preferred c-axis and a*-axis orientation. The first inner ring corresponds to 2θ of 12.16°. The other eleven rings were as follows: $(110)_\alpha$, $(113)_\gamma$, $(300)_\beta$,$(040)_\alpha$, $(130)_\alpha$, $(117)_\gamma$, $(111)_\alpha$, $(041)_\alpha$, $(131)_\alpha$, $(060)_\alpha$ and $(220)_\alpha$.

Figure 3.38 shows the schematic diagram of the twelve Debye ring pattern of the SCORIM samples.

3.8 Thermal Analysis of Injection Moulded iPP

The heat of fusion (ΔH) and melt temperature (T_m) were measured with a Perkin-Elmer DSC-2 connected to a Thermal Analysis Data Station (TADS-1).

For the standard tensile bar conventional moulding, the measuring temperature range was from 320K to 545K. The heating rate was 10°C/min and the cooling rate was 320°C/min. Figures 3.39 and 3.40 show the measured DSC profiles at the gate region and 8/10 length of the flow path of tensile bar mouldings under each processing condition. The DSC results shown in Table 3.10 indicated that the melting temperature (T_m) was effected slightly by using different processing conditions. The maximum melt temperature was obtained (438.76K) from the gate region by using higher nozzle temperature (220°C) and higher injection velocity (60%). The maximum difference of the melting temperature was 0.80K at the gate region. The maximum melt temperature was obtained (439.22K) from 8/10 length of the flow path by using lower nozzle temperature (200°C) and higher injection velocity (60%). The maximum difference of the melting temperature was 0.63K at 8/10 length of the flow path. The lower injection velocity resulted in moulded iPP exhibiting greater heat of fusion (ΔH) and crystallinity ($X_{\Delta H}$) for both injection temperatures. The maximum heat of fusion and crystallinity were obtained at gate regions ($\Delta H = 90.28J/g$, $X_{\Delta H} = 65.9\%$) and 8/10 length of the flow path ($\Delta H=87.45J/g$, $X_{\Delta H}= 63.8\%$) by using lower nozzle temperature (200°C) and lower

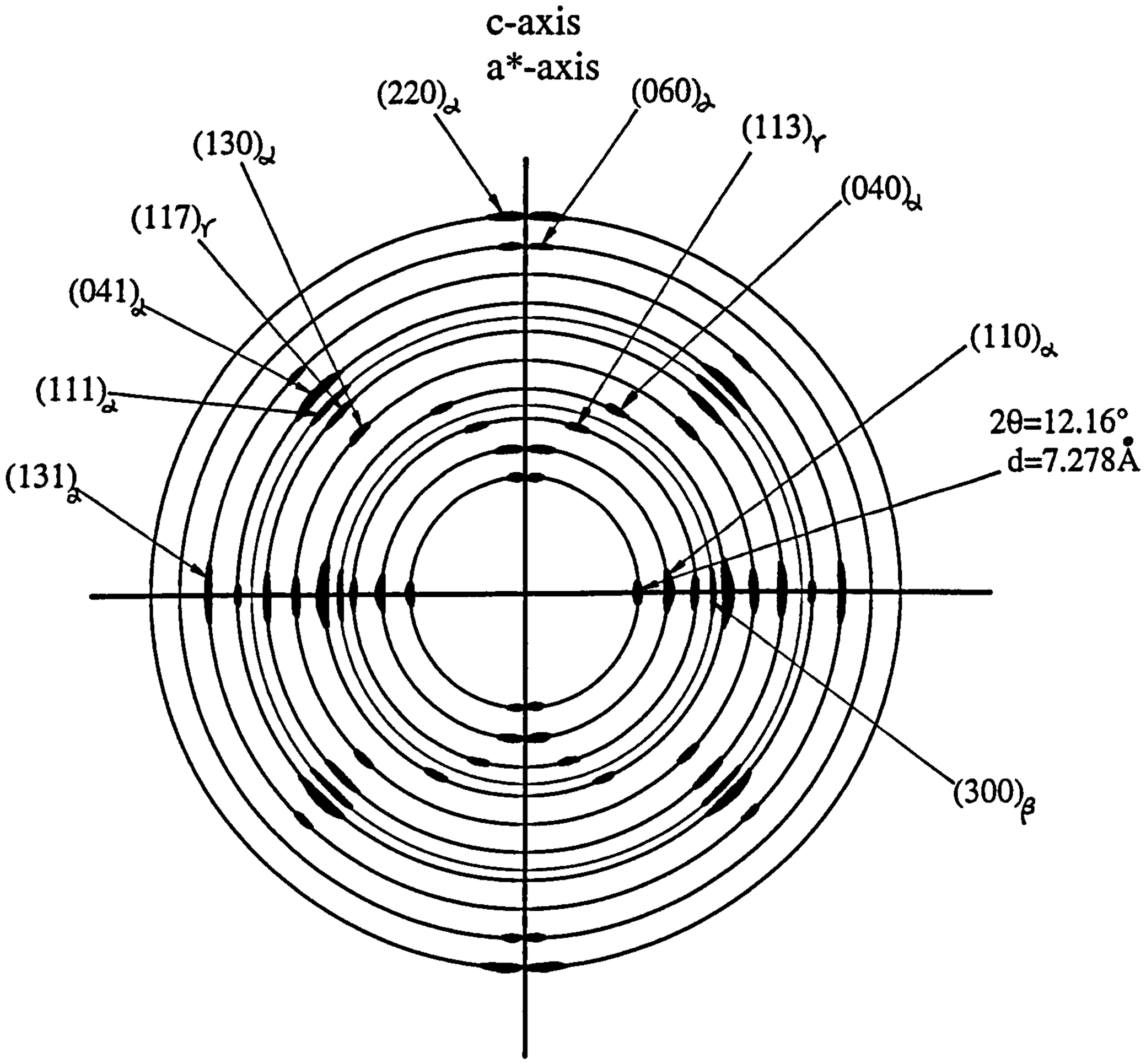

Figure 3.38 Schematic diagram of Debye pattern and indices

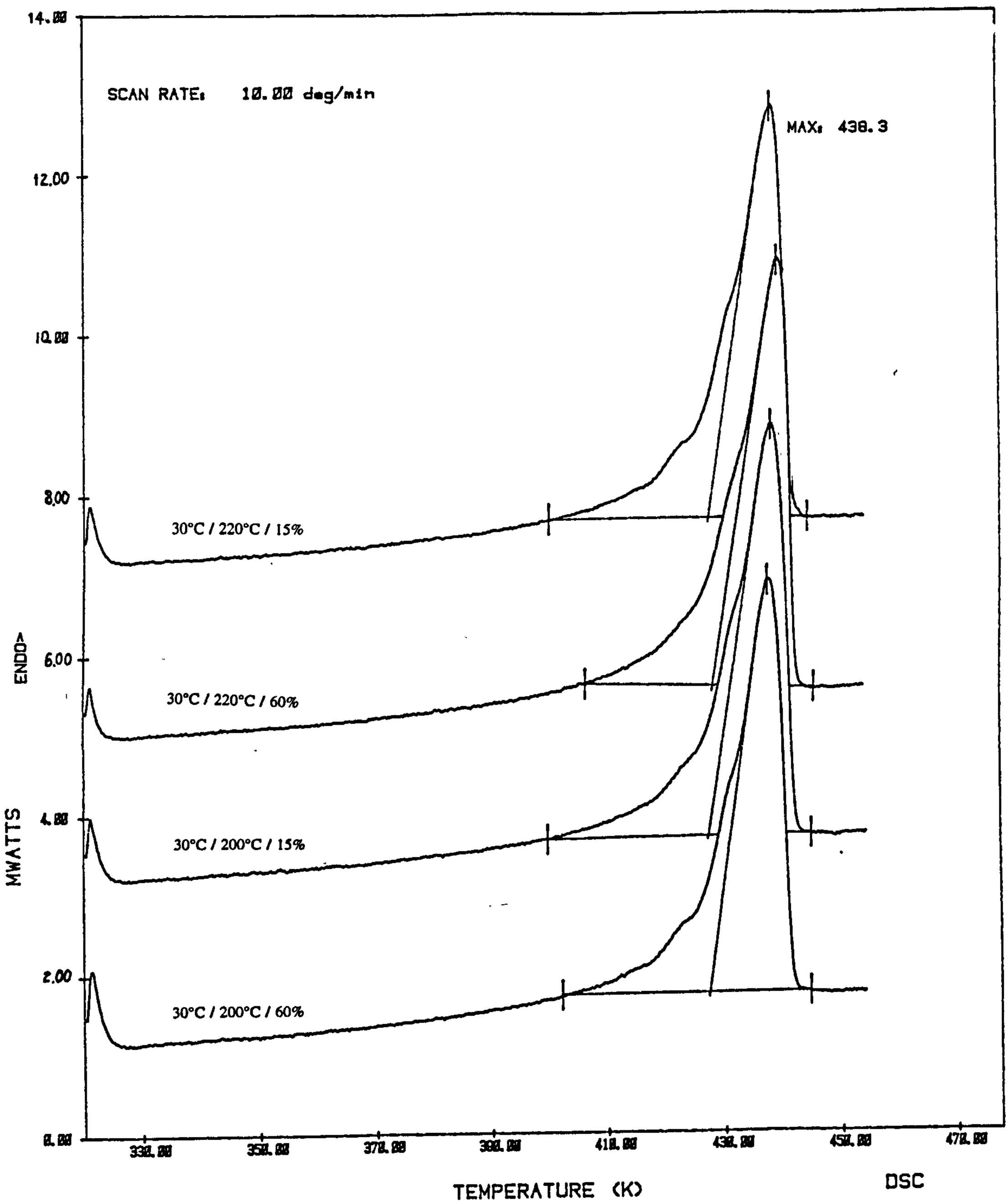

Figure 3.39 DSC thermogram of standard tensile bar conventional mouldings at the gate region with different processing conditions

(Processing conditions: mould temperature / nozzle temperature / injection speed)

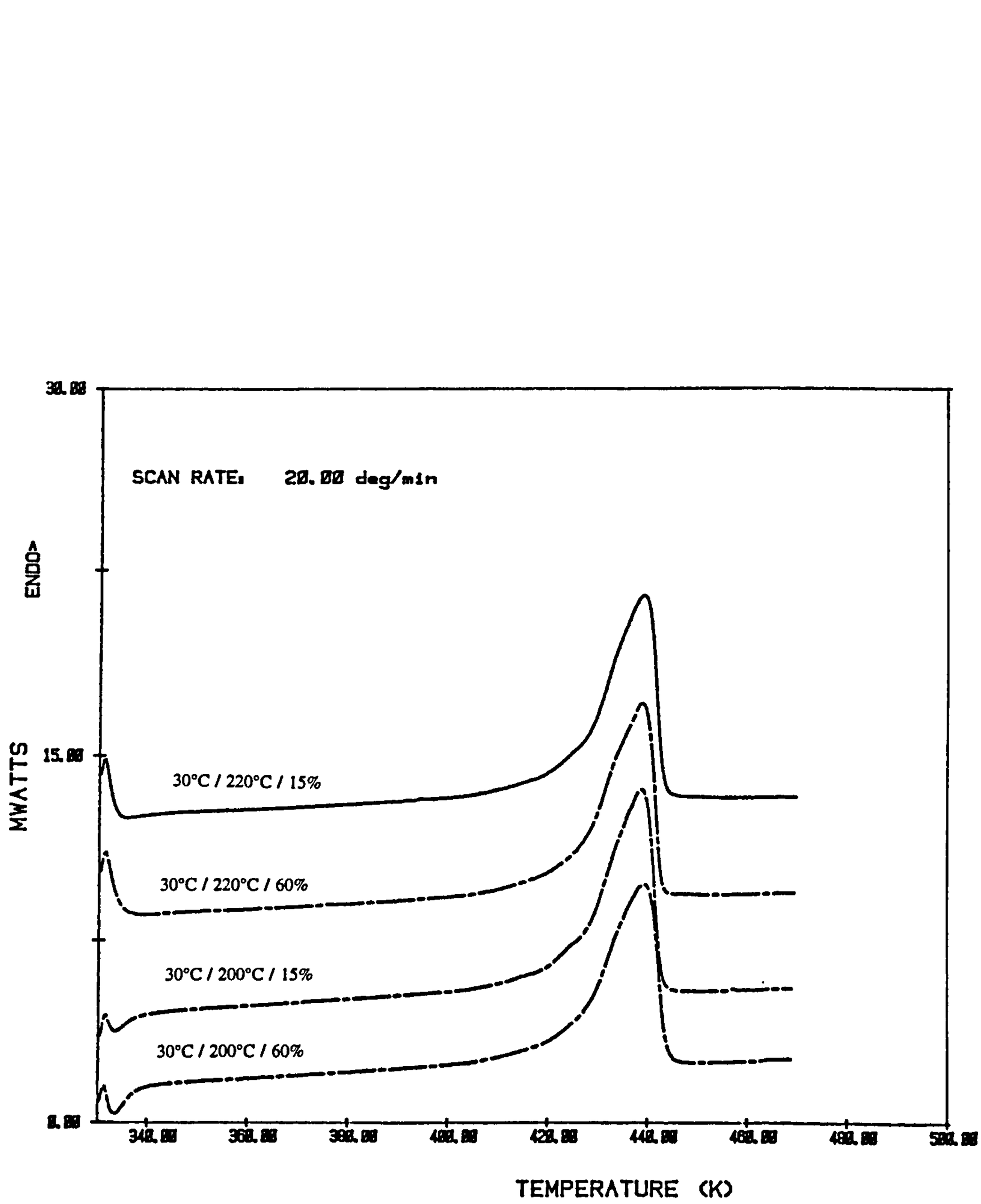

Figure 3.40 DSC thermogram of standard tensile bar of conventional injection mouldings at 8/10 length of the flow path with different processing conditions
(Processing conditions: mould temperature / nozzle temperature / injection speed)

Table 3.10 DSC measuring results at the gate region and 8/10 of the flow path of conventional standard tensile bar mouldings

Mould temperature/ Melt temperature/ Injection velocity	Gate region			8/10 of the flow path length		
	T_m (K)	ΔH (J/g)	$X_{\Delta H}$ (%)	T_m (K)	ΔH (J/g)	$X_{\Delta H}$ (%)
30°C / 220°C / 15%	438.30	88.85	64.2	439.06	85.70	62.5
30°C / 220°C / 60%	438.76	86.51	63.1	438.76	83.76	61.1
30°C / 200°C / 15%	438.71	90.28	65.9	438.59	87.45	63.8
30°C / 200°C / 60%	437.96	89.18	64.9	439.22	85.63	62.5

injection velocity (15%).

For the MLFM and conventional ring mouldings, the DSC measurements were made on each gate and weld line regions. The measuring temperature range was from 320K to 485K. The heating rate was 10°C/min and the cooling rate was 320°C/min. Figures 3.41 — 3.43 show the thermogram of MLFM and conventional ring mouldings at each region. The results of melting temperature and heat of fusion are shown in Figure 3.44. Generally, the MLFM ring samples exhibited higher melting temperature and higher heat of fusion compared with conventional ring samples. The maximum heat of fusion (ΔH=99.04J/g) obtained was exhibited at gate C by use of the MLFM-R2 program and the maximum melt temperature (T_m=427.61K) obtained was at gate D by use of the MLFM-R1 program.

3.9 Summary

The effects of processing conditions on the micromorphology and mechanical properties of iPP was investigated. Both SCORIM and conventional techniques were employed for iPP injection mouldings by using three mould of different shapes, i.e. conventional single-gated tensile bar, conventional and four live-feed four-gated rings, conventional and SCORIM two-gated rectangular bars. The experimental results show that the mechanical properties of those mouldings are significantly enhanced by using the SCORIM technique.

The spherulitic structure of the conventional mouldings exhibited the skin-core morphology. The micromorphology of the SCORIM mouldings show the preferred oriented laminate structure within the mouldings. No shear related structure was observed in the section of conventional mouldings.

TEM observations confirmed the existence of the shish-kebab structure in the SCORIM mouldings and equiaxed α-phase spherulites in the conventional moulding.

The variation in anisotropy identified by microhardness measurement is consistent with the recorded x-ray diffraction patterns and light microscopy. In comparison

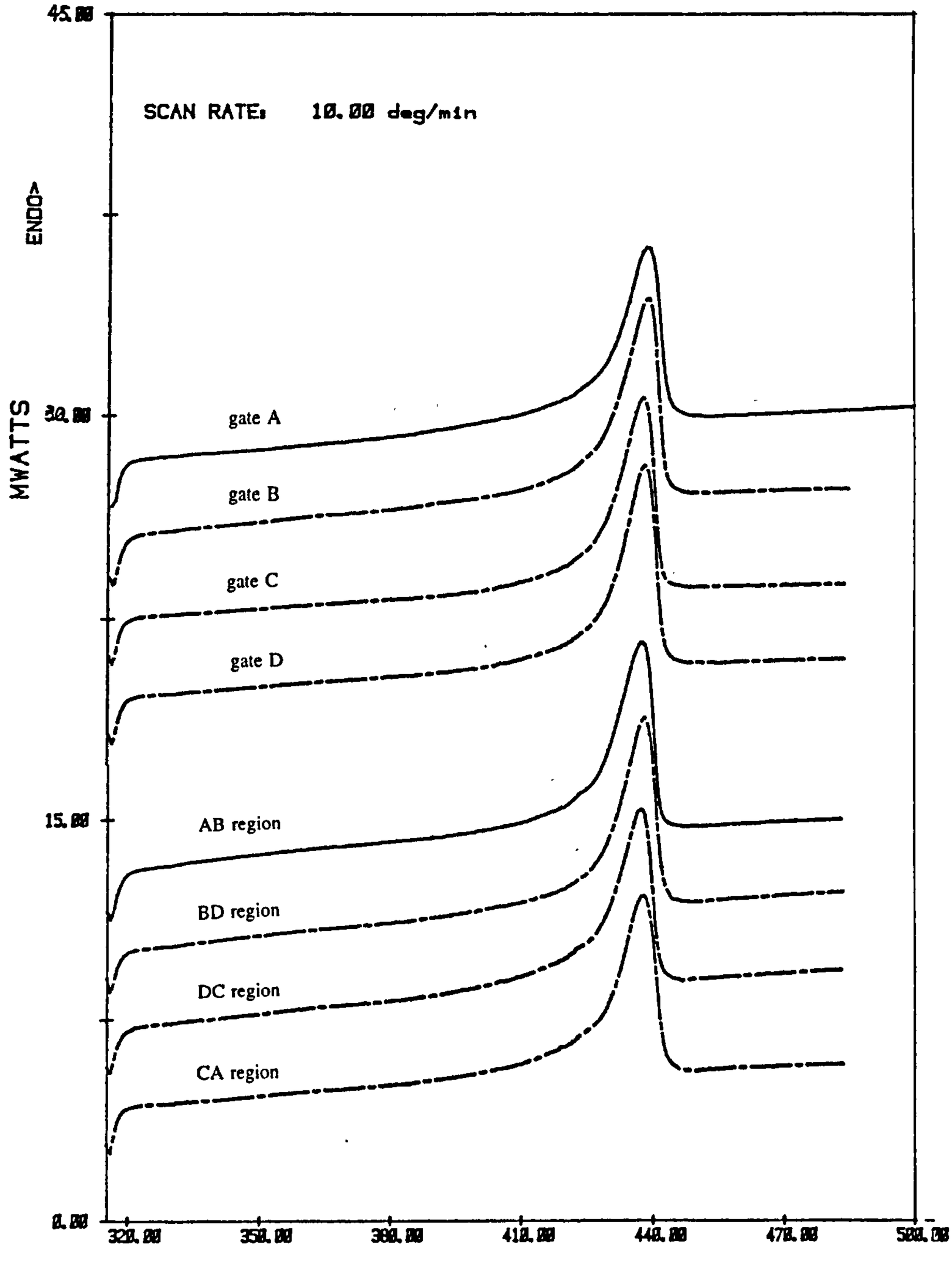

Figure 3.41 DSC thermogram of MLFM-R1 ring mouldings at each gate and weld line region

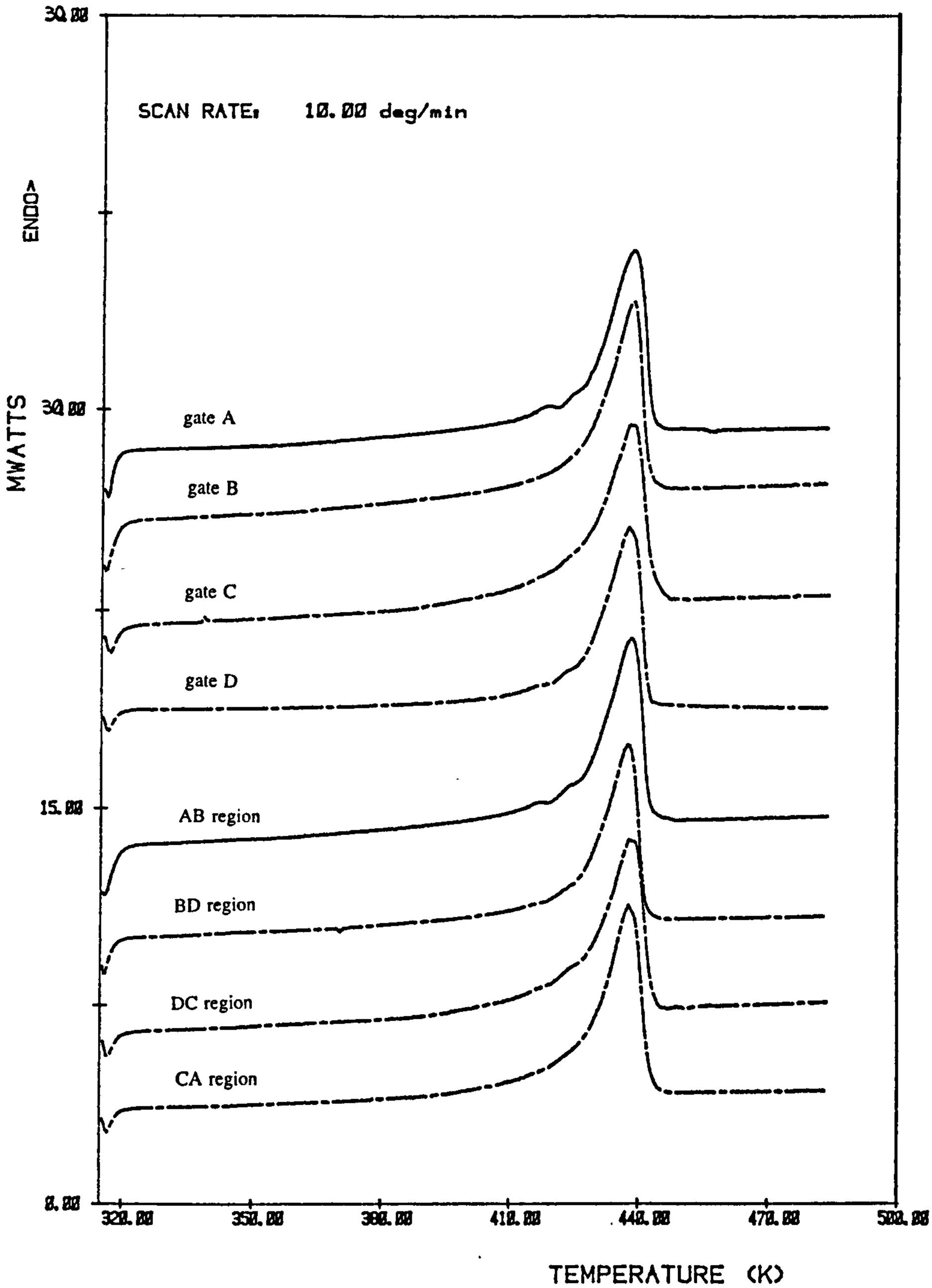

Figure 3.42 DSC thermogram of MLFM-R2 ring mouldings at each gate and weld line region

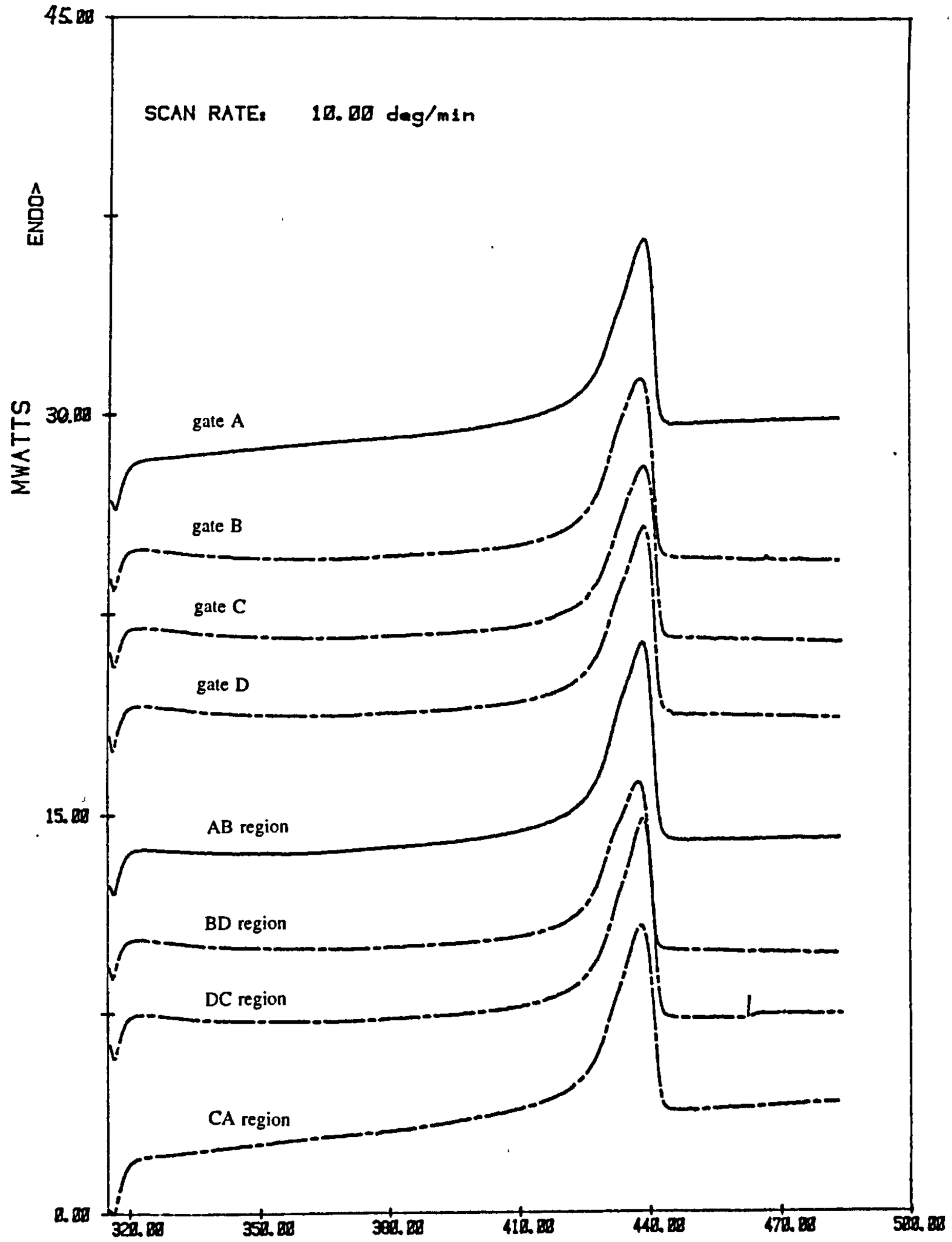

Figure 3.43 DSC thermogram of conventional ring mouldings at each gate and weld line region

(a)

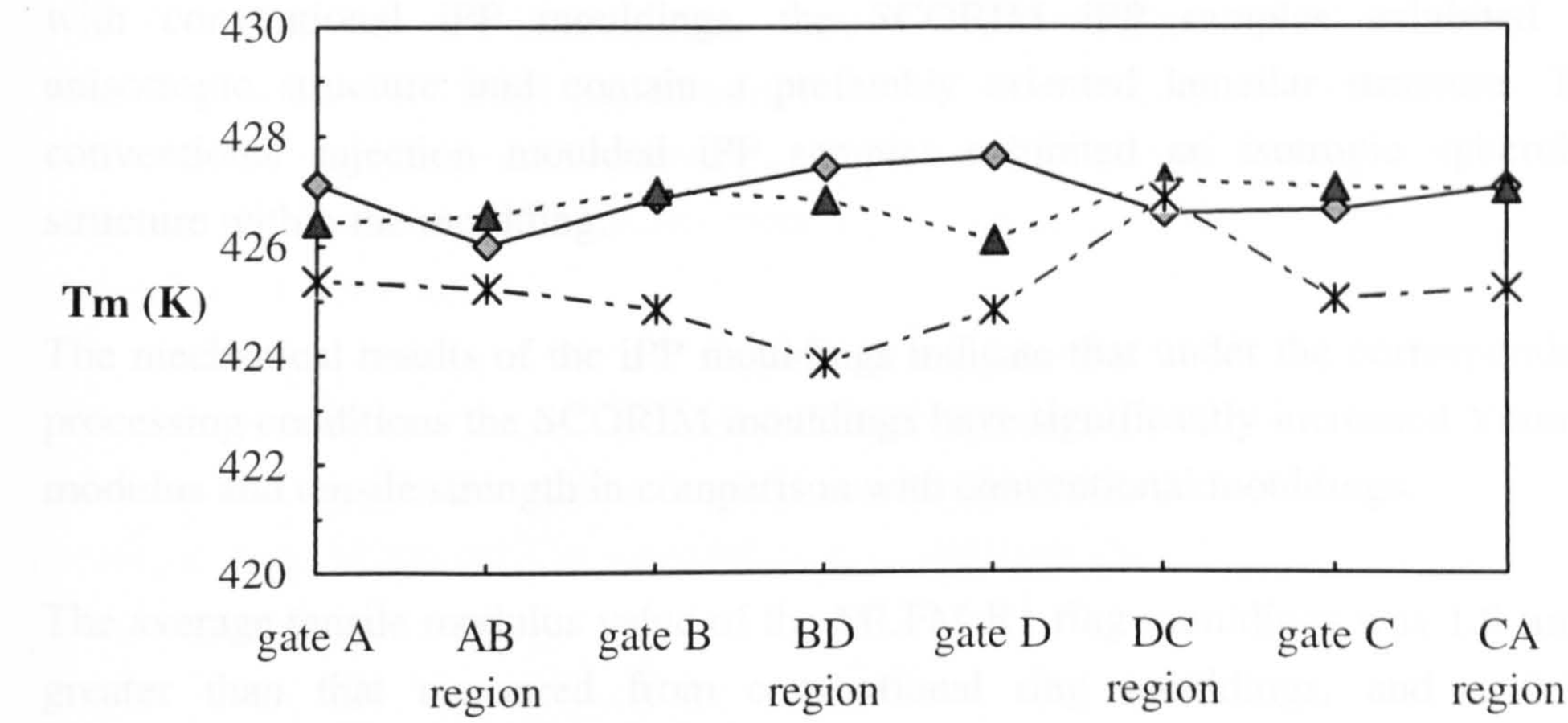

(b)

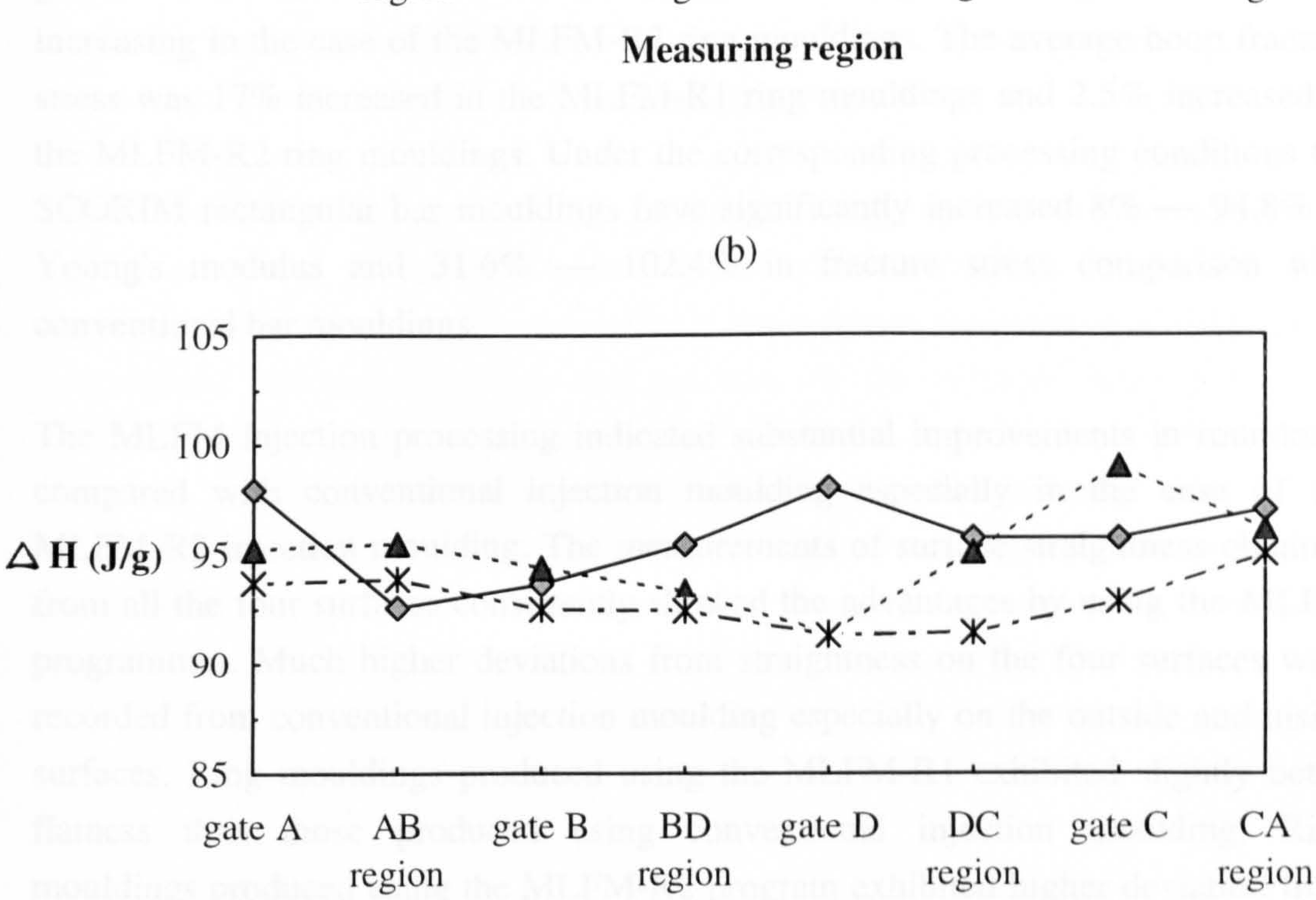

Figure 3.44 DSC measuring results of MLFM and conventional injection ring mouldings

(a) melting temperature T_m (b) heat of fusion ΔH

with conventional iPP mouldings, the SCORIM iPP samples exhibited an anisotropic structure and contain a preferably oriented lamellar structure. The conventional injection moulded iPP samples exhibited an isotropic spherulite structure within the moulding.

The mechanical results of the iPP mouldings indicate that under the corresponding processing conditions the SCORIM mouldings have significantly increased Young's modulus and tensile strength in comparison with conventional mouldings.

The average tensile modulus value of the MLFM-R1 ring mouldings was 1.9 times greater than that measured from conventional ring mouldings, and a 9.3% increasing in the case of the MLFM-R2 ring mouldings. The average hoop fracture stress was 17% increased in the MLFM-R1 ring mouldings and 2.5% increased in the MLFM-R2 ring mouldings. Under the corresponding processing conditions the SCORIM rectangular bar mouldings have significantly increased 8% — 94.8% in Young's modulus and 31.6% — 102.4% in fracture stress comparison with conventional bar mouldings.

The MLFM injection processing indicated substantial improvements in roundness compared with conventional injection moulding especially in the case of the MLFM-R2 injection moulding. The measurements of surface straightness obtained from all the four surfaces consistently showed the advantages by using the MLFM programmes. Much higher deviations from straightness on the four surfaces were recorded from conventional injection moulding especially on the outside and inside surfaces. Ring mouldings produced using the MLFM-R1 exhibited slightly better flatness than those produced using conventional injection moulding. Ring mouldings produced using the MLFM-R2 program exhibited higher deviation from flatness than either the MLFM-R1 or conventional moulding.

In comparison with conventional ring samples, the wide angle x-ray scattering profiles of the SCORIM samples exhibited a new intense reflection at a Bragg angle (2θ) of 19.68° for MLFM-R1, 19.83° for MLFM-R2 and 19.80° for SCORIM-2C corresponding to the $(117)_\gamma$ reflection in the γ-phase. Generally, the values of α-phase index A, ß-phase index B and crystallinity index C of the SCORIM samples were greater than that of conventional samples.

The WAXS Debye ring pattern obtained from the section parallel to the melt flow direction of the SCORIM samples in the skin, sub-skin, shear and core regions exhibited the more pronounced arcing and represented the preferred orientation. The isotropic ring pattern was obtained from each layer in the section perpendicular to the melt flow direction.

The Debye ring pattern of the conventional moulding exhibited the less level intensity of arcing in the cross section parallel to melt flow direction, and exhibited isotropic rings in the section perpendicular to the melt flow direction in each layer and representing an isotropic structure.

Generally, the MLFM ring samples exhibited higher melting temperature and higher heat of fusion compared with conventional ring samples.

Thus it can be concluded that the mechanical properties of the mouldings are dependent on the processing conditions and micromorphology. There are many factors that effect the process —— melting temperature, temperature profile, mould temperature, injection velocities and pressures in the cylinder, holding pressure time, cooling time and melt flowing patterns. Polymer materials have different heat histories, molecular weights, molecular weight distributions, degrees of polymerisation and impurities. Careful selection of appropriate processing parameters can produce mouldings with required properties for practical applications.

CHAPTER 4
EFFECTS OF PROCESSING CONDITIONS ON THE MICROMORPHOLOGY AND MECHANICAL PROPERTIES OF iPP WITH THE ADDITION OF NUCLEATING AGENTS

4.1 Selection of Injection Moulding Processing Conditions for iPP with the Addition of Nucleating Agents

Nucleating agents are widely used in the plastics industry to regulate the spherulite size of crystalline polymer materials. Nucleation and crystallisation can be described as the thermal and kinetic processes which allow the formation of a stable solid phase with a regular ordered geometry from a structurally disordered phase. The addition of nucleating agents to polymers with a medium crystal growth rate has been widely practised in plastics fabrication, not only for the improvement in mechanical properties and optical clarity [129, 130], but also for the shortening of cycle times in injection moulding processes [131]. The study on the nucleation of crystallisation in polymers and mainly in polypropylene has been extensively carried out for the last few decades, as a response to its increased industrial use [132, 133]. Although the nucleation process may be either homogeneous or heterogeneous, the former is practically never achieved in polymer crystallisation [134]; yet heterogeneous nucleation generally implies that the crystallisation is carried out in the presence of some deliberately added foreign substance [135, 136]. Such substances are better known as nucleating agents, the influence of which on the polymer crystallisation is then evaluated [137].

The aim here is to study the close relationship between processing conditions and mechanical properties of iPP with the addition of nucleating agents by using conventional and SCORIM techniques. The processing of isotactic polypropylene modifies to a great extent the behaviour of the polymer during crystallisation because of the role of nucleating agents play and the presence of shear stresses. The activity of a nucleating agent has been estimated by the number of nuclei [138]. The multiplication of the number of nuclei of heterogeneous crystallisation prevents a three-dimensional spherulitic development of the lamellae. The application of the shear stress in polypropylene promotes the orientation of the macromolecular chains in the stress direction, which will allow the growth of crystalline lamellae. A wide range of techniques have been used to investigate the crystallisation and physical properties of nucleated grades of polypropylene. These included: light microscopy, TEM, mechanical testing, x-ray diffraction, WAXS Debye flat plate technique, density measurement and DSC.

4.1.1 Conventional and SCORIM Processes

Conventional and SCORIM techniques were employed in the experiments, and different concentrations of the nucleating agents were used. The SCORIM processes were further investigated using the following different oscillating modes for the application of cyclic shear stress to the solidifying melt:

1) shear was supplied by oscillating both pistons moving in phase simultaneously under different compression pressure;
2) oscillating shear was supplied by both pistons moving in phase simultaneously at the same compression pressure;
3) shear was supplied to the mould cavity by moving pistons out of phase alternately under different compression pressure.

Two mould configurations, with one gate at the head of the standard tensile bar and two gates at both sides of rectangular bar were studied. Figures 2.1 and 2.4 show whole sections of both bar mouldings, parallel and perpendicular to the melt flow direction.

The results described throughout this study were those obtained on samples moulded from polypropylene containing different concentrations of nucleating agents, and these were prepared in the following two ways:

(1) iPP containing 0.1, 0.15, 0.2, 0.3 and 2 wt.% of Geniset MD and ADK STAB (NA-11) nucleating agents was used (the melting flow index of the basic iPP at 230°C is 10.5g/10mins). The necessary amounts of iPP and different concentrations of nucleating agents were mixed manually. A Sandretto Torino 6GV-50 injection machine was used to prepare conventional injection mouldings which were single-gated standard tensile bars. The processing conditions are shown in the following table. For different concentrations these results were compared with those of iPP without adding nucleating agents.

melt temperature (°C)	barrel temperature (°C)	mould temperature (°C)	injection speed (%)
220	200, 190, 180, 170	40	30

(2) The mixture of iPP and 0.15 wt.% Geniset MD was used. A Demag D150 NCIII-K injection machine was used to prepare conventional and SCORIM samples which were 6×6×60 mm two-gated rectangular bars. The processing conditions are shown in Tables 4.1. The cavity melt pressures were measuren by a transducer located at the centre of the bar moulding. The values given in Table 4.1 are the average cavity pressure values were taken from the cavity pressure records which were printed from the graphic datas on the machine control. The number 1(N), 2(N) and 3(N) following the abbreviations con- and SCORIM- stand for polypropylene, iPP+0.15wt.% Geniset MD and iPP+0.15wt.% ADK STAB, respectively.

Two series of conventional injection process were set for both iPP without and with the addition of nucleating agents (con-N1 and con-N2). Four different series of the SCORIM process were set for both iPP without and with the addition of nucleating agents (SCORIM-N1, SCORIM-N2, SCORIM-N3 and SCORIM-N4). For all the SCORIM mouldings the initial volume displacement of the SCORIM piston was 5cc for each piston movement and the time for one movement was 2sec. The SCORIM action was maintained during the solidfication of the moulded section as determined by the pressure transducer. In all case the moulded section had solidfied before the holding pressure time shown in Table 4.1 had elapsed. The SCORIM profiles were adjusted for each series of the moulding conditions to give a controlled shearing/solidfication curve as indicated by the cavity pressure transducer.

4.1.2 Compression Moulding

The sample sheets were prepared using a Moore (Serial No.1563) hot press at 180°C by 40 tons pressing the mixture for 3 mins between two steel plates with a 2mm thickness spacer after 5 mins melting without pressure. Then the hot plate was moved immediately to Moore (Serial No.1121) cold press machine. The samples were cooled for 2 mins under 40 tons pressure.

The materials used to prepare compression mouldings were GYM43-iPP and Geniset MD nucleating agent. The compression moulded samples were examined by light microscopy to gain the basic morphology characteristics of the iPP resin and the nucleating agents.

Table 4.1 Conventional and SCORIM processing conditions for the rectangular bar moulding of iPP with and without the addition of nucleating agents

Temperature (°C):

Sample I. D.	con-N1	SCORIM-N1	SCORIM-N2	SCORIM-N3	con-N2	SCORIM-N4
Nozzle temperature	230	220	230	230	280	280
Barrel temperature	200 195 190 185 180				220 195 190 185 180	
Mould temperature	70	30	70	70	70	70

Pressure (bar):

Hold Pressure: 120 Injection Pressure: 80

average cavity pressure (bar):

Sample I. D.	con-N1	con-N2	SCORIM-N1	SCORIM-N2	SCORIM-N3	SCORIM-N4
polypropylene	1715	1715	1678	1678	1602	3033
iPP+0.15wt.% Geniset MD	1715	1637	1939	1950	1884	3410
iPP+0.15wt.% ADK STAB	—	1755	—	—	—	2974

Time (sec):

Sample I. D.	con-N1	con-N2	SCORIM-N1	SCORIM-N2	SCORIM-N3	SCORIM-N4
Hold Pressure Time	66.5	96.5	74.8	68.5	66.5	135.0
Cooling Time	20	20	25	20	20	20

Speed (rpm):

Injection Speed: 100 Plastics Screw Speed: 32

Screw Return After Plastics: 10

4.2 Light Microscopy Study of Microstructure of iPP with the Addition of Nucleating Agents

Polarized light microscopic observations on iPP crystallised with and without the addition of nucleating agents were carried out, for the purpose of confirming the nucleation effects of nucleating agents on crystallisation. In this study the sections were taken from the injection moulded tensile bar samples by microtomy, and the compression sheet mouldings were cut and prepared by pressing the piece on a hot stage. In order to illustrate the spherulitic growth, both injection moulding samples and compression moulding samples were observed in a polarizing light microscope. The results show that there are significant differences in morphology of iPP with and without the addition of nucleating agents substrates obtained from both compression moulded sheets and standard tensile bar conventional injection mouldings (see Figures 4.1 and 4.2).

In Figure 4.1, the polarized light micrograph (a) shows the typical Maltese cross structure of polypropylene spherulites; polarized light micrograph (b) shows the fine structure of the compression moulding produced from Geniset MD nucleating agent, which was a mixture of 7.5% dimethylbenzylidene sorbitol (MDBS) with polypropylene homopolymer carrier; light micrograph (c) shows the ADK STAB (NA-11) nucleating agent powder.

Figure 4.2 shows polarized light micrographs of iPP with and without the addition of nucleating agents obtained by conventional injection moulding of standard tensile bar, where fine-grain spherulitic structure of iPP with the addition of nucleating agent is clearly evident. The introduction of nucleating agents progressively reduces the spherulitic size [139]. From a comparison of micrographs, it clearly emerges that the Geniset MD and ADK STAB determine a strong nucleating effect, as evidenced by the fact that the average dimensions of nucleated-iPP spherulites are comparatively smaller in the samples containing 0.3 wt.% of nucleating agents (micrographs d and e) than in the samples containing 0.1 wt.% of nucleating agents (micrographs b and c). The injection moulded iPP without adding nucleating agent crystallised without restriction, growing quite freely to develop large-size spherulites (see micrograph a).

In the samples of iPP with the addition of nucleating agents, most of the cross-

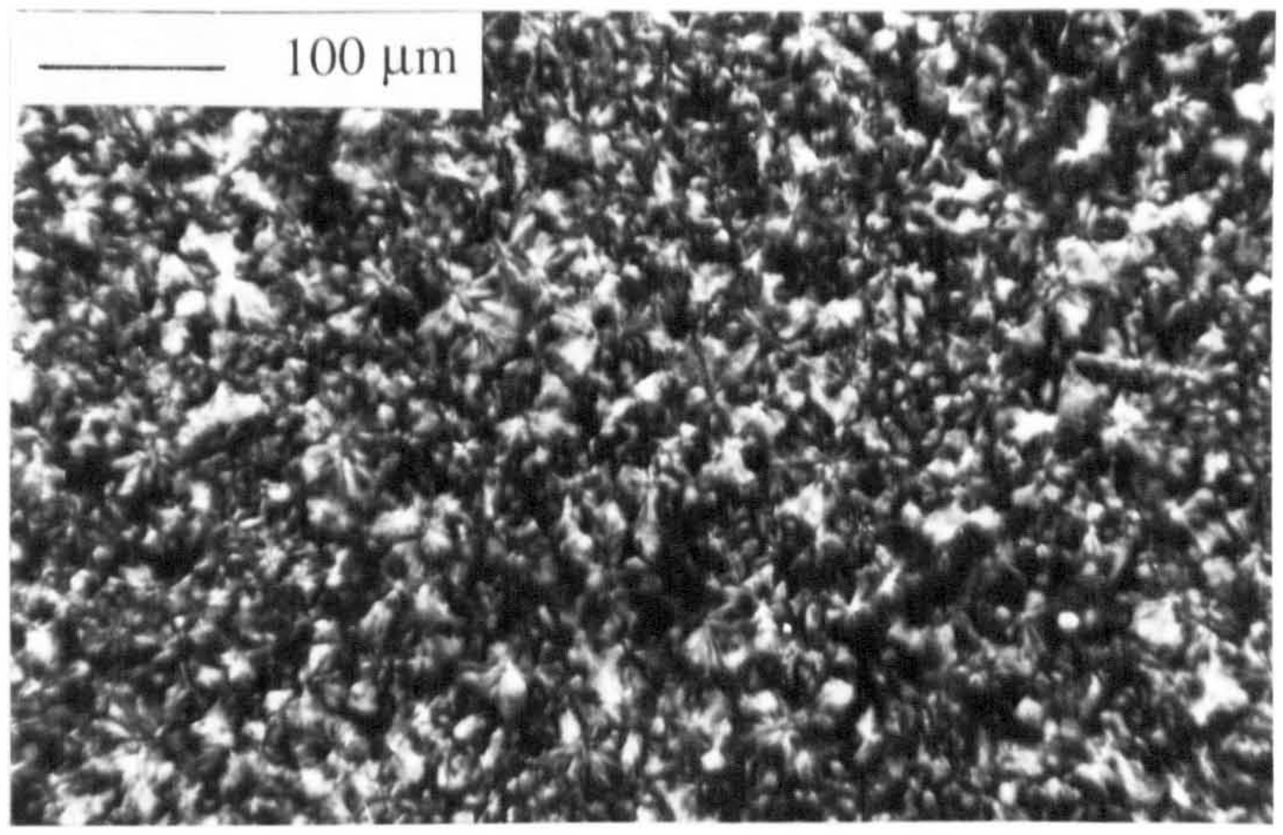

(a) polypropylene compression sample
magnification: 20×10

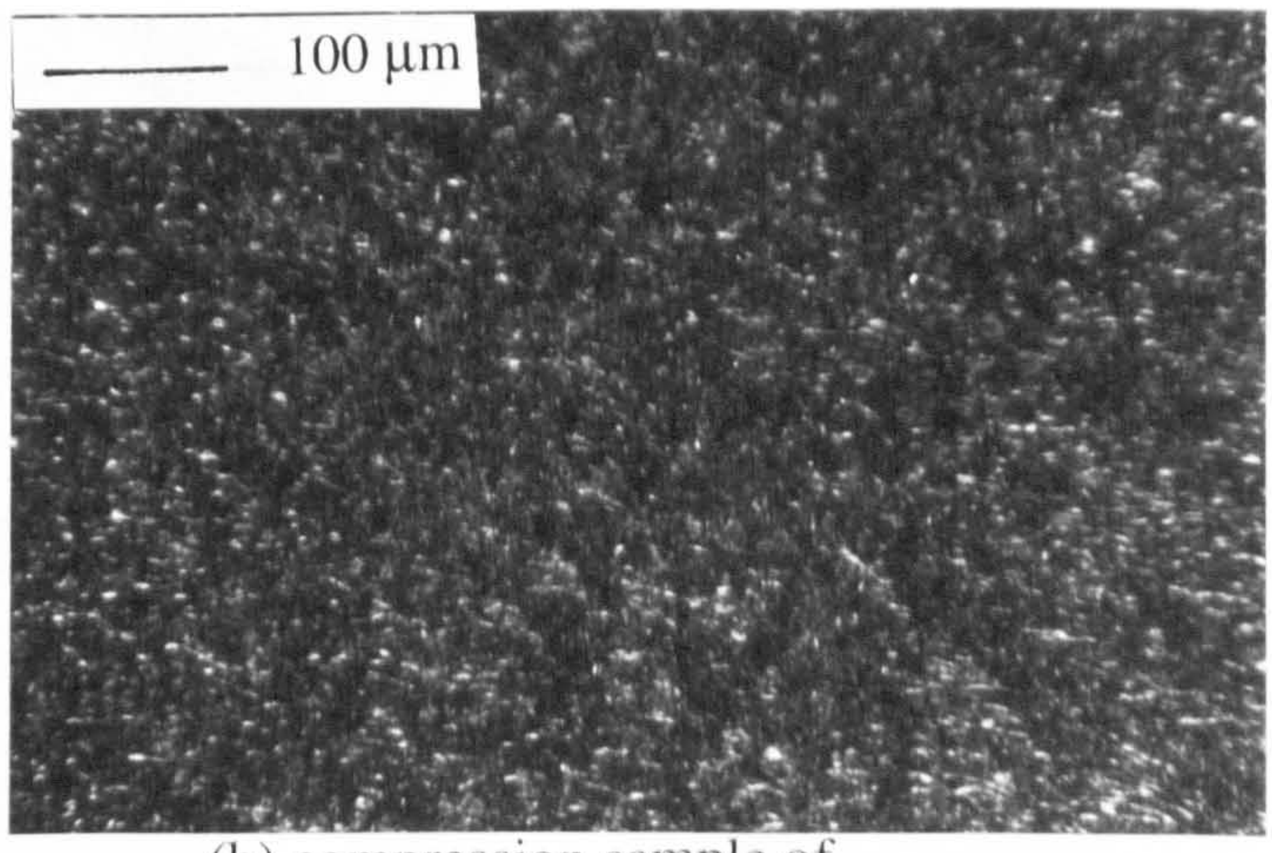

(b) compression sample of
Geniset MD nucleating agent
magnification: 20×10

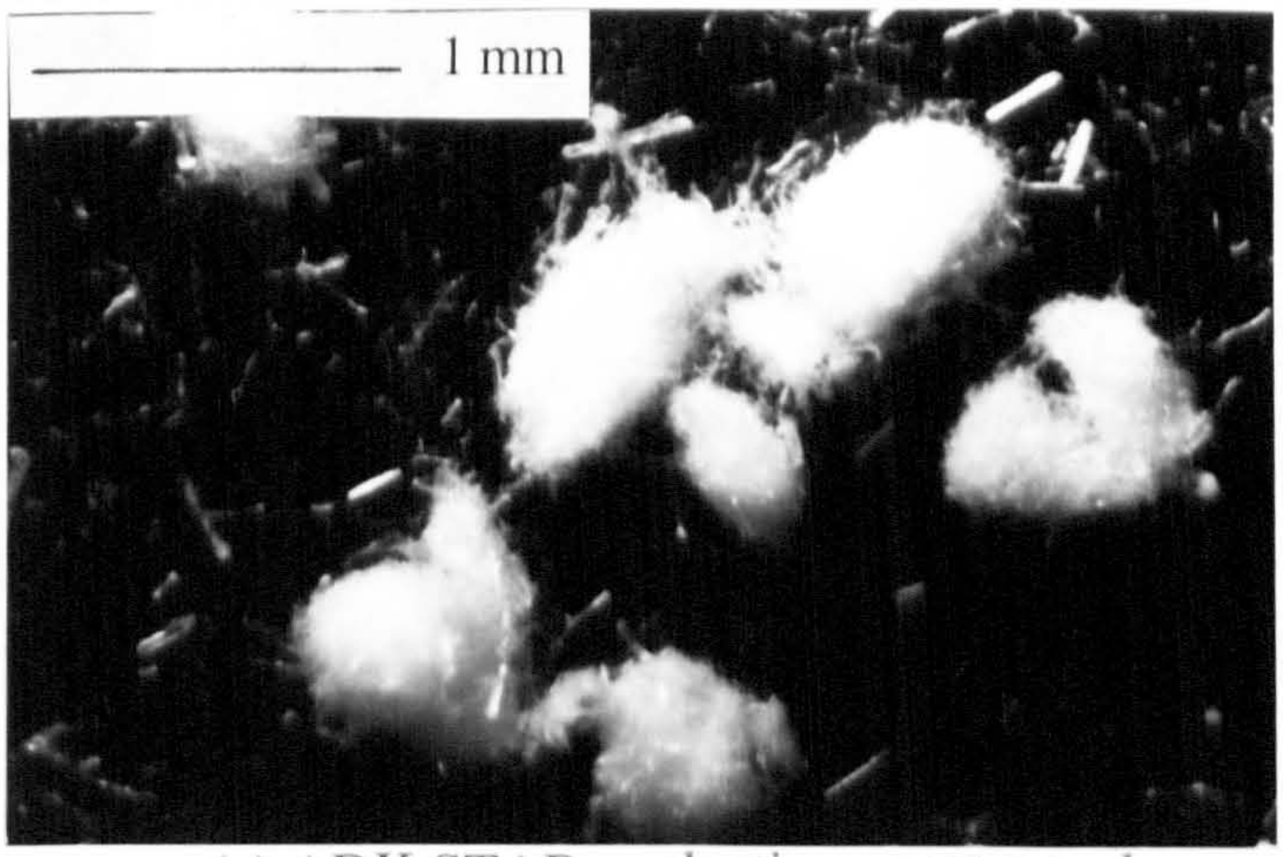

(c) ADK STAB nucleating agent powder

Figure 4.1 Micrographs of polypropylene and nucleating agents
(a) (b) compression samples of iPP and Geniset MD nucleating agent
(c) optical photo of ADK STAB nucleating agent powder

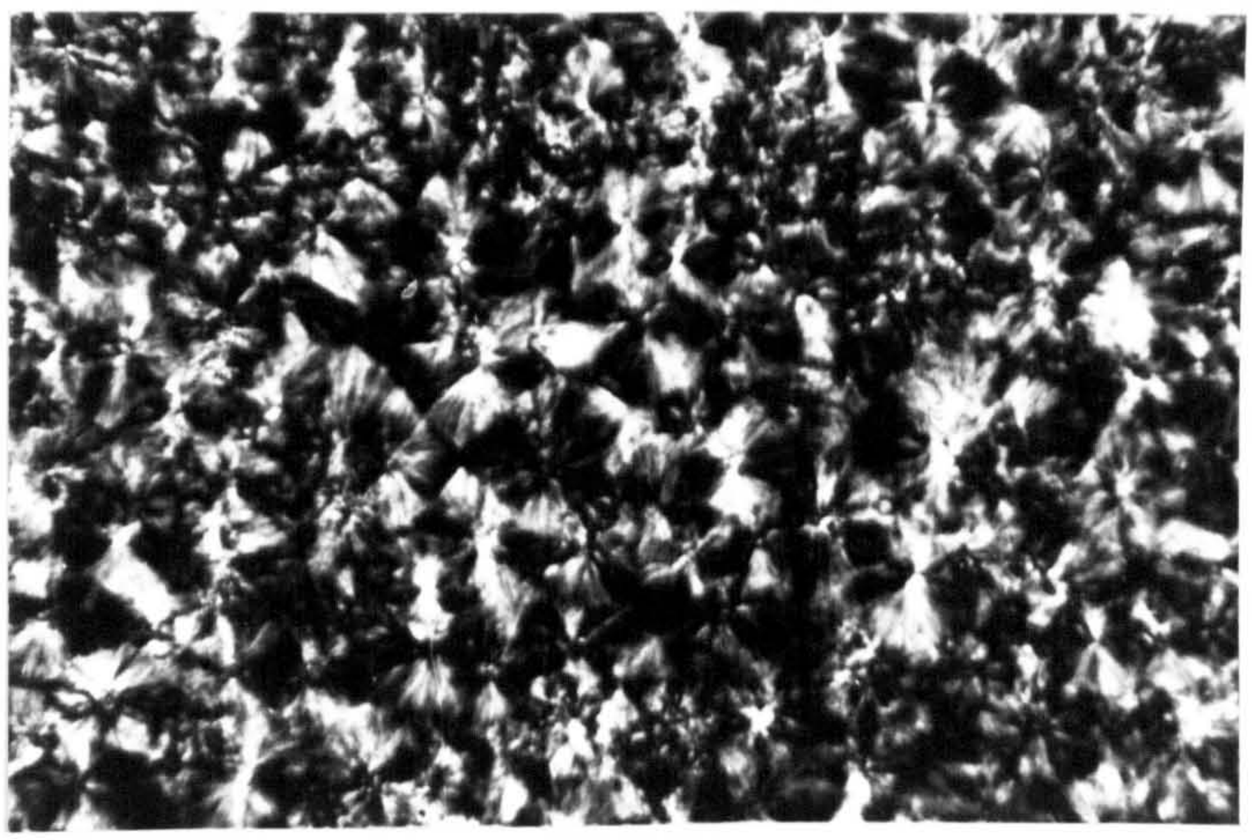

(a) polypropylene

(b) iPP+0.1wt.%Geniset MD

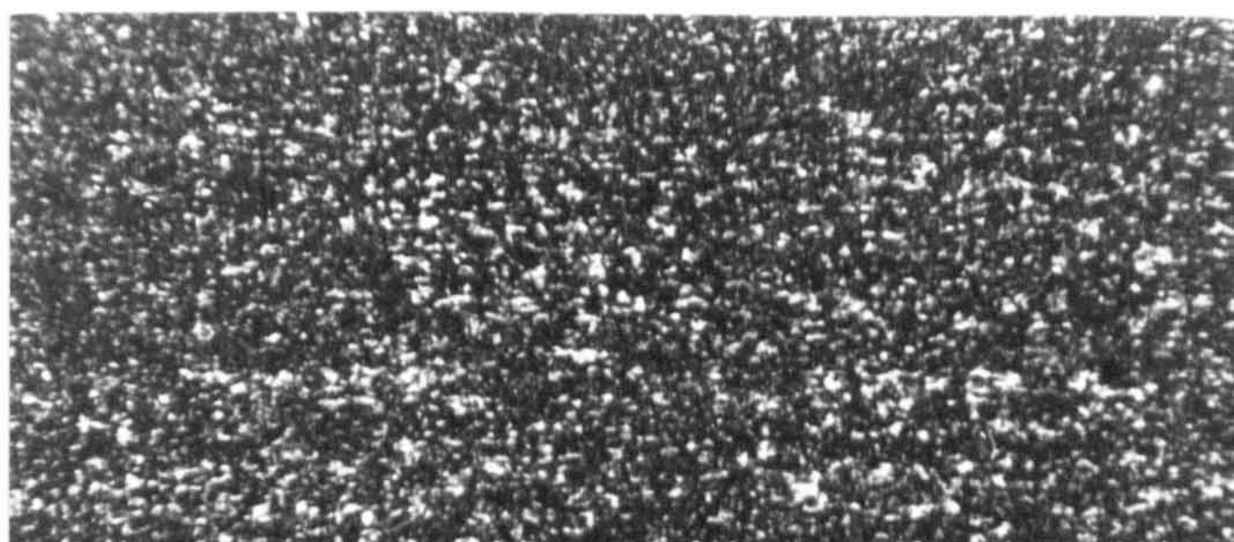

(c) iPP+0.1wt.%ADK STAB

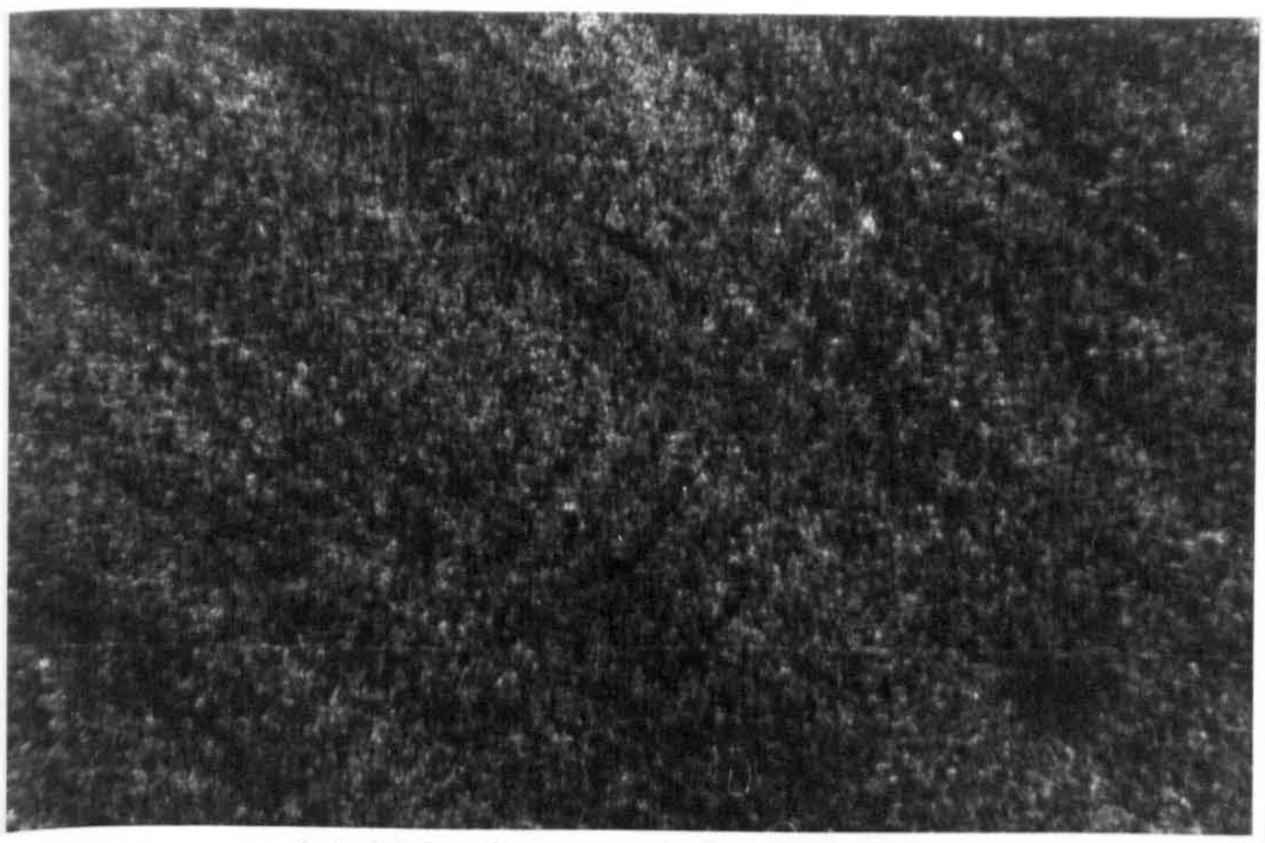

(e) iPP+0.3wt.%Geniset MD

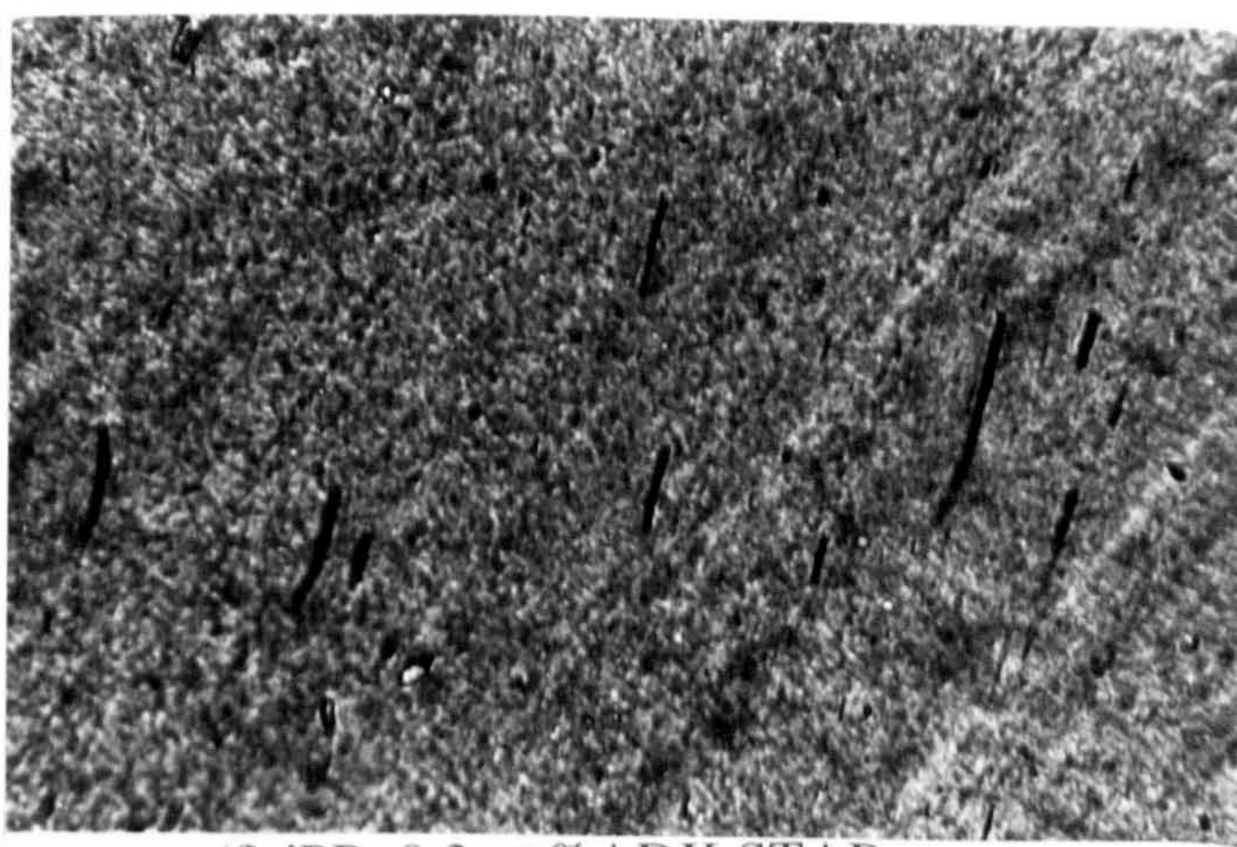

(f) iPP+0.3wt.%ADK STAB

100 μm

Figure 4.2 Micrographs of tensile bar conventional mouldings of iPP with the addition of nucleating agents

magnification: 40×10

section consisted of very fine spherulites and the effect on the substrate has been such that the density of nucleating agent will prevent lateral growth of the spherulites. The fine crystalline structure of iPP with the addition of nucleating agent can reduce the reflection and absorption of light within the polymer matrix. This increased the light transmittance of polypropylene and improved the optical clarity. The fine structure may be classified as non-spherulitic/crystalline, where high nucleation does not allow the crystalline growth to reach spherulitic completion but precipitates a random distribution of stacked lamellae, elsewhere described as grain-like morphology [140], or as axialites [141].

Due to the limiting thickness of the microtomed samples, the details of the nucleated samples were difficult to observe at higher magnification by polarized light microscopy, and were studied by using TEM as described in the following section.

4.3 TEM Studies of iPP with the Addition of Nucleating Agents

The moulding produced by SCORIM-2N4 was selected for etching for the purpose of preparing replicas for examination with the transmission electron microscope. Figure 4.3 shows the TEM micrographs of fibrous textures in the middle layer. The orientation of c-axis is parallel to the melt flow direction.

During the SCORIM processing, the melt material in the mould cavity was oriented preferably by oscilating pressure and formed lamellar structure in the melt flow direction. The predominant appearance in the morphology of the SCORIM-2N4 is the shish-kebab texture. Figure 4.3c shows the main skeleton structure under the high magnification. The enhanced modulus observed with the SCORIM-2N4 mouldings can be attributed to the greater degree of the orientation of c-axis and a*-axis. In fact there is a large proportion of the section through the SCORIM-2N4 moulding which shows a more pronounced fibrous alignment in the direction of the length of the bar. Maximum mechanical performance of the moulding in this direction has, therefore, been achieved in this region. The micro holes appeared in the TEM micrographs in Figure 4.3 were the unsolved polyacrylic acid (PAA) and the white lines were the crack of replica.

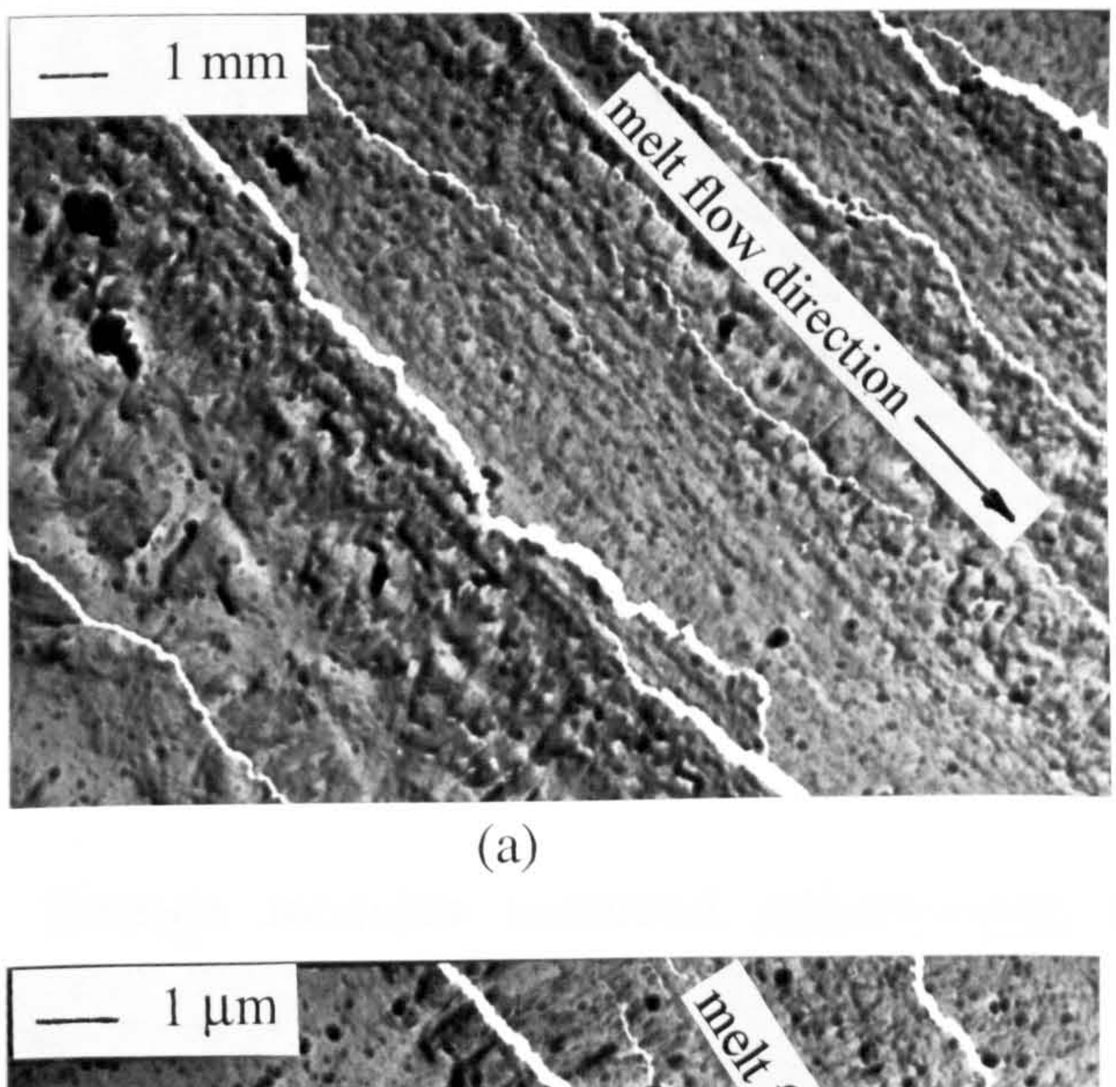

(a)

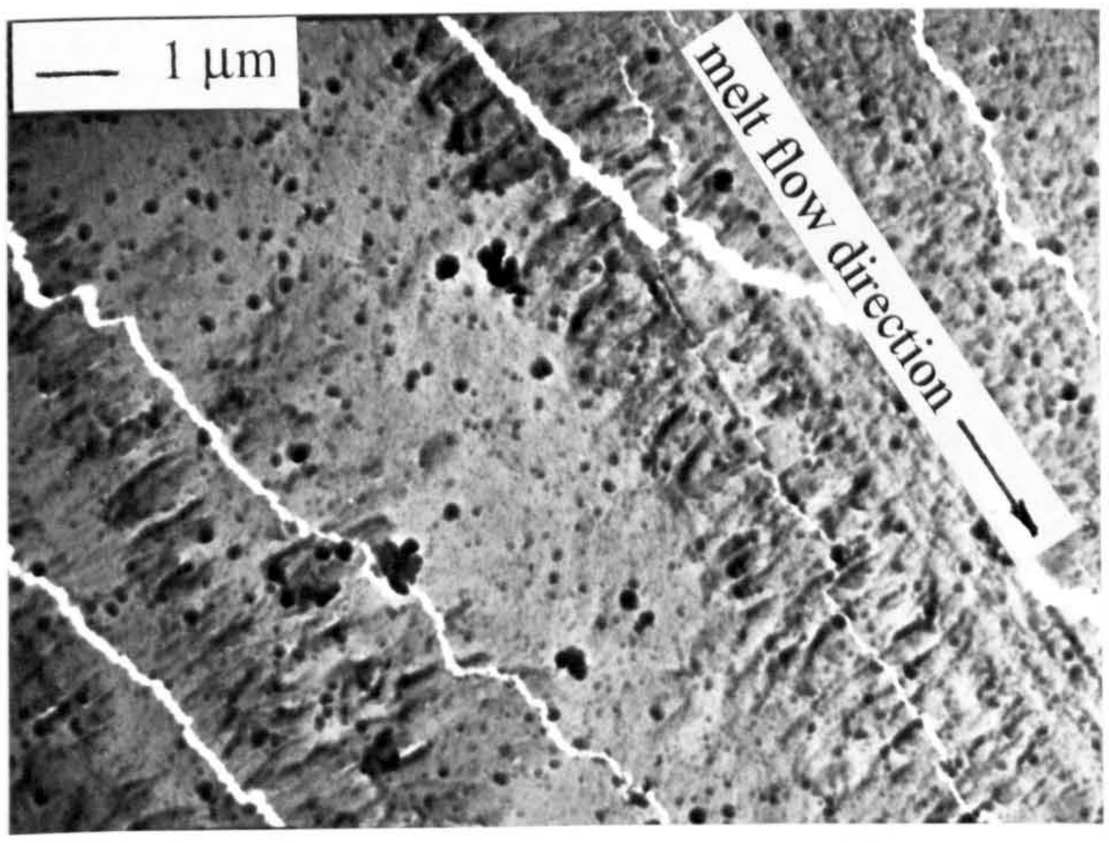

(b)

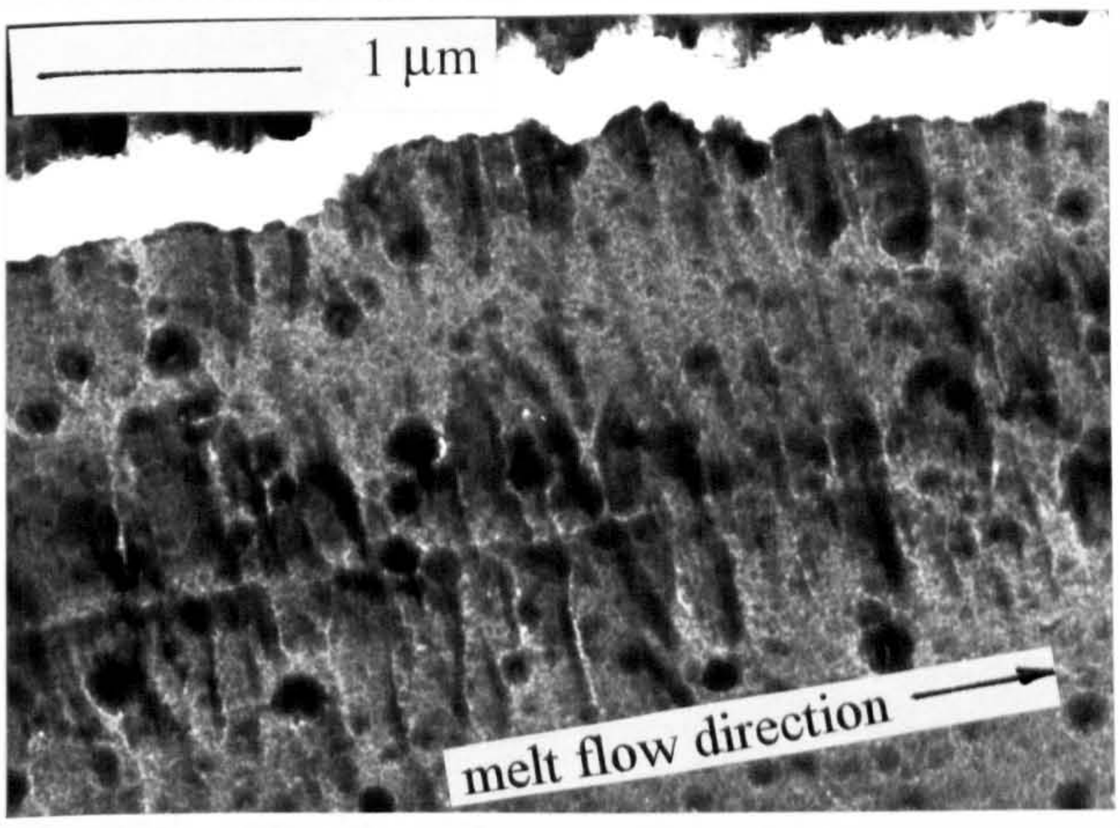

(c)

Figure 4.3 TEM micrographs of the middle layer of SCORIM-2N4 rectangular bar moulding

(a) magnification: ×5,000 (b) magnification: ×6,600 (c) magnification: ×20,000

4.4 Effect of Nucleating Agents on Mechanical Properties of iPP

In the mechanical testing, the Young's modulus and tensile stresses (yield stress, peak stress and breaking stress) were all found to increase gradually with increasing concentration of Geniset MD nucleating agent (Figure 4.4a,b) when the testing bars were produced by conventional injection mouldings (standard tensile bar).

The values of Young's modulus increased progressively with increasing the concentration of Geniset MD nucleating agent from 0 to 2 wt.%. For the tensile stresses, when the concentration of Geniset MD nucleating agent was changed from 0 to 0.1 wt.%, the yield stress was increased by 19.1%, the peak stress by 10.5% and the breaking stress by 41.8%. When the concentration of Geniset MD nucleating agent was increased from 0.1 to 2 wt.%, the yield stress and peak stress increased by 13.1% and 11.6% respectively, and the increase in the breaking stress was 49.3%.

On the other hand the strain to break of standard tensile bar conventional injection mouldings falls rapidly at first and then slowly with increasing concentration of Geniset MD nucleating agent. The trend is shown in Figure 4.4c. When the concentration of Geniset MD nucleating agent was increased from 0 to 0.1 wt.%, the mouldings exhibit a significant decrease in the strain to break, which was 82.0% for strain to break. When the concentration of Geniset MD nucleating agent exceed 0.1 wt.%, the strain to break falls slowly with increasing concentration. The change in yield strain and peak strain were less marked with increasing concentration of the Geniset MD nucleating agent. The mechanical results of conventional injection mouldings of iPP with the addition of Geniset MD are shown in Table 4.2b.

Figure 4.5 shows the changes in the Young's modulus and tensile stresses (yield stress, peak stress and breaking stress) of iPP with the addition of ADK STAB as a function of nucleating agent concentration. The occurrence of the increasing Young's modulus and tensile stresses can be seen in iPP with increasing concentration of ADK STAB (see Figure 4.5a,b). On the other hand, the strain to break of iPP with ADK tended to decrease with increasing concentration of the nucleating agent (see Figure 4.5c). The yield strain and peak strain exhibited small changes with increasing concentration of ADK nucleating agent. The mechanical results of conventional injection mouldings of iPP with the addition of ADK STAB

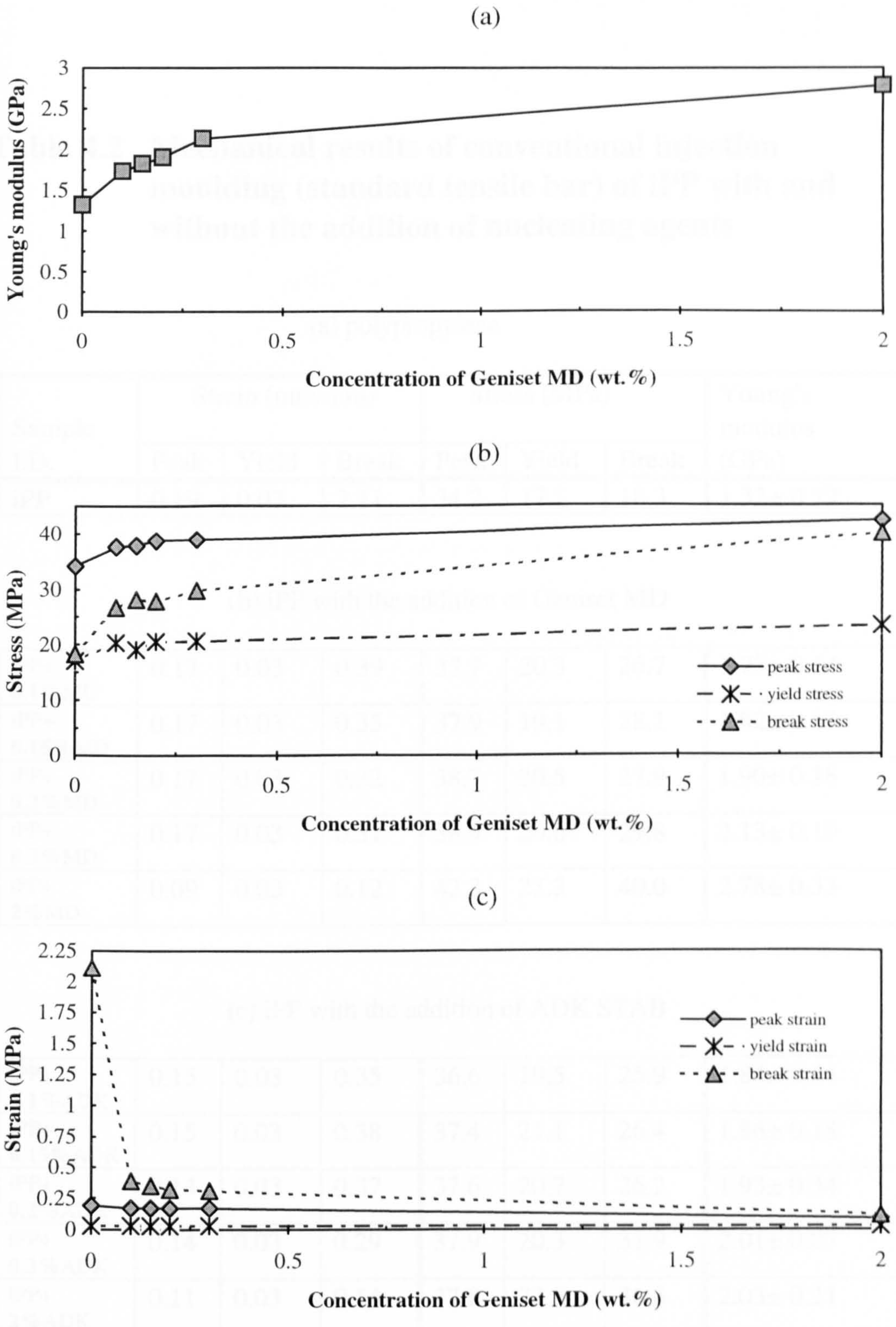

Figure 4.4 Mechanical results of tensile bar of conventional injection mouldings of iPP with the addition of Geniset MD

(a) Young's modulus (b) tensile stress (c) tensile strain

Table 4.2 Mechanical results of conventional injection moulding (standard tensile bar) of iPP with and without the addition of nucleating agents

(a) polypropylene

Sample I.D.	Strain (mm/mm)			Stress (MPa)			Young's modulus (GPa)
	Peak	Yield	Break	Peak	Yield	Break	
iPP	0.19	0.03	2.11	34.2	17.1	18.3	1.32± 0.22

(b) iPP with the addition of Geniset MD

iPP+ **0.1%**MD	0.17	0.03	0.39	37.7	20.3	26.7	1.73± 0.14
iPP+ **0.15%**MD	0.17	0.03	0.35	37.9	19.1	28.1	1.82± 0.11
iPP+ **0.2%**MD	0.17	0.03	0.32	38.7	20.5	27.9	1.90± 0.18
iPP+ **0.3%**MD	0.17	0.03	0.31	38.9	20.6	29.8	2.13± 0.19
iPP+ **2%**MD	0.09	0.03	0.12	42.3	23.3	40.0	2.78± 0.33

(c) iPP with the addition of ADK STAB

iPP+ **0.1%**ADK	0.15	0.03	0.35	36.6	19.5	25.9	1.84± 0.14
iPP+ **0.15%**ADK	0.15	0.03	0.38	37.4	21.1	26.4	1.86± 0.18
iPP+ **0.2%**ADK	0.14	0.03	0.37	37.6	20.7	26.2	1.93± 0.34
iPP+ **0.3%**ADK	0.14	0.03	0.29	37.9	20.3	31.9	2.01± 0.07
iPP+ **2%**ADK	0.11	0.03	0.14	37.8	22.5	36.8	2.03± 0.21

(a)

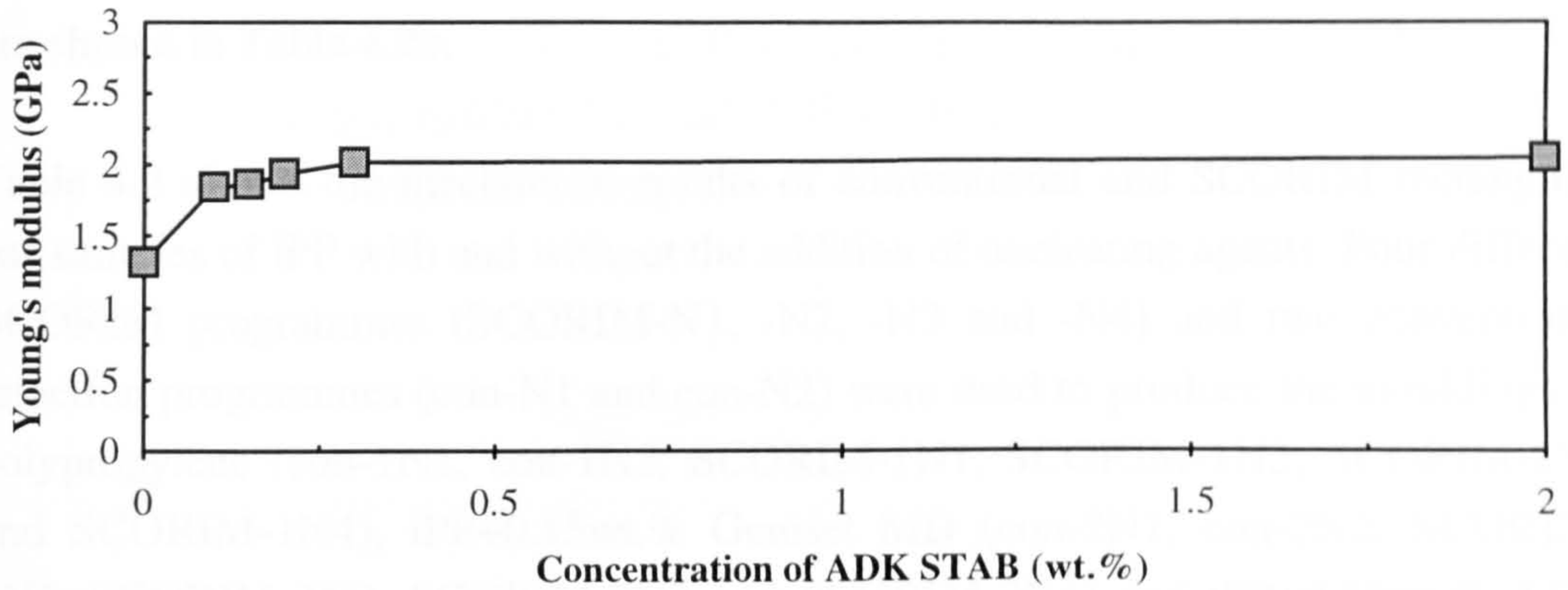

(b)

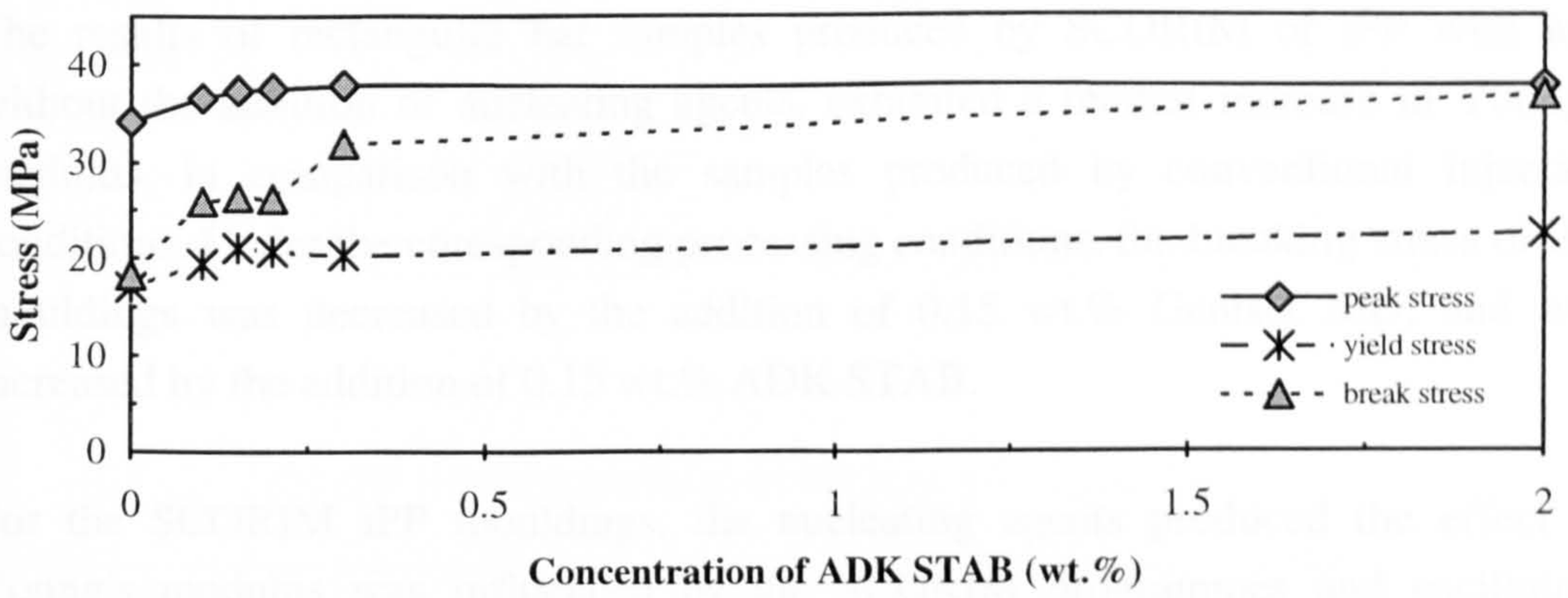

(c)

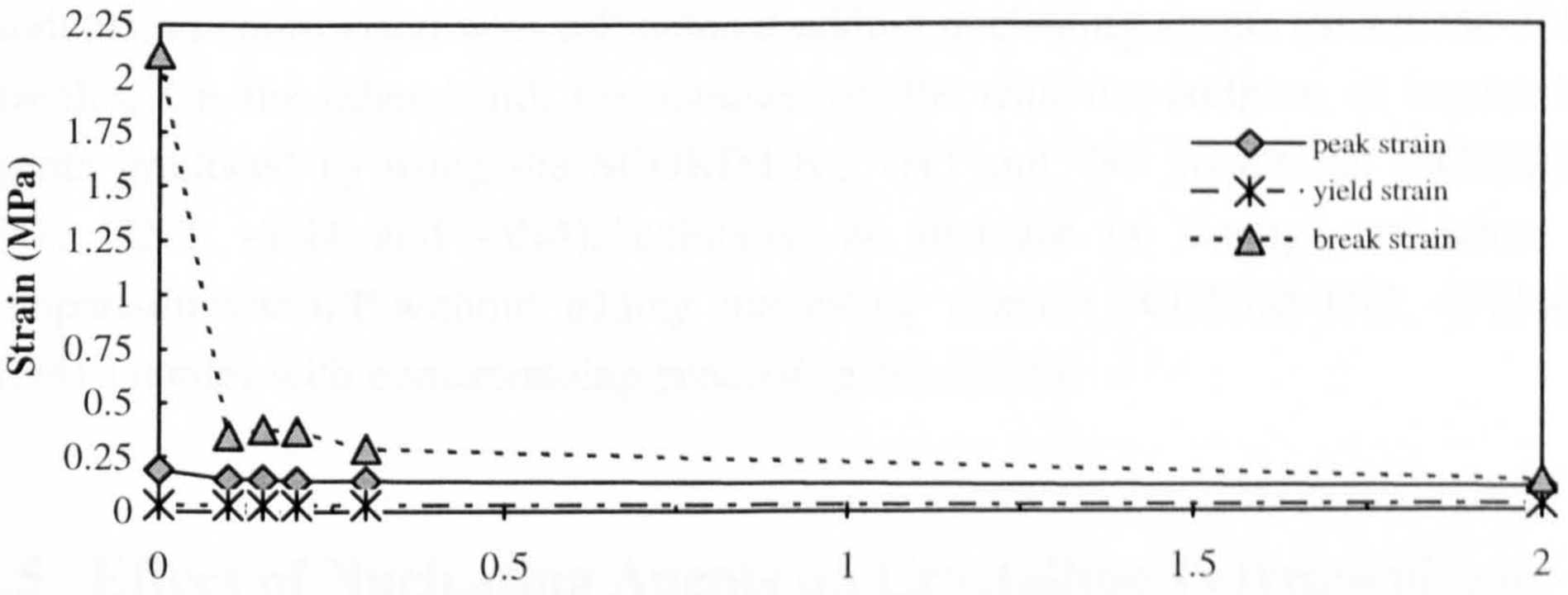

Figure 4.5 Mechanical results of tensile bar of conventional injection mouldings of iPP with the addition of ADK STAB

(a) Young's modulus (b) tensile stress (c) tensile strain

are shown in Table 4.2c.

Table 4.3 shows the mechanical results of conventional and SCORIM rectangular bar samples of iPP with and without the addition of nucleating agents. Four different SCORIM programmes (SCORIM-N1, -N2, -N3 and -N4) and two conventional injection programmes (con-N1 and con-N2) were used to produce the mouldings of polypropylene (con-1N1, con-1N2, SCORIM-1N1, SCORIM-1N2, SCORIM-1N3 and SCORIM-1N4), iPP+0.15wt.% Geniset MD (con-2N1, con-2N2, SCORIM-2N1, SCORIM-2N2, SCORIM-2N3 and SCORIM-2N4) and iPP+0.15wt.% ADK STAB (con-3N2, SCORIM-3N4).

The results of rectangular bar samples produced by SCORIM of iPP with and without the addition of nucleating agents, exhibited a modest increase in Young's modulus, in comparison with the samples produced by conventional injection conditions. Under the coresponding processing conditions, the breaking stress of iPP mouldings was decreased by the addition of 0.15 wt.% Geniset MD, and was increased by the addition of 0.15 wt.% ADK STAB.

For the SCORIM iPP mouldings, the nucleating agents produced the effect in Young's modulus was influenced by the SCORIM programmes and oscillating modes applied. For the SCORIM-N1 program, the mouldings (SCORIM-2N1) of iPP with the addition of 0.15wt.% Geniset MD showed a decrease in Young's modulus, in comparison with iPP without adding nucleating agents (SCORIM-1N1) samples. On the other hand, the samples of iPP with the addition of nucleating agents produced by using the SCORIM-N2, -N3 and -N4 conditions (SCORIM-2N2, -2N3, -2N4 and -3N4), exhibited an increase in Young's modulus, in comparison with iPP without adding nucleating agents (SCORIM-1N2, -1N3 and -1N4) samples with corresponding processing conditions.

4.5 Effect of Nucleating Agents on Crystalline Polymorphism and Orientation in iPP as Revealed by X-ray Diffractometer

4.5.1 The Wide Angle X-ray Diffraction Measurement of iPP with and without the Addition of Nucleating Agents

The wide angle x-ray scattering profiles of injection moulded iPP samples were

Table 4.3 Mechanical results of conventional and SCORIM rectangular bar of iPP with and without the addition of nucleating agents

(a) polypropylene

Sample I.D.	Strain (mm/mm)			Stress (MPa)			Young's Modulus (GPa)
	Peak	Yield	Break	Peak	Yield	Break	
SCORIM-1N4	0.24	0.012	0.49	48.6	15.7	45.2	2.35±0.23
SCORIM-1N3	0.84	0.007	1.45	56.0	24.4	53.6	2.73±0.30
SCORIM-1N2	0.64	0.006	1.10	55.4	23.4	51.1	2.62±0.32
SCORIM-1N1	0.82	0.046	1.22	57.4	19.9	55.9	3.30±0.99
Con-1N2	0.11	0.014	5.61	31.7	14.5	17.5	1.78±0.23
Con-1N1	0.31	0.008	18.50	39.6	23.2	28.3	1.54±0.87

(b) iPP with the addition of 0.15wt.% Geniset MD

SCORIM-2N4	0.23	0.008	0.38	47.5	9.5	45.0	2.60±0.68
SCORIM-2N3	1.09	0.004	2.36	53.3	17.9	48.7	3.54±0.72
SCORIM-2N2	0.93	0.043	1.73	51.1	18.1	48.3	2.66±0.47
SCORIM-2N1	0.71	0.050	1.11	50.3	20.8	47.4	2.42±0.87
Con-2N2	0.11	0.015	4.68	31.5	14.0	17.6	1.76±0.36
Con-2N1	0.30	0.050	11.30	35.0	17.9	22.3	1.55±0.31

(c) iPP with the addition of 0.15wt.% ADK STAB

SCORIM-3N4	0.24	0.015	0.45	49.3	18.5	46.3	2.47±0.37
Con-3N2	0.11	0.014	2.11	33.8	14.9	20.0	2.12±0.42

recorded at a scanning rate of 0.02degree/sec over an angle range 8°<2θ<32° or 8°<2θ<38°. The wavelength of the x-ray beam (λ) was 1.5418Å. The peak intensity values of the α-, ß- and γ- phases were obtained from the scattering profiles. α-phase orientation index A, ß-phase index B, crystallinity index C, γ-phase index G and percentage γ (γ%) were calculated from the corresponding peak heights that were also used for analysis of the degrees of crystallinity.

For the tensile bar conventional injection mouldings, the x-ray scattering profiles of 2θ angle *vs.* peak intensity of crystal phase are shown in Figures 4.6 and 4.7. For Geniset nucleated-iPP mouldings (see Figure 4.6), the intensities of $(111)_\alpha$ and $(041)_\alpha$ peaks were decreased with the higher concentration of Geniset MD nucleating agent. The x-ray scattering profiles exhibited the peaks of $(300)_\beta$ and $(117)_\gamma$ in the concentration of 0.15 and 2wt.% Geniset MD. The crystallographic data of iPP with the addition of 0.15wt.% and 0.3wt.% Geniset MD samples are shown in Table 4.4. For the conventional injection mouldings of ADK nucleated-iPP (Figure 4.7), the x-ray profiles showed a significant increased intensity for $(040)_\alpha$ peak and decreased intensity for $(111)_\alpha$ and $(041)_\alpha$ peaks. The peaks of $(300)_\beta$ and $(117)_\gamma$ were only found in the x-ray scattering profile of iPP+2wt.% ADK. The crystallographic data of iPP with the addition of 0.1wt.% and 2wt.% ADK STAB samples are shown in Table 4.5.

The results of calculated A, B, C, G indices and γ% are shown in the Table 4.4. The results indicate that the α-phase index A was increased with increasing concentration of both nucleating agents. It is noticed that the ß-phase was not found in the lower concentration of both Geniset MD and ADK nucleated-iPP mouldings. Both nucleating agents produced the effects in increased crystallinity index C.

Figures 4.8, 4.9 and 4.10 show the x-ray scattering profiles of 2θ angle *vs.* peak intensity of the conventional and SCORIM rectangular bar mouldings of iPP with and without the addition of nucleating agents. The samples produced by SCORIM of iPP with and without the addition of nucleating agents exhibited higher intensities for $(110)_\alpha$, $(040)_\alpha$, $(130)_\alpha$, $(060)_\alpha$ and $(220)_\alpha$ peaks in comparison with the samples produced by conventional injection conditions. The intensity of $(117)_\gamma$ peak of each SCORIM sample was increased significantly, and at the same time the intensities of $(111)_\alpha$ and $(041)_\alpha$ peaks were decreased. The crystallographic data of iPP without and with the addition of 0.15wt.% Geniset MD rectangular bar samples

Figure 4.6 X-ray diffractogram of tensile bar conventional injection mouldings of iPP with the addition of Geniset MD

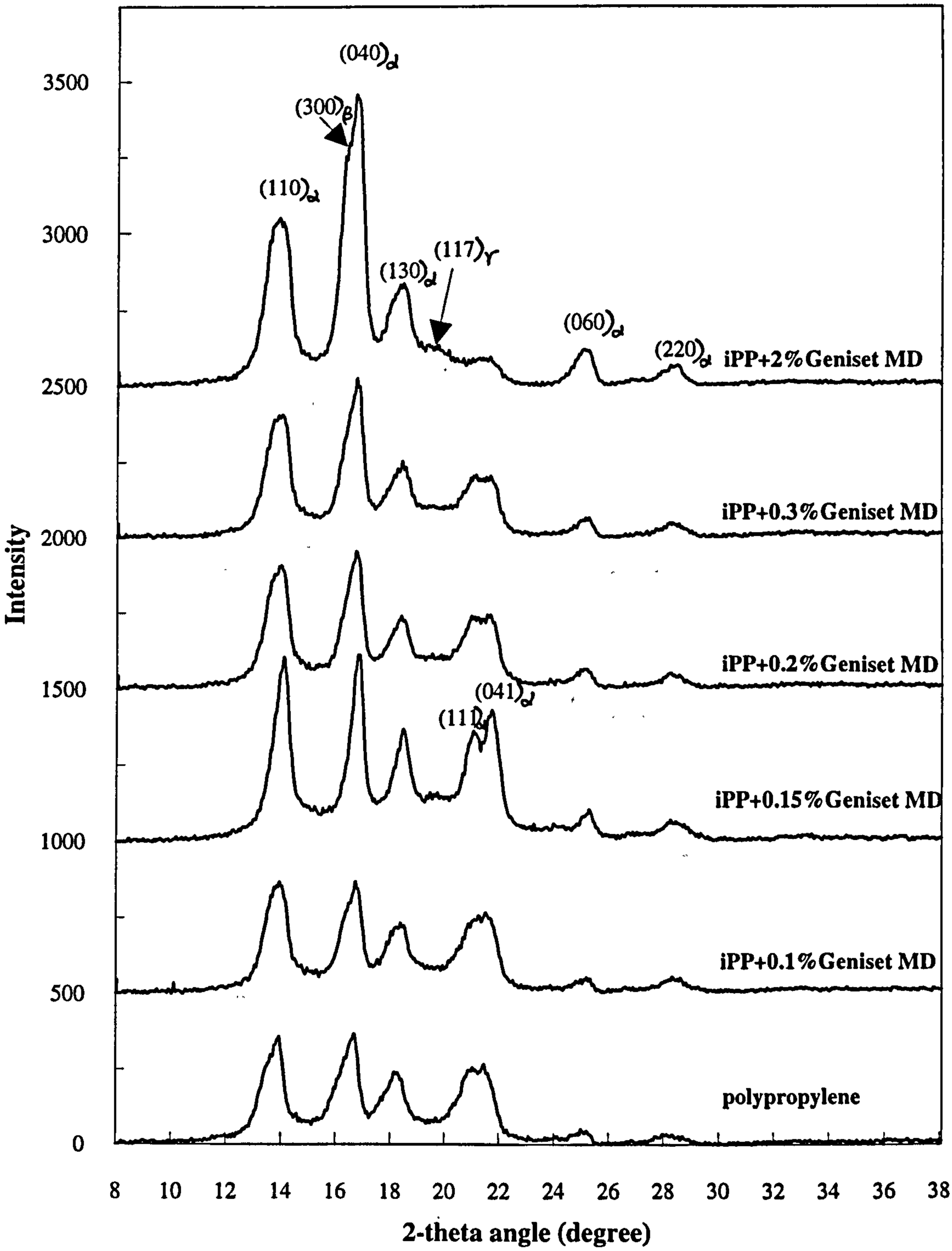

Figure 4.7 X-ray diffractogram of tensile bar conventional injection mouldings of iPP with the addition of ADK STAB

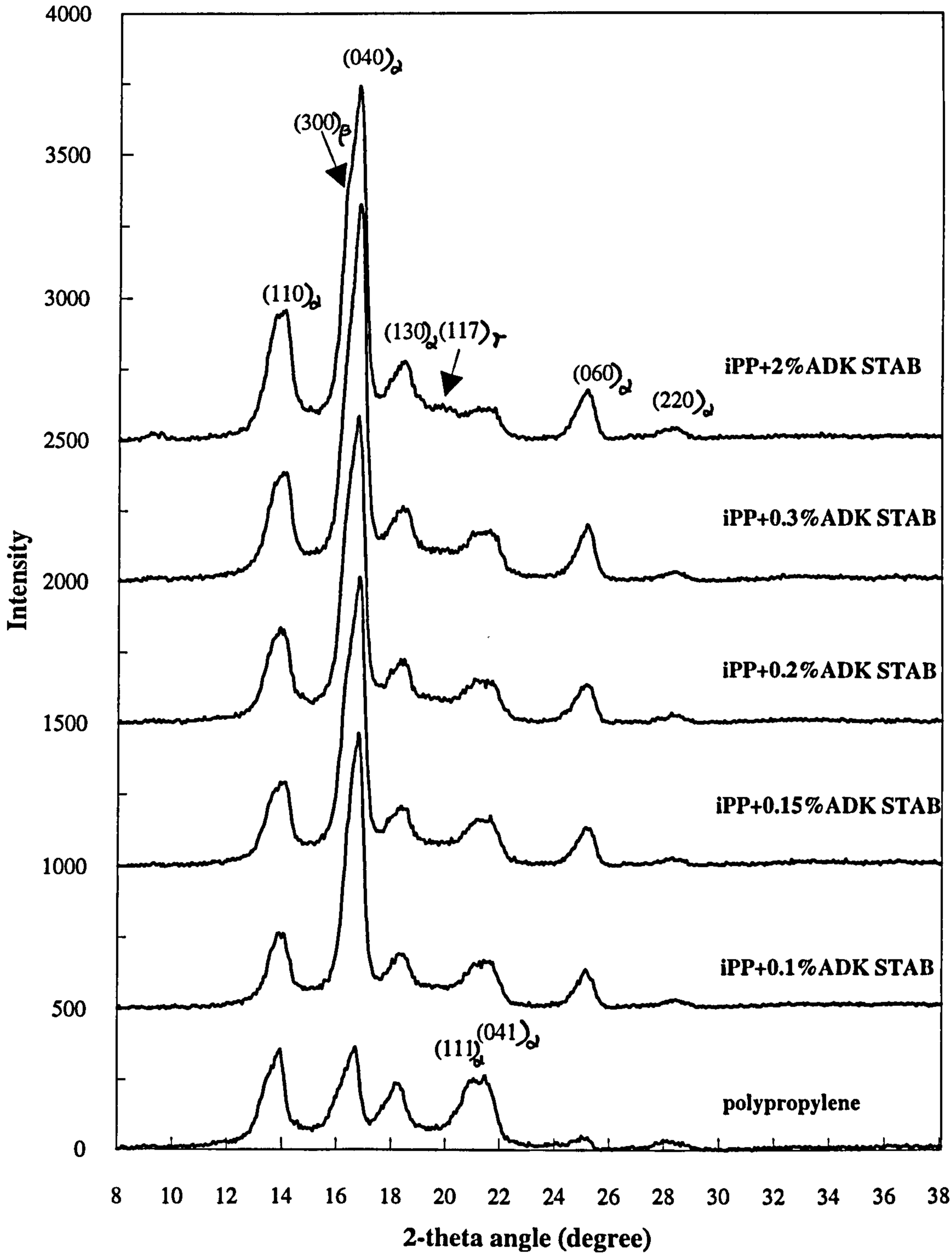

Table 4.4 X-ray diffraction data of tensile bar conventional injection mouldings of iPP with the addition of Geniset MD nucleating agent

a. iPP+0.15wt.% Geniet MD moulding

2θ (degree)	d-spacing (Å)	$d^* = \lambda/d$	Miller index (hkl)	Crystal phase	Relative intensity (%)
14.04	6.309	0.244	110	α	98
16.80	5.277	0.292	040	α	100
18.48	4.801	0.321	130	α	59
19.76	4.493	0.343	117	γ	25
21.10	4.210	0.366	111	α	58
21.80	4.077	0.378	041	α	69
25.41	3.505	0.440	060	α	16
28.42	3.140	0.491	220	α	10

b. iPP+0.3wt.% Geniset MD moulding

2θ (degree)	d-spacing (Å)	$d^* = \lambda/d$	Miller index (hkl)	Crystal phase	Relative intensity (%)
13.97	6.337	0.243	110	α	77
16.74	5.297	0.291	040	α	100
18.44	4.812	0.320	130	α	48
21.20	4.191	0.368	111	α	39
21.72	4.091	0.377	041	α	38
25.29	3.521	0.438	060	α	12
28.41	3.141	0.491	220	α	8

Table 4.5 X-ray diffraction data of tensile bar conventional injection mouldings of iPP with the addition of ADK STAB nucleating agent

a. iPP+0.1wt.% ADK STAB moulding

2θ (degree)	d-spacing (Å)	$d^* = \lambda/d$	Miller index (hkl)	Crystal phase	Relative intensity (%)
13.86	6.390	0.241	110	α	27
16.78	5.284	0.292	040	α	100
18.31	4.845	0.318	130	α	20
21.32	4.167	0.370	111	α	17
21.81	4.075	0.378	041	α	16
25.26	3.525	0.437	060	α	13
28.62	3.119	0.494	220	α	2

b. iPP+2wt.% ADK STAB moulding

2θ (degree)	d-spacing (Å)	$d^* = \lambda/d$	Miller index (hkl)	Crystal phase	Relative intensity (%)
14.01	6.323	0.244	110	α	36
16.39	5.408	0.285	300	ß	75
16.76	5.291	0.291	040	α	100
18.45	4.809	0.321	130	α	22
19.85	4.472	0.345	117	γ	10
21.16	4.199	0.367	111	α	8
21.82	4.073	0.379	041	α	9
25.32	3.517	0.438	060	α	13
28.62	3.119	0.494	220	α	2

Table 4.6 α-phase index A, ß-phase index B, crystallinity index C, γ-phase index G and percentage γ of standard tensile bar conventional injection mouldings

(a) polypropylene

Sample I.D.	A	B	C	G	γ%
iPP	0.576	0	2.15	-	-

(b) iPP with the addition of Geniset MD

iPP+0.1%MD	0.601	0	2.63	-	-
iPP+0.15%MD	0.609	0	2.57	0.015	9.7
iPP+0.2%MD	0.646	0	2.10	-	-
iPP+0.3%MD	0.690	0	2.40	-	-
iPP+2%MD	0.909	0.295	3.14	0.015	10.9

(c) iPP with the addition of ADK STAB

iPP+0.1%ADK	0.628	0	2.69	-	-
iPP+0.15%ADK	0.652	0	2.32	-	-
iPP+0.2%ADK	0.717	0	2.42	-	-
iPP+0.3%ADK	0.690	0	2.42	-	-
iPP+2%ADK	0.813	0.319	2.81	0.014	14.7

Figure 4.8 X-ray diffractogram of conventional and SCORIM rectangular bar mouldings of polypropylene

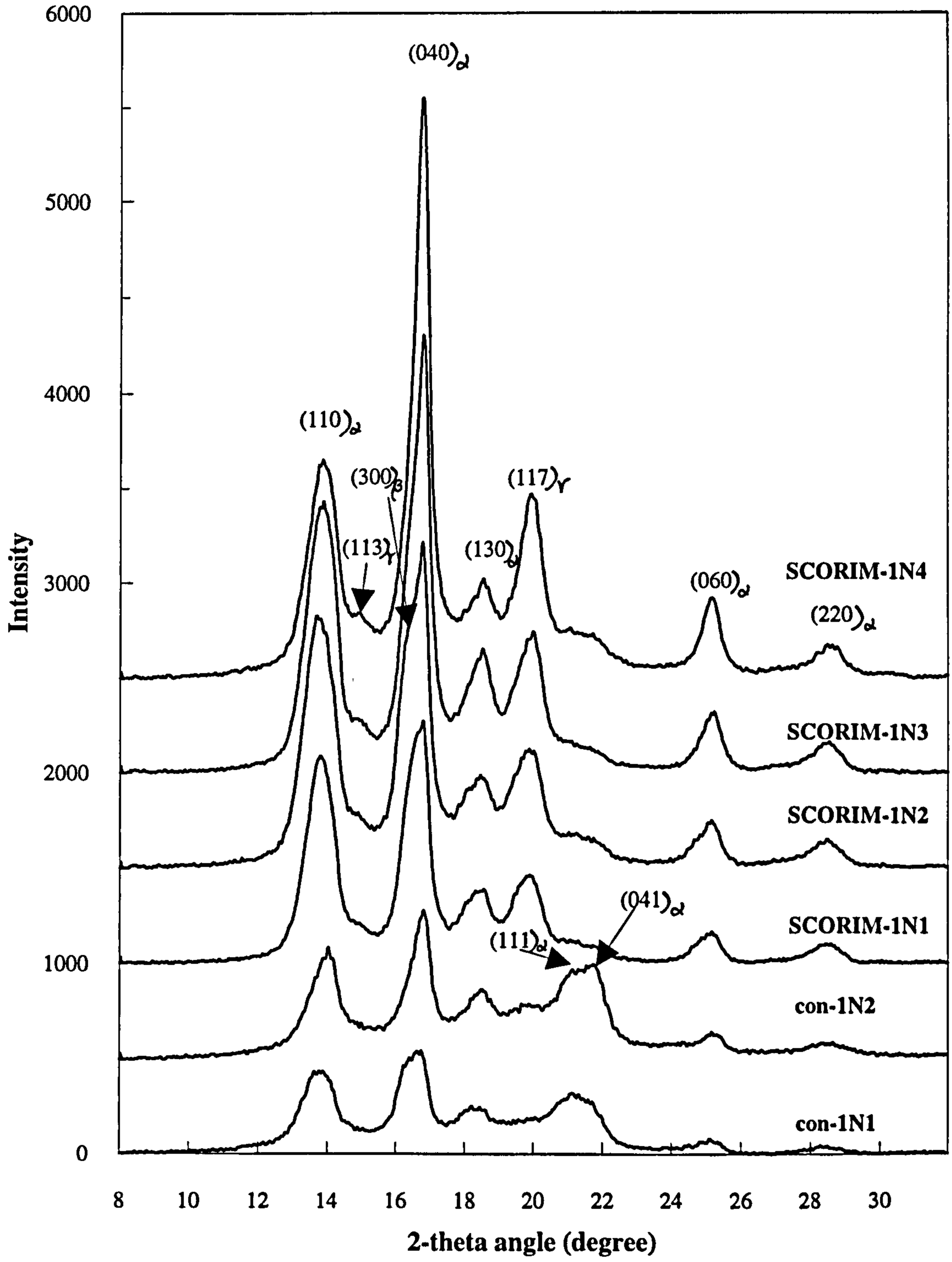

Figure 4.9 X-ray diffractogram of conventional and SCORIM rectangular bar mouldings of iPP+0.15wt.%Geniset MD

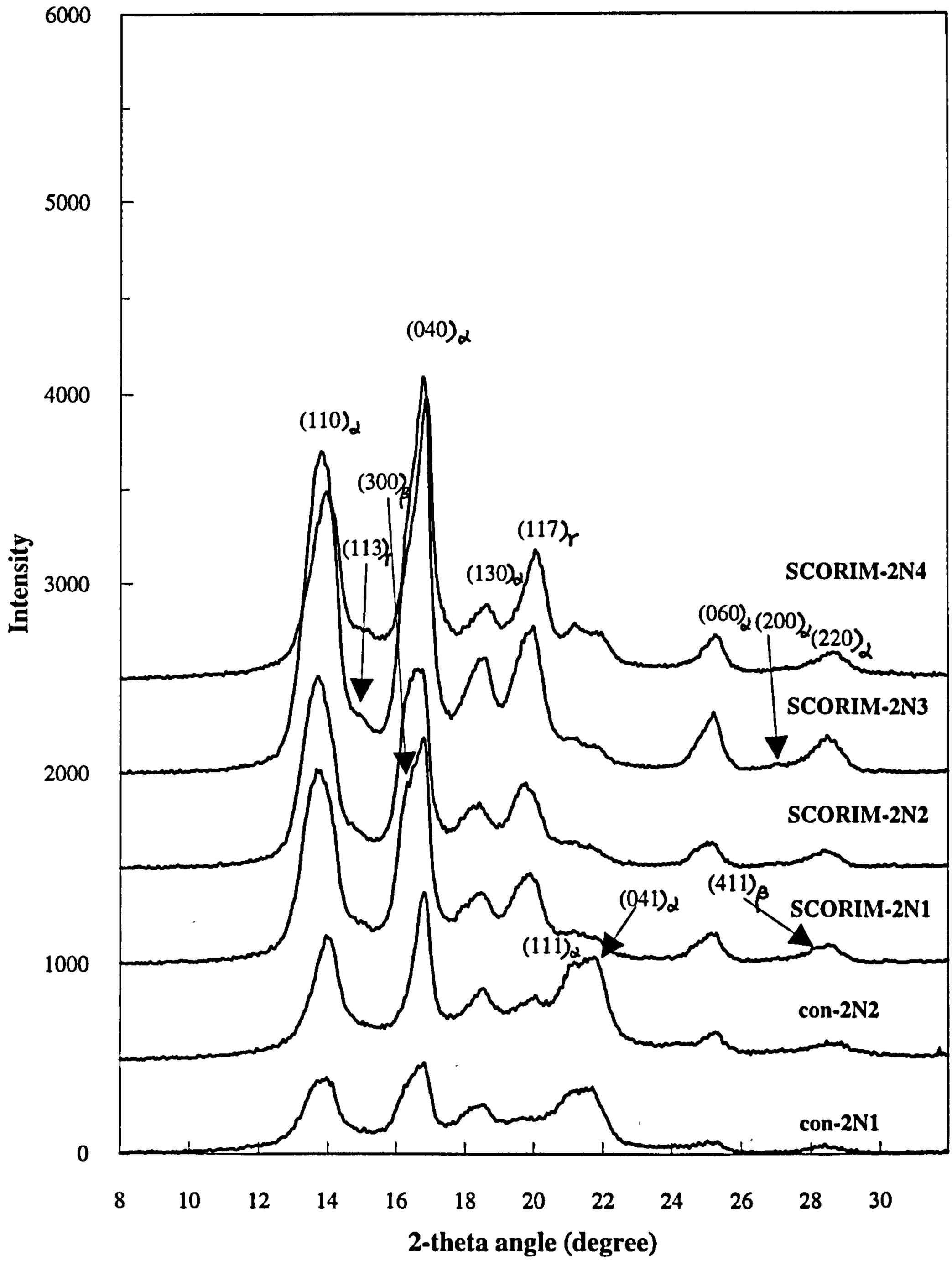

Figure 4.10 X-ray diffractogram of conventional and SCORIM rectangular bar mouldings of iPP+0.15wt.%ADK STAB

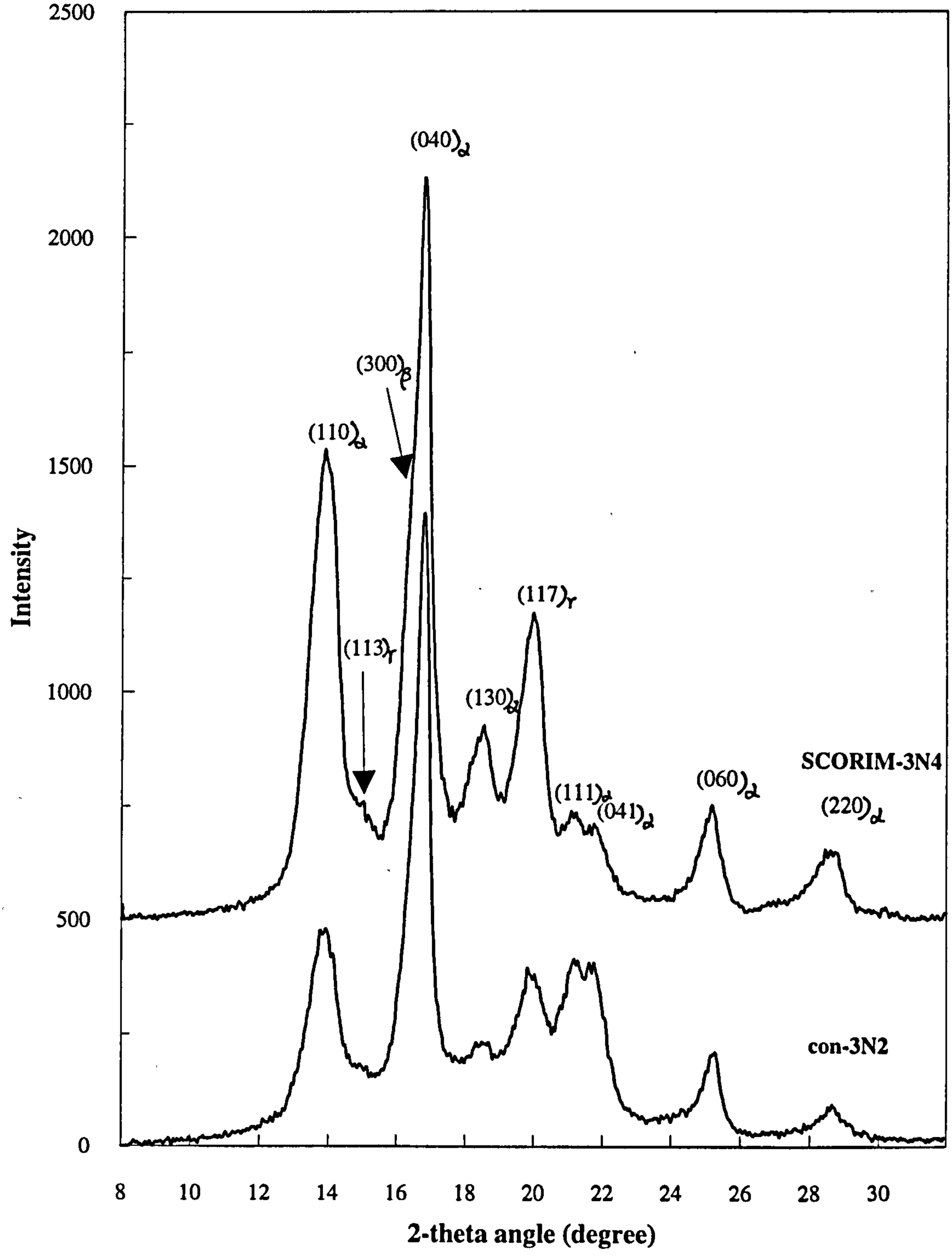

are shown in Tables 4.7 and 4.8.

Table 4.9 shows the results of A, B, C, G indices and γ% of SCORIM and conventional rectangular bar samples. In comparison with rectangular bar conventional injection mouldings, the samples of iPP with and without the addition of nucleating agents exhibited a significant increase in α-phase orientation index A, γ-phase index G, γ% and the crystallinity index C by using the SCORIM process. For conventional and SCORIM iPP mouldings, the nucleating agents produced the effects in A, B, C, G indices and γ% were influenced by the processing conditions applied (see Table 4.1).

For the conventional-N1 program, the nozzle temperature, mould temperature and holding pressure time were 230°C/70°C/66.5sec. Geniset nucleated-iPP mouldings (con-2N1) exhibited lower A, B, C, G indices and γ% than polypropylene mouldings (con-1N1).

In comparison with the conventional-N1 program, the conventional-N2 provided the higher nozzle temperature (280°C) and longer holding pressure time (96.5sec) for rectangular bar mouldings. The values of α-phase index A, γ-phase index G and γ% of Geniset nucleated-iPP samples (con-2N2) were all greater than polypropylene samples (con-1N2). ADK nucleated-iPP samples (con-3N2) exhibited higher α-phase index A, crystallinity index C, γ-phase index G and γ% than both polypropylene (con-1N2) and Geniset nucleated-iPP (con-2N2) samples. On the other hand the peak of $(300)_{\beta}$ was not found in the conventional mouldings produced by using con-N2 programmes (con-1N2, -2N2 and -3N2).

Under the SCORIM-N1 processing condition, the nozzle temperature and mould temperature were 220°C/30°C, iPP+0.15wt.% Geniset MD samples (SCORIM-2N1) exhibited higher ß-phase index B, crystallinity index C, γ-phase index G, γ% and lower α-phase orientation index, in comparison with polypropylene samples (SCORIM-1N1). The peak of $(300)_{\beta}$ was not found in x-ray scattering profile of the SCORIM-1N1.

The nozzle temperature and mould temperature of the SCORIM-N2 and -N3 were all 230°C/70°C. Geniset nucleated-iPP samples produced under both processing conditions (SCORIM-2N2 and -2N3) exhibited higher values of ß-phase index B, crystallinity index C, γ-phase index G and γ%, in comparison with polypropylene

Table 4.7 X-ray diffraction data of conventional-1N1 and SCORIM-1N2 rectangular bar mouldings of Polypropylene

a. Conventional-1N1 moulding

2θ (degree)	d-spacing (Å)	$d^* = \lambda/d$	Miller index (hkl)	Crystal phase	Relative intensity (%)
13.84	6.399	0.241	110	α	80
16.37	5.415	0.285	300	β	92
16.72	5.304	0.291	040	α	100
18.21	4.873	0.316	130	α	46
20.06	4.425	0.348	117	γ	35
21.15	4.201	0.367	111	α	58
21.61	4.113	0.375	041	α	52
25.15	3.541	0.435	060	α	14
28.36	3.147	0.490	220	α	7

b. SCORIM-1N2 moulding

2θ (degree)	d-spacing (Å)	$d^* = \lambda/d$	Miller index (hkl)	Crystal phase	Relative intensity (%)
13.61	6.507	0.237	110	α	77
14.08	6.290	0.245	113	γ	56
16.35	5.422	0.284	300	ß	77
16.73	5.300	0.291	040	α	100
18.43	4.815	0.320	130	α	28
19.86	4.469	0.345	117	γ	36
21.25	4.181	0.369	111	α	10
21.60	4.115	0.375	041	α	9
25.20	3.534	0.436	060	α	14
28.56	3.125	0.493	220	α	8

Table 4.8 X-ray diffraction data of conventional-2N2 and SCORIM-2N4 rectangular bar mouldings of iPP with the addition of 0.15wt.% Geniset MD

a. Conventional-2N2 moulding

2θ (degree)	d-spacing (Å)	$d^* = \lambda/d$	Miller index (hkl)	Crystal phase	Relative intensity (%)
13.89	6.375	0.242	110	α	74
16.78	5.284	0.292	040	α	100
18.52	4.790	0.322	130	α	42
20.03	4.432	0.348	117	γ	38
21.17	4.197	0.367	111	α	58
21.75	4.085	0.377	041	α	61
25.27	3.524	0.438	060	α	15
28.56	3.125	0.493	220	α	9

b. SCORIM-2N4 moulding

2θ (degree)	d-spacing (Å)	$d^* = \lambda/d$	Miller index (hkl)	Crystal phase	Relative intensity (%)
13.88	6.375	0.242	110	α	66
14.84	5.967	0.258	113	γ	18
16.45	5.384	0.286	300	ß	59
16.82	5.267	0.293	040	α	100
18.58	4.771	0.323	130	α	26
20.03	4.429	0.348	117	γ	45
21.19	4.190	0.368	111	α	19
21.73	4.086	0.377	041	α	15
25.29	3.518	0.438	060	α	15
28.72	3.106	0.496	220	α	8

Table 4.9 α-phase index A, ß-phase index B, crystallinity index C, γ-phase index G and percentage γ of conventional and SCORIM rectangular bar mouldings

(a) polypropylene

Sample I.D.	A	B	C	G	γ%	crystallinity (%)
CON-1N1	0.672	0.302	1.73	0.035	27.5	49.13
CON-1N2	0.581	0	1.27	0.033	25.7	42.04
SCORIM-1N1	0.964	0	2.23	0.096	54.7	62.91
SCORIM-1N2	0.954	0.280	2.80	0.102	60.8	61.02
SCORIM-1N3	0.971	0	2.43	0.102	53.5	64.88
SCORIM-1N4	0.922	0	2.66	0.158	75.0	59.00

(b) iPP with the addition of 0.15wt% Geniset MD

CON-2N1	0.563	0.226	1.68	0.027	22.4	48.61
CON-2N2	0.598	0	1.26	0.040	32.1	44.44
SCORIM-2N1	0.941	0.271	2.48	0.104	61.7	57.17
SCORIM-2N2	0.959	0.301	2.86	0.118	60.8	64.70
SCORIM-2N3	0.970	0.235	2.85	0.110	58.8	66.94
SCORIM-2N4	0.889	0	1.88	0.164	74.1	54.40

(c) iPP with the addition of 0.15wt% ADK STAB

CON-3N2	0.627	0	1.62	0.099	83.2	56.92
SCORIM-3N4	0.899	0	2.13	0.145	67.9	64.85

samples (SCORIM-1N2 and -1N3).

The SCORIM-N4 injection program provided a higher nozzle temperature (280°C) and the longest holding pressure time (135.0sec) for iPP with and without the addition of nucleating agents. Both iPP without and with nucleating agents samples produced under such higher temperature and pressure (SCORIM-1N4, -2N4 and -3N4), exhibited the highest values of γ-phase index G and γ%, and lower values of α-phase orientation index A and crystallinity index C within the SCORIM process. The ß-phase index B of the SCORIM-N4 mouldings (SCORIM-1N4, -2N4 and -3N4) were all zero.

4.5.2 WAXS Debye Flat Plate Measurements of iPP with and without the Addition of Nucleating Agents

Figures 4.11 —— 4.14 show the Debye patterns obtained from section taken from the midpoints and parallel to the melt flow direction of injection moulded iPP. The testing positions were taken from the middle layer in the cross section. The distance from the sample surface to the film was 37.6mm, and the film exposure time was 3.5 hours. The Debye patterns of iPP with and without the addition of nucleating agents exhibited different levels of preferred orientation.

Figure 4.11 shows the Debye ring patterns of the rectangular bar conventional injection mouldings (con-1N2 and -2N2) of iPP without and with the addition of 0.15wt.% Geniset MD. Nine Debye rings were observed. The first inner ring was indexed as 2θ equal to 12.16° corresponding to a d-spacing was 7.28 Å. The other eight rings were indexed as $(110)_\alpha$, $(113)_\gamma$, $(040)_\alpha$, $(130)_\alpha$, $(117)_\gamma$, $(111)_\alpha$+$(041)_\alpha$, $(060)_\alpha$, and $(220)_\alpha$. Crystallographic data is shown in Table 4.6a and 4.7a.

Figure 4.12 shows the Debye ring patterns of the SCORIM rectangular bar samples (SCORIM-1N2 and -2N2) of iPP without and with the addition of 0.15wt.% Geniset MD. The SCORIM-1N2 sample exhibited twelve rings in the Debye pattern. The first inner ring corresponding to 2θ of 12.16°. The other eleven rings were $(110)_\alpha$, $(113)_\gamma$, $(300)_ß$, $(040)_\alpha$, $(130)_\alpha$, $(117)_\gamma$, $(111)_\alpha$, $(041)_\alpha$, $(131)_\alpha$, $(060)_\alpha$ and $(220)_\alpha$. Crystallographic data is shown in Table 4.6b and 4.7b.

Figures 4.13 and 4.14 show that Debye ring patterns obtained from the section taken

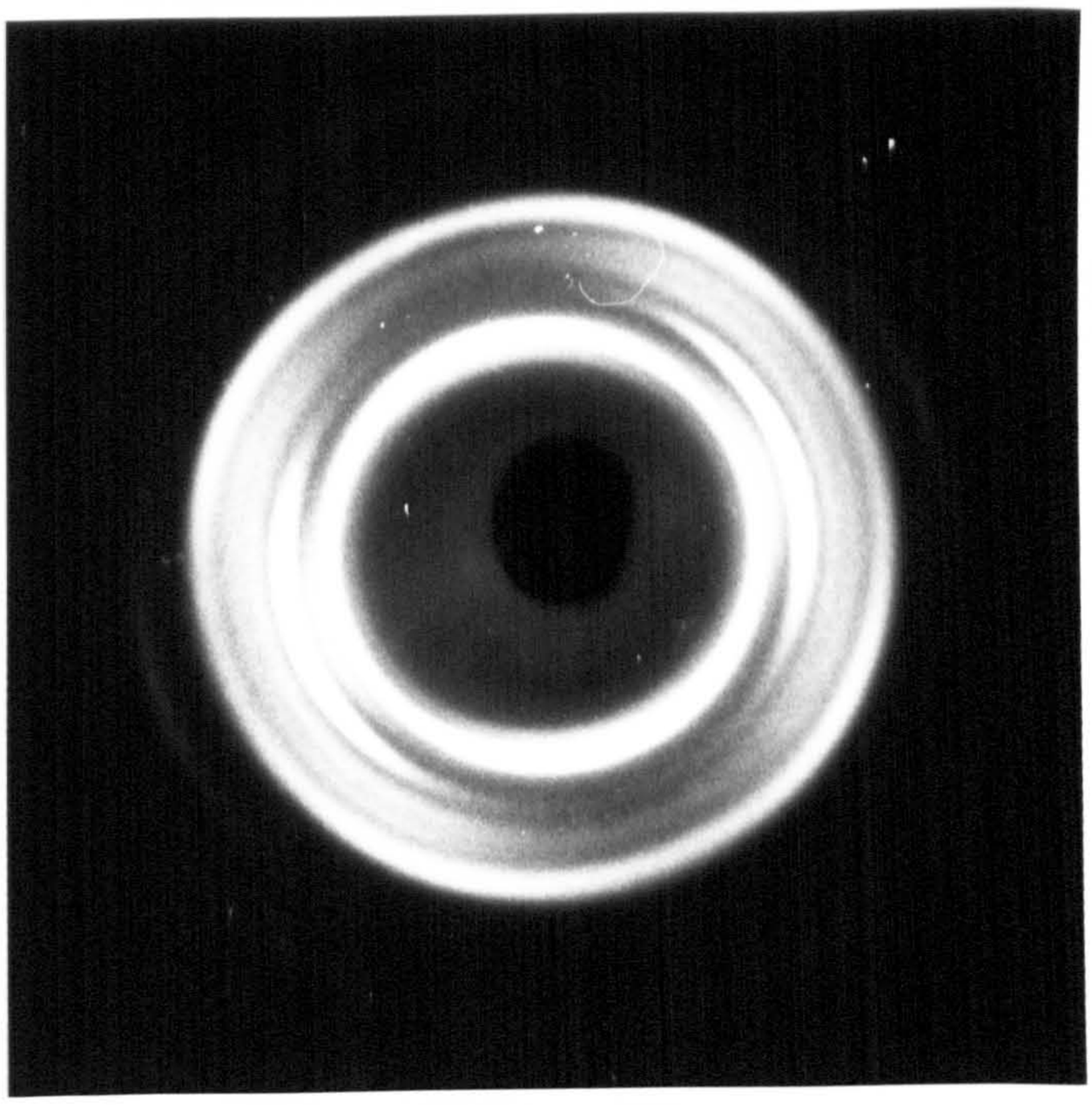

(a) conventional-1N2

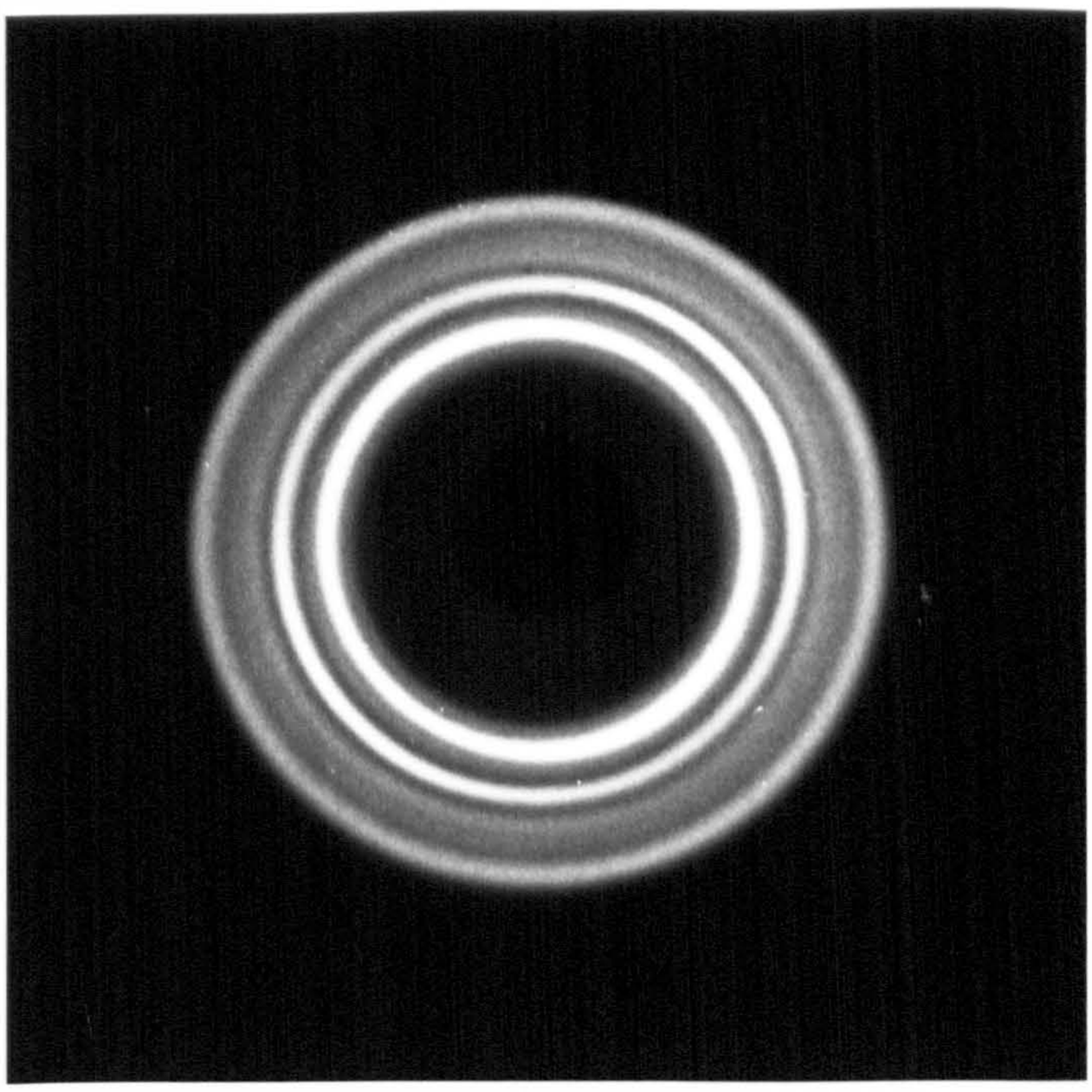

(b) conventional-2N2

Figure 4.11 Photographs of Debye pattern of rectangular bar conventional injection mouldings

(a) conventional-1N2 (polypropylene)

(b) conventional-2N2 (iPP+0.15wt.%Geniset MD)

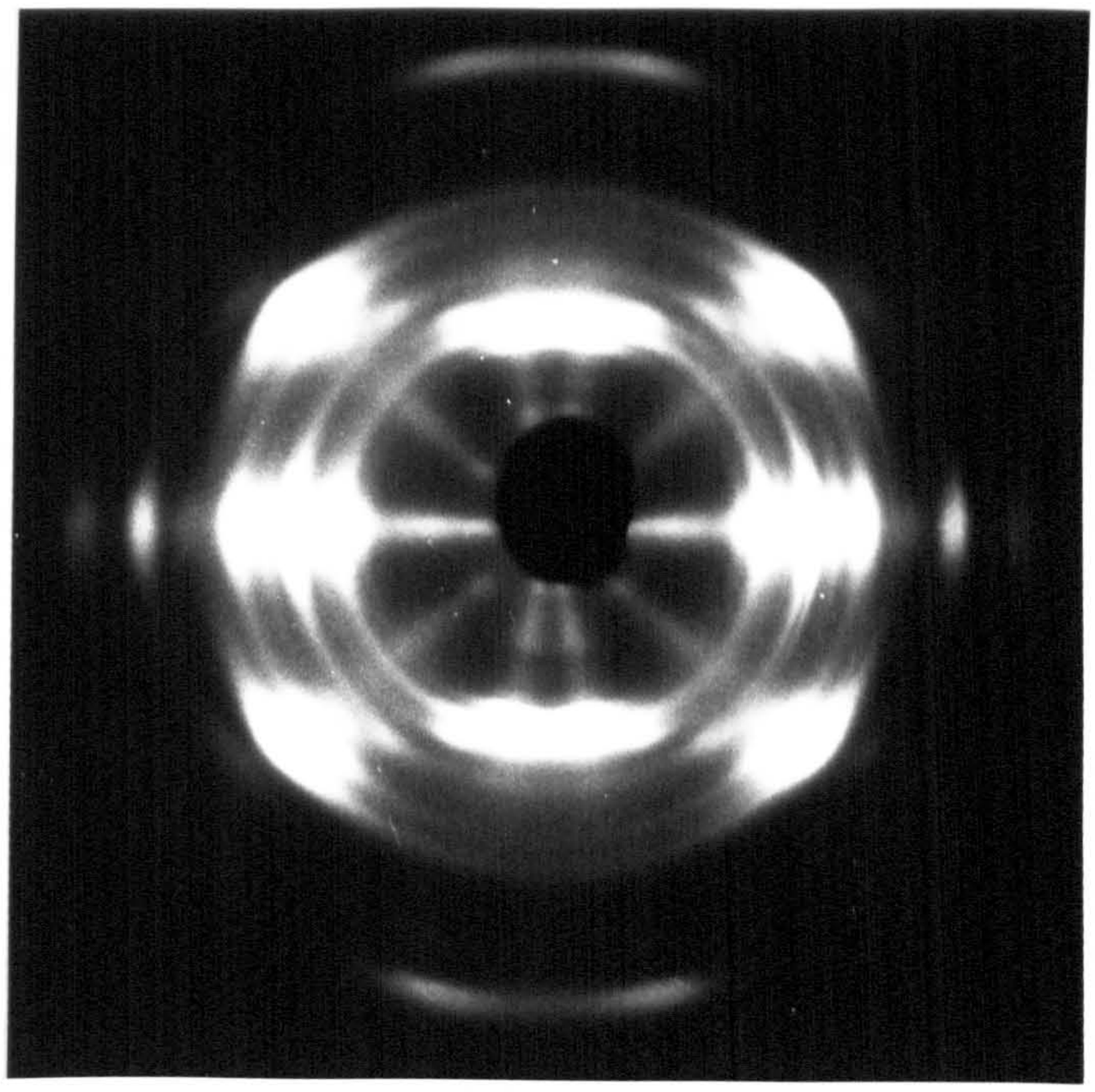

(a) SCORIM-1N2

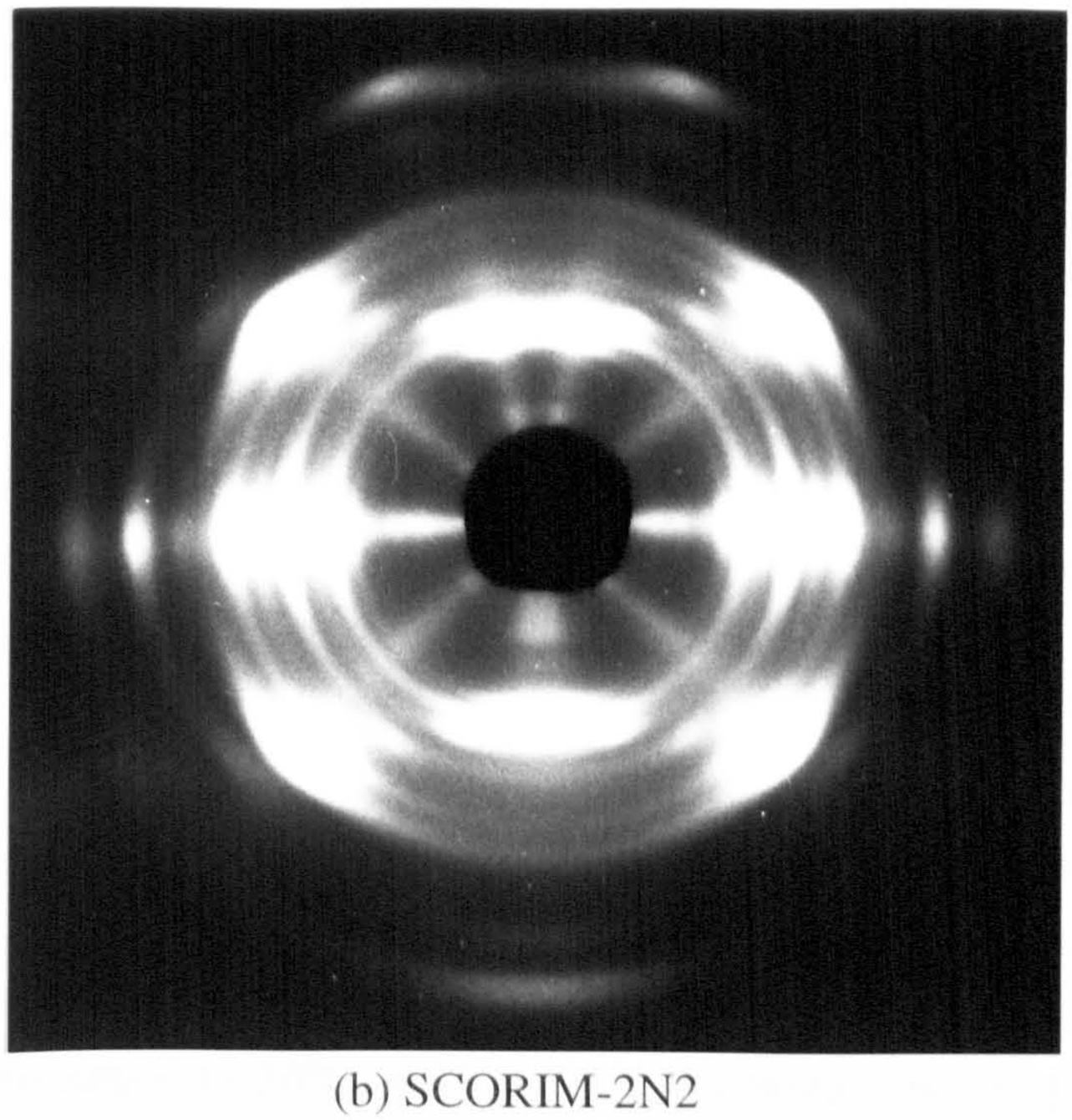

(b) SCORIM-2N2

Figure 4.12 Photographs of Debye pattern of rectangular bar SCORIM mouldings

(a) SCORIM-1N2 (polypropylene)

(b) SCORIM-2N2 (iPP+0.15wt.%Geniset MD)

from the midpoints and parallel to the melt flow direction of the SCORIM-1N4 and -2N4 samples. The measuring positions were taken from the skin, middle and core regions.

For the SCORIM polypropylene mouldings, the testing points were taken from 0.46, 1.24 and 3.43mm away from the surface of the SCORIM-1N4 sample (see Figure 4.13). Eleven Debye rings were observed. The first inner ring was 2θ equal to 12.16°. The other ten rings were $(110)_\alpha$, $(113)_\gamma$, $(040)_\alpha$, $(130)_\alpha$, $(117)_\gamma$, $(111)_\alpha$, $(041)_\alpha$, $(131)_\alpha$, $(060)_\alpha$ and $(220)_\alpha$.

For the SCORIM moulding of iPP+0.15wt.% Geniset MD, thirteen rings were observed in the Debye pattern of the SCORIM-2N4 sample (Figure 4.14). The first inner ring equal to 2θ of 12.16°. The other twelve rings were $(110)_\alpha$, $(113)_\gamma$, $(300)_\beta$, $(040)_\alpha$, $(130)_\alpha$, $(117)_\gamma$, $(111)_\alpha$, $(041)_\alpha$, $(131)_\alpha$, $(060)_\alpha$, $(200)_\alpha$and $(220)_\alpha$.

Figure 4.15 shows the schematic diagram of the thirteen Debye ring pattern obtained from the SCORIM-2N4 samples of iPP with the addition of 0.15wt.% Geniset MD. The prominent feature of the occurence of the inner unidenfied ring with 2θ equal to 12.16° corresponding to a d-spacing 7.28Å, and the occurence of two γ-phase rings $(113)_\gamma$ and $(117)_\gamma$ were reported in a publication accoreding to the results obtained in this thesis [142].

4.6 Thermal Analysis of Injection Moulded iPP with and without the Addition of Nucleating Agents

The effect of nucleating agent in different concentrations on the crystallisation of injection moulded iPP was studied. The thermal treatment was contained two steps. Firstly, the sample was heated from 50°C to 250°C at 10°C/min and kept at 250°C for 1min before crystallisation in order to remove the thermal history, and then slowly cooled down to 50°C at 20°C/min; Secondly, the sample was reheated to 250°C at 10°C/min and kept at 250°C for 1 min, and then quickly recooled down to 50°C at 320°C/min in order to minimize the time spent by the sample in the melt state. The melting temperature (T_m) and heat of fusion (ΔH) of iPP mouldings with different concentration of nucleating agents were obtained from the DSC melting thermogram by reheating the samples. All the measuring iPP samples at different

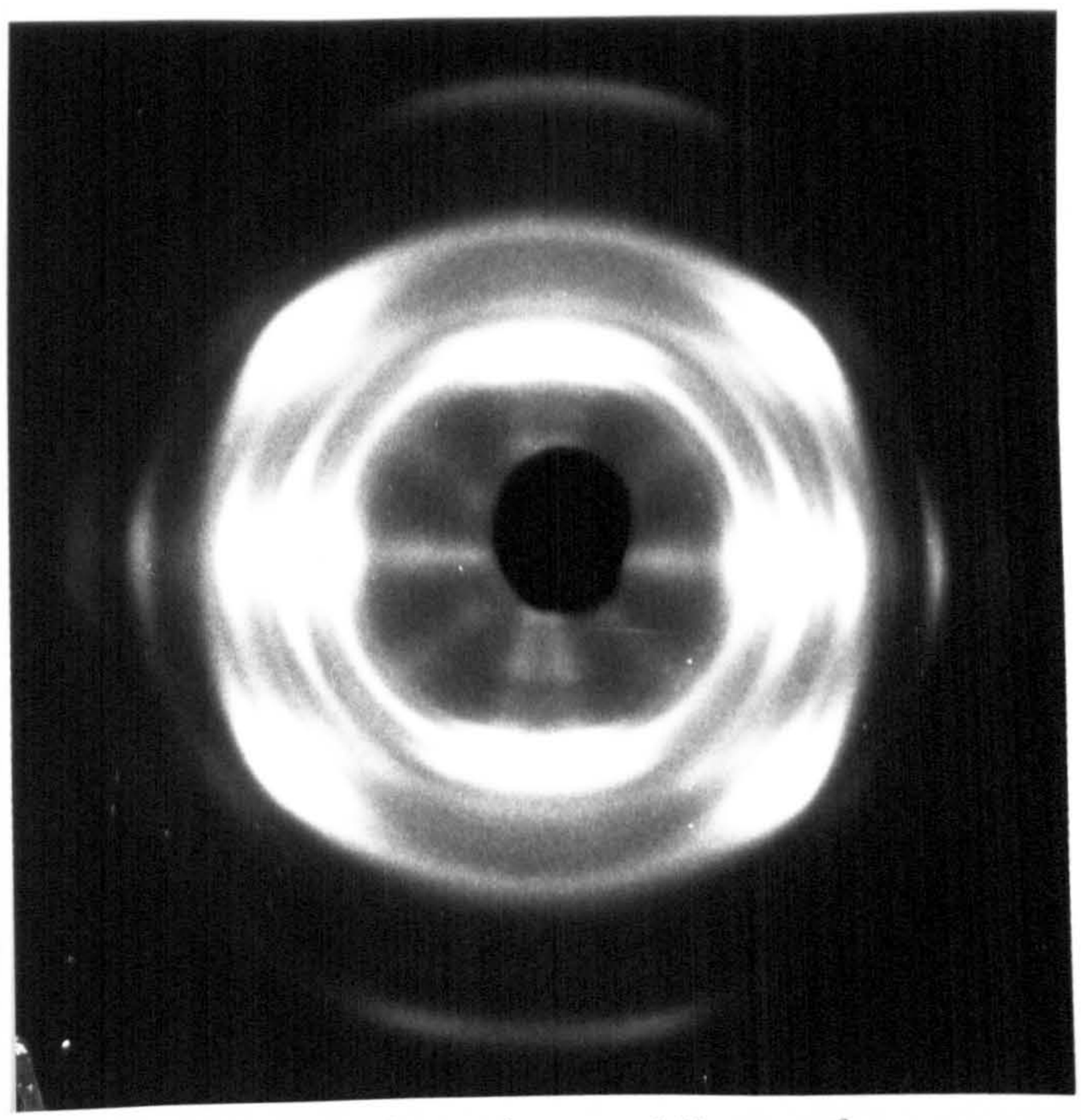

(a) 0.46mm from the moulding surface

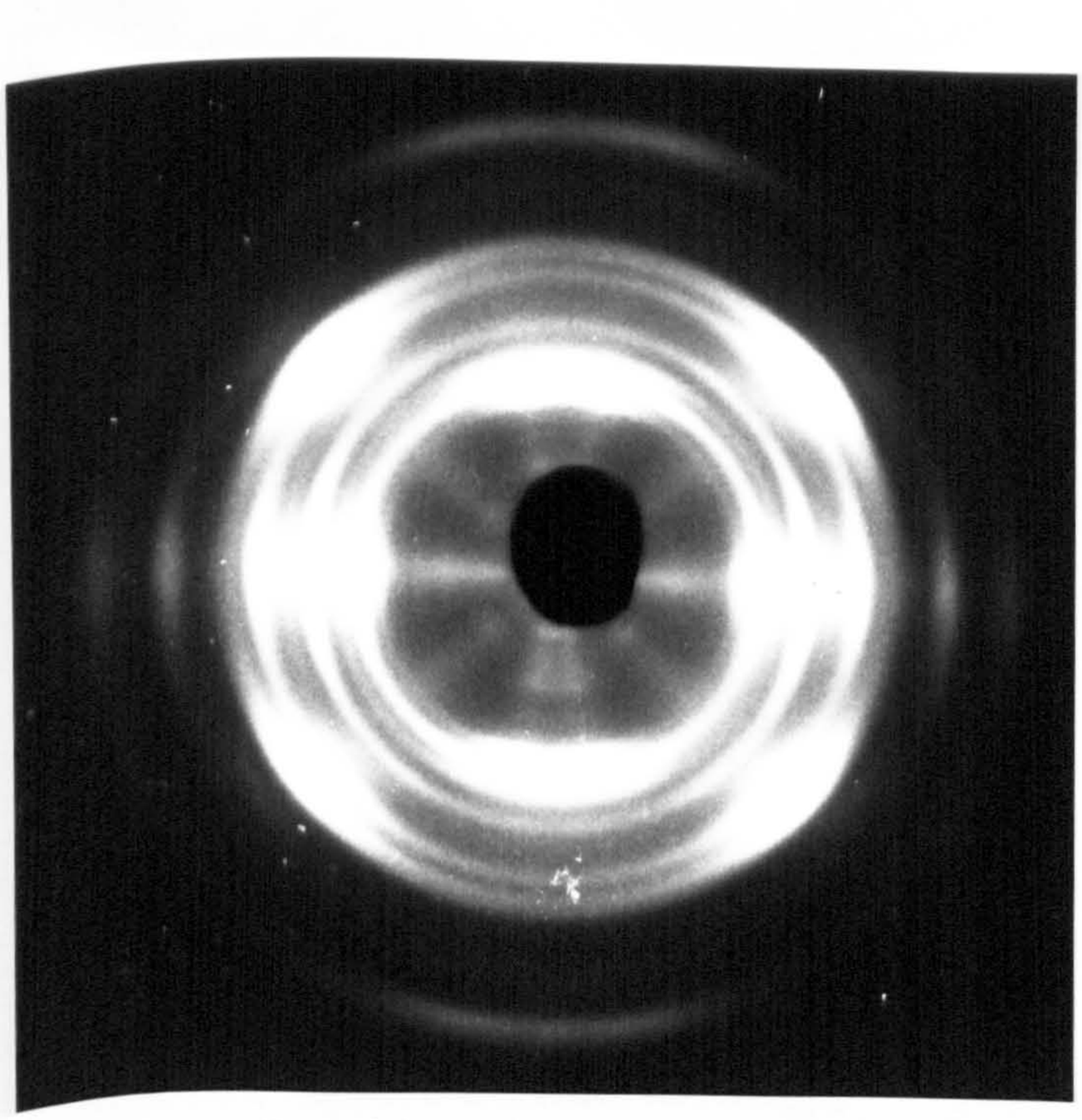

(b) 1.24mm from the moulding surface

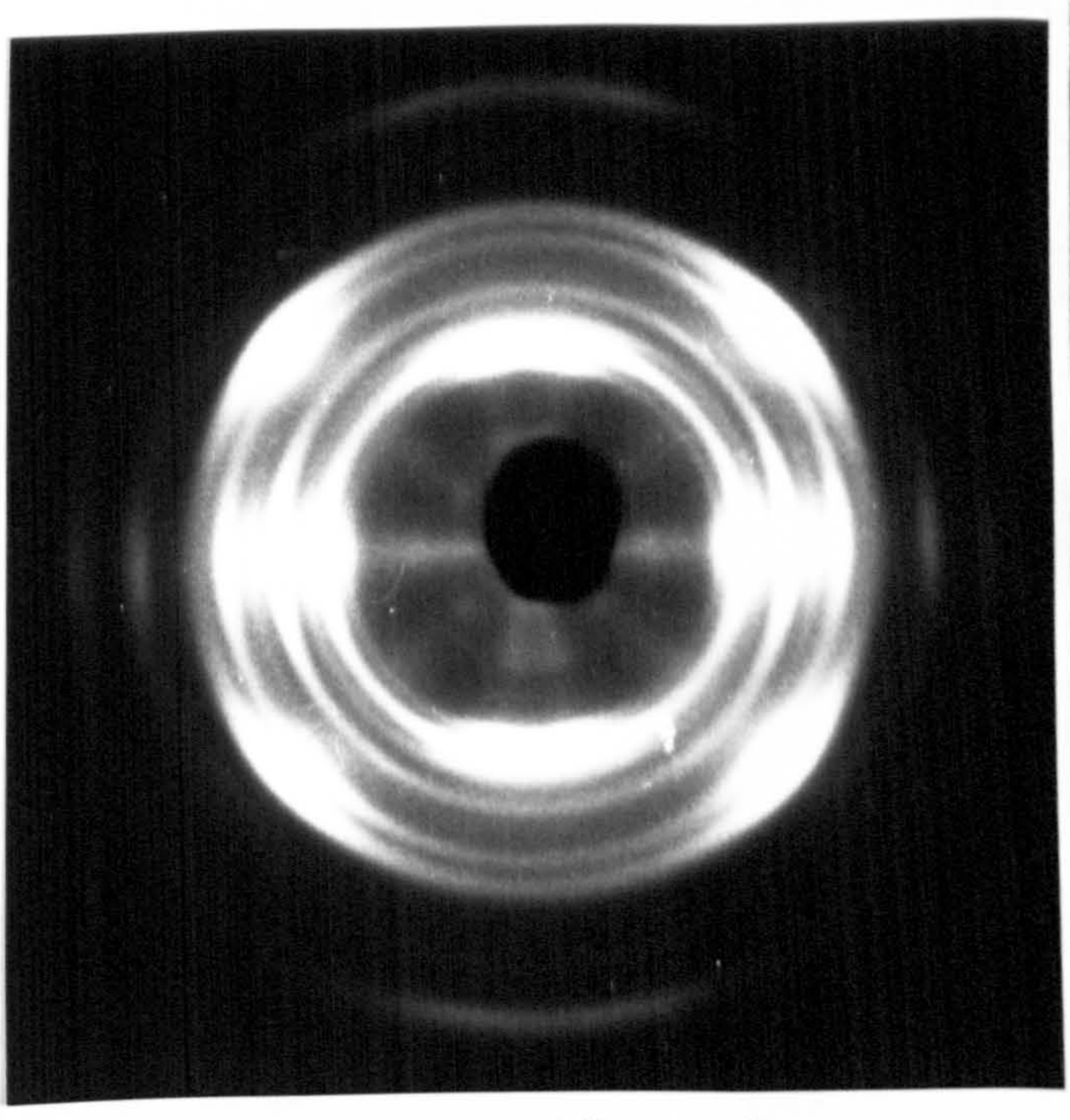

(c) 3.43mm from the moulding surface

Figure 4.13 Photographs of Debye pattern of SCORIM-1N4 rectangular bar moulding of polypropylene

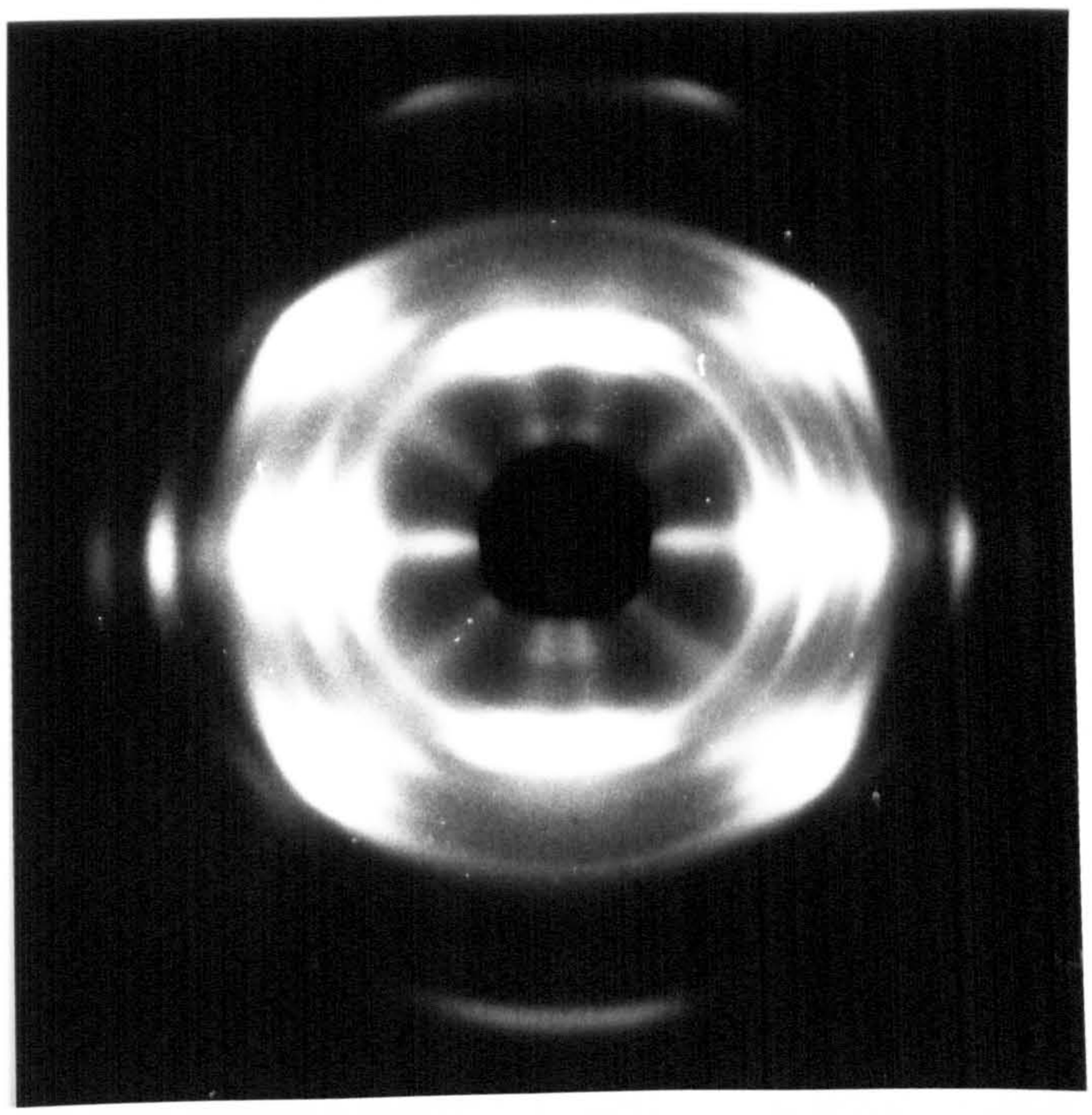

(a) middle layer

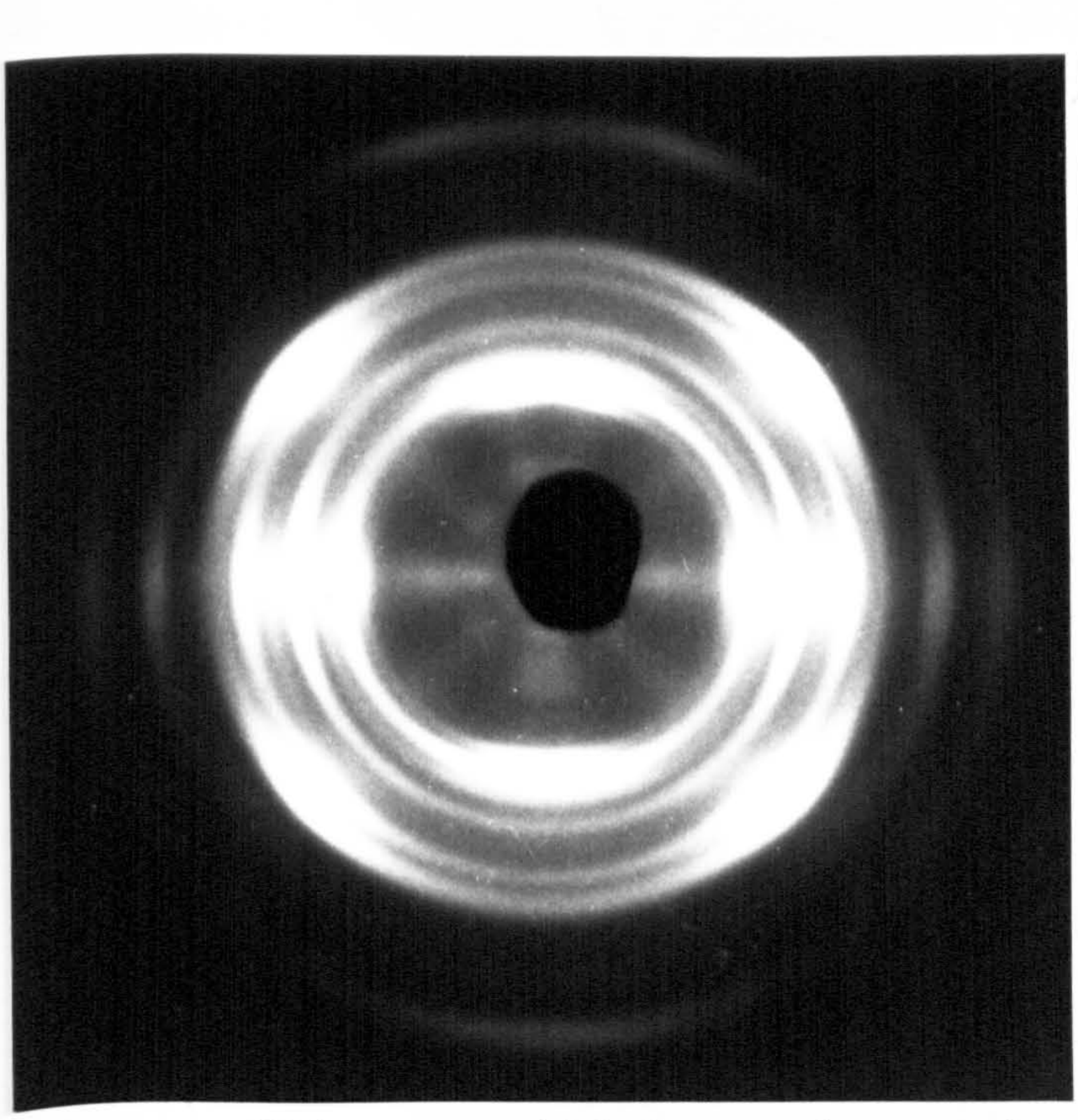

(b) between middle layer and core region

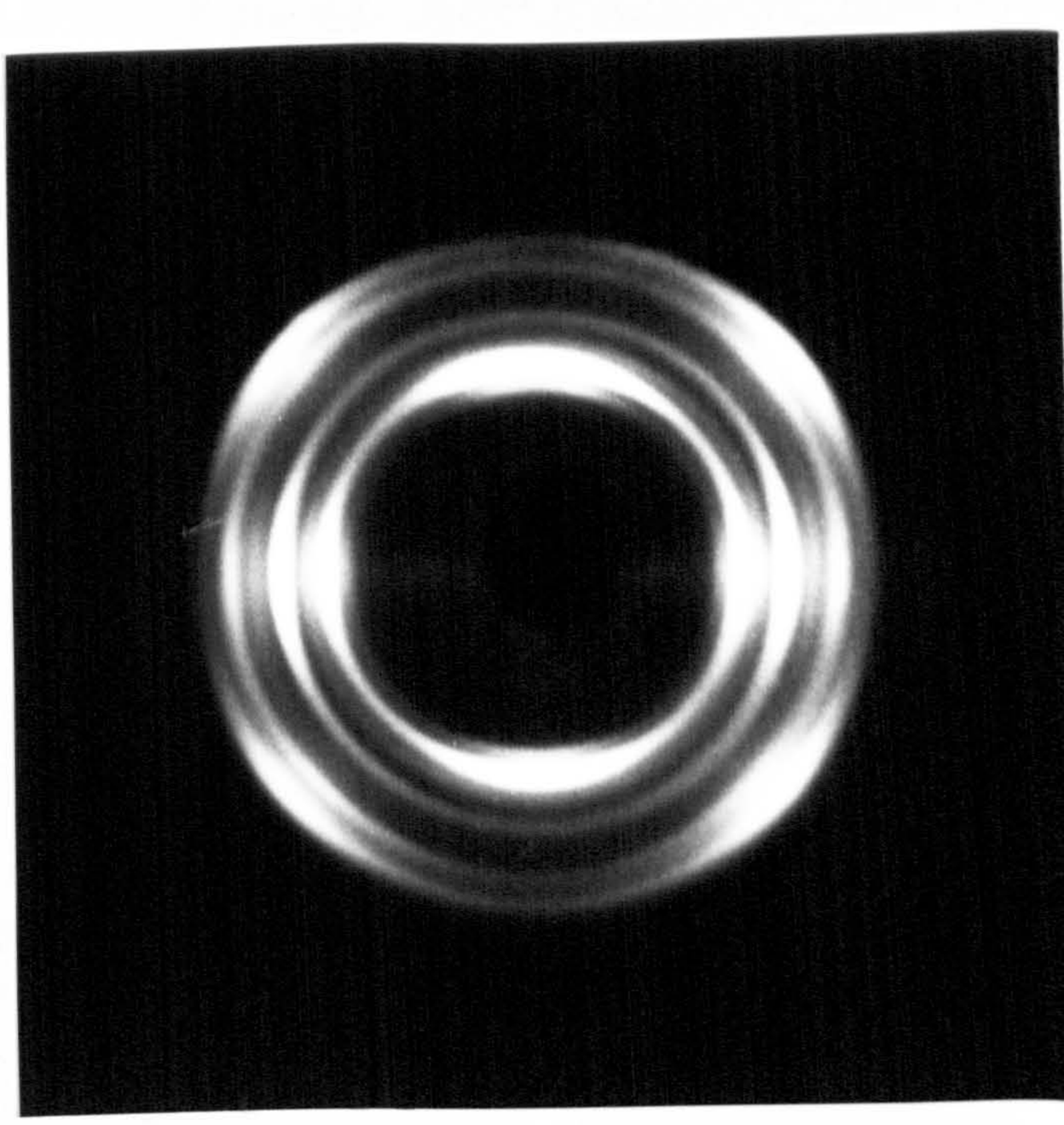

(c) core region

Figure 4.14 Photographs of Debye pattern of SCORIM-2N4 rectangular bar moulding of iPP+0.15wt.% Geniset MD

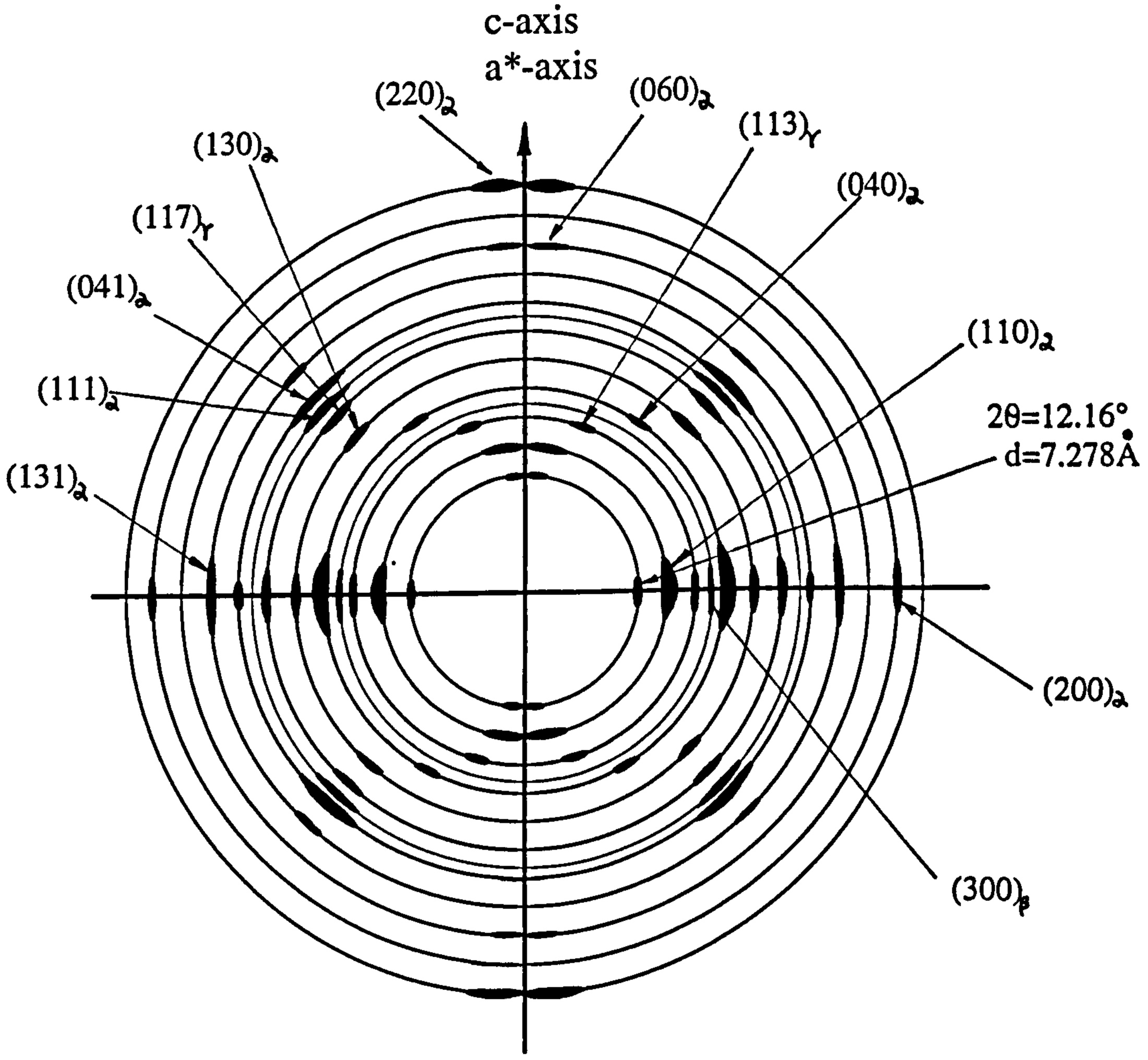

Figure 4.15 Schematic diagram of Debye pattern and indices

concentration of nucleating agents were given the same thermal treatment.

Figures 4.16 and 4.17 show the reheating thermogram of tensile bar conventional injection mouldings of iPP with the different concentration of nucleating agents (the concentration is indicated beside the curves). Similar differences in crystallisation and melting behaviour of polypropylene containing different concentrations of nucleating agents were obtained. Table 4.8 shows the melting temperature of endotherm (T_m), peak temperature of endotherm ($T_{m,p}$), temperature range of peak (ΔT), the heat of fusion (ΔH) and crystallinity ($X_{\Delta H}$) of tensile bar conventional injection mouldings of Geniset and ADK nucleated-iPP.

The Geniset MD nucleated-iPP samples exhibited the lower melting temperature (T_m) than that of ADK nucleated-iPP samples with the higher concentration of nucleating agents, and lower than that of ADK nucleated-iPP samples at the higher concentration (see Figure 4.18a). The heat of fusion (ΔH) reached a maximum at the lower concentration of both nucleating agents, before it decreased with further increase in the concentration of nucleating agents. This phenomenon may be due to the nucleating agent in high concentrations forming agglomerates to give an effect of a low concentration of the agent. The heat of fusion (ΔH) of Geniset MD nucleated-iPP samples was lower than that of ADK nucleated-iPP samples at the lower concentration, and higher than that of ADK nucleated-iPP samples at the higher concentration (see Figure 4.18b). To control the concentration of the nucleating agent is important for the purpose of optimising the crystallinity of the injection moulded iPP.

For both conventional and SCORIM rectangular bar samples, the thermogram of iPP with and without the addition of 0.15wt.% Geniset MD are shown in Figures 4.19 and 4.20. The results of the melting temperature of endotherm (T_m), peak temperature of endotherm ($T_{m,p}$), temperature range of peak (ΔT), the heat of fusion (ΔH) and crystallinity ($X_{\Delta H}$) were shown in Table 4.9.

Figure 4.21 shows the melting temperature (T_m) and the heat of fusion (ΔH) of crystallisation *vs.* conventional and SCORIM processing conditions of iPP with and without the addition of Geniset MD. The conventional injection moulded iPP containing 0.15% Geniset MD (con-2N1 and -2N2) exhibited higher melting temperature (T_m) and higher the heat of fusion (ΔH) than that recorded for

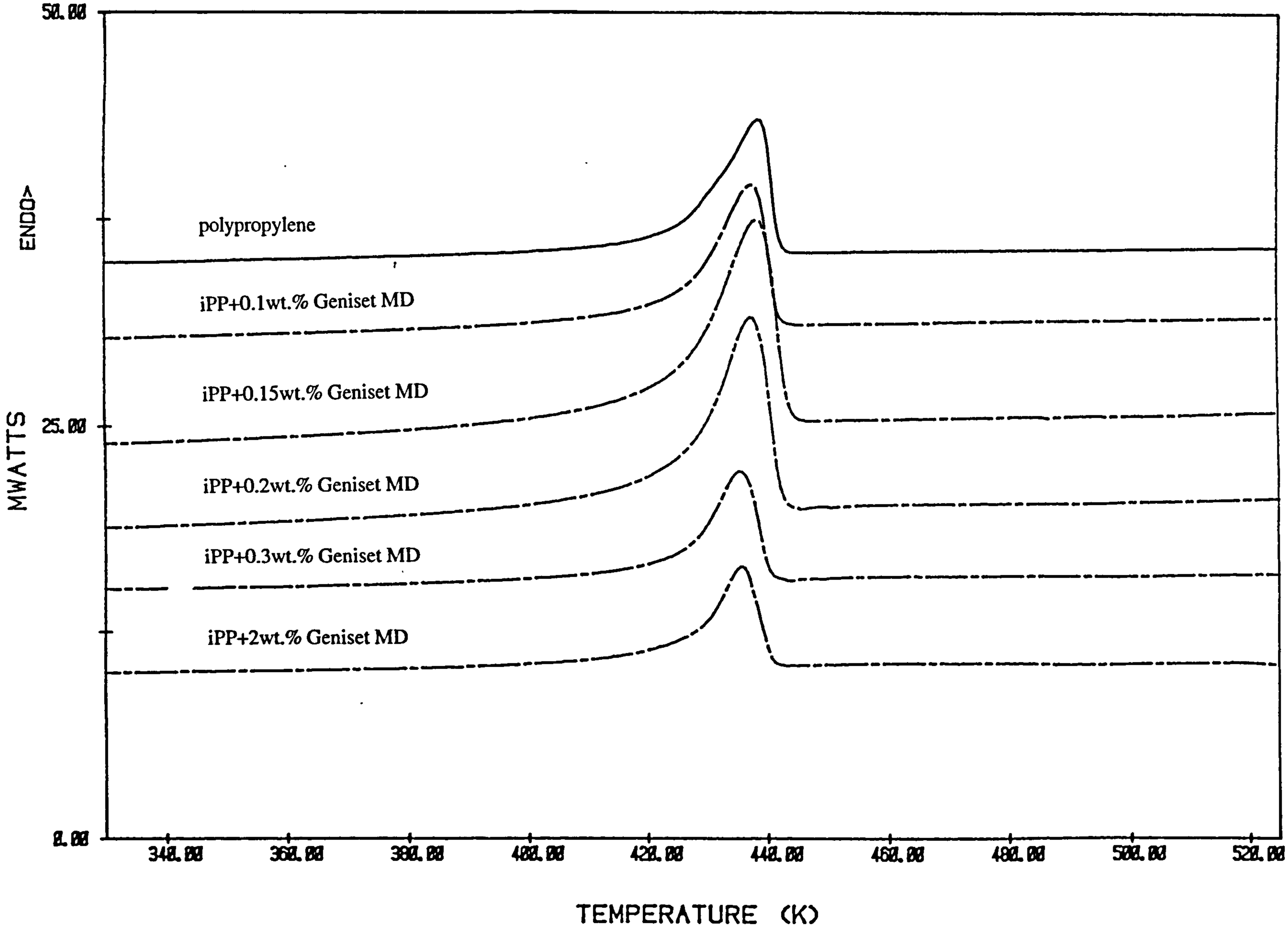

Figure 4.16 DSC thermogram of tensile bar conventional injection moulding of iPP with the addition of Geniset MD

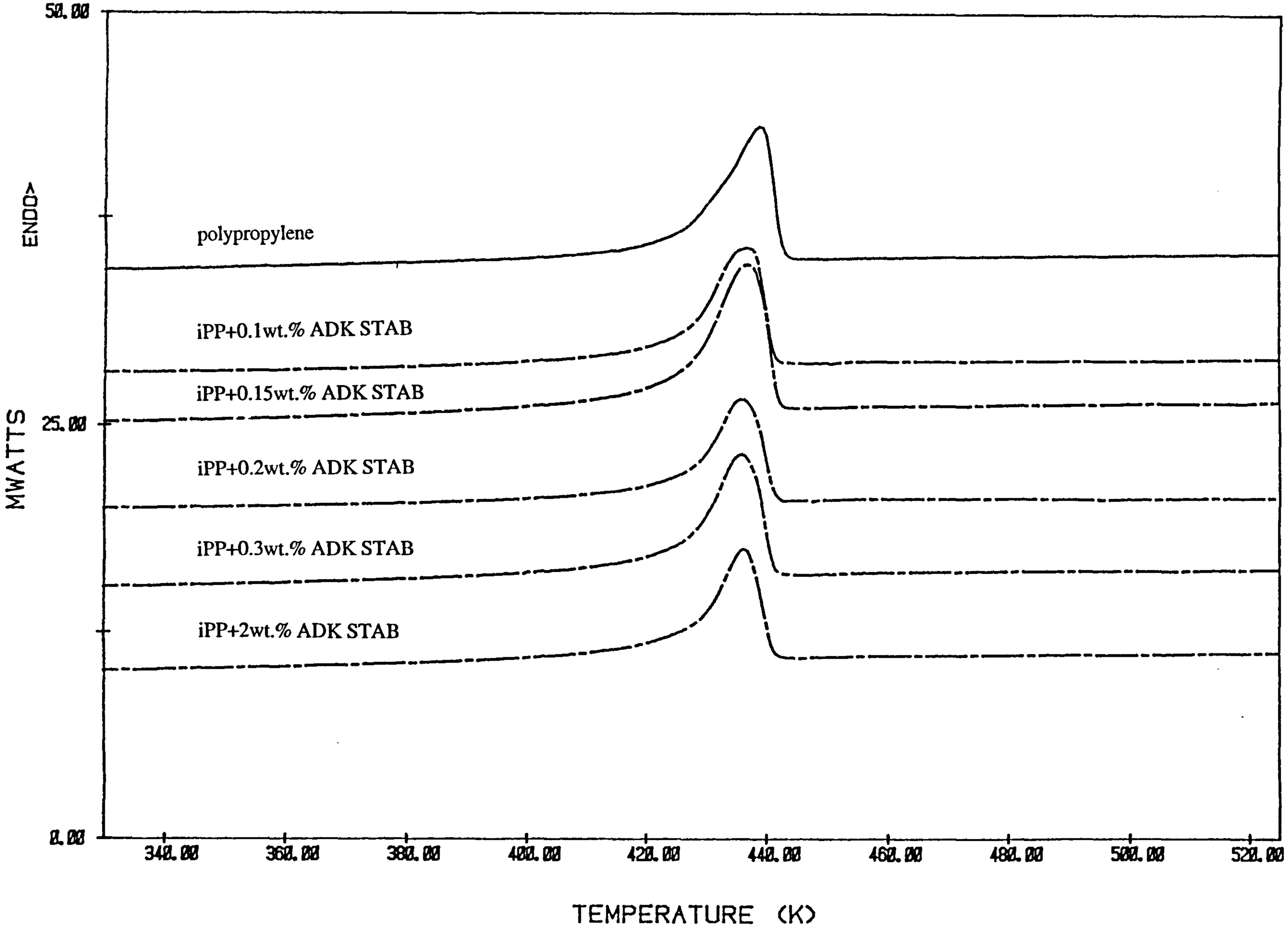

Figure 4.17 DSC thermogram of tensile bar conventional injection moulding of iPP with the addition of ADK STAB

Table 4.10 DSC results of conventional injection mouldings (standard tensile bar) of iPP with the addition of nucleating agents

(a) polypropylene

Sample ID	T_m (K)	ΔT (K)	$T_{m,D}$ (K)	Heat of fusion ΔH (J/g)	Crystallinity $X_{\Delta H}$ (%)
iPP	427.36	37.83	432.43	81.92	59.76

(b) iPP with the addition of Geniset MD

iPP+0.1%MD	426.69	35.32	438.34	80.81	58.95
iPP+0.15%MD	427.27	44.14	432.32	85.76	62.56
iPP+0.2%MD	430.93	43.70	437.08	92.40	67.41
iPP+0.3%MD	431.95	42.59	437.57	93.56	68.25
iPP+2%MD	430.80	40.64	437.91	90.97	66.36

(c) iPP with the addition of ADK STAB

iPP+0.1%ADK	432.41	42.46	436.75	88.90	64.85
iPP+0.15%ADK	432.24	42.98	436.99	90.23	65.82
iPP+0.2%ADK	431.93	48.45	436.34	94.21	68.73
iPP+0.3%ADK	431.76	44.93	436.68	90.92	66.33
iPP+2%ADK	431.37	43.96	438.20	90.50	66.02

(a)

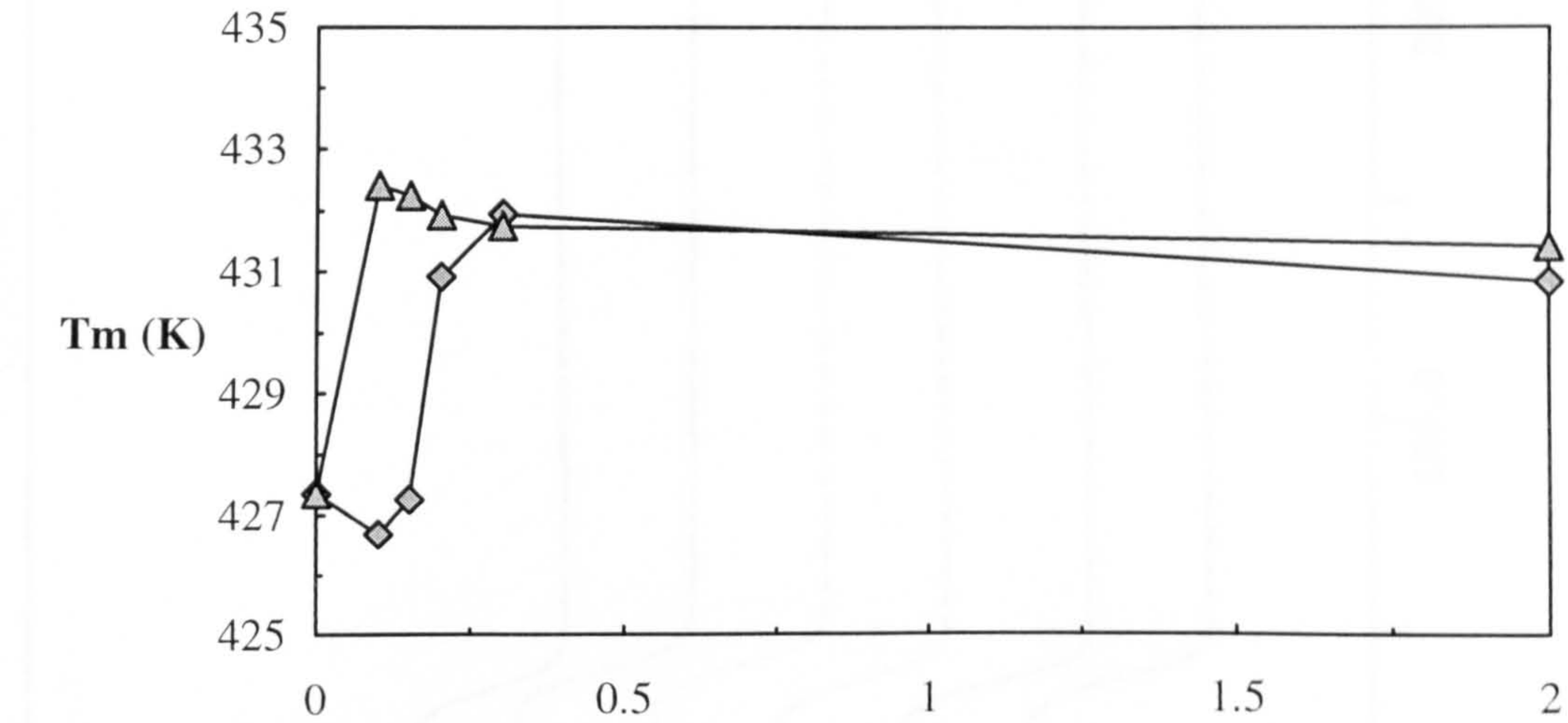

(b)

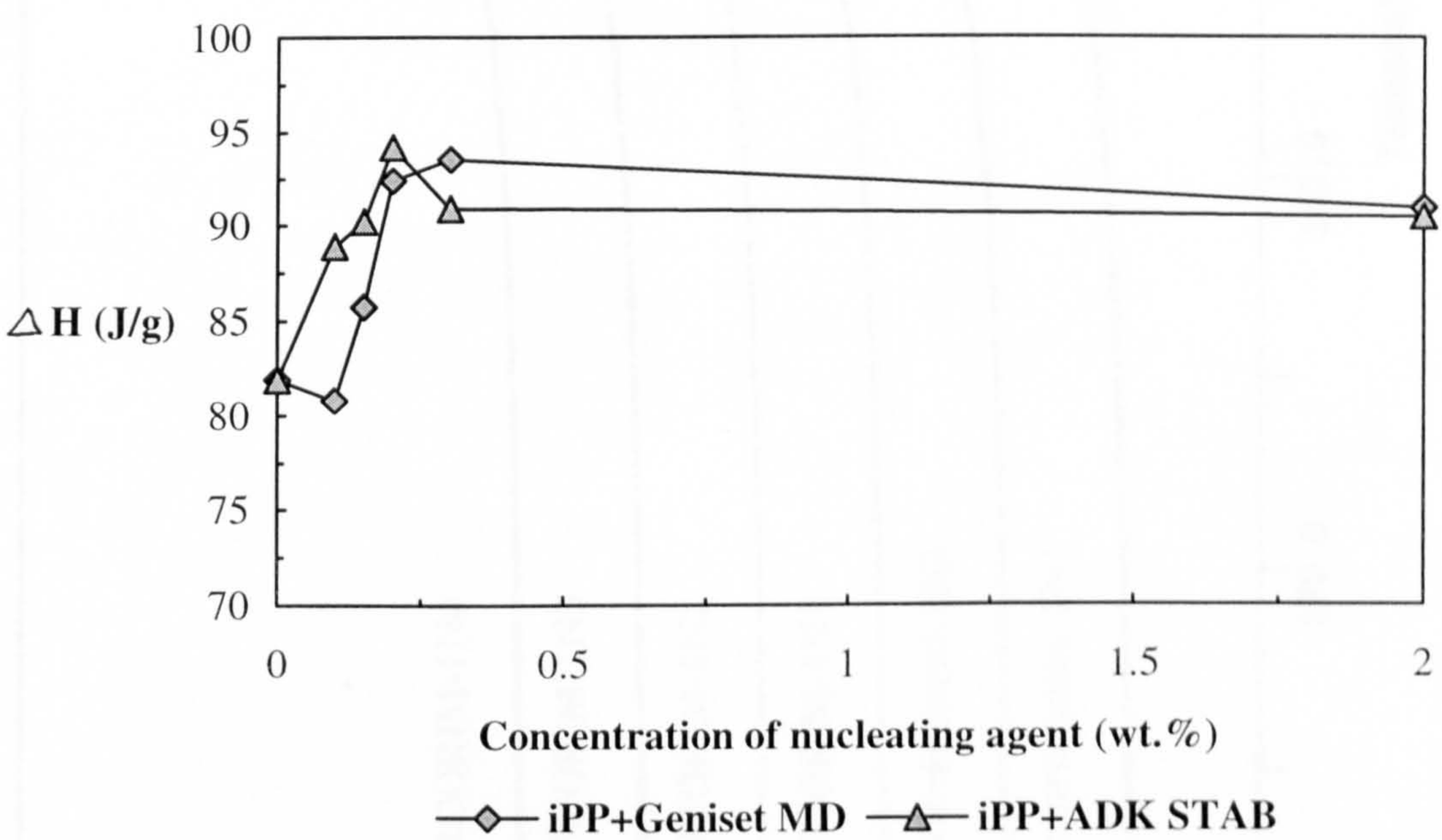

Figure 4.18 DSC measuring results of tensile bar conventional mouldings of iPP with the addition of nucleating agents

(a) melting temperature T_m (b) heat of fusion ΔH

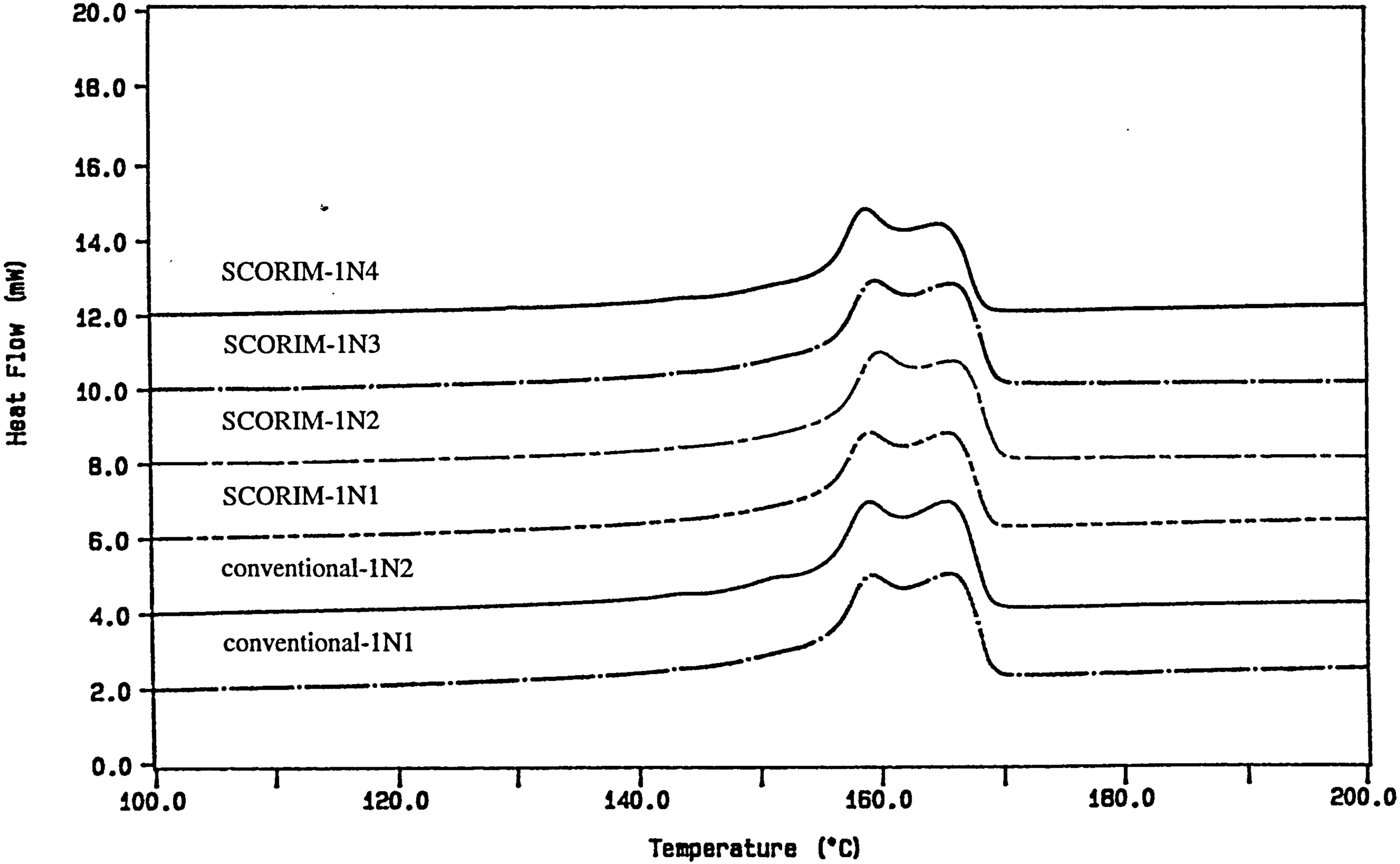

Figure 4.19 DSC thermogram of conventional and SCORIM rectangular bar moulding of iPP

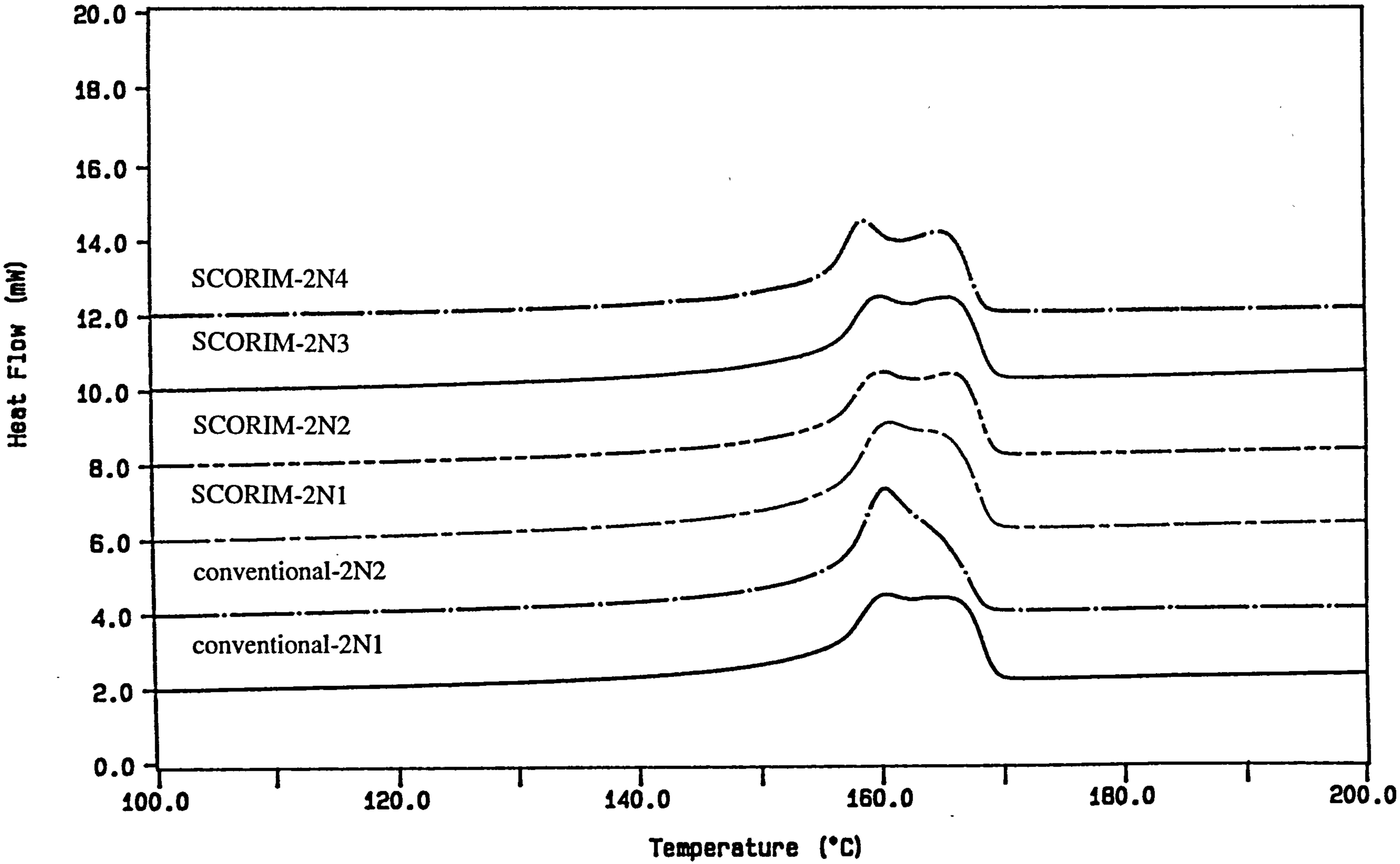

Figure 4.20 DSC thermogram of conventional and SCORIM rectangular bar moulding of iPP+0.15 wt% Geniset MD

Table 4.11 DSC results of conventional and SCORIM mouldings (rectangular bar) of iPP with and without the addition of nucleating agents

(a) polypropylene

Sample ID	T_m (K)	ΔT (K)	$T_{m.D}$ (K)	Heat of fusion ΔH (J/g)	Crystallinity $X_{\Delta H}$(%)
Con-1N1	428.01	31.00	438.57	77.14	56.27
Con-1N2	427.36	45.50	438.48	87.31	63.69
SCORIM-1N1	427.72	36.17	432.41	80.91	59.02
SCORIM-1N2	428.25	49.50	433.26	86.90	63.39
SCORIM-1N3	428.09	41.33	432.90	82.81	60.41
SCORIM-1N4	430.83	42.83	432.26	86.35	62.99

(b) iPP with the addition of Geniset MD

Con-2N1	428.08	35.33	433.42	82.24	60.00
Con-2N2	428.74	47.50	433.45	89.81	65.52
SCORIM-2N1	428.30	38.00	433.83	80.60	58.80
SCORIM-2N2	427.91	39.00	433.21	81.50	59.45
SCORIM-2N3	428.01	35.17	433.18	79.12	57.71
SCORIM-2N4	427.80	43.64	431.97	85.90	62.67

(c) iPP with the addition of ADK STAB

Con-3N2	432.94	38.00	437.44	87.39	63.75
SCORIM-3N4	430.29	44.33	436.10	89.04	65.22

(a)

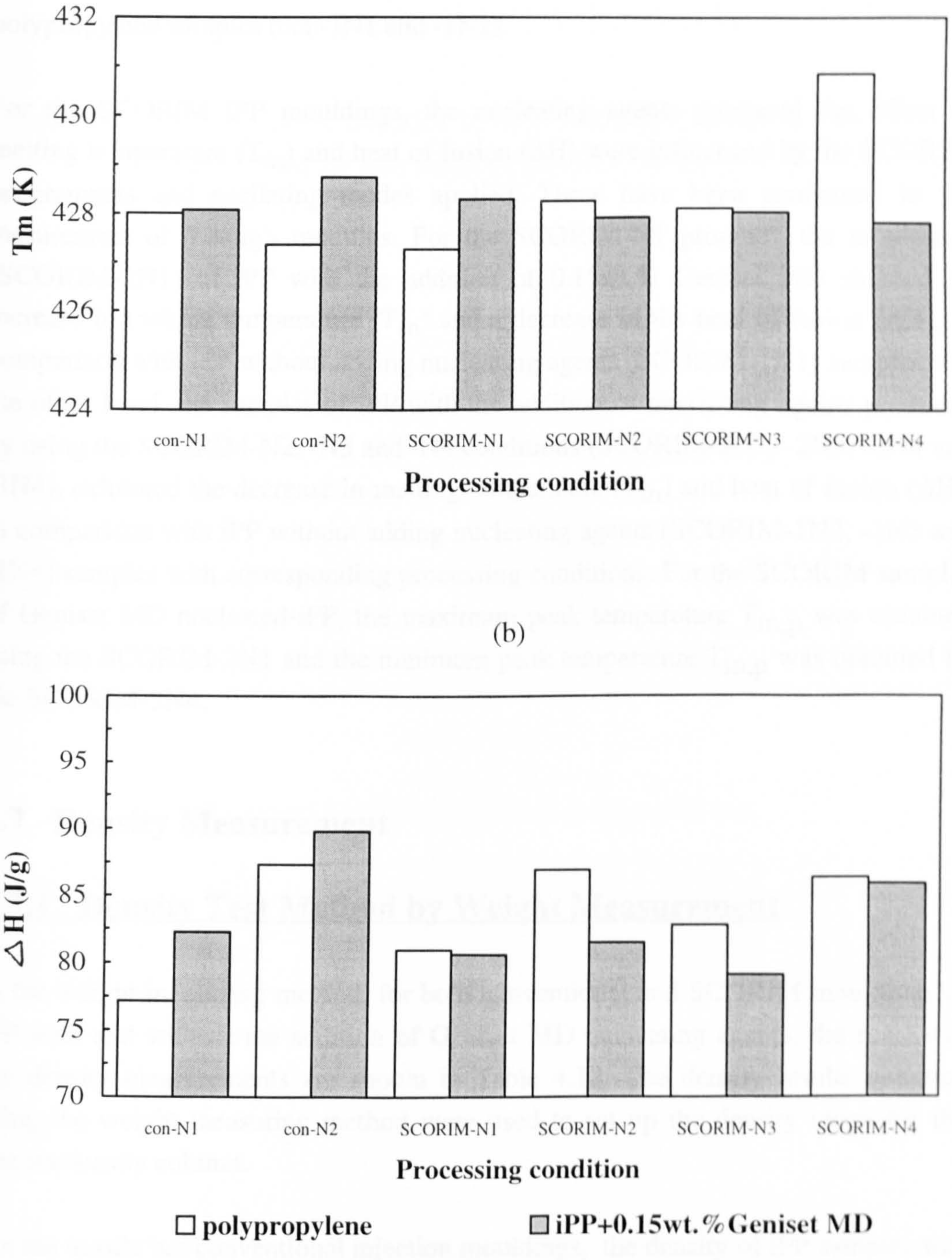

Figure 4.21 DSC measuring results of rectangular bar conventional and SCORIM mouldings of iPP without and with the addition of Geniset MD

(a) melting temperature T_m (b) heat of fusion ΔH

polypropylene samples (con-1N1 and -1N2).

For the SCORIM iPP mouldings, the nucleating agents produced the effect in melting temperature (T_m) and heat of fusion (ΔH) were influenced by the SCORIM programmes and oscilating modes applied. These have been confirmed in the mesurement of Young's modulus. For the SCORIM-N1 program, the mouldings (SCORIM-2N1) of iPP with the addition of 0.15wt.% Geniset MD showed an increase in melting temperature (T_m) and a decrease in the heat of fusion (ΔH), in comparison with iPP without adding nucleating agents (SCORIM-1N1) samples. On the other hand, the samples of iPP with the addition of nucleating agents produced by using the SCORIM-N2, -N3 and -N4 conditions (SCORIM-2N2, -2N3, -2N4 and -3N4), exhibited the decrease in melting temperature (T_m) and heat of fusion (ΔH), in comparison with iPP without adding nucleating agents (SCORIM-1N2, -1N3 and -1N4) samples with corresponding processing conditions. For the SCORIM samples of Geniset MD nucleated-iPP, the maximum peak temperature $T_{m,p}$ was obtained using the SCORIM-2N1 and the minimum peak temperature $T_{m,p}$ was obtained by the SCORIM-2N4.

4.7 Density Measurement

4.7.1 Density Test Method by Weight Measurement

In the weight measuring method, for both conventional and SCORIM mouldings of iPP with and without the addition of Geniset MD nucleating agents, the results of the density measurements are shown in Table 4.12. The density results obtained using the weight measuring method were used to set up the density range for the Tecam density column.

For the tensile bar conventional injection mouldings, the density of iPP samples was increased with increasing concentration of both Geniset MD and ADK nucleating agents (see Table 4.12a). For the rectangular bar samples (see Table 4.12b), the density of the SCORIM samples of iPP without and with the addition of 0.15wt.% Geniset MD samples were greater than that of conventional samples, respectively. The maximum value of the density in all conventional and SCORIM samples was obtained by the tensile bar sample of iPP+2wt.% Geniset MD, with a density of 0.9138 g/cm^3. The minimum value of the density in all conventional and SCORIM

Table 4.12 Results of density of iPP with and without the addition of nucleating agents by weight measuring method

(a) conventional injection mouldings (standard tensile bar)

Sample I.D.	$D^{23°C}$ (g/cm^3)	Crystallinity X_d (%)	Sample I.D.	$D^{23°C}$ (g/cm^3)	Crystallinity X_d (%)
iPP	0.9053	96.7			
iPP+0.1%MD	0.9075	97.0	iPP+0.1%ADK	0.9079	97.0
iPP+0.15%MD	0.9079	97.0	iPP+0.15%ADK	0.9079	97.0
iPP+0.2%MD	0.9085	97.1	iPP+0.2%ADK	0.9084	97.1
iPP+0.3%MD	0.9101	97.2	iPP+0.3%ADK	0.9084	97.2
iPP+2%MD	0.9138	97.6	iPP+2%ADK	0.9104	97.3

(b) conventional and SCORIM mouldings (rectangular bar)

Con-1N1	0.8981	96.0	Con-2N1	0.9027	96.4
SCORIM-1N1	0.9081	97.0	SCORIM-2N1	0.9056	96.8
SCORIM-1N2	0.9041	96.6	SCORIM-2N2	0.9061	96.8
SCORIM-1N3	0.9052	96.7	SCORIM-2N3	0.9054	96.7

samples was obtained by rectangular bar sample of polypropylene (con-1N1) which was 0.8981 g/cm³. The method to calculate the density range is shown in Appendix 4.

4.7.2 Tecam Density Column Method

Table 4.13 reflects the nucleating effect on density measurements of iPP as revealed by the Tecam density column method. For the tensile bar conventional injection mouldings (see Figure 4.22a), the density results indicated that the density of both Geniset MD and ADK nucleated-iPP samples increases with increasing the concentration of both nucleating agents. The changes in the density with increasing content of nucleating agents is pronounced up to 1%.

For the rectangular bar mouldings of iPP with the addition of 0.15wt.% Geniset MD (see Figure 4.22b), the density of the SCORIM samples were greater than that of conventional injection moulding samples. For the polypropylene rectangular bar samples, the maximum value of density was obtained by the SCORIM-1N1 moulding which was 0.9087 g/cm³. For the rectangular bar samples of iPP+0.15wt.% Geniset MD, the maximum value of density was obtained by the SCORIM-2N3 moulding which was 0.9088 g/cm³.

4.8 Summary

The study of the effect of nucleating agents on the mechanical properties and micromorphology of injection moulded iPP evaluated:

1) After adding nucleating agents, iPP mouldings consisted of very fine spherulitic structure and improved optical clarity. The nucleating agents produced the effect in injection moulded iPP of increasing the number of the nuclei, and decreasing the dimensions of the spherulites.

2) Young's modulus and tensile strength of iPP were enhanced by the addition of nucleating agents and increased gradually with increasing concentration of nucleating agents when the mouldings were produced by conventional injection process. On the other hand, the tensile strains were decreased with increasing concentration of nucleating agents. The more pronounced increase in modulus and

Table 4.13 Results of density of iPP with and without the addition of nucleating agents by Tecam density column measuring method

(a) convention injection mouldings (standard tensile bar)

Sample ID	$D^{24°C}$ (g/ml)	Sample ID	$D^{24°C}$ (g/ml)
iPP	0.9057		
iPP+0.1%MD	0.9080	iPP+0.1%ADK	0.9079
iPP+0.15%MD	0.9096	iPP+0.15%ADK	0.9085
iPP+0.2%MD	0.9101	iPP+0.2%ADK	0.9089
iPP+0.3%MD	0.9106	iPP+0.3%ADK	0.9090
iPP+2%MD	0.9141	iPP+2%ADK	0.9125

(b) conventional and SCORIM mouldings (rectangular bar)

Con-1N1	0.9031	Con-2N1	0.9046
SCORIM-1N1	0.9087	SCORIM-2N1	0.9083
SCORIM-1N2	0.9083	SCORIM-2N2	0.9076
SCORIM-1N3	0.9082	SCORIM-2N3	0.9088

(a)

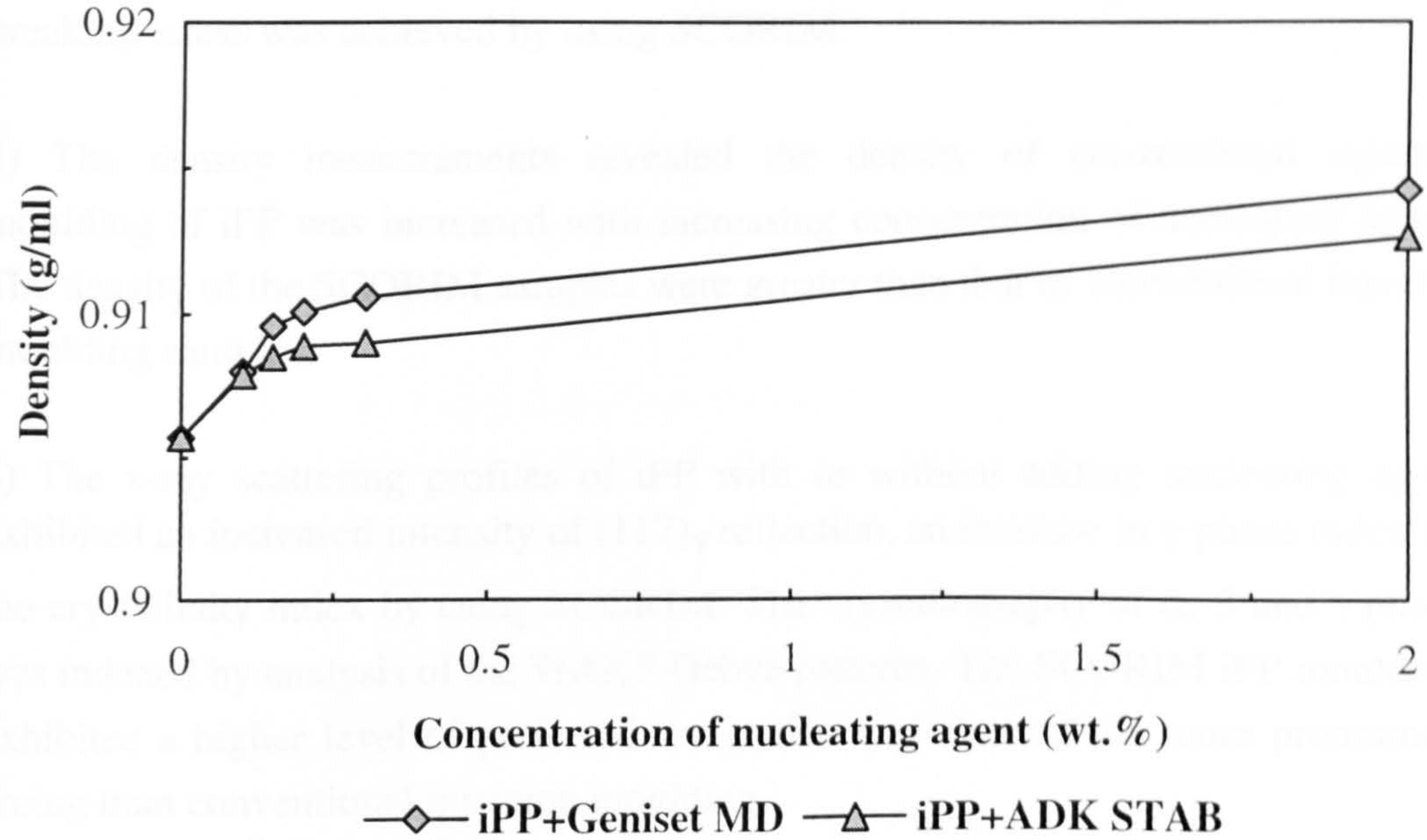

(b)

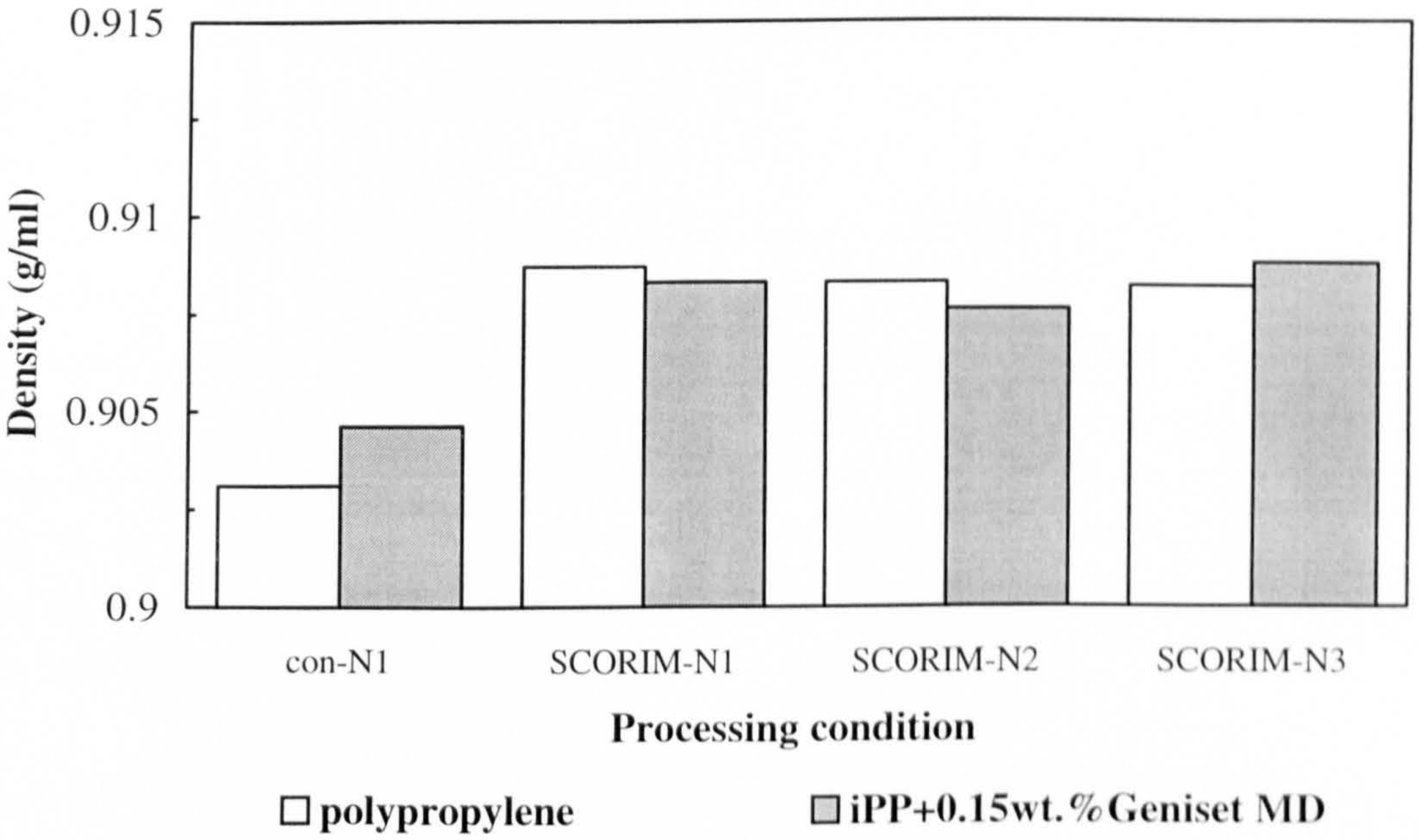

Figure 4.22 Density measuring results of injection mouldings of iPP with and without the addition of nucleating agents

(a) tensile bar conventional injection mouldings

(b) rectangular bar conventional and SCORIM mouldings

breaking stress was achieved by using SCORIM.

3) The density measurements revealed the density of conventional injection moulding of iPP was increased with increasing concentration of nucleating agents. The density of the SCORIM samples were greater than that of conventional injection moulding samples.

4) The x-ray scattering profiles of iPP with or without adding nucleating agents exhibited an increased intensity of $(117)_\gamma$ reflection, an increase in γ-phase index and the crystallinity index by using SCORIM. The crystallography of α, ß and γ phases was indexed by analysis of the WAXS Debye patterns. The SCORIM iPP mouldings exhibited a higher level of preferred orientation and showed the more pronounced arcing than conventional injection moulding.

5) The influence of nucleating agents in higher concentration on the crystallisation of iPP gave an effect of a lower concentration of the agents.

CHAPTER 5 DISCUSSION

5.1 Effect of Processing Parameters on the Micromorphology and Mechanical Properties of iPP

It is well known that microstructure is a dominant factor in determining the properties of materials. The micromorphology of injection moulded polypropylene can be controlled by the processing parameters, and in general it is determined by a contribution of materials formulation, molecular weight characteristics and compound composition, and processing conditions and in-cavity geometry. The mechanical properties of polypropylene are dependent on the morphology of the mouldings. In order to produce final plastic parts with required physical characteristics, it is essentially important to control and manipulate the processing procedure and formulation of the compound, thus optimising the performance properties of the injection moulded polypropylene. The research reported in this thesis explored the influences of composition, in essence a limited range of nucleating agents, and processing methods, namely conventional and SCORIM, and aspects of the micromorphology, dimensional control and the mechanical properties of a single grade of polypropylene.

5.1.1 Conventional Injection Moulded Standard Tensile Bar

In injection moulded polypropylene plastics, changes in moulding conditions such as melt temperature and injection speed can greatly influence the microstructure and consequently the mechanical properties of the end products. The experimental results obtained from conventional injection moulded standard tensile bars describe the basic investigation of the microstructure and mechanical properties of injection moulded polypropylene (grade GYM43).

The normal form of polypropylene which is crystallised from the melt develops through the growth of spherulites. A birefringent assemblage of crystals start usually from a heterogeneous nucleus and spread out in a spherical fashion until they fill practically the entire volume of the bulk crystallised polymer.

Optical light microscopy showed that all of the tensile bars moulded over the range of conditions displayed the typical skin-core morphology as characteristic of polypropylene. Figures 3.1(a,b) show the micrographs taken from the cross section

parallel to the melt flow direction of the tensile bar of conventional injection moulded iPP, which contained a very thin spherulitic structure skin, a birefringent row nucleated intermediate layer and a typically spherulitic core. The spherulites in the core region are randomly nucleated. The intermediate layer is not easily observed in the cross section because the birefringence of the row-nucleated spherulites viewed perpendicular to the cylindrical axes of the rows differs little from that of the spherulites in the core region. The appearance of the three zones in the gate region of the samples was used to investigate the micromorphology of the moulding, as this is a sensitive region within the moulding to the use of different processing temperatures and speeds.

An interesting feature apparent from the micrographs of the gate area is the inlet region immediately after the gate, and the width of the intermediate layer at the gate shoulders, both affected by the injection conditions. The injection speed control is achieved through a pre-set speed profile. The speed programme is provided by 10 speed command points for a given shot. The results expressed:

1) the mouldings produced at the same melt temperature, those produced under higher injection speed (60%) exhibited a larger inlet region immediately after the gate, and a greater width of the intermediate layer which achieved to increase Young's modulus and higher yield stress values. Kubat and Rigdahl reported that the stiffness of the mouldings increased up to a certain limit and decreased beyond this limit as the injection speed increased [143]. On the other hand the strain at peak and yield showed almost the same values for all processing conditions.

2) the greatest Young's modulus and lowest breaking stress values were obtained by using higher injection speed (60%) associated with lower melt temperature (200°C).

The results of mechanical testing conventional standard tensile bar samples of injection moulded iPP can be concluded as: the tensile properties of conventional injection moulded iPP were dependent on the processing parameters (melt temperature, injection speed) and the morphology of the mouldings. The lower the processing temperature and the higher the injection speed that were applied, the greater the Young's modulus and the lower breaking stress that obtained.

5.1.2 Conventional and Multiple Live-feed Injection Moulded Rings

Distinct differences in micromorphology, dimensions and mechanical characteristics occur with changes in injection moulding conditions. Changes in injection moulding technique may also result in different microstructures, dimensions and mechanical properties of moulded polypropylene. MLFM technique leads to an enhancement of the preferred orientation, strengthen internal weld lines and modify the micromorphology in injection moulded thermoplastics [74, 80, 82].

The MLFM ring mouldings were investigated to identify the improvements in uniformity of micromorphology and mechanical properties of injection moulded polypropylene. The MLFM ring mouldings exhibited a significant enhancement in tensile modulus and hoop fracture stress in comparison with conventional injection ring mouldings. The micrographs of the MLFM ring samples exhibited fibrous lamellar structure in the region near the gates, together with a wider width of the intermediate layer at the shoulders of the four gates (see Figures 3.3-3.5). This resulted in the MLFM-R1 ring samples exhibit 1.9 times greater tensile modulus and 17% increase in hoop fracture stress than that of conventional injection ring samples (see Figure 3.21). For the MLFM-R2 samples, the results show a 9.3% increase in tensile modulus and a 2.5% increase in hoop fracture stress.

The processing difference between MLFM-R1 and MLFM-R2 ring mouldings was the oscillating piston profiles (see Figure 2.2). In the case of the MLFM-R1, two pairs of pistons on the diagonal line (A and D, B and C) were moved down and up under the same compression and decompression pressures, and at the same frequency, but with a phase difference of 180°. The melt in the mould cavity was repetitively injected alternately from the packing chambers on the diagonal line at the same frequency. For the MLFM-R2, four pistons (A, D, B, C) were moved down and up under the same compression and decompression pressures at the same frequency and in phase. Under the MLFM-R2 processing, the melt in the mould cavity was compressed and decompressed by the four packing pistons at the same frequency.

The difference of the processing conditions effected the moulding roundness by

measuring the distortions of the ring mouldings. The ring mouldings produced using the MLFM injection processing exhibited less values of the maximum and minimum distortions from moulding roundness on the outside and inside dimensions than conventional injection ring mouldings. The MLFM-R2 ring sample exhibited the least distortion from moulding roundness than either MLFM-R1 or conventional samples. Comparison of the conventional ring sample and the MLFM-R2 sample, showed that the MLFM-R2 sample exhibited the better circumference which was

a 63.6% decrease in the value of the maximum distortion in the outside diameter,
a 60.6% decrease in the value of the maximum distortion in the inside diameter,
a 43.9% decrease in the value of the minimum distortion in the outside diameter and
a 58.1% decrease in the value of the minimum distortion in the inside diameter.

The MLFM-R1 ring sample exhibited lower value of the maximum difference of moulding flatness (68.6μm) than that of conventional ring samples (71.1μm). The ring samples produced by using the MLFM-R2 program exhibited higher deviation (79.8μm) from moulding flatness than either MLFM-R1 or conventional samples.

The measurements of surface straightness obtained from all the four surfaces consistently showed the advantages by using the MLFM programmes. Much higher deviations from surface straightness on the four surfaces were recorded from conventional injection mouldings especially on the outside and inside surfaces. This is attributed to the presence of macro-voids in the core region of all conventional ring samples. The lowest values of the maximum deviation were obtained on the top and bottom surfaces by the MLFM-R1 ring moulding, and on the outside and inside surfaces by the MLFM-R2 ring moulding. The lowest values of the minimum deviation were obtained on the outside and bottom surfaces by the MLFM-R1 ring moulding, and on the top and inside surfaces by the MLFM-R2 ring moulding.

The results of mechanical measurements exhibit that substantial enhancement in stiffness and internal weld line strength, and improvements in moulding dimensions, results from the action of MLFM processing. The processes lead to erase the internal weld line and provide the optimum circumferential alignment. The resultant uniformity of microstructure throughout the circumference of the ring also results in substantial dimension control.

5.1.3 SCORIM and Conventional Injection Moulded iPP Rectangular Bars

The microstructure and physical properties of injection moulded iPP can be significantly influenced by the application of the shear controlled orientation technique. The shear controlled orientation injection moulding (SCORIM) provided the preferred orientation on the microstructure by controlled shearing of the polypropylene melt in the mould cavity before and during solidification [75, 143]. A range of characterisation techniques have been used in the assessment of microstructure and physical property changes caused by the application of macroscopic shear during solidification.

Transmitted polarized light micrographs of the SCORIM rectangular bar mouldings showed the distribution of shear bands which is presented as lamellar rings on the cross sections perpendicular to the melt flow direction. The samples were taken 1mm away from the gate (as shown in Figure 3.7) and from the main part (Figures 3.8a,b,c) of the bar mouldings. The area near the gate was the more sensitive region within the whole moulding to different processing conditions (mould temperature, nozzle temperature, holding pressure and the piston operating modes).

The Young's modulus results indicated the significant increase in stiffness of the SCORIM bar mouldings (see Table 3.2) in comparison with the corresponding conventional injection moulding bars. The recorded Young's modulus also reflected the preferred orientation of the microstructure in all the SCORIM mouldings. The emanation of crystalline morphology from a central aggregate and the typical α-phase spherulite were observed in the TEM micrographs of the conventional-2C rectangular bar sample (see Figure 3.14).

For the SCORIM-1A, -1B and -1C samples produced under the same lower mould temperature (40°C) and nozzle temperature (215°C), the use of a lower hold pressure (40 bar) resulted in mouldings (SCORIM-1A) with greater Young's modulus of 2.63GPa (see Table 3.3 Group-1). The cavity pressure associated with the SCORIM-1A moulding was lower than that of the SCORIM-1B and the SCORIM-1C. When the melt was injected into the mould cavity under the lower mould temperature and lower cavity pressure, the melt was frozen rapidly especially

for the skin layer. This skin layer probably consists of chain extended materials typical of highly oriented melt. The mechanical testing results obtained from the layer removal procedures indicated that the greater modulus was provided by skin layer within the SCORIM-1A moulding (see Table 3.4b). The fibrous micromorphology exhibited in the cross section is attributed to the level of shear that polymer melt experience prior to freezing and resulted greater Young's modulus.

For the SCORIM-2A, -2B and -2C samples produced under the same higher mould temperature (80°C) and lower nozzle temperature (215°C), the use of a higher hold pressure (120 bar) resulted in mouldings (SCORIM-2C) with the greater Young's modulus of 3.81GPa (see Table 3.3 Group-2). The use of high mould temperature tends to cause sheared and oriented molecules before the completion of solidification. The melt flow capable of producing significant molecular chain uncoiling and extension by apply a macroscopic shear before and during solidification. The molecular extended melt is shock cooled on contacting the mould wall and substantially retains the orientation induced by the flow. The resulting fibrous lamellar structure obtained (see Figure 3.8b) possessed high tensile strength and exhibited greater Young's modulus and breaking stress.

For the SCORIM-1B, -2B and -3B samples, using the same hold pressure (80 bar), the use of a higher moulding temperature (80°C) and higher nozzle temperature (265°C) resulted in the mouldings (SCORIM-3B) with the greater Young's modulus of 3.97GPa (see Table 3.3 Group-3). Under the higher mould temperature and higher melt temperature, the molecular chain was sufficient mobile and the force between molecular chains was decreased. The higher temperature processing causes the solidifying melt to undergo shear, and induces effectively fibrous alignment by applying oscillating pressure and results in enhancing the Young's modulus of the mouldings.

The SCORIM polypropylene parts have a complex skin-core morphology, consisting generally of a highly oriented fine structure skin, a lamellar shear-nucleated intermediate layer and a spherulitic core. The thickness of the oriented skin is a function of the polymer melt temperature and varies inversely with temperature. The thickness of the intermediate layer varies with injection pressure but in a complex manner. Preferred orientation in the skin and intermediate layer

exert profound effects on mechanical properties. The mechanical testing results obtained from the layer removal procedures provided the data necessary for estimation of the moduli in different regions within mouldings and delineated by different microstructures. The skin layer exhibits a much higher modulus. Both sub-skin layer and the shear layer can also provide some contribution to the modulus of the moulding. The modulus of the core region shows the lowest value within the moulding. So the higher modulus of the mouldings, the wider width of the skin layer and the smaller region of the core.

The SCORIM-2CM1 and SCORIM-2CM2 programmes were modified from the SCORIM-2C program according to the layer removal procedure. The results indicated that the use of different SCORIM processing programmes for the same mould temperature and nozzle temperature resulted in different microstructures (see Figure 3.9). The mouldings produced using SCORIM-2CM1 and SCORIM-2CM2 programmes related to different oscillating packing options which were principally differences in applying higher shearing pressure in the mould cavity. The shish-kebab structure was observed within the skin, sub-skin and in the intermediate layer which was shown in the TEM micrographs (as shown in Figures 3.10 and 3.11). The shear controlled orientation processing provided a mixture c-axis and a*-axis orientation to the melt flow direction, and enhanced alignment of the molecular chains in the microstructure of SCORIM-2CM1 and SCORIM-2CM2 samples. This leads to exhibition the greatest Young's modulus and breaking stress in the mouldings (see Table 3.3 Group-4).

The mechanical results of the SCORIM rectangular bar samples of injection moulded iPP can be concluded as:

1) the injection moulded iPP exhibits substantial structural heterogeneity along the melt flow direction which is particularly dependent on the processing temperatures and holding pressure used during injection moulding process. The micromorphology is sensitive to processing conditions and moulding techniques.

2) the Young's modulus dependence upon processing temperatures and pressure. The following observations were made with reference to Table 3.3 which summarises the holding pressure, melt temperature and mould temperature for a range of the SCORIM mouldings:

a) when the lower mould temperature (40°C) associated with the lower melt

temperature (215°C) were applied, the lower holding pressure (40bar) exhibited the greater Young's modulus.

b) when the higher mould temperature (80°C) associated with the lower melt temperature (215°C) were applied, the higher holding pressure (120bar) caused the greater Young's modulus.

c) when the medium holding pressure (80bar) was applied, the higher mould temperature (80°C) and the higher melt temperature (265°C) combined resulted in the greater Young's modulus.

The mechanical properties of the mouldings are dependent on the processing conditions. The shear controlled orientation injection process can displace sufficient molten material within the mould to create a macroscopic shearing and enhance fibrous alignment of the melt. It is believed that by careful application of the SCORIM processing conditions, the physical properties of moulded materials could be controlled in such a way that their performance would be increased to suit the requirements of the artefact.

5.1.4 Effect of Nucleating Agents on the Micromorphology and Mechanical Properties of Injection Moulded iPP

The microstructure and mechanical properties can be manipulated using different processing conditions, and encourages further optimisation of the injection moulding process by changes in the SCORIM processing programmes and compounds. The addition of nucleating agents to polymers has been widely practised in the plastics fabrication not only for the improvement in impact properties and optical clarity [129, 130], but also for the shortening of cycle times in conventional injection moulding processes [131, 57]. However, the relationship between the physical characteristics of nucleating agents and the SCORIM processing conditions has not been investigated, and may provide for new possibilities in microstructure control.

The fine spherulitic structures of tensile bar conventional injection mouldings of iPP with the addition of nucleating agents are remarkable in the transmitted polarized light micrographs. As seen in the Figure 4.2, the fineness of the morphological detail in the sample containing 0.3wt.% of Geniset MD is finer than that of the sample containing 0.3wt.% of ADK STAB. Under the same concentration, Geniset

MD is more effective in nucleation activity than ADK STAB. The mechanical results revealed that the effect of increasing Young's modulus of iPP+0.3wt.% Geniset MD samples were stronger than that of iPP+0.3wt.% ADK STAB samples (see Table 4.2). The mechanical results summarised in Table 4.2.

Figures 4.4 and 4.5 show the effect of Geniset MD and ADK STAB nucleated-iPP of tensile bar conventional injection moulding samples on tensile properties. The trend of the correlation is as would be expected and shows that in all cases the addition of nucleating agents produces significantly enhancement of the Young's modulus and the tensile stresses (yield stress, peak stress and breaking stress). On the other hand tensile strains (yield strain, peak strain and breaking strain) decrease with an increase the concentration of the nucleating contents. The mechanical characteristics of nucleated-polypropylene have been found to increase with the increase drastically in the concentration up to 0.3wt.% of nucleating agents. Mitra and Misra attributed the decrease in the nucleation effect in the high concentration of the nucleating agent might form agglomerates to give an effect of low concentration of the agent [137]. Young and his colleagues' work also gained the results of the decrease in the nucleation effect in the high concentration of the nucleating agent was due to decrease number of nuclei by agglomeration [138].

The observed density obtained from the Tecam density column showed that the density of the tensile bar conventional injection moulded iPP samples increased with increasing concentration of both Geniset and ADK nucleating agents (see Figure 4.22a). In the mechanical measurements, Young's modulus and tensile stresses were increased with increasing concentration of the two nucleating agents. The nucleating agents produced the effect in injection moulded iPP to increase the number of the nuclei and decrease the dimensions of spherulites.

Polypropylene crystallisation begins at crystallisation sites. Nucleators increase the number of crystallisation sites in a polymer, resulting in an increase in the overall crystallisation rate and a decrease in the spherulite size [58]. Smith et al. found the enhanced crystallisation rate also results in intercrystalline links. Intercrystalline links are bridges between and within spherulites generated by one polypropylene chain that has one segment crystallised in one spherulite and another segment crystallised in another spherulite or another part of the same spherulite. Thus, one polypropylene chain can "link" two spherulites together. Nucleators, through

intercrystalline links and smaller spherulites, improve the impact strength, tensile elasticity modulus, tensile strength and clarity of polypropylene [59].

For the rectangular bar mouldings of iPP with the addition of nucleating agents, the lamellar morphology resulting from high levels of chain extension was found to relate with the SCORIM processing programmes and shearing pressure applied corresponding with the mechanical properties. It is evident from the results presented that the microstructure can have a profound effect upon Young's modulus of the SCORIM polypropylene mouldings. The mechanical properties have also been shown to depend on the processing conditions and resultant micromorphology.

5.2 Effect of Processing Parameters on the Mechanical Properties and Crystalline Polymorphism of Injection Moulded iPP

Polymorphism is a pronounced effect in crystalline isotactic polypropylene. It is well known that isotactic polypropylene can crystallise into more than one crystallographic form (α, ß or γ) and that these are incorporated into spherulites of different type [144] depending on the cooling rate and the level of stress and pressure during crystallisation. The monoclinic α modification was characterised by Natta and Corradini [24]. The hexagonal ß and triclinic γ forms have been described by Turner-Jones [116] and by Samuels and Yee [145].

The crystalline regions are normally folded-chain lamellas, whereas the non-crystalline regions are composed of crystal fold surfaces, tie molecules, impurities and uncrystallisable additives. Normally the crystalline and non-crystalline regions associate into larger, ordered arrangements such as spherulites or fibrils [127]. The morphology of melt crystallised polymers is known to depend on the processing conditions.

5.2.1 Conventional Injection Moulded Standard Tensile Bar

The α-phase orientation index A, ß-phase index B and crystallinity index C were calculated from the corresponding peak heights in the x-ray diffraction profiles. The results of A, B and C indices of the standard tensile bar conventional injection

moulded iPP are shown in Table 3.5.

In the mechanical tests, Young's modulus was measured in the 10mm gauge length in the main part of the tensile bar conventional injection mouldings. The position of the 8/10 length of the flow path was in the tensile testing range of the sample. The greater Young's modulus and yield stress in the conventional injection moulding bars were obtained by using higher injection speed (60%), where the mouldings exhibited the higher α-phase index, higher crystallinity index, and lower ß-phase index. The conventional injection moulding bars produced by using lower melting temperature (200°C) and lower injection speed (15%) resulted in the highest breaking stress associated with the lowest α-phase index A, lower crystallinity index C and a relatively high ß-phase index B.

The x-ray diffraction profiles of standard bar conventional injection mouldings at the 8/10 length of the flow path exhibited higher ß-phase concentration associated with high injection speed. Murphy reported the extent of ß spherulite nucleation was high in polypropylene mouldings and reflected the poor impact properties [146].

The following results can be concluded for the conventional injection moulded iPP:
1) when the mouldings produced by using same melting temperature, the changing of injection speed can be effected to the α-phase orientation index A and ß-phase index B. Young's modulus depends essentially on the changing of α- and ß-phase index.

2) the higher injection speed (60%) was used in the conventional injection moulding bars, the higher α-phase orientation index and the lower ß-phase index exhibited, the greater Young's modulus was obtained.

5.2.2 MLFM and Conventional Injection Moulded iPP Rings

From the wide angle x-ray scattering profiles of MLFM and conventional injection ring mouldings, α-phase orientation index A, ß-phase index B, γ-phase index G, crystallinity index C and percentage γ-phase (γ%) were calculated and shown in Table 3.6. Generally, the values of A, B, G, C indices and γ% of the MLFM ring samples at each gate and weld line regions were all greater than that of conventional injection ring samples (see Figure 3.27). There were no γ-phase reflections present

in x-ray scattering profiles gained from any region of conventional injection ring moulding. This is the major difference between MLFM and conventional injection ring mouldings. In the mechanical behaviour, the values of tensile modulus and hoop fracture stress of the MLFM ring mouldings were greater than that of conventional injection ring mouldings (see Figures 3.21).

Comparing the injection conditions used for the ring mouldings, the average cavity pressure and holding pressure time of the MLFM ring mouldings were two or three times higher than that of conventional injection ring mouldings. The average cavity pressure and holding pressure time set in the machine for ring mouldings are shown as follow:

Processing	Conventional	MLFM-R1	MLFM-R2
Cavity pressure (bar)	425	911	956
Hold pressure time(sec)	80	300	150

During the MLFM injection processing, high shear forces were applied to the melt in the mould cavity by oscillating pressure to enhance the alignment of the molecular chains. The high shearing pressure and longer holding pressure time applied on the MLFM mouldings resulted the greater γ-phase index G and γ%. Lotz and Morrow reported the fact that γ-iPP is obtained by high pressure and slow cooling, and the reduced importance of chain folding [35, 147].

Comparing the injection processing conditions set for the ring mouldings, the higher average cavity pressure and longest holding pressure were applied on the MLFM-R1 ring mouldings. For the MLFM ring samples, the higher oscillating pressure applied in the mould cavity could cause the increasing γ% and decreasing the chains folding. The values of ß-phase index B of the MLFM-R1 ring sample were smaller than that of the MLFM-R2 ring sample with the corresponding regions. In comparison with conventional ring samples, the MLFM-R1 ring samples exhibited a significant enhancement in mechanical characteristics than the MLFM-R2 ring samples (see Figures 3.21). The average tensile modulus value of the MLFM-R1 ring samples is 1.9 times greater than that measured from conventional injection ring mouldings, and a 9.3% increase in the MLFM-R2 ring samples. The average hoop fracture stress was 17% increase in the MLFM-R1 ring mouldings and 2.5% increase in the MLFM-R2 ring mouldings in comparison with the conventional

injection ring mouldings.

The conclusion for the MLFM and conventional injection ring mouldings are:
1) The higher shearing pressure and the longer holding pressure time applied in MLFM, the greater γ% and γ-phase index G obtained, and reduced the chains folding in the micromorphology.
2) The greater A, C, G indices and γ% resulted in enhancement tensile modulus in the MLFM ring mouldings through the β-phase index B was relatively increased.

5.2.3 SCORIM and Conventional Injection Moulded iPP Rectangular Bar Mouldings

In comparison with the conventional-2C rectangular bar sample, the x-ray scattering profile from the SCORIM-2C sample exhibited greater intensity of γ-phase $(117)_\gamma$ peak and much weaker intensity of α-phase $(111)_\alpha$ and $(041)_\alpha$ peaks (see Figure 3.28). Table 3.7 shows the results of α-phase orientation index A, ß-phase index B, γ-phase index G, crystallinity index C and percentage γ-phase (γ%) of the SCORIM-2C and conventional-2C samples. The values of A, B, G, C indices and γ% of the SCORIM-2C bar sample were all greater than that of conventional-2C sample.

The higher shearing pressure applied in the SCORIM-2C mouldings, the higher intensity of γ-phase and the less degree of the chain folding. The effect of increasing concentrations of α-phase and γ-phase led to increase the preferred orientation and reduce the chain folding, and relate to enhancement of Young's modulus and breaking stress in the SCORIM-2C rectangular bar mouldings in comparison with conventional-2C bar mouldings, though the ß-phase index B slightly increased.

5.2.4 SCORIM and Conventional Injection Moulding of iPP with the Addition of Nucleating Agents

5.2.4.1 Effect of Processing Parameters on the Mechanical Properties of Injection Moulded iPP with the Addition of Nucleating Agents

For the standard tensile bar conventional injection mouldings, both Geniset MD nucleated-iPP and ADK STAB-nucleated iPP samples exhibited a similar manner in

mechanical measurements. The Young's modulus and tensile stresses (yield stress, peak stress and breaking stress) were all found to increase gradually with increasing concentration of nucleating agents (see Figures 4.4a,b and 4.5a,b). On the other hand the strain to break of standard tensile bar conventional injection mouldings falls rapidly at first and then slowly with increasing concentration of nucleating agents (see Figures 4.4c and 4.5c). The change in yield strain and peak strain were less marked with increasing concentration of the nucleating agents.

Comparison of the effects of nucleating agents in conventional injection moulded iPP, the Young's modulus of iPP with the addition of ADK STAB exhibited a greater increase than that of iPP with the same concentration of Geniset MD when the concentration of nucleating agent was up to 0.2wt.%, and a less increase when the concentration of nucleating agent was higher than 0.3wt.%.

For the rectangular bar conventional injection mouldings, both iPP without and with the addition of 0.15wt.% Geniset MD samples also behave in a similar manner in tensile testing. The nozzle temperature of conventional-N1 (230°C) was lower than that of conventional-N2 (280°C). The mould temperature of conventional-N1 and -N2 were the same (70°C). The holding pressure time of conventional-N1 (66.5sec) was shorter than for conventional-N2 (96.5sec). The tensile stresses (yield, peak and breaking) decreased when a higher Young's modulus was achieved following the application of the longer holding pressure time and a higher melt temperature. Conversely, the Young's modulus decreased when the higher tensile strength was achieved following the shorter holding pressure time and a lower melt temperature. The addition of 0.15wt.% Geniset MD nucleating agent does not cause a significant change in the mechanical behaviour of the rectangular bar conventional injection moulded iPP.

In comparison with the rectangular bar conventional injection mouldings, both SCORIM iPP without and with the addition of 0.15wt.% Geniset MD samples exhibited a significant increase in Young's modulus and tensile strength. An increase of 2.54 times in Young's modulus occurs as a consequence of polypropylene SCORIM-1N1 processing, and 1.68 times in iPP with the addition of 0.15wt.% Geniset MD SCORIM-2N3 processing.

For the SCORIM-1N mouldings of polypropylene, the highest Young's modulus

(3.91GPa) is achieved for the SCORIM-1N1 sample. The SCORIM-1N1 was produced with the lowest melt temperature (220°C) and mould temperature (30°C). This represents a greater than two-fold increase in Young's modulus and gives the highest stiffness for polypropylene within the SCORIM-1N group. In comparison with the SCORIM-1N1 mouldings, the SCORIM-1N2 and SCORIM-1N3 mouldings produced by using the higher mould temperature (70°C) and the SCORIM-1N4 mouldings produced by using the higher melt temperature (280°C) were all presented the lower Young's modulus than the SCORIM-1N1 mouldings. The SCORIM-1N4 process produced the lowest Young's modulus (2.35GPa), in comparison with the other SCORIM-1N mouldings.

The tensile results for the SCORIM-2N mouldings produced from iPP with the addition of 0.15wt.% Geniset MD nucleating agent exhibit a different behaviour. The highest Young's modulus (2.98GPa) is achieved for the SCORIM-2N3 which has a higher mould temperature (70°C) and the shortest holding pressure time (66.5sec) within the SCORIM-2N group. The SCORIM-2N2 and SCORIM-2N4 exhibit slightly lower Young's modulus than the SCORIM-2N3. The SCORIM-2N1 mouldings exhibits the lowest Young's modulus (2.42GPa) which associated with the lowest melt temperature (220°C) and mould temperature (30°C) in comparison with the other SCORIM-2N mouldings. The SCORIM-2N2 and SCORIM-2N3 mouldings produced by using the higher mould temperature (70°C) and the SCORIM-2N4 mouldings produced by using the higher melt temperature (280°C) were all presented the higher Young's modulus than the SCORIM-2N1 mouldings.

The SCORIM-N4 profiles (SCORIM-1N4 and SCORIM-2N4), which result in twice the cavity pressure that is achieved with the SCORIM-N1 profiles (SCORIM-1N1 and SCORIM-2N1), also lead to the lowest tensile strength for both iPP without and with the addition of 0.15wt.% Geniset MD mouldings. The holding pressure time for the SCORIM-N4 profiles is the longest (135.0sec) and the melt temperature is the highest (280°C) within the SCORIM. The two stages for the SCORIM-N4 profiles have a very long duration, during which very high cavity pressures are achieved. A very high percentage of γ-phase and a lower overall crystallinity were recorded for the SCORIM-N4 profile mouldings, in comparison with the other SCORIM mouldings. Therefore degradation of the tensile strength of the mouldings may have occurred. There is an increase of 55.4% in yield stress, 15.2% in peak stress and 18.6% in breaking stress with the application of the

SCORIM-1N3 profiles in comparison with the SCORIM-1N4 profiles. At the same case, an increase of 88.4% in yield stress, 12.2% in peak stress and 8.2% in breaking stress with the application of the SCORIM-2N3 profiles in comparison with the SCORIM-2N4 profiles.

5.2.4.2 Effect of Processing Parameters on the Crystalline Polymorphism of Injection Moulded iPP with the Addition of Nucleating Agents

For the standard tensile bar conventional injection mouldings, the x-ray scattering profiles of 2θ angle *vs.* peak intensity of crystal phase are shown in Figures 4.6 and 4.7. For Geniset nucleated-iPP mouldings (see Figure 4.6), the intensities of $(111)_\alpha$ and $(041)_\alpha$ peaks were decreased with the higher concentration of Geniset MD nucleating agent. The x-ray scattering profiles exhibited the peaks of $(300)_\beta$ and $(117)_\gamma$ in the concentration of 0.15wt.% and 2wt.% Geniset MD. For the conventional injection mouldings of ADK nucleated-iPP (Figure 4.7), the x-ray profiles showed a significant increased intensity for $(040)_\alpha$ peak and decreased intensity for $(111)_\alpha$ and $(041)_\alpha$ peaks. The peaks of $(300)_\beta$ and $(117)_\gamma$ were only found in the x-ray scattering profile of iPP+2wt.% ADK. Tables 4.4 and 4.5 summarise the measurements of 2θ angles. d-spacing, d*, relative intensities of the diffraction peaks, crystal phase and the Miller indices associated with the reflection recorded from Geniset MD nucleated-iPP and ADK STAB nucleated-iPP samples, respectively.

For the rectangular bar conventional and SCORIM mouldings of iPP without and with the addition of nucleating agents, Figures 4.8, 4.9, and 4.10 show the x-ray scattering profiles of 2θ angle *vs.* peak intensity of crystal phase.

Con-1N1 and con-1N2 exhibit γ-phase (117) reflection. The $(117)_\gamma$ peak for con-1N2 is more intense than the $(117)_\gamma$ peak for con-1N1. While con-1N1 exhibits a β-phase (300) reflection which the con-1N2 mouldings do not exhibit any β-phase peaks. Another important difference between con-1N1 and con-1N2 is the intensity of the doublet which comprises $(111)_\alpha$ and $(041)_\alpha$ reflections. Con-1N2 shows the higher intensity for $(111)_\alpha$+$(041)_\alpha$ peaks than con-1N1. Con-2N1 and con-2N2 exhibit a similar behaviour as con-1N1 and con-1N2. Both exhibit a $(117)_\gamma$

reflection but this reflection is more intense for con-2N1 than for con-2N2. A (300) β-phase reflection is observed for con-2N1 but it is not observed for con-2N2. Again the intensity of $(111)_\alpha$+$(041)_\alpha$ peaks is more intense for con-2N2 than for con-2N1.

The SCORIM-1N mouldings of iPP without adding of nucleating agents exhibit two γ-phase peaks which correspond to $(113)_\gamma$ and $(117)_\gamma$. The intensity of the $(111)_\alpha$ +$(041)_\alpha$ peaks is more pronounced for the SCORIM-1N4 than the other three SCORIM-1N mouldings (SCORIM-1N1, -1N2 and -1N3). All of the four SCORIM-1N mouldings, only the SCORIM-1N2 exhibits a (300) β-phase reflection.

As with the SCORIM-1N mouldings, all the SCORIM-2N mouldings exhibit $(113)_\gamma$ and $(117)_\gamma$ reflections. The intensity of the $(111)_\alpha$+$(041)_\alpha$ peaks is higher for the SCORIM-2N4 than the other three SCORIM-2N mouldings (SCORIM-2N1, -2N2 and -2N3). The SCORIM-2N1 shows a weak reflection at 2θ angle of 28.24°, corresponding to a d-spacing of 3.156Å, which appears as a shoulder on the $(220)_\alpha$ peak. This reflection may be identified as $(411)_\beta$. The SCORIM-2N3 mouldings exhibit a $(200)_\alpha$ reflection at 2θ angle of 27.10° whereas this reflection is not present in the conventional injection mouldings. The main characteristic of the SCORIM-2N mouldings is the presence of more $(300)_\beta$ reflection. Only the SCORIM-2N4 does not show this reflection. The presence of more β-phase in the SCORIM-2N mouldings than the SCORIM-1N mouldings may be attributed to the Geniset MD nucleating agent.

5.2.4.3 Effect of Processing Parameters on the Mechanical Properties and Crystalline Polymorphism of Injection Moulded iPP with the Addition of Nucleating Agents

The α-phase orientation index A, β-phase index B, γ-phase index G, crystallinity index C and the percentage γ were calculated for all conventional and SCORIM mouldings of iPP without and with the addition of nucleating agents. All of the results are shown in Tables 4.6 and 4.9. The relative orientations of the section of the mouldings used for WAXS Debye patterns and x-ray diffractometry were the same for all samples, thereby providing for the standardisation of the technique for

mouldings exhibiting different texture and anisotropy of physical properties.

For the standard tensile bar conventional injection mouldings of Geniset MD nucleated-iPP and ADK STAB nucleated-iPP, the results of A, B, C, G indices and γ% were calculated and shown in Table 4.6.

The values of α-phase orientation index A increased with increasing concentration of Geniset MD nucleating agent. The ß-phase index B was zero when the concentration of Geniset MD nucleating agent did not exceed 0.3wt.%. In the mechanical measurements, the values of Young's modulus and tensile stresses of the tensile bar conventional injection mouldings were found (see Figure 4.4a,b) to increase gradually with increasing concentration of Geniset MD nucleating agent. The x-ray scattering profile of iPP with the addition of 0.15wt.% and 2wt.% Geniset MD samples exhibited ß and γ-phase reflections.

The A, B, C, G indices and γ% of ADK STAB nucleated-iPP showed the similar results to Geniset MD nucleated-iPP in Table 4.6c. The values of α-phase orientation index A increased with increasing the concentration of ADK nucleating agent. In mechanical testing, the values of Young's modulus and tensile stresses were increased progressively with increasing concentration of ADK nucleating agent (see Figure 4.5). The ß and γ-phase reflections were only found in the x-ray scattering profile of iPP with the addition of 2wt.% ADK.

From the above observation, the results of standard tensile bar conventional injection moulded iPP can be concluded:
(1) the increase of concentration of nucleating agent was linked to the increase in α-phase orientation index A and resulted in the increase Young's modulus and tensile strength.

(2) when the concentration of nucleating agent was up to 0.3wt.%, significant increases in α-phase index A and Young's modulus and tensile stresses are noted for increasing the concentration of nucleating agent.

(3) the high concentration of nucleating agent has less effect on increasing Young's modulus and tensile stresses. The decrease in the nucleation effect in the high concentration of the nucleating agent might form agglomerates to give an effect of

low concentration of the nucleating agent.

(4) the γ and ß-form reflections were found in the x-ray scattering profiles of high concentration nucleated-iPP mouldings.

(5) the increase of α-phase results in increasing the orientation structure. The appearance of γ-phase leads to extentsion molecular chains. The production of row nucleated ß-phase structure causes a reduction in the strength of mouldings.

For the rectangular bar conventional and SCORIM mouldings of iPP without and with the addition of 0.15wt.% Geniset MD, the results of A, B, C, G indices and γ% were calculated and shown in Table 4.9. The crystallinities of each sample were also calculated.

For the rectangular bar mouldings of both iPP without and with the addition of nucleating agents, the SCORIM mouldings exhibited considerably higher α-phase orientation indices, higher intensity of γ-phase and presented greater γ% and γ-phase index G in comparison with conventional injection mouldings. The crystallinity indices and the crystallinities of all the SCORIM mouldings are also higher than those of the conventional injection mouldings. The β-phase indices of the mouldings con-1N2, con-2N2, SCORIM-1N1, SCORIM-1N3, SCORIM-1N4 and SCORIM-2N4 are all zero. These results are consistent with the differences in the Young's modulus of the mouldings.

The results concerning γ-phase firms the association of γ-phase with the chain extended morphology. During the SCORIM process, high shear pressure applied to the melt in the mould cavity to create the high alignment of the molecular chains and reduce the chain folding. The γ% for the mouldings are also consistent with the γ-phase indices. Both the SCORIM-1N and SCORIM-2N mouldings exhibit a high proportion of γ-phase as evident from the γ-phase indices. The values of γ% for the SCORIM mouldings (SCORIM-1N and SCORIM-2N) are two or three times higher than that of conventional injection mouldings (con-1N and con-2N) of the corresponding groups. The γ-phase in injection mouldings can be seen as a sign of enhanced mechanical properties, through since it is also associated with low molecular weight polypropylene, as a single parameter it does not have too much of a significance. However the presence of a high γ-phase content is certainly

consistent with high molecular alignment and consequently high mechanical performance compared with the injection mouldings that do not exhibit a pronounced degradation.

The con-N1 mouldings produced by lower nozzle temperature (230°C) and shorter holding pressure time (66.5sec) in comparison with con-N2 mouldings (280°C/96.5sec). Con-1N1 and con-2N1 mouldings exhibit ß-phase which is identified by the ß-phase indices. The ß-phase index B of con-1N2 and -2N2 samples was zero, both mouldings did not show the ß-phase (300) reflection in the x-ray diffraction profiles (see Figures 4.8 and 4.9). The con-1N2 and con-2N2 samples exhibited greater Young's modulus than con-1N1 and con-2N1, respectively (see Table 4.3). Murphy's work had been carried on the investigation into the impact properties of the same grade of polypropylene. The research reported the extent of ß spherulite nucleation was low and resulted in good impact strength [146].

In the SCORIM-1N group samples, the $(300)_{\beta}$ reflection was only observed in the x-ray profile of the SCORIM-1N2 sample. The SCORIM-1N1 has the greatest Young's modulus of the SCORIM-1N mouldings (see Table 4.3a), which is consistent with the highest α-phase index and higher crystallinity, although γ-phase index is relatively low compared with that of the SCORIM-1N2, -1N3 and -1N4 mouldings (see Table 4.9a).

Comparison of the SCORIM-1N1 and -1N2 samples, produced under the same cavity pressure, the melting temperature and mould temperature of the SCORIM-1N1 sample (220°C/30°C) were lower than that of the SCORIM-1N2 sample (230°C/70°C). There was no ß-phase reflection in x-ray diffraction profile of the SCORIM-1N1 sample. The lower processing temperature of the SCORIM-1N1 sample exhibited the higher α-phase index A and lower γ% associated with the greater Young's modulus than the SCORIM-1N2 sample.

Comparison of the SCORIM-1N2 and -1N3 samples, produced under the same melt temperature and mould temperature, and the cavity pressure of the SCORIM-1N3 sample (1,602bar) was lower than that of the SCORIM-1N2 sample (1,678bar). There was no ß-phase reflection in x-ray diffraction profile of the SCORIM-1N3 sample. The lower processing pressure of the SCORIM-1N3 moulding exhibited the

higher α-phase index A and relatively lower γ% associated with the greater Young's modulus than the SCORIM-1N2 sample.

The SCORIM-1N4 has the lowest Young's modulus of the SCORIM-1N mouldings and this is also consistent with its lowest α-phase index and crystallinity. The SCORIM-1N4 sample was subjected to the highest cavity pressure and melting temperature within the SCORIM-1N group and resulted in the greatest γ% and γ-phase index G recorded within the SCORIM-1N group.

After adding 0.15wt.% Geniset MD nucleating agent to the GYM43 iPP, the group of SCORIM-2N samples exhibited differences in x-ray diffraction profiles in comparison with the corresponding processing of the SCORIM-1N samples. The SCORIM-2N1, -2N2 and -2N3 all exhibited pronounced ß-phase in their x-ray scattering profiles and resulted the changing in Young's modulus.

In the SCORIM-2N group, the greatest Young's modulus was obtained for the SCORIM-2N3 mouldings (see Table 4.3b), which exhibited the highest α-phase orientation index, the highest crystallinity and a relatively high γ-phase index (see Table 4.9b).

In comparison with the SCORIM-2N3 sample, the SCORIM-2N1 sample was produced at lower melting temperature, lower mould temperature and higher cavity pressure (220°C/30°C/1,939bar) than that of the SCORIM-2N3 sample (230°C/70°C/1,884bar). The lower processing temperature and the higher cavity pressure of Geniset MD nucleated SCORIM-2N1 sample exhibited a lower α-phase orientation index, a lower crystallinity, a higher γ-phase index and higher β-phase index, and all are associated with a lower Young's modulus.

Comparison of the SCORIM-2N2 and -2N3 samples, produced under the same melt temperature and mould temperature, the cavity pressure of the SCORIM-2N2 sample (1,950bar) was higher than that for the SCORIM-2N3 sample (1,884bar). The higher processing pressure of Geniset MD nucleated SCORIM-2N2 sample exhibited a lower α-phase index, a lower crystallinity, a relatively greater γ-phase index and higher ß-phase index associated with the lower Young's modulus.

The SCORIM-2N4 samples exhibited the lowest Young's modulus in the SCORIM-

2N group samples, consistent with the lowest value of α-phase index. The SCORIM-2N4 moulding was associated with the highest cavity pressure and melting temperature in the SCORIM-2N group samples. This condition resulted in the greatest γ% and γ-phase index G within the SCORIM-2N group samples.

For the rectangular bar moulding of iPP without and with adding nucleating agents, the x-ray diffraction and related mechanical properties can be summarised as:

1) the SCORIM mouldings exhibited a significant increase in Young's modulus and tensile strength in comparison with the conventional injection mouldings. An increase of 2.54 times in Young's modulus occurs as a consequence of polypropylene SCORIM process, and 1.68 times in iPP with the addition of 0.15wt.% Geniset MD SCORIM process.

2) the SCORIM mouldings exhibited considerably higher α-phase orientation indices, higher intensity of γ-phase and presented greater γ% and γ-phase index G in comparison with conventional injection mouldings. The crystallinity indices and the crystallinities of all the SCORIM mouldings are also higher than those of the conventional injection mouldings.

3) α-phase index was the main fraction for Young's modulus. The higher α-phase index was related to the higher Young's modulus of the moulding. The ß-phase index had little effect on the stiffness of the moulding.
a) when the same melt and mould temperatures were applied, the lower cavity pressure obtained resulted in the higher α-phase index, higher crystallinity and lower ß-phase index associated with higher Young's modulus.
b) when the same cavity pressure was obtained, the lower melt and mould temperatures applied resulted in the higher α-phase index and lower ß-phase index associated with higher Young's modulus.

4) During the shear control orientation injection moulding processing, the high shear pressure was applied to the mould cavity. The higher cavity pressure resulted in an increase in γ% and γ-phase index.

5) all of the parameters are interdependent, and also clearly indicates the complex relationship between the mechanical properties and the occurrence of specific

crystalline phases.

5.3 Thermal Analysis of iPP with the Addition of Nucleating Agents by Differential Scanning Calorimetry

For both SCORIM and conventional injection mouldings produced from iPP without and with the addition of nucleating agents, the DSC scans were obtained by heating to 250°C at a rate of 10°C/min, holding for 1 min, slowly cooling at 10°C/min to 50°C and then reheating. The observed melting temperature and heat of fusion were obtained from the DSC melting thermograms by reheating the samples at a rate of 10°C/min.

During heating, crystallites formed from chains of short iPP sequences will melt and those with longer sequences can recrystallise to form more perfect thick crystallites. The extent of this "morphological rearrangement" will be very dependent upon the heating rate. Only at slow rates will there be enough time for crystallites to be developed which are sufficiently perfect to be stable [117]. As the temperature drops, the longest iPP sequences crystallised first, with progressively shorter sequences effected a fractionation on a chain structure basis which was reflected in the melt distribution on reheating.

For the tensile bar conventional injection moulding of iPP with the addition of both Geniset MD and ADK STAB nucleating agents, the melting temperatures ranges were changed with increasing concentration of the nucleating agents. The widest melting ranges of iPP injection mouldings obtained were 0.15wt.% Geniset MD nucleated-iPP and 0.2wt.% ADK nucleated-iPP (see Table 4.10). The wide melting ranges observed after slow cooling exhibited a wide distribution of iPP sequence lengths. After slow cooling, crystallisation at different temperatures give rise to crystallites of different thickness and perfection and hence different melting points. The higher melting peak related to that some chains of very long iPP sequences. The highest melting peaks of iPP injection mouldings obtained were 0.1wt.% Geniset MD nucleated-iPP and 2wt.% ADK nucleated-iPP.

The heat of fusion ΔH and the degree of crystallinity of iPP with the addition of nucleating agents samples were increased to a limiting value with lower

concentration of nucleating agents, and then reduce with higher concentrations of nucleating agents. The size and melt distribution of endothermic curves appropriately reflect the proportion and degree of modification of the amorphous morphology present. The degree of modification of amorphous morphology depended on the different concentrations of the different nucleating agents. As the results for the tensile bar conventional injection moulding, the greatest degree of crystallinity of Geniset MD nucleated-iPP was obtained by using 0.3wt.% concentration and the greatest degree of crystallinity of ADK STAB nucleated-iPP was obtained by using 0.2wt.% concentration. The degree of crystallinity of iPP conventional injection mouldings were all increased with lower concentration of both Geniset MD and ADK nucleating agents and reduced with higher concentration of nucleating agents (see Figure 4.18).

For the rectangular bar conventional injection moulding, the melting temperature (T_m) of endotherm and the peak temperature ($T_{m,p}$) of endotherm of 0.15wt.% Geniset MD nucleated-iPP samples were higher than that of iPP without adding nucleating agent (see Table 4.11). The higher melting peak temperature is associated with the longer iPP sequences of the molecular chains. The observation of transmitted light microscopy confirmed the finer morphology in the Geniset MD nucleated-iPP conventional injection mouldings. On the other hand, the temperature ΔT_m of the endothermic peak, the heat of fusion ΔH and the degree of crystallinity of 0.15wt.% Geniset MD nucleated-iPP conventional injection mouldings were greater than that of iPP without adding nucleating agent (see Table 4.11). Thus after adding 0.15wt.% Geniset nucleating agent, the iPP conventional injection mouldings exhibited a wider distribution of iPP sequence lengths. The proportion of amorphous morphology of conventional moulded iPP was decreased by adding 0.15wt.% Geniset MD nucleating agent.

For the rectangular bar SCORIM moulding, the heat of fusion ΔH and the degree of crystallinity of 0.15wt.% Geniset MD nucleated iPP samples were lower than that recorded for the iPP without adding nucleating agent (see Table 4.11). After adding the nucleating agent, the number of nuclei was increased and the dimension of the spherulites was decreased during nucleation and crystallisation. The balance between growth on nuclei present and their dispersion due to thermal motions was in favour of the latter. This expressed the small dimensions and perfectness of the crystallinity in iPP with the addition of 0.15wt.% Geniset MD samples.

For the rectangular bar of the conventional and SCORIM mouldings of iPP without and with the addition of 0.15wt.% Geniset MD, the γ-phase of polypropylene was found in the x-ray scattering profiles. The melting behaviour was accompanied by increasing amounts of γ-form which must have developed from chains of progressively shorter iPP sequences, but still crystallisable. The difference of the peak temperature $T_{m,p}$ of the SCORIM mouldings between iPP without and with the addition of 0.15wt.% Geniset MD samples was very small with the corresponding processing conditions (see Table 4.11). After adding Geniset MD nucleating agent, the nucleated-iPP gives crystallites of similar melting point by using the SCORIM process. The results indicated that the difference of the length of the longest iPP sequence between iPP without and with the addition of 0.15wt.% Geniset MD samples was very small. On the other hand, the increasing amounts of γ -form had little effect in developing the length of the iPP sequence, but had a great influence in enhancing the alignment of the molecular chains and reducing the molecular chain folding of the iPP mouldings.

The results are summarised:

(1) employment of nucleating agent at a given set of processing conditions enables a degree of control over percentage crystallinity, spherulite size and the rate of crystallisation.

(2) the proportion of amorphous morphology of iPP conventional injection mouldings was decreased with adding nucleating agents.

(3) the degree of crystallinity of iPP conventional injection mouldings was increased to a limiting value with adding lower concentration of nucleating agents and then reduced with adding higher concentration of nucleating agents.

(4) by using the SCORIM injection processing, iPP mouldings adding 0.15wt.% Geniset nucleating agent had little effect in producing a melting distribution characteristic of the chain distribution present.

CHAPTER 6
CONCLUSIONS AND RECOMMENDATIONS FOR FUTURE WORK

6.1 Conclusions

The objective of this study was to investigate the relationship between processing conditions, micromorphology and mechanical properties of isotactic polypropylene. Through this comprehensive experimental study, the objective has been achieved, and the detailed micromorphology studies under different moulding conditions can be used to optimise and achieve the mechanical properties of injection moulded polypropylene for practical applications.

The application of SCORIM on the four live-feed ring moulding resulted to strengthen internal weld lines and provide the optimum circumferential alignment and enhance mechanical properties. The dimensions of iPP ring mouldings were also controlled in moulding roundness, moulding flatness and surface straightness by four live-feed procedure.

The tensile modulus of the MLFM-R1 ring mouldings was 1.9 times greater than that measured from conventional injection ring mouldings, and a 9.3% increase in the case of the MLFM-R2 ring mouldings. The hoop fracture stress for the MLFM-R1 ring mouldings was increased by 17% and for the MLFM-R2 ring mouldings by 2.5%.

The conventional injection moulded iPP exhibited the skin-core morphology which containing a very thin spherulitic structure skin, a birefringent row nucleated intermediate layer and a typically spherulitic core. The shear controlled orientation injection process can displace sufficient molten material within the mould to create a macroscopic shearing action and enhance fibrous alignment of the melt. The micromorphology of iPP injection mouldings produced by SCORIM exhibited the preferred orientated laminated shish-kebab structure in the skin, sub-skin and the intermediate layers which exert profound effects on mechanical properties. The thickness of the oriented skin is a function of the polymer melt temperature and varies inversely with temperature. The thickness of the shear layer varies with injection pressure but in a complex manner.

The Young's modulus of the SCORIM bar mouldings were dependent upon processing temperatures and pressure. According to the iPP used in this research project, the following observations were obtained:

a) when the lower mould temperature was applied, the lower melt temperature associated with the lower holding pressure exhibited the greater Young's modulus;
b) when the higher mould temperature was applied, the lower melt temperature associated with the higher holding pressure caused the greater Young's modulus;
c) when the medium holding pressure was applied, the higher mould temperature and the higher melt temperature combined resulted in the greatest Young's modulus;

The effect of the SCORIM process was dependent on many processing parameters, including duration time, frequency of piston movement, mode of piston operation and pressure. Among them, the oscillating mode of the pistons and the piston operating pressure were the main functions for gaining the significant enhancement to obtain the maximum mechanical properties. Careful selection of appropriate pistons movements and pressure of SCORIM can produce rectangular bar mouldings with 8.0% —— 94.8% enhancement in Young's modulus and 31.6% —— 102.4% increase in fracture stress comparison with conventional injection moulding under the corresponding processing conditions.

The fine spherulitic structures of conventional injection mouldings of iPP with the addition of Geniset MD and ADK NA-11 nucleating agents are remarkable in the view of the transmitted polarized light microcopy. The increase of concentration of nucleating agent in conventional iPP moulding was linked to the increase in α-phase index, density and crystallinity associated with the increase of Young's modulus and tensile strength. On the other hand the tensile strains decrease with an increase of the nucleating contents. The mechanical characteristics of iPP were found that the decreased in the nucleation effect in the high concentration of the nucleating agent might form agglomerates to give an effect of low concentration of the agent.

For the rectangular bar mouldings of both iPP without and with the addition of nucleating agents, the SCORIM mouldings exhibited considerably higher α-phase orientation indices, higher intensity of γ-phase and presented greater γ% and γ-phase index G in comparison with conventional injection mouldings. The crystallinity indices and the crystallinities of all the SCORIM mouldings are also higher than those of the conventional injection mouldings.

According to the higher shearing pressure and longer holding pressure time applied on SCORIM, the greater γ% and γ-phase index G were obtained, the high alignment

of the molecular chains was gained and the chains folding was reduced in the micromorphology, and associated with enhancement of Young's modulus. The values of γ% for the SCORIM mouldings are two or three times higher than that of conventional injection mouldings.

The increase of α-phase results in increasing the orientation structure. The appearance of γ-phase leads to extension of molecular chains. The production of row nucleated ß-phase structure associated with a reduction in the strength of the moulding.

Employment of a nucleating agent enables a degree of control over percentage crystallinity, spherulite size and the rate of crystallization. The heat of fusion ΔH and the degree of crystallinity of iPP were increased with lower concentrations of nucleating agent, and decreased with higher concentrations of nucleating agent.

The melting behaviour was accompanied by increasing amounts of γ-form in the SCORIM iPP. After adding Geniset MD (60/1) nucleating agent, the iPP gives crystallites of similar melting point by using the SCORIM process. The increasing amounts of γ-form had little effect in developing the length of the iPP sequence, but had a great influence in reducing the molecular chain folding and enhancing the stiffness of the iPP mouldings.

6.2 Recommendations for Future Work

It is believed that by appropriate application of the SCORIM processing conditions, the physical properties of moulded materials could be controlled in such a way that their performance would be increased to suit the requirements of the artefact. The arising recommendations for the further work are as follows:

1) The further work can be carried out on the physical characteristics of the iPP with nucleating agents with the other crystalline polyolefines materials by the SCORIM processing.

2) Further studies of morphology need to be extended to a wider range of fillers in polymer matrix by the SCORIM process, it is suggested that polymer/inorganic filler, polymer/rubber filler, polymer/flame retardant filler, be included.

3) A continuation of the investigation is suggested on the development of α, ß and γ crystal phases, which are controlled by the SCORIM process and effect the morphology and mechanical properties.

4) Further investigation is needed to identify the unidentified crystalline form that results from the application of the SCORIM iPP.

REFERENCES

1. Kamal M. and Moy F. H., Microstructure in polymer processing a case study-injection molding. ***Polym. Eng. Rev.***, Vol.2, No.4, p381-416, (1983).
2. Zachariades A. E. and Chung B., ***Advances in Polymer Progress***, Vol.7, No.4, p397-409, (1987).
3. Billiani J. and Feischmann E., ***Polym. Degradation and Stability***, Vol.28, No.1, p67-75, (1990).
4. Kresser T. O. J., ***"Polypropylene"***. Reinhold Pub. Corporation, New York, (1960).
5. Frank H. P., ***"Polypropylene"***. Macdonald Tech. & Sci., London, (1969).
6. Hall C., ***"Polymer materials"***. Macmillan Press Ltd., (1981).
7. Fawcett E. W., Gibson R. O., Perrin M. W. and Williams E. G., ***British Patent*** 471,590 (accepted Sept.6, 1937).
8. Fontana C. M., Herold R. J., Kinney E. J. and Miller R. C., ***Ind. Eng. Chem.***, Vol.44, p2955-62, (1952).
9. Ziggler K., Holzkamp E., Breil H. and Lanning W. C., ***Ind. Eng. Chem.***, Vol.48, p1152, (1956).
10. Natta G., Pino P., Cooradini P., Danusso F., Mantica E., Mazzanti G. and Moraglio G., ***J. Am. Chem. Soc.***, Vol.77, p1708, (1955).
11. d'Ouville E. L., ***"Polythene"***. 2nd Edition, Renfrew A. and Morgan P. eds., Illife & Sons Ltd, London, (1960).
12. Vandenberg E. J.,(to Hercules, Inc.) ***U.S. Patent*** 3,051,690, filed July 29, 1955; issued Aug. 28, (1962).
13. Short J. N., ***Rubb. Plast. News***, May 26, p22-23, (1980).
14. Hull R. L., Foster R. H. and Bowles W. A., SPE Technical Papers, ***RETEC Meeting*** Feb. 27-28, Houston, p239-245, (1984).
15. Scherpereel D. E., Polypropylene-build in toughness when processing. ***Plast. Eng.***, Dec., p46-49, (1973).
16. Monasse B. J., ***J. Mater. Sci.***, Vol.30, No.19, p5002-12, (1995).
17. Heino M. T., Vainio T. P., Seppala L., ***Polymers and Polym. Comp.***, Vol.1, No.6, p439-49, (1993).
18. Pigram A. J. and Freer R. J., ***J. Mater. Sci.***, Vol.29, No.24, p6420-26, (1994).
19. Bassett D. C., ***"Principles of polymer morphology"***. Cambridge University Press, (1981).
20. Bunn C. W., ***"Fibres from synthetic polymers"***. Hill R. ed.,

Amsterdam:Elsevier, p240-300, (1953).

21. Keller A., ***Rep. Prog. Phys.***, Vol.31, p623, (1968).

22. Rees D. V. and Bassett D. C., ***J. Mater. Sci.***, Vol.6, p1021, (1971).

23. Schultz J. M., ***"Polymer materials science"***. Englewood Cliffs, NJ:Prentice Hall, (1974).

24. Natta G. and Cooradini P., Structure and properties of isotactic polypropylene. ***Nuovo. Cimento.***, Vol.15, p40-51, (1960).

25. Pennings, A. J., ***J. Polym. Sci.***, Vol.59, p55, (1977).

26. Frank F. C. and Tosi M. P., ***Proc. Roy. Soc.*** A, Vol.263, p323, (1961).

27. Lauritzen J. I. and Hoffman J. D., ***J. Res. Nat. Bur. Std.***, Vol.64A, p73, (1960).

28. Sanchez T. C., ***J. Macromol. Sci. Rev. Macromol. Chem.***, Vol.10, p113, (1974).

29. Keith H. D., Padden F. J. JR., Walter N. M. and Wyckoff H. W. Evidence for a second crystal form of polypropylene. ***J. Appl. Phys.***, Vol.30, No.10, p1485-88, (1959).

30. Turner-Jones A. and Cobbold A. J. The ß crystalline form of isotactic polypropylene. ***Polym. Lett.***, Vol.6, p539-46, (1968).

31. Morrow D. R. and Newman B. A., ***J. Appl. Phys.***, Vol.39, p4944, (1968).

32. Kardos J. L., Christiansen A. W. and Baer E., ***J. Polym. Sci.*** A-2, Vol.4, p777, (1966).

33. Sauer J. A. and Pae K. D., ***J. Appl. Phys.***, Vol.30, p4950, (1968).

34. Pae K. D., Morrow D. R. and Sauer J. A., Interior morphology of bulk polypropylene. ***Nature***, Vol.211, p514-15, (1966).

35. Morrow D. R., ***J. Macromol. Sci.***, B3, p53-65, (1969).

36. Brückner S. and Meille S. V., Non-parallel chains in crystalline γ-isotactic polypropylene. ***Nature***, Vol.340, p455-57, (1989).

37. Meille S. V., Brückner S. and Porzio W., ***Macromol.***, Vol.23, p4114, (1990).

38. Ferro D. R., Bruckner S., Meiller S. V. and Ragazzi M., ***Macromol.***, Vol.25, No.20, p5231-35, (1992).

39. Rincon J. M., ***Polym.-Plast. Tech. Eng.***, Vol.31, No.3-4, p309-357, (1992).

40. Bowman J., The structure and mechanical properties of an injection-moulded acetal copolymer. ***J. Mater. Sci.***, Vol.16, p1151-66, (1981).

41. Keith H. D. and Padden F. J., ***J. Appl. Phys.***, Vol.35, p1270, (1964).

42. Bunn C. W., ***J. Polym. Sci.***, A, Vol.2, p835, (1954).

43. White J. L., ***Pure Appl. Chem.***, Vol.55, p765-776, (1983).

44. Turley S. G. and Keskkula H., ***J. Appl. Polym. Sci.***, Vol.9, p2693, (1965).

45. Murphy M. W., ***Ph.D Thesis***: Relationships between micromorphology and impact properties of injection moulded isotactic polypropylene. Brunel University, (1986).

46. Murphy M. W., Thomas K. and Bevis M. J., Relationships between injection mouldings conditions, micromorphology and impact properties of polypropylene: 1. A typical commercial grade. ***Plast. Rubb. Mater. Appl.***, Vol.9(1), p3-16, (1988).

47. Trotignon J. P., Lebrun J. L. and Verdu J., Crystalline polymorphism and orientation in injection moulded polypropylene. ***Plast. Rubb. Process Appl.***, Vol.2, p247-51, (1982).

48. Way J. L., Atkinson J. R. and Nutting J., The effect of spherulite size on the fracture morphology of polypropylene. ***J. Mater. Sci.***, Vol.9, p293-99, (1974).

49. Krsova A. and Neuhausl E., Morphology of injection-moulded polyolefine gate zones. ***J. Mater. Sci. Lett.***, Vol.8, No.4, p376-80, (1989).

50. AKay M., ***Polymers and Polym. Comp.***, vol.2, No.6, p349-54, (1994).

51. Alonso M, Gonzalez A., deSaja J. and Requejo A., ***Plast. Rubb. Process. Appl.***, Vol.20, No.3, p165-170, (1993).

52. ZaiKov G. and Polishchuk A., ***Inter. J. Polym. Mater.***, Vol.27, No.1-2, p11-14, (1994).

53. Nichols K., Sole J., Barger M., Pavlowski D. and Bicerano J., ***ANTEC, Conference Proceeding***, No.pt2, p1433-34, (1994).

54. Long Y, Tiganis B. and Shanks R., ***J. Appl. Polym. Sci.***, Vol.58, No.3, p527-35, (1995).

55. Dubey V, Bajpai R., Parashar P. and Datt S., ***Polym. Testing***, Vol.11, No.3, p225-231, (1992).

56. Watkins J. and Kasunic J., ***Eng. Plast.***, Vil.7, No.2, p122-138, (1994).

57. Bensbergen F. L., ***J. Polym. Sci. Polym. Symp.***, Vol.59, p11-29, (1977).

58. Khanna Y. P., ***Macromol.***, Vol.26, p3639-43, (1993).

59. Smith T. L., Masilamani D., Bui L. K., Branbilla R., Khanna Y. P. and Gabriel K. A., ***J. Appl. Polym. Sci.***, Vol.52, No.5, p591-96, (1994).

60. Amellal K. and Lafleur P. G., ***Plast. Rubb. Process. Appl.***, Vol.19, No.4, p227-39, (1993).

61. Bellet. M., Corsini C., Assaker D., Mercier P. and Wouters P., ***J. Reinforced Plast. Comp.***, Vol.12, No.5, p498-505, (1993).

62. Czvikovszky T., ***Mechanical Eng.***, Vol.38, No.4, p209-24, (1994).

63. Mutel B., Taleb A., Dessau X., Goundmand P., Gengembre L. and Grimblot J., ***Thin Solid Films***, Vol.266, No.2, p119-28, (1995).

64. Mikos A., Sarakinos G., Leite S., Vacanti J. and Langer R., ***Biomater.***, Vol.14, No.5, p323-30, (1993).

65. Devries R., Shick R. and Johnson M., *Mater. Research Society Symp. Proceedings*, Vol.381, p165-73, (1995).

66. MatuanaMalanda L., Park C. and Balatinecz J., ***ANTEC, Conference Process.***, Vol.2, p2394-99, (1995).

67. Stehling F. and Meka P., ***J. Appl. Polym. Sci.***, Vol.51, No.1, p105-19, (1993).

68. Whelan A. and Craft J. L., ***"Developments in injection moulding"***. Appl. Sci. Pub. Ltd., London, (1978).

69. Isayev A. I. and Crouthamel D. L.: Residual Stress Development in the Injection Moulding of Polymers. ***Polym. Plast. Tech. Eng.***, Vol.22, No.2, p177-232, (1984).

70. Whelan A., ***"Injection moulding machines"***. Elsevier Appl. Sci. Pub., London and New York, (1984).

71. Thienel P. and Menges G., ***Polym. Eng. Sci.***, Vol.18, p314, (1978).

72. Chen S. and Chen Y., ***Comput. Structure***, Vol.52, No.5, p6420-26, (1994).

73. Coates P., Haynes A. and Speight R., ***Polym.***, Vol.35, No.18, p3831-43, (1994).

74. Allan P. S. and Bevis M. J., ***British Patent*** 2170-140-B.

75. Allan P. and M. J. Bevis, ***Plast. Rubb. Comp. Process. Appl.***, Vol.16, No.2, p133-137, (1991).

76. Allan P. S. and Bevis M. J., The production of void-free thick-section mouldings. 1. Shot-weight and dimensional reproducibility. ***Plast. Rubb. Process. Appl.***, Vol.3, p85-91, (1983).

77. Allan P. S. and Bevis M. J., The production of void-free thick-section injection-flow mouldings. 2. Preferred orientation and residual stress measurements. ***Plast. Rubb. Process. Appl.***, Vol.3, p331-336, (1983).

78. Allan P. S. and Bevis M. J., Producing void-free thick-section thermoplastic and fibre resinforced thermoplastics mouldings. ***Plast. Rubb. Int.***, Vol.9(2), p32-36, (1984).

79. Allan P. S. and Mortazavi M. J., The effect of oscillating packing pressure on the residual stress in thick-section polyethylene injection mouldings. ***Plast. Rubb. Process. Appl.***, Vol.5, p71-78, (1985).

80. Allan P. S. and Bevis M. J., Multiple live-feed injection moulding. ***Plast. Rubb. Process. Appl.***, Vol.7, p3-10, (1987).

81. Allan P. S. and Bevis M. J., Multiple live-feed processing as a route for fibre management in composite materials. ***Inst. Phys. Conf. Ser.***, No.III, p13-23, (1990).

82. Allan P. S. and Bevis M. J., Development and application of multiple live-feed moulding for the management of fibres in moulded parts. ***Composites Manufacturing***, Vol.1, No.2, p79-84, (1990).

83. Ziabicki A. and Kedzierska K., ***J. Appl. Polym. Sci.***, Vol.2, p14, (1959).

84. Ziabicki A. and Kedzierska K., ***J. Appl. Polym. Sci.***, Vol.6, p111, (1962).

85. Sheehan W. C. and Cole T. B., ***J. Appl. Polym. Sci.***, Vol.8, p2339, (1964).

86. Danford M. D., Spruiell J. E. and White J. L., ***J. Appl. Polym. Sci.***, Vol.22, p3351, (1978).

87. Omotoso M. A., White J. L. and Fellers J. F., ***J. Appl. Polym. Sci.***, Vol.25, p1573, (1980).

88. Dees J. R. and Spruiell J. E., ***J. Appl. Polym. Sci.***, Vol.18, p1053, (1974).

89. Hill M. J. and Keller A., ***J. Macromol. Sci.-Phys.***, B3, p153, (1969).

90. Spruiell J. E. and White J. L., ***Polym. Eng. Sci.***, Vol.15, p660, (1975).

91. Katayama K., Amano T. and Nakamura K., ***Kolloid-z Polym.***, Vol.226, p125, (1968).

92. Nadkarni V. M. and Schultz J. M., ***J. Polym. Sci. Phys.***, Vol.15, p2151, (1977).

93. Gibson A., Ward I. M., Cole B. N. and Parsons B., ***J. Mater. Sci. Lett.***, Vol.9, p1193, (1974).

94. Kojima S., Desper C. R. and Porter R. S., ***J. Polym. Sci. Phys.***, Vol.16, p1721, (1978).

95. Mead W. T., Desper C. R. and Porter R. S., ***J. Polym. Sci. Phys.***, Vol.17, p859, (1979).

96. White J. L. and Agarwal A., ***Polym. Eng. Sci.***, Vol.21, p859, (1980).

97. Nagasawa T., Matsumura T., Hoshino S. and Kobayoshi K., ***Appl. Polym. Symp.***, Vol.20, p275, (1973).

98. Hashimoto T., Todo A., Murakami Y. and Kawai H., ***J. Polym. Sci. Phys.***, Vol.10, p521, (1978).

99. Maddams W. F. and Preedy J. E., ***J. Appl. Polym. Sci.***, Vol.22, p2739, (1978).

100. Choi K. J., Spruiell J. E. and White J. L., ***J. Polym. Sci. Phys.***, Vol.20, p27, (1982).

101. Kamal M. R. and Kening, ***Polym. Eng. Sci.***, Vol.12, p302, (1974).

102. Clark E. S., ***Plast. Eng.***, Vol.30, No.3, p73, (1974).

103. Kamal M. and Moy F. H., ***Chem. Eng. Commun.***, Vol.12, p253, (1980).

104. Jensen M. and Whisson R. R., ***Polym.***, Vol.14, p193, (1973).

105. Kantz M. R., Newman H. D. JR. and Stigale F. H., The skin-core morphology and structure-property relationships in injection-molded polypropylene. ***J. Appl. Polym. Sci.***, Vol.16, p1249-60, (1972).

106. Koda H., ***J. Appl. Polym. Sci.***, Vol.12, p2257, (1968).

107. Menges G. and Wubken G., ***SPE Antec***, Vol.19, p519, (1973).

108. Bakerdjian Z. and Kamal M. R., ***Polym. Eng. Sci.***, Vol.17, p96, (1977).

109. Fleissner M. and Paschke E., ***Kunststoffe***, Vol.61, p195, (1971).

110. Clark E. S., ***Polym. Preprint,*** Vol.14, p268, (1973).

111. Boehme E., ***Kunststoffe***, Vol.60, p273, (1970).

112. Kamal M. and Moy F. H., ***Polym. Eng. Sci.***, Vol.20, p957, (1980).

113. Kamal M. and Moy F. H., ***"Rheology, V.3: Applications"***. Astarita G., Marrucci G. and Nicolais L. ed., Plenum Pub. Corp., New York, (1980).

114. Woebcken W. and Heise B., ***Kunststoffe***, Vol.68, p99, (1978).

115. Ladd M. F. C. and Palmer R. A., ***"Structure determination by x-ray crystallography"***. Plenum Press, New York, (1977).

116. Turner-Jones A., Aizlewood J. M. and Beckett D. R., Crystalline forms of isotactic poltpropylene. ***Makromol. Chem.***, Vol.75, p134-58, (1964).

117. Turner-Jones A. Development of the γ-crystal form in random copolymers of propylene and their analysis by DSC and x-ray methods. ***Polym.***, Vol.12, p487-508, (1971).

118. Mijovic J. S. and Koutsky J. A., Etching of polymeric surface: A review. ***Polym.-Plast. Tech. Eng.***, Vol.9, No.2, p139, (1977).

119. Buseck P. R., Epelboin Y. and Rimsky A., ***ACTA Crystallographica Section A-Foundations of Crystallography***, Vol.44, No.Nov, p975-986, (1988).

120. Murphy M. W., Thomas K. and Bevis M. J., ***Plast. Rubb. Mater. Appl.***, Vol.9, No.2, p117-27, (1988).

121. Moy F. H. and Kamal M. R., ***Polym. Eng. Sci.***, Vol.20, p957, (1980).

122. Clark E. S. and Garber C. A., ***Int. J. Polym. Mater.***, Vol.1, p31, (1971).

123. Heckmann W. and Johnson U., ***Colloid Polym. Sci.***, Vol.252, p876, (1974).

124. Clark E. S., ***Meeting of the American Phys. Soc.***, Dallas, (1970).

125. Fujiyama M., Wakino T. and Kawasaki Y., ***J. Polym. Sci.***, Vol.35, p29, (1988).

126. Matsumoto K., Miura I. and Hayashida K., ***Kobunshi Ronbunshu***, Vol.36, p401, (1979).

127. Dragaun H., Hubeny H. and Muschik H., Shear-induced ß-form crystallization in tsotactic polypropylene. ***J. Polym. Sci., Polym. Phys. Ed.***, Vol.15, p1779-89, (1977).

129. Jansen Ir. J., "***Plastic additives handbook***". 2nd Ed., Gachter R. and Huller H. eds., Hanser Pub., Munich, (1983).

130. Avella M., Martuscelli E., Sellitti C. and Garagnani E., Crystallization behaviour and mechanical properties of polypropylene-based composites. ***J. Mater. Sci.***, Vol.22, No.9, p3185-93, (1987).

131. Johnsen U. and Spilgies G., ***Kolliod-Z. Z. Polym.***, Vol.250, p1174, (1972).

132. Janimak J. J., Zhang A. and Cheng S. Z. D., Surface nucleation kinetics in crystallization study of isotactic polypropylene fractions. Polym. Preprints, ***Division Polym. Chem., American Chem. Soci.***, Vol.30, No.2, p313-14, (1989).

133. Fillo B., Wittmann J. C., Lotz B. and Thireey A., Self-nuclaetion and recrystallization of isotactic polypropylene (α-phase) incestigated by differential scanning calorimetry. ***J. Polym. Sci.***, part B: polym. Phys., Vol.31, No.10, p1383-93, (1993).

134. Binsbergen F. L., ***J. Polym. Sci., Polym. Phys. Ed.***, Vol.12, p117, (1973).

135. Alghazawi M. and Sheldon R. P., Heterogeneous nucleation studies on polypropylene. ***J. Polym. Sci., Polym. Lett. Ed.***, Vol.21, No.5, p347-51, (1983).

136. Pospisil L., Lancar J. and Rybnikar F., Activated heterogeneous nucleation of isotactic polypropylene. ***J. Mater. Sci. Lett.***, Vol.9, No.4, p495-96, (1990).

137. Mitra D. and Misra A., Study on the effect of Dibenzylidene sorbitol as a nucleating agent on the crystallization and morphology of poly(ethylene terephthalate). ***J. Appl. Polym. Sci.***, Vol.36, No.2, p387-403, (1988).

138. Young C. K., Chung Y. K. and Sung C. K., Crystallization characteristics of isotactic polypropylene with and without nucleating agents. ***Polymer Eng. Sci.***, Vol.31, No.14, p1009-14, (1991).

139. Akay M., Influence of total processing history on polypropylene structure and properties. ***British Polym. J.***, Vol.21, p285-93, (1989).

140. Tadmor Z. and Gogos C. G., "***Principles of polymer processing***". John Wiley, New York, (1979).

141. Bovey F. A. and Winslow F. H., "***Macromolecules: An introduction to polymer science***". Academic Press, New York, (1979).

142. Gurhan K., Zhong Z., Allan P. and Bevis M. J., ***Polym***. Vol.37, No.11,

p2077-2085, (1996).

143. Gibson J. R., Allan P. S. and Bevis M. J., Recent developments in shear controlled orientation of reinforcement in polymer matrix mouldings. ***Plast. Rubb. Int.***, Oct./Nov., p12-14, (1991).

144. Padden F. J. and Keith H. D., Spherulitic crystallization in polypropylene. ***J. Appl. Phys.***, Vol.30, No.10, p1479-85, (1959).

145. Samuels R. J. and Yee R. Y., ***J. Polym. Sci.***, Vol.10, A-2, p385, (1972).

146. Murphy M. W., Thomas K. and Bevis M. J., Relationship between micromorphology and local impact strength in injection moulded polypropylene artefacts. ***Plast. Rubb. Process. Appl.***, Vol.7, No.4, p241-42, (1987).

147. Lotz B., Graff S. S. and Wittmann J. C., ***J. Polym. Sci. Polym. Phys. Ed.***, Vol.24, p2017-32, (1986).

APPENDICES

Appendix 1. Calculation of the Young's modulus (E)

Young's modulus searched for a elastic region in the curve following Hooke's law.

$$E = \frac{\sigma}{\varepsilon}$$

where σ and ε are the stress and strain values at yield point or end of the curve.

$$\text{The stress} \quad \sigma = \frac{F}{A} = \frac{F}{W \cdot D}$$

The moving time of crosshead (t_S) and the paper chart (t_C) were same.

$$t_S = \frac{d}{V_S} \qquad t_C = \frac{l}{V_C}$$

$$\therefore \quad \frac{d}{V_S} = \frac{l}{V_C} \qquad l = \frac{V_C \cdot d}{V_S}$$

$$\text{The strain} \quad \varepsilon = \frac{l}{L} = \frac{V_C \cdot d}{V_S \cdot L}$$

$$\therefore \text{ Young's modulus } E = \frac{\sigma}{\varepsilon} = \frac{\dfrac{F}{W \cdot D}}{\dfrac{V_C \cdot d}{V_S \cdot L}} = \frac{F \cdot V_S}{W \cdot D \cdot d \cdot V_C} \cdot L \qquad (2—3)$$

where F is the load applied (KN);
L is gauge length (mm);
V_S is the crosshead speed (mm/min);
V_C is the chart speed (mm/min);
W and D are the width and thickness of the sample respectively (mm);
d is the chart moving distance (mm).

Appendix 2. The equations used to calculate the crystal phases indices

(1) α-phase orientation index A where

$$A = \frac{h_{\alpha 1}}{h_{\alpha 1} + h_{\alpha 4}} \qquad (2—5)$$

(2) ß-phase index B where

$$B = \frac{h_{\beta}}{h_{\alpha 1} + h_{\alpha 2} + h_{\alpha 3} + h_{\beta}} \qquad (2—6)$$

(3) Crystallinity index C where

$$C = \frac{h_{\alpha 1} + h_{\alpha 2} + h_{\alpha 3} + h_{\alpha 4} + h_{\beta}}{5ha} \qquad (2—7)$$

(4) percentage γ crystallinity (γ%) where

$$\gamma\% = \frac{H_{\gamma}}{H_{\gamma} + H_{\alpha 3}} \qquad (2—8)$$

(5) γ-phase index G where

$$G = \frac{h_{\gamma}}{h_{\alpha 1} + h_{\alpha 2} + h_{\alpha 3} + h_{\alpha 4}} \qquad (2—9)$$

$$\text{(6) the degree of crystallinity} = \frac{\text{Area}_{(\text{crystalline})}}{\text{Area}_{(\text{crystalline})} + \text{Area}_{(\text{amorphous})}} \qquad (2—10)$$

Appendix 3. The calculation method used to analyse the crystallographic date

$$\text{tg } 2\theta = \frac{r}{L} \qquad \therefore \theta = \frac{1}{2}\,\text{arctg}\left(\frac{r}{L}\right) \qquad (2\text{—}12)$$

$$\lambda = 2d\cdot\sin\theta \qquad \therefore d = \frac{\lambda}{2\cdot\sin\theta} \qquad (2\text{—}13)$$

r : the radius of ring of Debye pattern (mm);

L : the distance from sample surface to the film (mm);

Appendix 4. The method to calculate the density range

Density of '*light*' liquid in the column (d):

$$\begin{aligned} d &= \text{lower density limit} - 20\% \times (\text{range}) \\ &= 0.8900 - 20\% \times (0.9200 - 0.8900) \\ &= 0.8840 \end{aligned}$$

Density of '*heavy*' liquid in the column (D):

$$\begin{aligned} D &= \text{upper density limit} + 30\% \times (\text{range}) \\ &= 0.9200 + 30\% \times (0.9200 - 0.8900) \\ &= 0.9290 \end{aligned}$$

Percentage of propan-2-ol in lower density liquid in the 1000ml mixture is given by '*a*' in the follow equation:

$$0.8840 = 0.785a + 1115 \cdot (1 - a)$$

$$a = 0.700 \text{ (l)} = 700 \text{ ml}$$

So the Digol should be 1000ml – 700ml = 300ml

Percentage of propan-2-ol in upper density liquid in the 1000ml mixture is given by '*b*' in the follow equation:

$$0.9290 = 0.785b + 1115 \cdot (1 - b)$$

$$b = 0.564 \text{ (l)} = 564 \text{ ml}$$

So the Digol should be 1000ml – 564ml = 436ml

Appendix 5. The method used to calculate modulus for rectangular bar mouldings by using the layer removal procedure

Step (1). square bar: Young's modulus: $E_{(skin+sub+shear+core)} = E_1$ (GPa)
Area: $A_{(skin+sub+shear+core)} = A_1$ (mm^2)

Step (2). square bar: Young's modulus: $E_{(sub+shear+core)} = E_2$ (GPa)
Area: $A_{(sub+shear+core)} = A_2$ (mm^2)

Step (3). round bar: Young's modulus: $E_{(shear+core)} = E_3$ (GPa)
Area: $A_{(shear+core)} = A_3$ (mm^2)

Step (4). round bar: Young's modulus: $E_{core} = E_4$ (GPa)
Area: $A_{core} = A_4$ (mm^2)

Young's modulus searched for a elastic region following Hooke's law.

$$\text{Modulus } E = \frac{\sigma}{\varepsilon} = \frac{F/A}{\varepsilon} = \frac{F}{A \cdot \varepsilon}$$

$$\therefore F = E \cdot A \cdot \varepsilon$$

$$E_{core} = E_4 \qquad (3\text{–}1)$$

$$F_{core} = E_{core} \cdot A_{core} \cdot \varepsilon = E_4 \cdot A_4 \cdot \varepsilon$$

$$\begin{aligned} F_{shear} &= F_{(shear+core)} - F_{core} \\ &= E_{(shear+core)} \cdot A_{(shear+core)} \cdot \varepsilon - E_4 \cdot A_4 \cdot \varepsilon \\ &= E_3 \cdot A_3 \cdot \varepsilon - E_4 \cdot A_4 \cdot \varepsilon \end{aligned}$$

$$A_{shear} = A_{(shear+core)} - A_{core} = A_3 - A_4$$

$$E_{shear} = \frac{F_{shear}}{A_{shear}\cdot\varepsilon} = \frac{E_3\cdot A_3\cdot\varepsilon - E_4\cdot A_4\cdot\varepsilon}{(A_3 - A_4)\cdot\varepsilon} = \frac{E_3\cdot A_3 - E_4\cdot A_4}{A_3 - A_4} \qquad (3\text{–}2)$$

$$\begin{aligned} F_{sub} &= F_{(sub+shear+core)} - F_{(shear+core)} \\ &= E_{(sub+shear+core)}\cdot A_{(sub+shear+core)}\cdot\varepsilon - E_3\cdot A_3\cdot\varepsilon \\ &= E_2\cdot A_2\cdot\varepsilon - E_3\cdot A_3\cdot\varepsilon \end{aligned}$$

$$A_{sub} = A_{(sub+shear+core)} - A_{(shear+core)} = A_2 - A_3$$

$$E_{sub} = \frac{F_{sub}}{A_{sub}\cdot\varepsilon} = \frac{E_2\cdot A_2\cdot\varepsilon - E_3\cdot A_3\cdot\varepsilon}{(A_2 - A_3)\cdot\varepsilon} = \frac{E_2\cdot A_2 - E_3\cdot A_3}{A_2 - A_3} \qquad (3\text{–}3)$$

$$\begin{aligned} F_{skin} &= F_{(skin+sub+shear+core)} - F_{(sub+shear+core)} \\ &= E_{(skin+sub+shear+core)}\cdot A_{(skin+sub+shear+core)}\cdot\varepsilon - E_2\cdot A_2\cdot\varepsilon \\ &= E_1\cdot A_1\varepsilon - E_2\cdot A_2\varepsilon \end{aligned}$$

$$A_{skin} = A_{(skin+sub+shear+core)} - A_{(sub+shear+core)} = A_1 - A_2$$

$$E_{skin} = \frac{F_{skin}}{A_{skin}\cdot\varepsilon} = \frac{E_1\cdot A_1\cdot\varepsilon - E_2\cdot A_2\cdot\varepsilon}{(A_1 - A_2)\cdot\varepsilon} = \frac{E_1\cdot A_1 - E_2\cdot A_2}{A_1 - A_2} \qquad (3\text{–}4)$$